ABC Imagem Cardiovascular

Volume 39 | Number 1

January/February/March 2026

Sociedade Brasileira de Cardiologia
ISSN-2675-312X

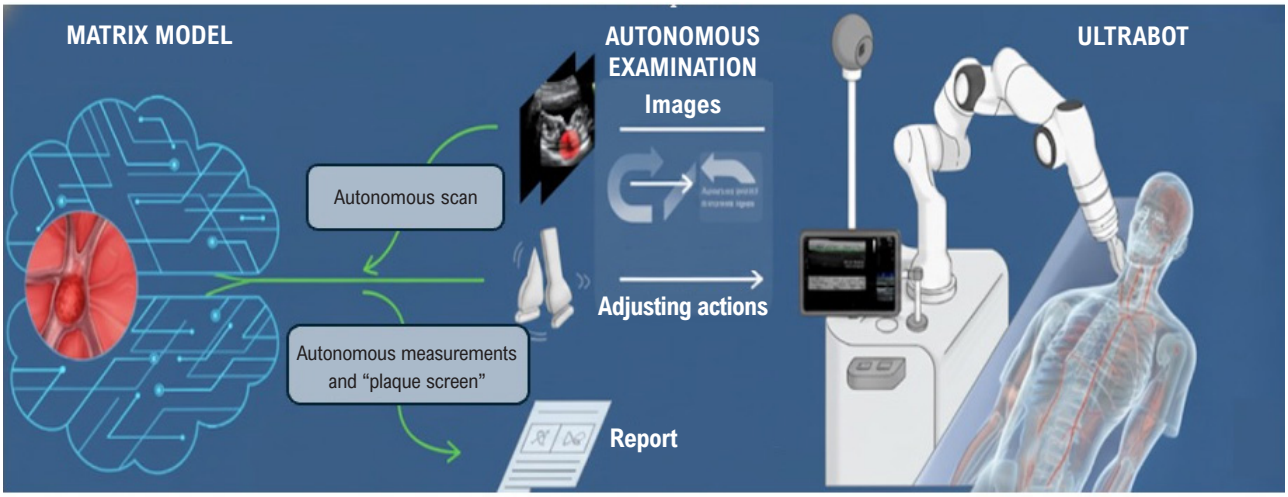

Figure 1 of the article: Top 1 Vascular Ultrasound in 2025: From Anatomy to Autonomy – Artificial Intelligence and Carotid Ultrasound

ABC Imagem Cardiovascular

Contents

Click on the title to read the article

Review Article / My Approach

Case Report

Brief Communication

Departament of Cardiovascular Imaging

President
Adenalva Lima de Souza Beck - DF

Vice President of Echocardiography
Marco Stephan Lofrano Alves - PR

Vice President of Nuclear Cardiology
Adriana Pereira Glavam - RJ

Vice President of Vascular Echography
Marcos Paulo Lacerda Bernardo - RJ

Vice President of Magnetic Resonance Imaging
Gabriela Liberato de Sousa - SP

Vice President of Computed Tomography
Antonio Tito Paladino Filho - SP

Vice President of Congenital Heart Disease and Pediatric Cardiology
Cristiane Nunes Martins - MG

Managing Director
Daniela do Carmo Rassi Frota - GO

Financial Director
Mohamed Hassan Saleh - SP

Journal Editor
Marcelo Dantas Tavares de Melo – PB

Consulting Board

Members
André Luiz Cerqueira de Almeida - BA
Carlos Eduardo Rochitte - SP
Marcelo Luiz Campos Vieira - SP
Samira Saady Morhy - SP
Silvio Henrique Barberato - PR

Scientific Committee

Coordinator
Marco Stephan Lofrano Alves - PR

Members
Adriana Pereira Glavam - RJ
Marcos Paulo Lacerda Bernardo - RJ
Gabriela Liberato de Sousa - SP
Antonio Tito Paladino Filho - SP
Cristiane Nunes Martins - MG

Echocardiography Certification Committee

Coordinator
Rafael Modesto Fernandes - BA

Adult Echo Members
Alex dos Santos Félix - RJ
Angele Azevedo Alves Mattoso - BA
Arthur Cortez Gonçalves - MG
Eliza de Almeida Gripp - RJ
Gracielly Rodrigues de Barros - ES
Liria Maria Lima da Silva - SP
Marcio Mendes Pereira - MA
Renato de Aguiar Hortegal - SP
Vitoria Regia Beserra Barbosa Ximenes - PI

Congenital Echo Members
Danielle Lopes Rocha - ES
Flavia Engers Salles Benites - MS
Halsted Alarcao Gomes Pereira Da Silva - SP
Maria Elisa Martini Albretch - SP

Seniors
Glaucia Maria Penha Tavares - SP
José Aldo Ribeiro Teodoro -SP
Marcelo Iorio Garcia - RJ
Márcio Miranda Brito - TO
Tatiane Mascarenhas Santiago Emerich - ES

Social Media Committee

Coordinator
Bruna Olandoski Erbano - PR
Alex dos Santos Félix - RJ

Members
Kelvin Henrique Vilalva - SP
Claudia Cosentino Gallafrio - SP
Karen Saori Shiraishi Sawamura - SP

Professional Defense and Institutional Relations Committee

Coordinator
Andrea de Andrade Vilela - SP

Members
Antonio Tito Paladino Filho - SP
Daniela do Carmo Rassi Frota - GO
Gracielly Rodrigues de Barros - ES
Isabel Cristina Britto Guimarães - BA
Simone Nascimento dos Santos - DF

Committee of Education and Accreditation

Coordinator
Edgar Bezerra de Lira Filho - SP

Members
Andrea de Andrade Vilela - SP
Daniela do Carmo Rassi Frota - GO
Edgar Daminello - SP
José Luiz Barros Pena - MG
Marcos Paulo Lacerda Bernardo - RJ
Sandra Nívea Dos Reis Saraiva Falcão - CE

Intersociety Committee

Coordinator
Silvio Henrique Barberato - PR

Members
Marcelo Luiz Campos Vieira - SP

Delegado DIC SISIAC
Ivan Romero Rivera - AL

DIC Youth Committee

Coordinator
Alexandre Costa Souza - BA

Members
Marcus Vinicius Silva Freire De Carvalho - BA
Camila Martins Ferreira – DF
Fernanda Maria Franco Castro - MG
Lucas Feldman Paz de Lima - RJ
Luiz Otavio de Arruda Santos - SP
Marina Albanez Albuquerque de Medeiros - PE

DIC Woman Committee

Coordinator
Marly Maria Uellendahl Lopes - SP

Members
Karen Saori Shiraishi Sawamura - SP
Simone Nascimento dos Santos - DF
Simone Cristina Soares Brandão - PE
Mônica Luiza de Alcantara - RJ
Marina Albanez Albuquerque de Medeiros - PE
Samira Saady Morhy - SP

ABC Imagem Cardiovascular

Volume 39, Nº 1, January/February/March 2026

Indexing: SciELO (Scientific Electronic Library Online), Lilacs (Latin American and Caribbean Health Sciences Literature), Latindex (Regional Cooperative Online Information System for Scholarly Journals from Latin America, the Caribbean, Spain and Portugal) and DOAJ (Directory of Open Access Journals)

Address: Av. Marechal Câmara, 160 – 3º andar – Sala 330
20020-907 • Centro • Rio de Janeiro, RJ • Brazil
Phone.: (21) 3478-2700
E-mail: abcimaging@cardiol.br
https://www.abcimaging.org/

Commercial Department
Phone: (11) 3411-5500
E-mail: comercialsp@cardiol.br

Editorial Production
SBC – Scientific Department

Graphic Design and Diagramming
SBC – Scientific Department

Coronary CT Angiography in 2025: Long-Term Evidence, Artificial Intelligence, and the Photon-Counting Era

Tiago A. Magalhães[1,2]
Hcor,[1] *São Paulo, SP – Brazil*
Complexo Hospital de Clínicas, Universidade Federal do Paraná (CHC-UFPR),[2] *Curitiba, PR – Brazil*

Coronary CT Angiography (CCTA) has become established as a first-line test in the evaluation of chest pain, supported by robust evidence of prognostic impact, advances in Artificial Intelligence (AI), and technological evolution with photon-counting CT. Publications in 2025 reposition CCTA as a central platform for risk stratification and therapeutic guidance in coronary artery disease.

The 10-year follow-up of the SCOT-HEART trial represents a major milestone in this process. Among 4,146 patients with stable chest pain randomized to standard care with or without CCTA, there was a sustained reduction in death from coronary heart disease or nonfatal myocardial infarction in the CCTA-guided group (HR 0.79; 95% CI 0.63–0.99).[1] Although revascularization rates did not differ between groups, the use of preventive therapies was more intensive and consistently maintained over time in the CCTA arm. These findings demonstrate that the direct identification of atherosclerosis leads to more aggressive preventive interventions, with durable effects on clinical outcomes, establishing CCTA as a disease-modifying tool in chronic coronary syndromes.

Complementing this perspective, the DISCHARGE trial evaluated outcomes in 3,561 individuals with stable chest pain and an intermediate pretest probability of Coronary Artery Disease (CAD), randomized to CCTA or invasive coronary angiography.[2] After 3.5 years of follow-up, quality of life and angina reduction were similar between strategies. Women had worse baseline status but experienced greater relative improvement in some domains. Thus, while SCOT-HEART confirms benefits in hard clinical endpoints, DISCHARGE demonstrates that CCTA-based evaluation does not result in worse outcomes compared with invasive angiography, reinforcing its role as the guideline-recommended initial diagnostic test.

In the field of artificial intelligence, 2025 marks the transition of CCTA toward a tool for personalized medicine. The Consensus Statement from the QCI Study Group, published in Nature Reviews Cardiology, recommends routine use of AI-assisted quantitative plaque analysis to guide preventive treatment.[3] The document proposes initiating pharmacologic therapy whenever plaque is present and intensifying treatment when plaque volume exceeds the age- and sex-adjusted 70th percentile. This shift moves clinical decision-making away from traditional risk scores toward imaging-derived biomarkers.

The review by Irannejad *et al*. in the International Journal of Cardiovascular Imaging details the current state of AI applications in CCTA, including automated arterial segmentation, plaque quantification, derivation of functional indices, and predictive models for adverse events.[4] Key challenges remain, including external validation, model transparency, and seamless integration into clinical workflows.

Direct evidence of AI algorithm performance is provided by the study of Maaniitty *et al*., published in the Journal of the American Heart Association.[5] In 1,772 patients with suspected CAD, a CCTA-derived ischemia algorithm demonstrated moderate to substantial agreement with a hybrid CCTA/PET reference standard ($\kappa \approx 0.61$) and similar prognostic performance, with a C-index of approximately 0.73 for death, myocardial infarction, or unstable angina over seven years of follow-up. These findings suggest that AI-enhanced tomographic strategies may serve as simpler and more cost-effective alternatives to hybrid imaging approaches.

On the hardware front, photon-counting CT represents a transformative advance. The review by Shiyovich *et al*. in JACC: Cardiovascular Imaging highlights substantial technological gains, including higher spatial resolution, reduced artifacts, and improved assessment of stents and calcified plaques.[6] Although largely based on observational studies, the evidence points to progressive adoption of this technology in specialized centers, expanding CCTA's ability to integrate anatomic assessment, plaque characterization, and, in the future, myocardial perfusion and late enhancement imaging.

The clinical translation of these benefits is demonstrated by Nakashima *et al*. in the Journal of Clinical Medicine.[7] In a matched cohort of 820 patients, photon-counting CT (PCCT) outperformed conventional CT in diagnostic accuracy for significant stenosis, plaque characterization, and appropriate referral for invasive coronary angiography, particularly in scenarios with heavy calcification. These results indicate that advances in photon-counting technology translate into greater precision in clinical care.

Taken together, these lines of evidence—prognostic impact, AI-driven therapeutic stratification, and next-generation hardware—support a new paradigm in which Coronary CT not only diagnoses disease but also guides long-term prevention and management. CCTA is approaching a unified platform for precision medicine in atherosclerosis.

Keywords

Tomography; Coronary Angiography; Coronary Artery Disease

Mailing Address: Tiago Magalhães •
Hospital do Coração. Desembargador Eliseu Guilherme, 147. Postal Code: 04004-030. São Paulo, SP – Brasil
E-mail: tiaugusto@gmail.com

DOI: https://doi.org/10.36660/abcimg.20250106i

Editorial

The challenge ahead lies in integrating these advances into validated clinical algorithms, incorporating them into guidelines, and disseminating them into everyday practice. The year 2025 may represent the point at which coronary CT moved beyond its traditional anatomic role to become a central axis of therapeutic decision-making in coronary artery disease.

References

1. Williams MC, Wereski R, Tuck C, Adamson PD, Shah ASV, van Beek EJR, et al. Coronary CT Angiography-Guided Management of Patients with Stable Chest paIn: 10-Year Outcomes from the SCOT-HEART Randomised Controlled Trial in Scotland. Lancet. 2025;405(10475):329-37. doi: 10.1016/S0140-6736(24)02679-5.
2. Rieckmann N, Neumann K, Maurovich-Horvat P, Kofoed KF, Benedek T, Bosserdt M, et al. Health Status Outcomes after Computed Tomography or Invasive Coronary Angiography for Stable Chest Pain: A Prespecified Secondary Analysis of the DISCHARGE Randomized Clinical Trial. JAMA Cardiol. 2025;10(7):728-39. doi: 10.1001/jamacardio.2025.0992.
3. Schulze K, Stantien AM, Williams MC, Vassiliou VS, Giannopoulos AA, Nieman K, et al. Coronary CT Angiography Evaluation with Artificial Intelligence for Individualized Medical Treatment of Atherosclerosis: A Consensus Statement from the QCI Study Group. Nat Rev Cardiol. 2026;23(2):100-15. doi: 10.1038/s41569-025-01191-6.
4. Irannejad K, Mafi M, Krishnan S, Budoff MJ. Artificial Intelligence in Coronary CT Angiography: Transforming the Diagnosis and Risk Stratification of Atherosclerosis. Int J Cardiovasc Imaging. 2025;41(9):1643-56. doi: 10.1007/s10554-025-03440-8.
5. Maaniitty T, Bär S, Nabeta T, Bax JJ, Saraste A, Knuuti J. Prognostic Value of a Coronary Computed Tomography Angiography-Derived Ischemia Algorithm: Comparison Against Hybrid Coronary Computed Tomography Angiography/Positron Emission Tomography Imaging. J Am Heart Assoc. 2025;14(22):e040726. doi: 10.1161/JAHA.124.040726.
6. Shiyovich A, Singh A, Blair CV, Cardoso R, Huck D, Peng G, et al. Photon-Counting Computed Tomography in Cardiac Imaging. JACC Cardiovasc Imaging. 2026;19(1):94-117. doi: 10.1016/j.jcmg.2025.07.022.
7. Nakashima M, Miyoshi T, Hara S, Miyagi R, Nishihara T, Miki T, et al. Photon-Counting CT Enhances Diagnostic Accuracy in Stable Coronary Artery Disease: A Comparative Study with Conventional CT. J Clin Med. 2025;14(17):6049. doi: 10.3390/jcm14176049.

Top 1 Vascular Ultrasound in 2025: From Anatomy to Autonomy – Artificial Intelligence and Carotid Ultrasound

Simone Nascimento dos Santos,[1] *Gustavo Dannenhauer*[2]

ECCOS,[1] *Brasília, DF – Brazil*

Clínica Biocor,[2] *Caxias do Sul, RS – Brazil*

Introduction

In recent years, we have witnessed a universal and unprecedented advancement of artificial intelligence (AI) across diverse medical scenarios, with a particularly relevant impact on diagnostic imaging, especially ultrasonography.

Ultrasonography is a widely available, low-cost, real-time method with rapid image acquisition and no exposure to ionizing radiation. Despite these advantages, ultrasonography remains limited by its operator- and equipment-dependent nature, which contributes to significant interobserver and interinstitutional variability, in addition to hindering large-scale standardization.[1,2]

In this editorial for *ABC Imagem Cardiovascular*, we discuss the revolutionary findings of the UltraBot system, as described in the article "Towards expert-level autonomous carotid ultrasonography with large-scale learning-based robotic system" by Jiang et al., published in *Nature Communications* in 2025.[3] The study illustrates a structural shift in the field, demonstrating the transition from rigid rule-based robotic systems to a fully autonomous model, driven by large-scale deep learning and imitation learning (Figure 1).

Discussion

Ultrasound examination traditionally depends on manual operation by a professional. This process requires not only prolonged technical training, but also a high capacity for motor and visual coordination, combined with clinical reasoning, to define the ideal positioning of the transducer in real time. Each examination requires individualized strategies adjusted to patients' anatomical and clinical variations.

This strong dependence on the operator's experience results in greater variability between examinations, compromising the standardization of results, with a potentially negative impact on diagnostic accuracy. In contrast, the advancement of highly autonomous medical robots has emerged as a promising solution, reducing the direct influence of human examiners and promoting greater uniformity in the diagnostic process.

In this context, the study by Jiang et al.[3] aimed to develop and validate a fully autonomous vascular ultrasound robot capable of operating at a level comparable to that of human specialists, which dynamically analyzes ultrasound signals collected from patients, adjusts probe trajectories and poses in real time, and accomplishes scanning and measurement tasks in real clinical scenarios. The authors opted for carotid artery ultrasonography due to its strong clinical relevance in detecting atherosclerotic plaques and its association with risk factors for cardiovascular diseases, which are responsible for the highest mortality rates worldwide.[4,5]

UltraBot differs from previous approaches by adopting a large-scale imitation learning framework trained on real examinations performed by specialists.[6-8] Unlike approaches based on predefined rules or simulated environments, the system simultaneously learns anatomy, navigation, and decision-making during acquisition, thus constituting a truly end-to-end model, from perception to action, with a high capacity for clinical generalization. The authors believe that their study not only highlights the system's potential but also charts a viable path to bridge the gap between theoretical research and real-world clinical adoption.

Large-scale data were collected from carotid artery examinations performed on real individuals, comprising 247,297 pairs of ultrasound images and encompassing a wide range of structural tissue variations observed in the real world as well as adaptation actions by expert operators.

The scanning success rate was greater than 90% in a diverse population (age: 19 to 70 years; body mass index: 16.5 to 30.8; both sexes), confirming strong generalization performance across anatomical variations, including successful scanning of patients with plaques.

UltraBot controls the transducer in six degrees of freedom, continuously adjusting its trajectory based solely on visual ultrasound signals, in a process that mimics sonographers' "hand-eye-brain" coordination. In addition, the system automatically measures intima-media thickness and lumen diameter, as well as screening for atherosclerotic plaques. It is interesting to note that the robot uses force sensors and external cameras, thus guaranteeing patient comfort and safety during the procedure.

Prior studies have also demonstrated the automatic processing of arterial segmentation, extracting parameters

Keywords

Doenças das Artérias Carótidas; Ultrassonografia; Inteligência Artificial.

Mailing Address: Simone Nascimento dos Santos •
ECCOS Diagnóstico Cardiovascular. SMDB Conj 16 Lote 5 Casa A. Postal code: 71680-160. Brasília, DF – Brazil
E-mail: simone.eccos@gmail.com

DOI: https://doi.org/10.36660/abcimg.20260001i

in a standardized, fast, and reproducible manner. He et al.[9] used a database with more than 3,000 three-dimensional images of carotid arteries, training a multitasking model for automatic wall segmentation, plaque detection, and vulnerability classification. Accuracy was 94%, with an area under the curve of 0.94, and a reduction of more than 80% in analysis time compared to manual review, demonstrating that AI was functional within real clinical workflows. Another relevant study is a follow-up of the UK database, the UK Biobank, which brings together images, genetic analyses, and clinical data, making it possible to correlate plaque phenotype with these variables.[10]

These findings pave the way for a truly integrated risk assessment, in which carotid ultrasound, for example, integrates with predictive models based on multimodal AI.

Deep learning is breaking down the cost and hardware complexity barriers.

Traditionally, measuring arterial stiffness and plaque morphological characteristics requires the use of high-resolution equipment, dedicated elastography devices, ultrasound enhancing agents, and three-dimensional transducers. With the advancement of deep learning algorithms, it is now possible to extract this information directly from conventional two-dimensional images.

A very interesting example is the concept of virtual elastography. AI analyzes subtle patterns of movement and pixel dispersion in conventional ultrasound videos and estimates tissue stiffness non-invasively, without requiring dedicated elastography hardware. In a recent study, Tang et al.[11] showed a correlation of 0.85 between the virtual technique and real elastography, with an average error of < 10%. This allows us to infer that we are close to transforming any ultrasound device into a tool capable of measuring arterial stiffness based on AI.

Modern deep learning models are able to run on simple hardware, such as clinical laptops, because they have been optimized for low computational demand. This allows advanced image analysis to be employed in clinical settings and even portable examinations.

Perhaps we are already part of an era in which deep learning can democratize high technology, in which AI not only assesses a single variable, but understands how each "layer" is related to risk of vascular events. This is a new concept known as "imaging at scale," which may be the next step in revolutionizing cardiovascular prevention.

Conclusion

UltraBot signals that high-precision autonomous ultrasound has ceased to be a distant promise and become a viable technical reality. For the cardiovascular imaging community, this advancement suggests a future in which technology does not replace physicians, but rather enhances their expertise, raising the standard of care through standardization, reproducibility, and democratization of access to accurate diagnoses.

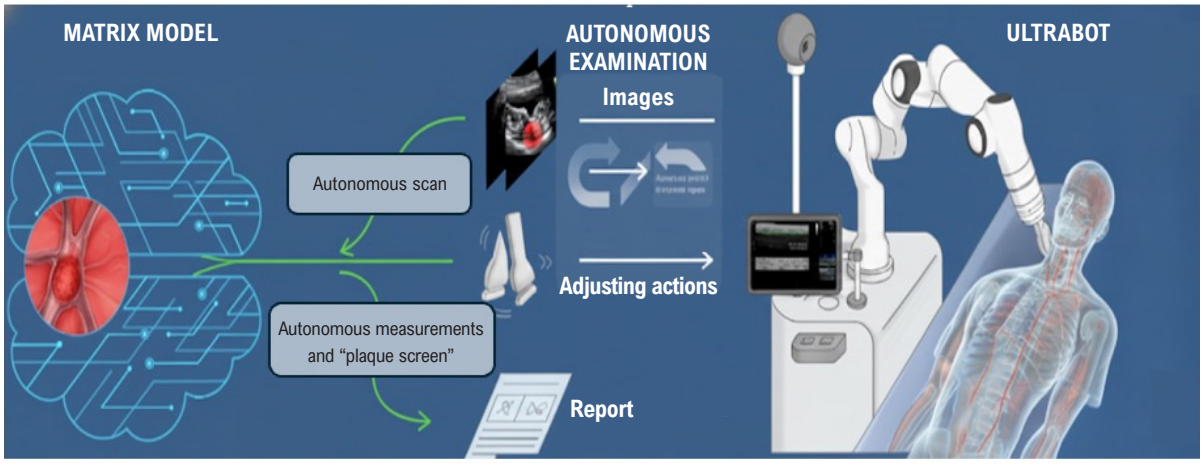

Figure 1 – *Autonomous robotic ultrasound examination. Employing a model based on deep learning and imitation learning, the robotic system automatically performs vascular scanning, biometric measurements, and atherosclerotic plaque screening, generating reports and demonstrating potential clinical applicability. Source: Adapted from Jiang et al.[3]*

References

1. Won D, Walker J, Horowitz R, Bharadwaj S, Carlton E, Gabriel H. Sound the Alarm: The Sonographer Shortage Is Echoing Across Healthcare. J Ultrasound Med. 2024;43(7):1289-301. doi: 10.1002/jum.16453.
2. Shah S, Bellows BA, Adedipe AA, Totten JE, Backlund BH, Sajed D. Perceived Barriers in the Use of Ultrasound in Developing Countries. Crit Ultrasound J. 2015;7(1):28. doi: 10.1186/s13089-015-0028-2.

3. Jiang H, Zhao A, Yang Q, Yan X, Wang T, Wang Y, et al. Towards Expert-Level Autonomous Carotid Ultrasonography with Large-Scale Learning-Based Robotic System. Nat Commun. 2025;16(1):7893. doi: 10.1038/s41467-025-62865-w.

4. Song P, Fang Z, Wang H, Cai Y, Rahimi K, Zhu Y, et al. Global and Regional Prevalence, Burden, and Risk Factors for Carotid Atherosclerosis: A Systematic Review, Meta-Analysis, and Modelling Study. Lancet Glob Health. 2020;8(5):e721-e729. doi: 10.1016/S2214-109X(20)30117-0.

5. Global Burden of Cardiovascular Diseases and Risks 2023 Collaborators. Global, Regional, and National Burden of Cardiovascular Diseases and Risk Factors in 204 Countries and Territories, 1990-2023. J Am Coll Cardiol. 2025;86(22):2167-243. doi: 10.1016/j.jacc.2025.08.015.

6. Huang D, Bi Y, Navab N, Jiang Z. Motion Magnification in Robotic Sonography: Enabling Pulsation-Aware Artery Segmentation. arXiv. 2023; arXiv:2307.03698. doi: 10.48550/arXiv.2307.03698.

7. Yanwei H, Xiao W, Wang C, Liu H, Huang R, Sun Z. Towards Fully Autonomous Ultrasound Scanning Robot With Imitation Learning Based on Clinical Protocols. IEEE Robot Autom Lett. 2021;6(2):3671-8. doi: 10.1109/LRA.2021.3064283.

8. Huang Q, Gao B, Wang M. Robot-Assisted Autonomous Ultrasound Imaging for Carotid Artery. IEEE Trans Instrum Meas. 2024.73:1-9. doi: 10.1109/TIM.2024.3353836.

9. He L, Yang Z, Wang Y, Chen W, Diao L, Wang Y, et al. A Deep Learning Algorithm to Identify Carotid Plaques and Assess their Stability. Front Artif Intell. 2024;7:1321884. doi: 10.3389/frai.2024.1321884.

10. Omarov M, Zhang L, Jorshery SD, Malik R, Das B, Bellomo TR, et al. Automated Deep Learning-Based Detection of Early Atherosclerotic Plaques in Carotid Ultrasound Imaging. medRxiv. 2025:2024.10.17.24315675. doi: 10.1101/2024.10.17.24315675.

11. Tang X, Zhang L, He D, Hu B, Jia C, Gu S, et al. Automatic Generation and Risk Stratification of Carotid Plaque in Virtual Shear Wave Elastography Using a Generative Adversarial Network. Comput Med Imaging Graph. 2025;124:102600. doi: 10.1016/j.compmedimag.2025.102600.

Nuclear Cardiology: From Consolidation to Integration

Simone Cristina Soares Brandão[1,2]

Universidade Federal de Pernambuco,[1] Recife, PE – Brazil

Brigham and Women's Hospital, Harvard Medical School,[2] Boston, MA – USA

Introduction

Over the past decade, nuclear cardiology has undergone a profound transformation.[1–5] What was once primarily a diagnostic tool focused on ischemia detection has evolved into a comprehensive platform for physiological understanding, risk stratification, and precision cardiovascular care.[2,6–12] In this context, the field has shifted from simply identifying disease to elucidating its underlying mechanisms, echoing Marie Curie's insight that "nothing in life is to be feared, it is only to be understood."

The year 2025 did not stand out for isolated disruptive discoveries, but rather for something equally important: clinical consolidation.[1,2,13] During this period, previously emerging concepts matured into actionable clinical paradigms, allowing the field to move from promise to practice.[1,13]

Positron emission tomography (PET) has become a central modality for the quantitative assessment of myocardial blood flow, microvascular dysfunction, and integrated myocardial pathophysiology.[1,7,10,12–14] Advances in radiotracers, scanner technology, and analytic frameworks have moved from proof-of-concept to structured clinical implementation, reinforcing the role of PET in contemporary cardiovascular imaging.[1,2,13]

In this context, 2025 represented a pivotal transition year for nuclear cardiology, defined by maturation, integration, and growing clinical relevance. This editorial reflects on key areas where consolidated evidence is available, highlights emerging applications that have gained momentum, and outlines ongoing and future directions, with PET positioned at the core of precision cardiovascular imaging.

From Ischemia Detection to Physiologic Phenotyping: Consolidation in 2025

One of the most defining developments in nuclear cardiology over recent years has been the shift from ischemia detection toward physiological phenotyping, a transition that reshaped clinical practice.[1,14] Central to this evolution is the recognition of coronary microvascular dysfunction (CMD) as a clinically meaningful phenotype rather than an incidental or secondary finding.[15] CMD is now increasingly understood as a key biological substrate underlying persistent symptoms, cardiometabolic disease, diffuse coronary atherosclerosis, and heart failure syndromes, even in the absence of obstructive epicardial disease.[1,7,10,13]

In this context, PET has emerged as the reference standard for the quantitative assessment of myocardial blood flow and myocardial flow reserve.[13] The ability to noninvasively quantify coronary physiology across the entire myocardium has reshaped clinical evaluation, enabling more accurate diagnosis, risk stratification, and therapeutic decision-making in patients with complex or diffuse disease patterns. By 2025, these quantitative PET-derived metrics have moved beyond research applications and are increasingly incorporated into routine clinical workflows at experienced centers.[1]

The clinical maturation of flurpiridaz further exemplifies this paradigm shift.[3,14,16,17] Once viewed primarily as a promising investigational tracer, flurpiridaz entered a phase of structured clinical implementation, supported by its favorable imaging characteristics, logistical advantages, and robust physiologic performance.[14,16] Its potential to expand access to PET myocardial perfusion imaging (i.e., improved image quality, flexible stress protocols, and streamlined workflows) represents a critical step toward broader adoption of physiologic imaging.[3,16] Together, these developments underscore a fundamental change in nuclear cardiology.

Expansion Beyond Obstructive Coronary Disease

In 2025, nuclear cardiology continued to expand beyond the traditional framework of obstructive coronary artery disease, reflecting a broader understanding of cardiovascular disease as a complex, dynamic biological system.[4,6] Cardiovascular pathology is recognized as the result of interacting metabolic, inflammatory, neurohormonal, and fibrotic processes that evolve over time,[10,11] with growing recognition of the tight interplay between myocardial metabolism and immune activation as fundamental drivers of disease expression.[18] No single metric can fully capture this complexity, helping explain the wide variability in clinical presentation, therapeutic response, and outcomes observed across patients.

Keywords

Positron Emission Tomography; Inflammation; Precision Medicine.

Correspondência: Simone Cristina Soares Brandão •
20 Chapel St., Apt. B411. Postal code: 02446.
Brookline, MA - USA
Email: ssoaresbrandao@bwh.harvard.edu

DOI: https://doi.org/10.36660/abcimg.20260007i

Within this context, molecular imaging has assumed a strategic role. Its value lies not only in detecting disease, but in visualizing and quantifying underlying biological processes in vivo; many of which represent potentially modifiable therapeutic targets. By interrogating inflammation, fibroblast activation, autonomic dysfunction, and microvascular physiology, nuclear cardiology provides a window into disease mechanisms that extend beyond luminal anatomy,[5,6] including metabolic stress–driven immune activation.[19]

Several clinical domains illustrate this expansion. In heart failure, PET imaging has enabled more refined phenotyping through the assessment of CMD, providing insights into myocardial remodeling and functional decline. In conduction diseases, particularly left bundle branch block, nuclear imaging has moved beyond descriptive findings to characterize mechanical dyssynchrony, regional perfusion patterns, and their association with adverse remodeling.[8] In cardio-oncology, cardiac FDG PET has emerged as a powerful tool for probing early metabolic and inflammatory myocardial responses to cancer therapy,[9,20] capturing biologic vulnerability that may precede, and is not reliably mirrored by, early functional deterioration.[21] These metabolic changes do not consistently correlate with early reductions in left ventricular ejection fraction or global longitudinal strain, indicating that FDG PET captures a distinct, biologically meaningful signal rather than serving as a surrogate for functional impairment alone.[9]

Collectively, these applications reflect a broader conceptual shift. Nuclear cardiology is transitioning from a predominantly diagnostic and prognostic discipline toward a driver of mechanism-based therapy. Imaging is increasingly used to guide patient selection, define optimal intervention windows, and monitor biological response to treatment.[6,22] In this evolving paradigm, the true value of nuclear cardiology lies in its ability to quantify biological processes that can be acted upon for the benefit of the patient.[2]

Technology and Tracers: From Innovation to Clinical Implementation

Advances in technology and radiotracers in nuclear cardiology were defined less by novelty and more by clinical readiness in 2025.[2,7,14,16,22,23] Improvements in the reproducibility of quantitative metrics, shorter workflows, and tighter integration between hardware and software platforms marked a transition from proof-of-concept to structured clinical implementation. Together, these developments strengthened confidence in quantitative PET and facilitated its broader adoption in routine clinical practice.[5,16]

Cardiac amyloidosis exemplifies this maturation. While bone-avid SPECT tracers remain foundational for diagnosis, recent advances extend beyond traditional approaches.[2] PET tracers, such as 124I-evuzamitide (AT-01) and emerging SPECT agents, including 99mTc-p5+14, highlight the potential for more specific tissue characterization.[22,23] These tools may enhance differentiation between light chain and transthyretin amyloidosis, support earlier disease detection, and improve integration of diagnosis, prognostication, and therapeutic decision-making.

Physiologic assessment has also advanced through refined flow quantification.[12,17] PET remains the reference standard for quantitative assessment of myocardial blood flow,[13] enabling evaluation of transmural and subendocardial perfusion and uncovering regional vulnerability not captured by global metrics alone.[12] Parallel validation studies using cadmium zinc telluride SPECT cameras demonstrate strong correlation with PET, signaling a future in which precision physiology may become accessible beyond specialized centers.[24]

Last, artificial intelligence and large-scale datasets are reshaping image interpretation and risk assessment.[25] Automated quantification, integration with biobanks, and sex- and age-specific reference values are improving robustness and reproducibility.[7] Registries (e.g., REFINE PET) now exceeding 35,000 patients, illustrate how data-driven approaches can connect imaging, physiology, and personalized cardiovascular care.[4,25]

Nuclear Cardiology in 2026: The Integration Era

Nuclear cardiology has clearly entered a new phase. The year 2025 represented more than incremental progress, it marked the consolidation of a discipline that now plays a decisive role in understanding cardiovascular physiology, refining diagnosis, and guiding patient management. Quantitative PET, supported by validated radiotracers, advanced hardware, and robust clinical evidence, has become central to this transformation.[1] At the same time, continued advances in quantitative methodologies and the development of increasingly sensitive and specific PET and SPECT tracers are expanding the biological and clinical insights accessible by nuclear cardiology.[3,22,23]

As we move through 2026, the emphasis is expected to shift from consolidation to integration. Phenotype-driven and prognosis-oriented imaging[8] supported by artificial intelligence, large-scale datasets,[25] and standardized quantitative metrics,[7] will increasingly inform clinical decision-making. In this evolving landscape, nuclear cardiology is no longer positioned as a complementary diagnostic modality but as a core component of precision cardiovascular medicine; thus, transforming complex biological signals into clinically actionable knowledge.[6] In this sense, the field continues to embody Marie Curie's insight: moving from what is feared to what is understood. While 2025 marked consolidation, 2026 marks the phase of integration and impact (Figure 1).

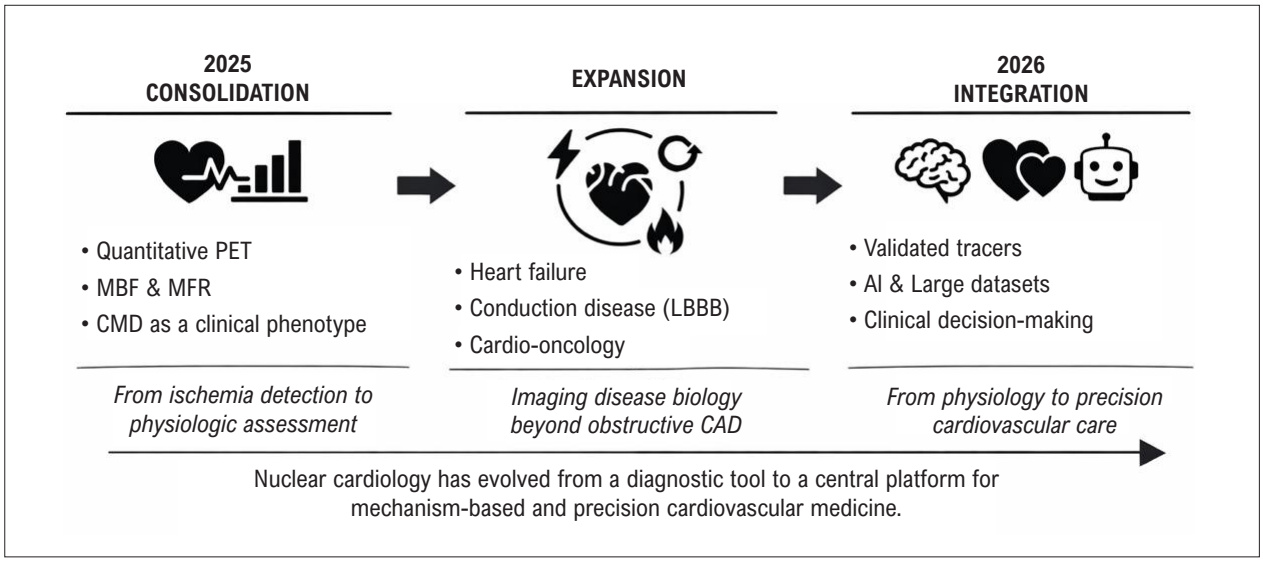

Figure 1 – *Evolution of nuclear cardiology from consolidation to integration (2025–2026). In 2025 (Consolidation), quantitative positron emission tomography (PET) with routine assessment of myocardial blood flow (MBF) and myocardial flow reserve (MFR) consolidated the shift from ischemia detection to physiologic assessment, establishing coronary microvascular dysfunction (CMD) as a clinical phenotype. The Expansion phase reflects the extension of nuclear cardiology beyond obstructive coronary artery disease (CAD) to imaging disease biology in heart failure, conduction disease, particularly left bundle branch block (LBBB), and cardio-oncology. In 2026 (Integration), validated tracers, artificial intelligence (AI)-driven analysis of large datasets, and imaging-guided clinical decision-making converge to enable precision cardiovascular care.*

References

1. Bateman TM, Al-Mallah MH, Alnabelsi TS, Arumugam P, Calnon DA, Chareonthaitawee P, et al. Clinical Indications for Positron Emission Tomography Myocardial Perfusion Imaging and Myocardial Blood Flow Quantification: An American Society of Nuclear Cardiology Position Statement. J Nucl Cardiol. 2025:102619. doi: 10.1016/j.nuclcard.2025.102619.
2. Aimo A, Chen YFF, Castiglione V, Passino C, Genovesi D, Giorgetti A, et al. Positron Emission Tomography in Cardiac Amyloidosis: Current Evidence and Future Directions. Heart Fail Rev. 2025;30(3):605-18. doi: 10.1007/s10741-025-10493-3.
3. Brandão SCS. A New Horizon in Nuclear Cardiology in Brazil: Impact and Barriers of F-18 Flurpiridaz. Arq Bras Cardiol: Imagem Cardiovasc. 2024;37(4):e20240118. doi: 10.36660/abcimg.20240118i.
4. Chareonthaitawee P. Our Adventure: A Year of Innovation, Collaboration, and Global Growth. J Nucl Cardiol. 2025;54:102569. doi:10.1016/j.nuclcard.2025.102569.
5. Di Carli MF. Another Year We Built Together. J Nucl Cardiol. 2025;54:102590. doi: 10.1016/j.nuclcard.2025.102590.
6. Thackeray JT. Theranostics in Nuclear Cardiology: Approaching Harbour or Boundless Horizon? J Nucl Cardiol. 2025;54:102481. doi: 10.1016/j.nuclcard.2025.102481.
7. Joseph L, Trinquart L, Lopez DM, Brandao S, Brown JM, Divakaran S, et al. Age- and Sex-Adjusted Myocardial Flow Reserve Percentiles for Personalized Cardiovascular Risk Assessment. medRxiv. 2025:2025.12.30.25343223. doi: 10.64898/2025.12.30.25343223.
8. Brandão SCS, Joseph L, Brown JM, Lopez D, Lemley M, Ramirez G, et al. Mechanical Dyssynchrony and Perfusion Heterogeneity Predict Adverse LV Remodeling in Patients with and without LBBB. medRxiv. 2026:2026.01.09.26343726. doi: 10.64898/2026.01.09.26343726.
9. Becker MMC, Buril RO, Wanderley MRB Jr, Berenguer DRF, Mourato FA, Costa IBSS, et al. Prospective Multicenter Evaluation of 18F-FDG PET/CT and Strain for Early Cardiotoxicity Detection in Lymphoma Patients. Cardiooncology. 2025;12(1):1. doi: 10.1186/s40959-025-00416-4.
10. Souza ACDAH, Troschel AS, Marquardt JP, Hadžić I, Foldyna B, Moura FA, et al. Skeletal Muscle Adiposity, Coronary Microvascular Dysfunction, and Adverse Cardiovascular Outcomes. Eur Heart J. 2025;46(12):1112-23. doi: 10.1093/eurheartj/ehae827.
11. Liang S, Hou P, Wang X, Liang W, Zhong S, Zhao R, et al. Comparison of 18F-FAPI-42 PET for Detecting Cardiac Fibroblast Activation in Dilated Cardiomyopathy with Histopathology and CMR. JACC Cardiovasc Imaging. 2025;18(9):997-1009. doi: 10.1016/j.jcmg.2025.05.021.
12. Xu X, Divakaran S, Weber BN, Hainer J, Laychak SS, Auer B, et al. Relationship of Subendocardial Perfusion to Myocardial Injury, Cardiac Structure, and Clinical Outcomes among Patients with Hypertension. Circulation. 2024;150(14):1075-86. doi: 10.1161/CIRCULATIONAHA.123.067083.
13. Vrints C, Andreotti F, Koskinas KC, Rossello X, Adamo M, Ainslie J, et al. 2024 ESC Guidelines for the Management of Chronic Coronary Syndromes. Eur Heart J. 2024;45(36):3415-537. doi: 10.1093/eurheartj/ehae177.
14. Lopez DM, Huck DM, Divakaran S, Brown JM, Weber BN, Lemley M, et al. Utility of 18F-Flurpiridaz PET Relative Flow Reserve in Differentiating Obstructive from Nonobstructive Coronary Artery Disease. Circ Cardiovasc Imaging. 2025;18(11):e018323. doi: 10.1161/CIRCIMAGING.125.018323.
15. Oliveira GMM, Almeida MCC, Valério CM, Giuffrida F, Espíndola L Neto, Izar MCO, et al. Position Statement on Cardiometabolic Health Across the Woman's Life Course - 2025. Arq Bras Cardiol. 2025;122(9):e20250615. doi: 10.36660/abc.20250615.
16. Rupa S, deKemp R, Horgan S, Al-Mallah MH, Bateman T, Case J, et al. Laboratory Considerations on the Use of F-18 Myocardial Perfusion Imaging Radiotracers: An ASNC Information Statement. J Nucl Cardiol. 2025;48:102230. doi: 10.1016/j.nuclcard.2025.102230.

17. Builoff V, Lemley M, Miller RJH, Fujito H, Ramirez G, Kavanagh P, et al. Subendocardial Quantification Enhances Coronary Artery Disease Detection in 18F-Flurpiridaz PET. Eur J Nucl Med Mol Imaging. 2025;52(9):3342-52. doi: 10.1007/s00259-025-07174-6.

18. Fragasso G, Stolfo D, Anker MS, Bayes-Genis A, Chioncel O, Heymans S, et al. The Crosstalk between Immune Activation and Metabolism in Heart Failure. A Scientific Statement of the Heart Failure Association of the ESC. Eur J Heart Fail. 2025;27(9):1700-19. doi: 10.1002/ejhf.3703.

19. Pereira A, Alvarez-Argote S, Meite I, Inui H, Sterling JK, Thorp EJ, et al. Metabolic Stress and Immune Activation in Heart Failure with a Preserved Ejection Fraction. Immunol Rev. 2026;337(1):e70103. doi: 10.1111/imr.70103.

20. Berenguer DRF, Arruda GFA, Becker MMC, Dourado MLC, Buril RO, Mourato FA, et al. Monitoring Myocardial Metabolic Changes in Lymphoma Patients Undergoing Chemotherapy Using FDG PET/CT. ABC Imagem Cardiovasc. 2025;38(4):e20250067. doi: 10.36660/abcimg.20250067i.

21. Galán-Arriola C, Pérez-Camargo D, Jorge I, Bautista V, Ayaon-Albarrán A, Pérez-Martínez C, et al. Anthracycline Cardiotoxicity: Role of Metabolic Vulnerability Induced by Cardiac Pressure Overload. Eur Heart J. 2026:ehaf1060. doi: 10.1093/eurheartj/ehaf1060.

22. Smiley DA, Einstein AJ, O'Gorman KJ, Santana D, Teruya S, Chan N, et al. Early Detection of Transthyretin Cardiac Amyloidosis Using 124I-Evuzamitide Positron Emission Tomography/Computed Tomography. JACC Cardiovasc Imaging. 2025;18(7):799-811. doi: 10.1016/j.jcmg.2025.01.018.

23. Martin E, Kassira A, Stuckey A, Whittle B, Guthrie S, Kennel SJ, et al. A Tale of Two Tracers - Amyloid Imaging with Investigational Radiotracers Iodine (124I) Evuzamitide and 99mTc-p5+14 (AT-05). J Nucl Cardiol. 2025:102451. doi: 10.1016/j.nuclcard.2025.102451.

24. Yahiro DS, Leite LF, Azevedo GL, Al-Mallah MH, Mesquita CT. Comparison of PET-CT and CZT-SPECT on Myocardial Blood Flow and Flow Reserve Measurement: A Systematic Review and Meta-Analysis. J Nucl Cardiol. 2025;52:102279. doi: 10.1016/j.nuclcard.2025.102279.

25. Ramirez G, Lemley M, Shanbhag A, Kwiecinski J, Miller RJH, Kavanagh PB, et al. The REgistry of Flow and Perfusion Imaging for Artificial Intelligence with Positron Emission Tomography (REFINE PET): Rationale and Design. J Nucl Cardiol. 2025;52:102449. doi: 10.1016/j.nuclcard.2025.102449.

Editorial

Recalibrating the Barometer: Echocardiography in Diastolic Dysfunction and the Era of New Algorithms

Maria Estefania Bosco Otto,[1,2] *Jorge Eduardo Assef,*[3] *Gustavo Nishida*[3]

Universidade de Brasília,[1] *Brasília, DF – Brazil*
Hospital DF Star,[2] *Brasília, DF – Brazil*
Instituto Dante Pazzanese de Cardiologia,[3] *São Paulo, SP – Brazil*

Diastolic dysfunction (DD) remains a diagnostic challenge, not for lack of available parameters, but because uncertainty emerges when complex physiology is reduced to static labels in echocardiographic reports. In clinical practice, physicians are often less concerned with the specific grade of DD and more interested in its prognostic implications and in whether increased filling pressures may explain dyspnea, guide further investigation, and support therapeutic decisions. It is precisely in this variable, mean left atrial pressure (MLAP) and left ventricular (LV) filling pressure (LVFP), that echocardiography must be most pragmatic, minimizing the number of "indeterminate" reports and offering an operational conclusion grounded in integrated physiology.[1-4]

The structured reasoning that supports this goal began with the 2009 American Society of Echocardiography/European Association of Echocardiography guideline on the evaluation of LV diastolic function,[1] a landmark document that organized modern thinking on diastole, established a shared language for key pathophysiological mechanisms, and systematized the interpretation of echocardiographic parameters. Beyond its conceptual value, it reinforced a critical principle for echocardiography laboratories: the assessment of diastole must translate into a clinically meaningful message, particularly when heart failure with preserved ejection fraction (HFpEF) is suspected.

The 2016 update of the guideline represented another important step by simplifying and improving the reproducibility of multiparametric assessment, focusing on widely available variables suitable for routine use.[2] In practice, however, the post-2016 experience revealed a persistent issue: in the real world, especially among patients with HFpEF, a substantial proportion of studies continued to be classified as having "indeterminate" diastolic function. While methodologically honest, this result is often clinically insufficient.[2-4]

The study by Lababidi et al.[3] represents a pragmatic turning point. In a multicenter cohort validated against invasive hemodynamics, they proposed a stepwise echocardiographic algorithm to estimate LVFP. The first stage relies on highly feasible measurements, while the second stage resolves discordance or incomplete data using additional parameters supported by strong pathophysiological rationale. Its editorial relevance is direct: the algorithm was designed to reduce the proportion of "indeterminate" cases and improve diagnostic accuracy (from 80% to 86% in patients with HFpEF) in determining LVFP.[3]

Following the publication of Lababidi et al.,[3] the 2025 guideline "recalibrates the barometer" by incorporating these proposed algorithms into a structured strategy for diastolic evaluation and HFpEF diagnosis.[4] This update not only refines the accuracy of DD classification but also improves the identification of increased LVFP, significantly reducing the proportion of cases classified as indeterminate.[4] These algorithms apply to patients in sinus rhythm and without mitral valve conditions that distort the assessment of relaxation and LVFP, such as mitral stenosis of any degree and moderate or severe mitral regurgitation or mitral annular calcification.

However, the 2025 guideline presents two key figures (Figures 2 and 3 of that document[4]) that, at a superficial reading, may appear to compete with one another and therefore generate operational uncertainty. In general terms, Figure 2 of that guideline evaluates the presence of DD, whereas Figure 3 classifies findings based on the estimated MLAP.[4] When interpreted as alternative pathways rather than complementary steps, they may perpetuate uncertainty and lead to conflicting results.

In this context, the letter by Assef & Nishida[5] gains practical relevance. They propose integrating these figures sequentially, redefining Figure 2 as Algorithm 1 (steps for diagnosing DD) and Figure 3 as Algorithm 2 (grading DD and estimating MLAP), both presented in Figure 1 of this Editorial, with clearer transition rules and tie-breaking criteria.[5] This integrated use facilitates interpretation and reduces the likelihood of misclassification. The editorial response from the guideline authors, by clarifying issues related to interpretation and applicability, further contributes to harmonizing understanding and reducing variability in the use of these tools.[6]

In practice, this integration has two immediate consequences. First, it preserves a core set of widely feasible measurements (transmitral Doppler, e′ velocities, E/e′ ratio, and pulmonary pressure estimation) as the initial decision-making step, while directing the use of additional parameters with strong pathophysiological rationale when needed. Second, so-called advanced parameters are placed in their proper role: not as technological embellishments, but as tools to resolve discordance and bring the report closer to the central clinical question, increased versus non-increased LVFP.[4,5]

Beyond workflow reorganization, the 2025 guideline incorporates two messages that directly reflect daily clinical practice. The first is the recognition of left atrial reservoir strain as an additional variable for diastolic assessment, particularly in populations with preserved ejection fraction, in whom the range

Keywords

Left Ventricular Dysfunction; Diastolic Heart Failure; Echocardiography.

Mailing Address: Maria Estefania Bosco Otto •
Universidade de Brasília. SQSW 301 Bloco F, Apto 508. Postal code: 70910-900. Brasília, DF – Brazil
E-mail: mariaestefaniaotto@gmail.com
Manuscript received January 12, 2026; revised January 29, 2026; accepted January 29, 2026; corrected in 15/04/2026.
Editor responsible for the review: Marcelo Tavares

DOI: https://doi.org/10.36660/abcimg.20260004i

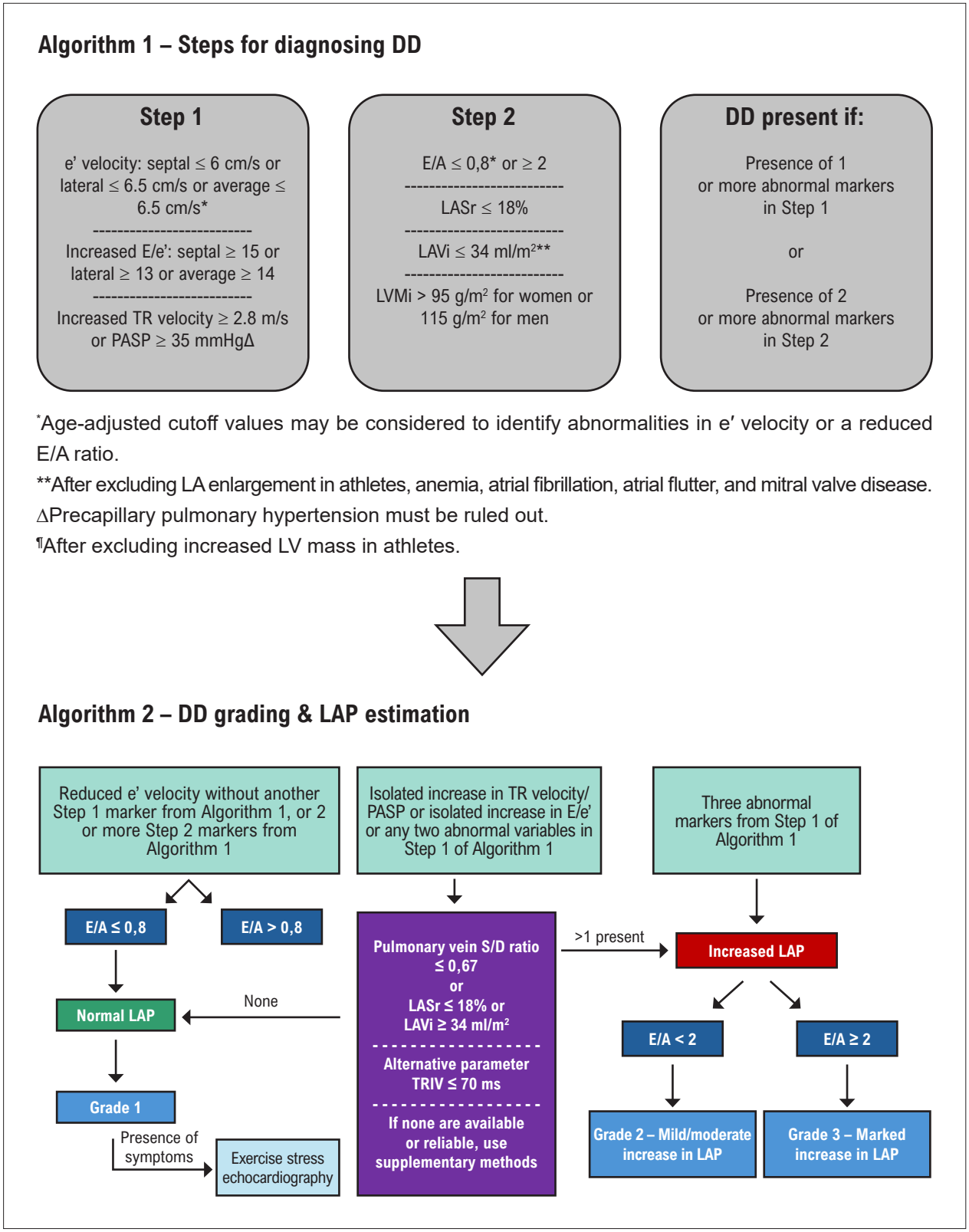

Figure 1 – *Integrated algorithm for DD (adapted from Assef & Nishida5 with permission). DD: diastolic dysfunction; IVRT: isovolumic relaxation time; LA: left atrium; LAP: LA pressure; LASr: LA strain, reservoir phase; LAVi: LA volume index; LV: left ventricle; LVMi: LV mass index; S/D: systolic-to-diastolic; PASP: pulmonary artery systolic pressure; TR: tricuspid regurgitation.*

of normality is broad and load dependence requires greater interpretative sophistication.[4,7] The second is the reinforcement that mitral annular tissue Doppler e' velocities should be interpreted in the context of age, acknowledging the physiological decline in relaxation associated with aging.[4] Together, these incorporations move in the same direction: reducing false conflicts among variables and increasing the likelihood of a coherent conclusion when the clinical picture is suggestive.[4-7]

Furthermore, the renewed role of pulmonary vein Doppler is consistent with the historical evolution of the field. As early as 2009, this parameter played a relevant role in inferring LVFP and distinguishing filling patterns.[1] By repositioning it as a tie-breaking variable, contemporary algorithms restore its ability to appropriately reduce the diagnostic gray zone.[1,5]

Integration with clinical algorithms represents the next step in reducing attribution errors in patients with multifactorial dyspnea. Approaches such as H_2FPEF help estimate pretest probability and identify those who may benefit from additional investigation.[8] Complementarily, the HFA-PEFF algorithm organizes diagnostic probability and guides decisions regarding functional testing or invasive hemodynamic assessment.[9]

Finally, improved diagnostic precision has an unavoidable practical consequence: HFpEF now has therapies that modify outcomes. Without turning this Editorial into a therapeutic review, it is important to recognize that trials such as EMPEROR-Preserved (empagliflozin) and DELIVER (dapagliflozin) established SGLT2 inhibitors as beneficial interventions in patients with HFpEF.[10,11] The more consistent the diagnosis of an HFpEF phenotype, the more appropriate the application of evidence-based treatment strategies.

In summary, "recalibrating the barometer" in DD means recovering what the 2009 guideline[1] conceptually organized, recognizing what the 2016 guideline[2] simplified, and applying what the 2025 guideline[4] operationalized: a stepwise, integrated, purpose-driven approach to classifying diastolic function and estimating MLAP.[3-7] New diastolic algorithms enable a clinically actionable conclusion, anchored in physiology, regarding the likelihood of increased LVFP. By sequentially integrating diastolic function classification with LVFP estimation, as proposed by Assef & Nishida,[5] inconsistencies observed in recent guidelines are substantially reduced, and echocardiographic reporting gains greater coherence and robustness, particularly when interpreted within the patient's clinical context.

Erratum

January, February, and March 2026 Issue, vol. 39(1): e20260004

In the Editorial "Recalibrating the Barometer: Echocardiography in Diastolic Dysfunction and the Era of New Algorithms," DOI: https://doi.org/10.36660/abcimg.20260004i, published in the journal Arquivos Brasileiros de Cardiologia: Imagem Cardiovascular, Arq Bras Cardiol: Imagem cardiovasc. 2026;39(1):e20260004, on page 2, in Figure 1, replace the line "iVAE ≤ 34 mL/m²" with "iVAE ≥ 34 mL/m²".

References

1. Nagueh SF, Appleton CP, Gillebert TC, Marino PN, Oh JK, Smiseth OA, et al. Recommendations for the Evaluation of Left Ventricular Diastolic Function by Echocardiography. J Am Soc Echocardiogr. 2009;22(2):107-33. doi: 10.1016/j.echo.2008.11.023.
2. Nagueh SF, Smiseth OA, Appleton CP, Byrd BF 3rd, Dokainish H, Edvardsen T, et al. Recommendations for the Evaluation of Left Ventricular Diastolic Function by Echocardiography: An Update from the American Society of Echocardiography and the European Association of Cardiovascular Imaging. J Am Soc Echocardiogr. 2016;29(4):277-314. doi: 10.1016/j.echo.2016.01.011.
3. Lababidi H, Rahi W, Smiseth OA, Billick K, Inoue K, Khan FH, et al. New Algorithm for Estimating Left Ventricular Filling Pressure by Echocardiography. Circulation. 2025;152(7):424-35. doi: 10.1161/CIRCULATIONAHA.125.074974.
4. Nagueh SF, Sanborn DY, Oh JK, Anderson B, Billick K, Derumeaux G, et al. Recommendations for the Evaluation of Left Ventricular Diastolic Function by Echocardiography and for Heart Failure with Preserved Ejection Fraction Diagnosis: An Update from the American Society of Echocardiography. J Am Soc Echocardiogr. 2025;38(7):537-69. doi: 10.1016/j.echo.2025.03.011.
5. Assef JE, Nishida G. Systematizing Diastolic Function Evaluation: From Algorithms to Practical Approach-Are we Finally Reaching Diagnostic Consistency? J Am Soc Echocardiogr. 2026;39(2):235-36. doi: 10.1016/j.echo.2025.09.023.
6. Nagueh SF, Sanborn DY, Oh JK, Anderson B, Billick K, Derumeaux G, et al. Reply to Multiple Letters regarding the American Society of Echocardiography's Recommendations for the Evaluation of Left Ventricular Diastolic Function. J Am Soc Echocardiogr. 2026;39(2):239-40. doi: 10.1016/j.echo.2025.10.010.
7. Nagueh SF, Khan SU. Left Atrial Strain for Assessment of Left Ventricular Diastolic Function: Focus on Populations with Normal LVEF. JACC Cardiovasc Imaging. 2023;16(5):691-707. doi: 10.1016/j.jcmg.2022.10.011.
8. Reddy YNV, Carter RE, Obokata M, Redfield MM, Borlaug BA. A Simple, Evidence-Based Approach to Help Guide Diagnosis of Heart Failure with Preserved Ejection Fraction. Circulation. 2018;138(9):861-70. doi: 10.1161/CIRCULATIONAHA.118.034646.
9. Pieske B, Tschöpe C, de Boer RA, Fraser AG, Anker SD, Donal E, et al. How to Diagnose Heart Failure with Preserved Ejection Fraction: the HFA-PEFF Diagnostic Algorithm: A Consensus Recommendation from the Heart Failure Association (HFA) of the European Society of Cardiology (ESC). Eur Heart J. 2019;40(40):3297-317. doi: 10.1093/eurheartj/ehz641.
10. Anker SD, Butler J, Filippatos G, Ferreira JP, Bocchi E, Böhm M, et al. Empagliflozin in Heart Failure with a Preserved Ejection Fraction. N Engl J Med. 2021;385(16):1451-61. doi: 10.1056/NEJMoa2107038.
11. Solomon SD, McMurray JJV, Claggett B, de Boer RA, DeMets D, Hernandez AF, et al. Dapagliflozin in Heart Failure with Mildly Reduced or Preserved Ejection Fraction. N Engl J Med. 2022;387(12):1089-98. doi: 10.1056/NEJMoa2206286.

Hypertrophic Cardiomyopathy: Standardization of Echocardiographic Assessment in an Era of New Therapies

Marcelo Goulart Paiva[1,2]

Unifesp EPM,[1] São Paulo, SP – Brazil

Hospital 9 de Julho,[2] São Paulo, SP – Brazil

Hypertrophic cardiomyopathy (HCM) has become the most common inherited myocardial disease, with an estimated global prevalence between 1:200 and 1:500. Despite its relatively high frequency in the general population, the disease remains significantly underdiagnosed. Only about 15% of affected individuals are clinically identified, due mainly to the wide variability of phenotypes and clinical manifestations.[1,2] Slightly more than half of patients may develop progressive symptoms or experience adverse events throughout their lifetime. Early identification, risk stratification, and cardiovascular therapies and interventions have reduced mortality rates to < 1.0% per year.[3]

The pathophysiology of HCM is based on myocardial hypertrophy in the absence of secondary causes, associated with hypercontractility and diastolic dysfunction, resulting from abnormal myosin activation. Approximately 75% of patients present with left ventricular outflow tract (LVOT) obstruction at rest or after provocative maneuvers. In the absence of an obstructive pattern, the disease course is usually favorable, oligosymptomatic, or asymptomatic, with a minority progressing to advanced stages.[3–5]

Transthoracic echocardiography (TTE) is essential for diagnosing HCM. Suspicion should arise in the presence of diastolic myocardial thickness ≥ 15 mm in the absence of any conditions that justify hypertrophy in a non-dilated ventricle. In patients with a family history of HCM or genetic mutation, diastolic myocardial thickness ≥ 13 mm is considered sufficient. Other indications for performing TTE include systolic murmur suggestive of dynamic obstruction in the LVOT and suggestive symptoms, such as dyspnea, chest pain, and syncope, related to dehydration, exercise, and the postprandial period.[1,2,6]

When HCM is suspected, TTE should contain the relevant information for case management, including the following: indexed left atrial volume; myocardial thickness of the septum and posterior wall; location of the segment with the greatest increase in thickness; left ventricular ejection fraction; global longitudinal strain; analysis of diastolic function; description of apical aneurysm when present; description of the presence and location of intraventricular gradient; description of systolic anterior motion of the mitral valve; mitral valve apparatus abnormalities; and mitral regurgitation.[2,3]

Given the labile nature of LVOT gradients, the absence of obstruction at rest does not exclude latent obstructive HCM. Provocative maneuvers such as the Valsalva maneuver or rapid squat-to-stand maneuver should be routinely used to unmask gradients. Furthermore, postprandial echocardiography has emerged as a powerful tool, as mesenteric vasodilation and the adrenergic response after a meal can significantly elevate gradients in more than a third of patients who would be erroneously classified as non-obstructive when fasting. Whenever resting maneuvers are inconclusive, exercise stress echocardiography (ESE) remains the gold standard for assessing the functional relevance of the obstruction and should be performed after a meal.[2,7]

Recent studies have demonstrated the relevance of hemodynamic assessment in hypertrophic cardiomyopathy under different physiological conditions, including rest, physical exertion, fasting, and the postprandial period. After food intake, even at rest, the presence of systolic anterior motion of the mitral valve and an increased left ventricular outflow tract gradient were observed, findings that became more pronounced during postprandial exertion. This case highlights the importance of a comprehensive use of the available diagnostic tools for characterizing obstruction, as such an approach contributes to therapeutic optimization and to guiding lifestyle measures.[8]

Using TTE and postprandial ESE to study 252 patients with HCM, Massera et al. identified a LVOT gradient ≥ 50 mmHg in 35.7% of patients without obstruction under baseline conditions, including 15.1% on the postprandial physical stress phase alone. More than 50% of patients undergoing invasive treatment or myosin inhibitors had a LVOT gradient ≥ 50 mmHg only on postprandial assessment (TTE and ESE).[7]

Accordingly, clinical routines should incorporate echocardiography with specific protocols for HCM, including provocative maneuvers and postprandial assessment. However, there is still a lack of standardization regarding the type of diet and the interval between the meal and echocardiographic assessment.

Keywords

Hypertrophic Cardiomyopathy; Echocardiography; Left Ventricular Outflow Obstruction

Mailing Address: Marcelo Goulart Paiva •
Unifesp EPM. Rua Periquito, 210, 92B. Postal code: 04023-062. São Paulo, SP – Brazil
E-mail: mgpaiva123@gmail.com

DOI: https://doi.org/10.36660/abcimg.20260027i

Editorial

References

1. Maron BJ, Desai MY, Nishimura RA, Spirito P, Rakowski H, Towbin JA, et al. Diagnosis and Evaluation of Hypertrophic Cardiomyopathy: JACC State-of-the-Art Review. J Am Coll Cardiol. 2022;79(4):372-89. doi: 10.1016/j.jacc.2021.12.002.
2. Mitchell CC, Frye C, Jankowski M, Symanski J, Lester SJ, Woo A, et al. A Practical Approach to Echocardiographic Imaging in Patients with Hypertrophic Cardiomyopathy. J Am Soc Echocardiogr. 2023;36(9):913-32. doi: 10.1016/j.echo.2023.04.020.
3. Fernandes F, Simões MV, Correia EB, Marcondes-Braga FG, Coelho-Filho OR, Mesquita CT, et al. Guidelines on the Diagnosis and Treatment of Hypertrophic Cardiomyopathy - 2024. Arq Bras Cardiol. 2024;121(7):e202400415. doi: 10.36660/abc.20240415.
4. Maron BJ, Desai MY, Nishimura RA, Spirito P, Rakowski H, Towbin JA, et al. Management of Hypertrophic Cardiomyopathy: JACC State-of-the-Art Review. J Am Coll Cardiol. 2022;79(4):390-414. doi: 10.1016/j.jacc.2021.11.021.
5. Abbasi M, Ong KC, Newman DB, Dearani JA, Schaff HV, Geske JB. Obstruction in Hypertrophic Cardiomyopathy: Many Faces. J Am Soc Echocardiogr. 2024;37(6):613-625. doi: 10.1016/j.echo.2024.02.010.
6. Ommen SR, Nishimura RA, Schaff HV, Dearani JA. Hypertrophic Cardiomyopathy: State of the Art. Mayo Clin Proc. 2025;100(3):557-66. doi: 10.1016/j.mayocp.2024.07.013.
7. Massera D, Long C, Xia Y, James L, Adlestein E, Alvarez IC, et al. Unmasking Obstruction in Hypertrophic Cardiomyopathy with Postprandial Resting and Treadmill Stress Echocardiography. J Am Soc Echocardiogr. 2024;37(10):971-80. doi: 10.1016/j.echo.2024.06.011.
8. Abreu MEB, Diógenes TCP, Chagas ISM,Xerex HM, Abreu JS. Repercussão Hemodinâmica da Cardiomiopatia Hipertrófica em Repouso e Durante o Esforço em Bicicleta Supina: Valor Adicional da Avaliação Pós-Prandial. Arq Bras Cardiol: Imagem cardiovasc. 2026;39(1):e20250049 . doi: 10.36660/abcimg.20250049

Original Article

Comparison of Cardiac Structural Changes After Surgical and Transcatheter Atrial Septal Defect Closure With Color Doppler Echocardiography

Tuğçe Akın,[1] Zeynep Bilge Yılmaz Dere,[1] Yılmaz Yozgat,[1] Halil Türkoğlu,[1] Murat Ugurlucan[2]
İstanbul Medipol Üniversitesi,[1] Fatih, Istambul – Turkey
Liv Hospital Vadi İstanbul,[2] Istambul – Turkey

Abstract

Background: Surgical and transcatheter techniques represent the two principal approaches for atrial septal defect (ASD) closure. Although both are widely used, comparative evidence regarding their mid-term effects on cardiac remodeling and right ventricular (RV) function remains limited.

Objectives: To compare mid-term cardiac structural remodeling and right ventricular functional recovery after surgical versus transcatheter ASD closure in pediatric patients using serial color Doppler echocardiographic assessment. Additionally, to determine whether either technique leads to faster or greater improvement in right heart morphology and function.

Methods: We retrospectively evaluated 69 pediatric patients who underwent ASD closure at a single center. A total of 39 patients underwent surgical repair (Group 1), and 30 patients underwent transcatheter closure (Group 2). Transthoracic color Doppler echocardiography was performed before the procedure and at 3 and 12 months after intervention. Measures of atrial and ventricular morphology and function were analyzed.

Results: At 3 months, the surgical group showed significantly greater improvement in right atrium (RA) major axis, RA volume, interventricular septal thickness in diastole, interventricular septal thickness in systole, and RV end-diastolic diameter (RVEDd) compared with the transcatheter group (all $p < 0.05$). At 12 months, surgical repair remained superior regarding improvement in RA major axis, RA volume, and RVEDd (all $p < 0.05$). Residual shunt was identified in only one patient in each group at 12 months.

Conclusions: Surgical ASD closure was associated with earlier and more consistent recovery of right atrial and ventricular geometry and function compared with transcatheter closure. These findings indicate that surgical closure may offer advantages for selected patients, particularly in relation to right heart remodeling during the first postoperative year.

Keywords: Atrial Heart Septal Defects; Operative Surgical Procedures; Echocardiography.

Introduction

Although multiple subtypes of atrial septal defect (ASD) exist, ostium secundum defects account for approximately 80% of all ASDs.[1,2] Echocardiography remains the cornerstone for diagnosis and longitudinal follow-up in this population.[3] Depending on the defect type and anatomical location, both surgical repair and transcatheter device closure are well-established therapeutic strategies.[4,5] Surgical repair is required for sinus venosus, coronary sinus, and ostium primum defects, whereas most secundum defects are suitable for transcatheter closure. The advent of color Doppler echocardiography has enabled a more comprehensive evaluation of myocardial function and cardiac chamber remodeling compared with conventional two-dimensional imaging.[5]

Previous investigations have demonstrated significant reductions in right atrial and right ventricular dimensions following ASD closure with either technique.[6-16] Nevertheless, comparative evidence describing the temporal trajectory of atrial and ventricular remodeling after surgical versus transcatheter closure, particularly in pediatric populations, remains limited.

Accordingly, this study aimed to evaluate the effects of surgical and transcatheter ASD closure on cardiac structure and myocardial function using transthoracic color Doppler echocardiography, with predefined assessments at baseline, 3 months, and 12 months after the procedure (Central Illustration).

Mailing Address: Tuğçe Akın •
İstanbul Medipol Üniversitesi, Department of Anatomy. Göztepe Mah, Kavacık, Atatürk, Cd. No:40, 34810. Beykoz, Fatih, Istanbul – Turkey
E-mail: tugceeaakin@gmail.com
Manuscript received February 6, 2026; revised February 9, 2026; accepted February 10, 2026
Editor responsible for the review: Marcelo Tavares

DOI: https://doi.org/10.36660/abcimg.20260014i

Original Article

Central Illustration: Comparison of Cardiac Structural Changes After Surgical and Transcatheter Atrial Septal Defect Closure With Color Doppler Echocardiography

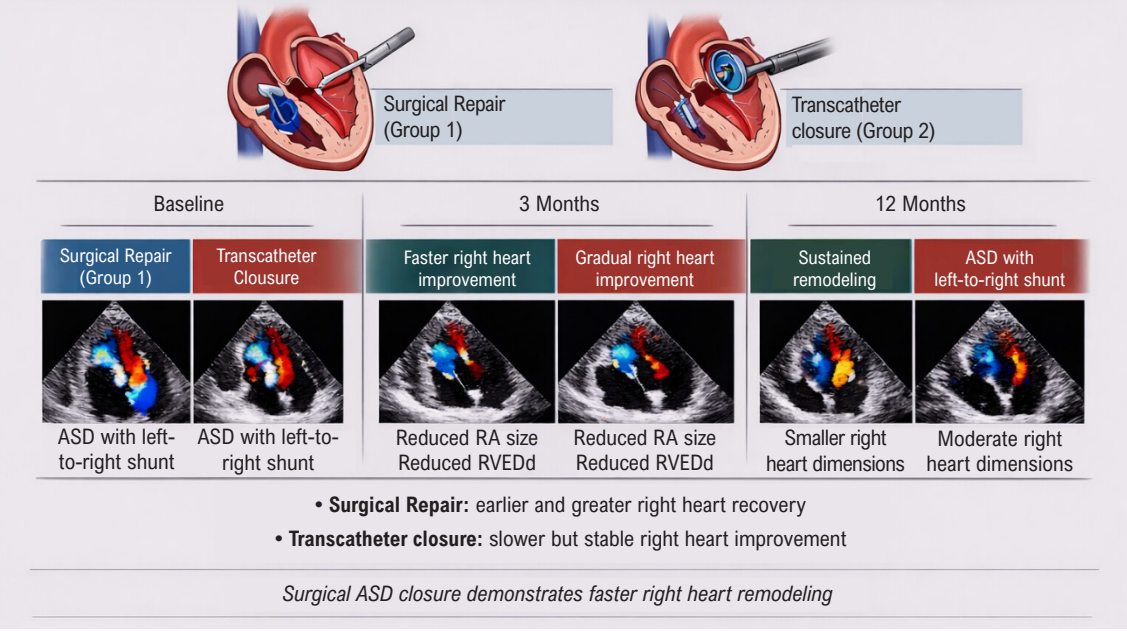

Arq Bras Cardiol: Imagem cardiovasc. 2026;39(1):e20260014

Comparison of Cardiac Structural Changes After Surgical and Transcatheter Atrial Septal Defect Closure With Color Doppler Echocardiography. ASD: atrial septal defect; RA: right atrium; RVEDd: right ventricle end-diastolic diameter.

Methods

Patient selection

This retrospective study was conducted at the Department of Pediatric Cardiology, Medipol Mega University Hospital. Data were obtained from the institutional electronic echocardiography database. A total of 69 patients who underwent ASD closure between 2013-2019 were included. Patients were categorized into two groups: surgical repair (Group 1, n = 39) and transcatheter closure (Group 2, n = 30).

Patients younger than 10 years, those with complex congenital cardiac anomalies, chronic comorbidities (e.g., anemia, hypothyroidism, cystic fibrosis), or those who underwent emergent surgical procedures were excluded.

The study was approved by the Human Research Ethics Committee at the Ethics Committee of Istanbul Medipol University, Istanbul, Turkey, and conducted in accordance with the Declaration of Helsinki.

Echocardiographic evaluation

All echocardiographic examinations were performed using transthoracic echocardiography (Vivid S6, M4S-RS 1.5-3.6 MHz probe, GE HealthCare, New York, USA) and analyzed with EchoPAC software (GE HealthCare, New York, USA). Imaging protocols followed the recommendations of the American Society of Echocardiography.

Parameters assessed included:

- Atrial morphology: right atrium (RA) and left atrium (LA) major/minor axes, RA and LA volumes, and tricuspid valve annular diameters (apical 4-chamber view) (Figure 1; Figure 2).
- Ventricular morphology and function: left ventricle (LV) end-diastolic diameter (LVEDd), LV end-systolic diameter (LVESd), right ventricle (RV) end-diastolic diameter (RVEDd), RV end-systolic diameter (RVESd), interventricular septal thickness in diastole, and interventricular septal thickness in systole (IVSs) (parasternal long-axis view, M-mode).
- Derived indices: LV ejection fraction and fractional shortening (FS).

Measurements were obtained before the procedure and at 3 and 12 months after the intervention.

Statistical analysis

Data were analyzed using IBM SPSS Statistics for Windows, version 20 (IBM Corp., Armonk, N.Y., USA). Continuous variables were expressed as mean ± standard deviation or median (minimum-maximum), depending on distribution, and categorical variables as number and percentage. Group comparisons were performed using Student's *t* test or the Mann-Whitney *U* test. Paired comparisons across time points were assessed using the paired samples *t*-test or Wilcoxon test.

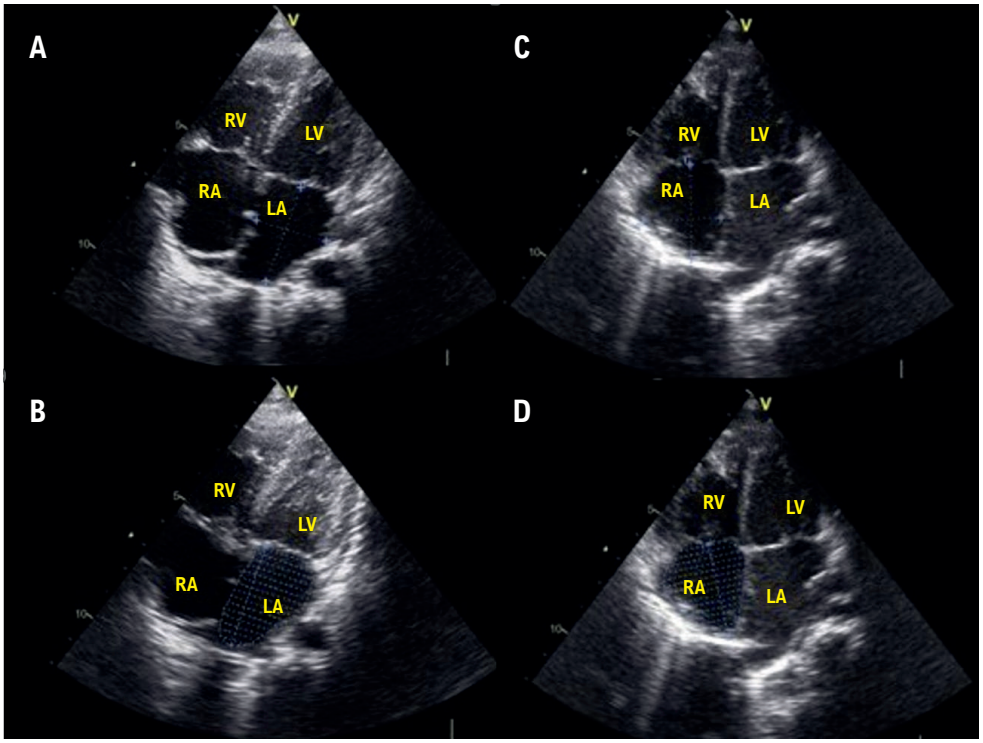

Figura 1 – *Measurement of major and minor axes (A) and volume (B) of the LA, and major and minor axes (C) and volume (D) of the RA. RA: right atrium; RV: right atrium; LA: left atrium; LV: left atrium.*

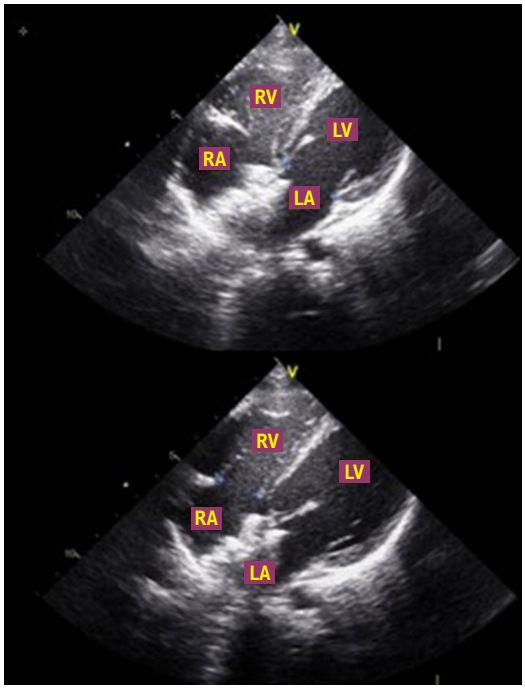

Figura 2 – *Mitral and tricuspid valve annuli measurements. RA: right atrium; RV: right atrium; LA: left atrium; LV: left atrium.*

A two-sided p-value < 0.05 was considered statistically significant. Power analysis using G*Power (v3.1.9.7) estimated an effect size of 0.56, which indicates that 57 participants per group would be required to achieve 95% power at $\alpha = 0.05$. Owing to data availability, 39 surgical and 30 transcatheter patients were included, which is acknowledged as a limitation.

Results

A total of 69 patients were included (38 women [55.1%], 31 men [44.9%]; mean age of 57.0 ± 26.6 months). The surgical group (n = 39) comprised 61.5% of women with a mean age of 50.4 ± 26.7 months, whereas the transcatheter group (n = 30) included 46.6% of women with a mean age of 65.6 ± 24.2 months. The mean ASD diameter was larger in the surgical group than in the transcatheter group (18.3 ± 6.2 mm vs. 12.3 ± 3.2 mm, p < 0.05). Secundum ASDs accounted for 71.8% of surgical cases and all transcatheter cases, while sinus venosus defects were present only in the surgical group (28.2%). Table 1 summarizes patient demographics.

At 3 months postoperatively in Group 1, significant reductions were observed in RA major axis, RA minor axis, RA volume, RVEDd, and RVESd, together with increases in FS, IVSs, and LV dimensions (all p < 0.05). These improvements largely persisted at 12 months, with further reductions in RA and RV dimensions and continued

increases in LV diameters. Detailed comparisons are presented in Table 2.

At 3 months in Group 2, RA major and minor axes, RA volume, and RVEDd significantly decreased, whereas LV dimensions increased (all $p < 0.05$). At 12 months, only LVEDd and LVESd continued to increase significantly compared with 3 months, while most right-sided parameters remained stable. Results are shown in Table 1.

Tabela 1 – Características demográficas dos pacientes

Variables	Surgical repair group (n = 39)	Transcatheter group (n = 30)
Age, months	50.40 ± 26.70	65.61 ± 24.20
Sex, n (%)		
Male	15 (38.4%)	16 (53.4%)
Female	24 (61.5%)	14 (46.6%)
ASD diameter, mm	18.33 ± 6.17	12.33 ± 3.18
Type of ASD		
Ostium secundum, n (%)	28 (71.79%)	30 (100%)
Sinus venosus, n (%)	11 (28.2%)	

ASD: atrial septal defect.

When changes from baseline were compared between groups, surgical repair demonstrated significantly greater improvement in RA major axis, RA volume, IVSs, and RVEDd at 3 months (all $p < 0.05$). At 12 months, RA major axis, RA volume, and RVEDd remained significantly more improved in the surgical group (all $p < 0.05$). Group comparisons are detailed in Table 4.

Discussion

In this single-center study, we compared postoperative cardiac remodeling in patients undergoing surgical versus transcatheter closure of ASDs. The main findings were: i) surgical closure resulted in faster improvement in right atrial dimensions and RVEDd during the early postoperative period; ii) these advantages persisted at 12 months; and iii) residual shunt rates were similarly low in both groups.

Our findings align with previous reports demonstrating rapid right heart reverse remodeling after ASD closure.[10-16] Chen et al.[10] reported significant reductions in right atrial dimensions following transcatheter repair, consistent with our observations in the device closure group. However, unlike Chen et al.,[10] we did not detect significant changes in LA parameters after transcatheter closure.

Hausdorf et al.[11] and Sezer et al.[12] described early improvements in RVEDd accompanied by gradual increases in LV dimensions after closure. Similarly, we observed marked reductions in RVEDd and increases in LVEDd

Table 2 – Echocardiographic parameters before and after surgical closure of atrial septal defect at 3 and 12 months

Parameter	Baseline	Postoperative (3 months)	Postoperative (12 months)	Baseline vs 3 months	Baseline vs 12 months	3 vs 12 months
LA major axis, mm	31.30 ± 3.41	29.30 ± 4.13	29.07 ± 3.94	0.011[a]	0.005[a]	0.788[a]
LA minor axis, mm	20.71 ± 3.45	21.71 ± 2.82	23.20 ± 3.06	0.064[a]	0.001[a]	0.024[a]
LA volume, cm^2	6.50 ± 1.29	6.06 ± 1.20	6.68 ± 1.20	0.054[a]	0.000[b]	0.004[a]
MVDL, mm	16.00 (14.00-18.00)	17.00 (15.00-19.00)	18.00 (17.00-20.00)	0.150[b]	0.000[b]	0.005[a]
RA major axis, mm	36.10 ± 5.01	28.76 ± 3.47	27.97 ± 4.64[a]	0.000[a]	0.000[a]	0.311[a]
RA minor axis, mm	30.23 ± 4.15	23.64 ± 3.07	23.32 ± 4.19[a]	0.000[a]	0.000[a]	0.667[a]
RA volume, mm^2	11.00 (8.40-12.20)	6.20 (5.40-6.90)	7.20 (6.40-7.67)[b]	0.000[b]	0.000[a]	0.000[b]
TVDL, mm	19.48 ± 4.16	17.79 ± 2.33	18.82 ± 2.62[a]	0.016[a]	0.489[a]	0.054[a]
RVESd, mm	20.27 ± 3.14[a]	16.35 ± 2.03[a]	15.52 ± 1.60[a]	0.000[a]	0.000[b]	0.021[a]
RVEDd, mm	29.05 ± 4.88[a]	20.87 ± 3.20[a]	19.90 ± 3.03[a]	0.000[a]	0.000[a]	0.087[a]
LVEDd, mm	28.61 ± 4.03	30.34 ± 4.37	33.24 ± 5.07	0.020[a]	0.000[a]	0.000[b]
LVEDs, mm	17.20 ± 2.24	19.23 ± 2.05	20.89 ± 2.89	0.000[a]	0.000[a]	0.001[a]
FS, %	35.94 ± 3.94	37.20 ± 3.64	37.56 ± 4.60	0.034[a]	0.119[a]	0.695[a]
IVSs, mm	9.36 ± 1.89	8.23 ± 1.44	9.82 ± 1.44	0.000[a]	0.235[a]	0.000[b]

[a]Paired samples t-test; mean ± standard deviation; [b]Wilcoxon test; median (minimum-maximum). FS: fractional shortening; IVSs: interventricular septal thickness in systole; LA: left atrium; LVEDd: left ventricular end-diastolic diameter; LVEDs: left ventricular end-systolic diameter; MVDL: mitral valve diameter (lateral); RA: right atrium; RVEDd: right ventricular end-diastolic diameter; RVESd: right ventricular end-systolic diameter; TVDL: tricuspid valve diameter (lateral).

Table 3 – Echocardiographic parameters before and after transcatheter closure of atrial septal defect at 3 and 12 months

Parameter	Baseline	Postoperative (3 months)	Postoperative (12 months)	Baseline vs 3 months	Baseline vs 12 months	3 vs 12 months
LA major axis, mm	31.80 ± 4.67	32.40 ± 3.73	32.76 ± 4.54	0.555[a]	0.389[a]	0.726[a]
LA minor axis, mm	21.30 ± 3.14	21.50 ± 3.00	22.70 ± 4.26	0.743[a]	0.076[a]	0.067[a]
LA volume, cm^2	6.47 ± 1.42	6.57 ± 1.18	6.78 ± 1.58	0.721[a]	0.182[a]	0.459[a]
MVDL, mm	18.60 ± 2.67	20.96 ± 2.73	20.00 (18.75-24.00)	0.000[a]	0.000[b]	0.664[a]
RA major axis, mm	33.63 ± 3.92	29.50 ± 4.35	29.63 ± 4.43	0.000[a]	0.000[a]	0.875[a]
RA minor axis, mm	28.00 (26.00-30.25)	22.50 (19.75-26.25)	23.16 ± 3.42	0.000[b]	0.000[a]	0.695[a]
RA volume, mm^2	8.52 ± 1.61	6.49 ± 2.02	6.35 (5.97-6.87)	0.000[a]	0.000[b]	0.275[b]
TVDL, mm	20.40 ± 3.61	20.13 ± 4.04	19.26 ± 3.81	0.738[a]	0.226[a]	0.361[a]
RVESd, mm	20.00 (18.00-22.25)	17.00 (15.75-19.25)	16.73 ± 3.41	0.001[b]	0.000[a]	0.195[a]
RVEDd, mm	25.98 ± 4.24	21.37 ± 3.10	20.16 ± 4.47	0.000[a]	0.000[a]	0.112[a]
LVEDd, mm	29.10 ± 5.74	32.88 ± 4.39	34.55 ± 3.07	0.000[a]	0.000[a]	0.015[a]
LVEDs, mm	17.00 (15.75-19.00)	19.00 (18.00-21.00)	21.44 ± 3.00	0.004[b]	0.000[a]	0.000[a]
FS, %	35.94 ± 3.94	37.20 ± 3.64	38.20 ± 5.23	0.034[a]	0.964[a]	0.289[b]
IVSs, mm	9.36 ± 1.89	8.23 ± 1.44	10.43 ± 1.67	0.000[a]	0.800[a]	0.600[b]

[a]Paired samples t-test; mean ± standard deviation; [b]Wilcoxon test; median (minimum-maximum). FS: fractional shortening; IVSs: interventricular septal thickness in systole; LA: left atrium; LVEDd: left ventricular end-diastolic diameter; LVEDs: left ventricular end-systolic diameter; MVDL: mitral valve diameter (lateral); RA: right atrium; RVEDd: right ventricular end-diastolic diameter; RVESd: right ventricular end-systolic diameter; TVDL: tricuspid valve diameter (lateral).

Tabela 4 – Comparação entre GC e GP

Parameter	SG: baseline (3 months)	TG: baseline (3 months)	SG: baseline (12 months)	TG: baseline (12 months)	SG: 3-12 months	TG: 3-12 months	p-value (baseline vs 3 months)	p-value (baseline vs 12 months)	p-value (3 vs 12 months)
LA major axis, mm	–2.00 ± 4.67	0.60 ± 5.49	–2.23 ± 4.72	0.96 ± 6.04	–0.23 ± 5.31	0.36 ± 5.68	0.038[a]	0.016[a]	0.655[a]
RA major axis, mm	–7.33 ± 5.42	–4.13 ± 3.79	–8.15 ± 5.39	–4.00 ± 5.09	–0.82 ± 4.99	0.13 ± 4.61	0.008[a]	0.002[a]	0.419[a]
RA volume, mm^2	–4.10 ± 2.69	–2.03 ± 2.17	–3.33 ± 2.51	–1.41 ± 3.48	0.80 (0.12 to 1.50)	0.55 (–1.12 to 1.45)	0.001[a]	0.010[a]	0.247[b]
RVEDd, mm	–8.28 ± 4.31	–4.61 ± 3.67	–9.28 ± 5.31	–5.82 ± 4.48	–1.00 ± 3.56	–1.21 ± 4.06	0.000[a]	0.006[a]	0.816[a]
IVSd, mm	–1.00 (–1.00 to 1.00)	0.00 (–1.00 to 1.43)	0.00 (–1.00 to 1.00)	0.00 (–1.00 to 1.00)	0.00 (–0.82 to 1.00)	0.00 (–1.25 to 1.00)	0.062[b]	0.568[b]	0.167[b]
IVSs, mm	–1.00 (–2.00 to 0.00)	0.00 (–1.00 to 1.00)	0.45 ± 2.34	0.10 ± 2.13	2.00 (0.00 to 3.00)	0.00 (–1.00 to 2.00)	0.006[b]	0.521[a]	0.006[b]

[a]Teste t pareado; média ± desvio padrão; [b]teste de Wilcoxon; mediana (mínimo-máximo). AD: átrio direito; AE: átrio esquerdo; dDFVD: diâmetro diastólico final do ventrículo direito; GC: grupo cirúrgico; GP: grupo percutâneo; SIVd: espessura do septo interventricular na diástole; SIVs: espessura do septo interventricular na sístole.

in both groups. Notably, this remodeling occurred more rapidly in the surgical group, suggesting that hemodynamic unloading of the right ventricle may be more effective with surgical repair, particularly in patients with larger defects or sinus venosus ASDs.

Our findings partially differ from those of Pawelec-Wojtalik et al.,[16] who reported greater increases in LVEDd and greater reductions in RVEDd in the transcatheter group. In our cohort, RVEDd improvement was significantly greater in the surgical group at both 3 and 12 months. This discrepancy may be explained by differences in patient age, baseline defect size, and the inclusion of sinus venosus ASDs, which are treated exclusively with surgery.

These results suggest that surgical closure may provide superior early and mid-term right ventricular remodeling, particularly in patients with large or complex ASDs. For appropriately selected secundum defects, transcatheter closure remains safe and effective; however, our data indicate that surgical repair may result in faster recovery of right-sided geometry and function.

Study limitations

This study has some limitations. First, the sample size was relatively small and did not meet the target identified in the power analysis, which may limit generalizability. Second, the retrospective single-center design introduces the possibility of selection bias. Third, all echocardiographic evaluations were performed using a single imaging platform, and advanced modalities (e.g., cardiac magnetic resonance) were not available.

Conclusion

Surgical closure of ASDs resulted in earlier and more consistent improvement in right atrial and right ventricular geometry compared with transcatheter closure. These advantages were evident as early as 3 months and persisted at 12 months after the procedure. Both approaches were safe and associated with similarly low residual shunt rates. Our findings suggest that surgical repair may be preferable for patients with larger defects or complex anatomy, whereas transcatheter closure remains an effective alternative for appropriately selected secundum ASDs.

Author Contributions

Conception and design of the research and acquisition of data: Akın T, Yozgat Y, Türkoğlu H, Ugurlucan M; analysis and interpretation of the data, writing of the manuscript and critical revision of the manuscript for intellectual content: Akın T; statistical analysis: Dere ZBY.

Potential Conflict of Interest

No potential conflict of interest relevant to this article was reported.

Sources of Funding

There were no external funding sources for this study.

Study Association

This study is not associated with any thesis or dissertation work.

Ethics Approval and Consent to Participate

This study was approved by the Ethics Committee on Animal Experiments of the Istanbul Medipol University under the protocol number 790.

Use of Artificial Intelligence

The authors did not use any artificial intelligence tools in the development of this work.

Availability of Research Data

All datasets supporting the results of this study are available upon request from the corresponding author.

References

1. Li J, Al Zaghal AM, Anderson RH. The Nature of the Superior Sinus Venosus Defect. Clin Anat. 1998;11(5):349-52. doi: 10.1002/(SICI)1098-2353(1998)11:5<349::AID-CA11>3.0.CO;2-J.
2. Oliver JM, Gallego P, Gonzalez A, Dominguez FJ, Aroca A, Mesa JM. Sinus Venosus Syndrome: Atrial Septal Defect or Anomalous Venous Connection? A Multiplane Transoesophageal Approach. Heart. 2002;88(6):634-8. doi: 10.1136/heart.88.6.634.
3. Silvestry FE, Cohen MS, Armsby LB, Burkule NJ, Fleishman CE, Hijazi ZM, et al. Guidelines for the Echocardiographic Assessment of Atrial Septal Defect and Patent Foramen Ovale: From the American Society of Echocardiography and Society for Cardiac Angiography and Interventions. J Am Soc Echocardiogr. 2015;28(8):910-58. doi: 10.1016/j.echo.2015.05.015.
4. Liava'a M, Kalfa D. Surgical Closure of Atrial Septal Defects. J Thorac Dis. 2018;10(Suppl 24):S2931-9. doi: 10.21037/jtd.2018.07.116.
5. Rainer RS, Wanat FE, Nanda NC, Chang LK. Multiple Secundum Type Atrial Septal Defects: Identification by Transthoracic Color Doppler Echocardiography. Echocardiography. 1990;7(5):567-9. doi: 10.1111/j.1540-8175.1990.tb00402.x.
6. Cowley CG, Lloyd TR, Bove EL, Gaffney D, Dietrich M, Rocchini AP. Comparison of Results of Closure of Secundum Atrial Septal Defect by Surgery versus Amplatzer Septal Occluder. Am J Cardiol. 2001;88(5):589-91. doi: 10.1016/s0002-9149(01)01750-7.
7. Du ZD, Hijazi ZM, Kleinman CS, Silverman NH, Larntz K; Amplatzer Investigators. Comparison between Transcatheter and Surgical Closure of Secundum Atrial Septal Defect in Children and Adults: Results of a Multicenter Nonrandomized Trial. J Am Coll Cardiol. 2002;39(11):1836-44. doi: 10.1016/s0735-1097(02)01862-4.
8. Jung SY, Choi JY. Transcatheter Closure of Atrial Septal Defect: Principles and Available Devices. J Thorac Dis. 2018;10(Suppl 24):S2909-22. doi: 10.21037/jtd.2018.02.19.

9. Vasquez AF, Lasala JM. Atrial Septal Defect Closure. Cardiol Clin. 2013;31(3):385-400. doi: 10.1016/j.ccl.2013.05.003.

10. Chen Q, Cao H, Zhang GC, Chen LW, Xu F, Zhang JX. Short-Term and Midterm Follow-Up of Transthoracic Device Closure of Atrial Septal Defect in Infants. Ann Thorac Surg. 2017;104(4):1403-9. doi: 10.1016/j.athoracsur.2017.02.085.

11. Hausdorf G, Schneider M, Fink C, Neudorf U, Fischer G, Tynan M, et al. Transcatheter Closure of Atrial Septal Defects within the Oval Fossa: Medium-Term Results in Children Using the 'ASDOS'-Technique. Cardiol Young. 1998;8(4):462-71. doi: 10.1017/s1047951100007125.

12. Sezer S, Özyurt A, Narin N, Pamukcu Ö, Sunkak S, Argun M, et al. The Immediate Haemodynamic Response and Right and Left Cardiac Remodelling after Percutaneous Transcatheter Closure of Secundum Atrial Septal Defect in Children: a Longitudinal Cohort Study. Cardiol Young. 2021;31(9):1476-83. doi: 10.1017/S1047951121000500.

13. Supomo S, Widhinugroho A, Nugraha AA. Normalization of the Right Heart and the Preoperative Factors that İnfluence the Emergence PAH after Surgical Closure of Atrial Septal Defect. J Cardiothorac Surg. 2020;15(1):105. doi: 10.1186/s13019-020-01148-5.

14. Hanninen M, Kmet A, Taylor DA, Ross DB, Rebeyka I, Vonder Muhll IF. Atrial Septal Defect Closure in the Elderly is Associated with Excellent Quality of Life, Functional İmprovement, and Ventricular Remodelling. Can J Cardiol. 2011;27(6):698-704. doi: 10.1016/j.cjca.2011.04.003.

15. Meyer RA, Korfhagen JC, Covitz W, Kaplan S. Long-Term Follow-Up Study after Closure of Secundum Atrial Septal Defect in Children: An Echocardiographic Study. Am J Cardiol. 1982;50(1):143-8. doi: 10.1016/0002-9149(82)90020-0.

16. Pawelec-Wojtalik M, Wojtalik M, Mrowczynski W, Surmacz R, Quereshi SA. Comparison of Cardiac Function in Children after Surgical and Amplatzer Occluder Closure of Secundum Atrial Septal Defects. Eur J Cardiothorac Surg. 2006;29(1):89-92. doi: 10.1016/j.ejcts.2005.10.017.

Original Article

Diagnostic Performance Of Contrast-Enhanced Echocardiography In Differentiating Cardiac Masses: A Systematic Review And Meta-analysis

João Guilherme G. Pedrosa,[1] Felizardo José Leandro Pereira,[1] Antonio Lacerda Cavalcanti Neto,[1] Renata Ramos Stropp,[1] Giordano Persuhn Rolim de Moura,[1] Marcelo Tavares,[1] Sadrak Lyon Dantas Pontes,[1] Alex dos Santos Felix[2]

UFPB,[1] João Pessoa, PB – Brazil

National Institute of Cardiology,[2] Rio de Janeiro, RJ – Brazil

Abstract

Background: Conventional echocardiography often struggles to differentiate intracardiac masses, particularly in patients with poor acoustic windows. Contrast-enhanced Echocardiography (CEE) overcomes this limitation by visualizing perfusion patterns — distinguishing avascular thrombi from vascularized tumors. We aimed to synthesize existing evidence to evaluate the diagnostic accuracy of CEE.

Objectives: To evaluate the diagnostic accuracy of CEE for differentiating cardiac masses in adults, using histopathology as reference and reporting AUC, sensitivity, specificity, PPV, and NPV.

Methods: Systematic searches of PubMed, Web of Science, Cochrane Library, and EMBASE were performed on August 10, 2025. Studies meeting PICOTT criteria were included; extracted data included sensitivity, specificity, AUC, and 2×2 tables. Pooled estimates were obtained using standard bivariate and SROC models for diagnostic meta-analysis. Statistical significance set at $P < 0.05$.

Results: Five prospective cohort studies (total n = 381 patients) were included. For tumor vs non-tumor, pooled sensitivity = 100% and specificity = 100% (95% CI 99.5–100%; $I^2 = 0\%$; heterogeneity P = 0.985), diagnostic odds ratio (DOR) = 3,890.65, AUC = 0.989. For malignant vs benign tumors, pooled sensitivity = 94.3% (95% CI 88.5–97.3%; $I^2 = 0\%$; P = 0.681), specificity = 96.1% (95% CI 91.5–98.2%; $I^2 = 0\%$; P = 0.970), DOR = 341.71, SROC AUC = 0.976.

Conclusions: CEE showed very high diagnostic accuracy in the available prospective series. However, the small number of studies and limited sample sizes warrant cautious interpretation; larger prospective multicenter studies with standardized CEE protocols are needed to confirm these results.

Keywords: Echocardiography; Contrast Media; Cardiac Neoplasms; Systematic Review; Meta-Analysis.

Introduction

Intracardiac masses represent a diagnostic challenge due to their diverse etiologies, including thrombi, benign tumors (such as myxomas), and malignant lesions, all with significantly different prognoses and treatment strategies. Transthoracic echocardiography (TTE) remains the initial and most accessible imaging modality in clinical practice, offering real-time assessment of morphology and hemodynamic effects. However, its diagnostic yield is often limited in patients with poor acoustic windows or atypical mass locations, which may lead to underdetection or misclassification of masses.[1,2] Transesophageal Echocardiography (TEE) imaging can improve visualization but still falls short in reliable tissue characterization, especially when compared with cardiac MRI or CT, which provide richer tissue contrast and spatial resolution but are more resource-intensive.[1,3]

Contrast-enhanced Echocardiography (CEE) has emerged as a compelling adjunct to overcome these limitations. By enhancing perfusion imaging, CEE can differentiate avascular thrombi, mildly perfused benign tumors, and hypervascular malignant lesions based on distinct vascular patterns.[4,5] For instance, the use of ultrasound-enhancing agents can vividly illustrate a mass's perfusion characteristics (Figure 1). This technique can reveal details such as peripheral contrast uptake with a necrotic core in a cardiac paraganglioma (Figure 2) and enables quantitative analysis that differentiates perfused from non-perfused components (Figure 3).

Initial prospective data have shown that CEE correctly identifies cardiac mass types in 90%– 97% of cases, even with trainee observers, highlighting its potential for routine

Mailing Address: João Guilherme G. Pedrosa •
UFPB. Campus I Lot. Postal Code: 58051-900. Cidade Universitaria, PB – Brazil
E-mail: joao.guilherme3@academico.ufpb.br
Manuscript received October 9, 2025, revised manuscript December 16, 2025, accepted January 26, 2026
Editor responsible for the review: Marcelo Tavares

DOI: https://doi.org/10.36660/abcimg.20250082i

Central Illustration: Diagnostic Performance Of Contrast-Enhanced Echocardiography In Differentiating Cardiac Masses: A Systematic Review And Meta-analysis

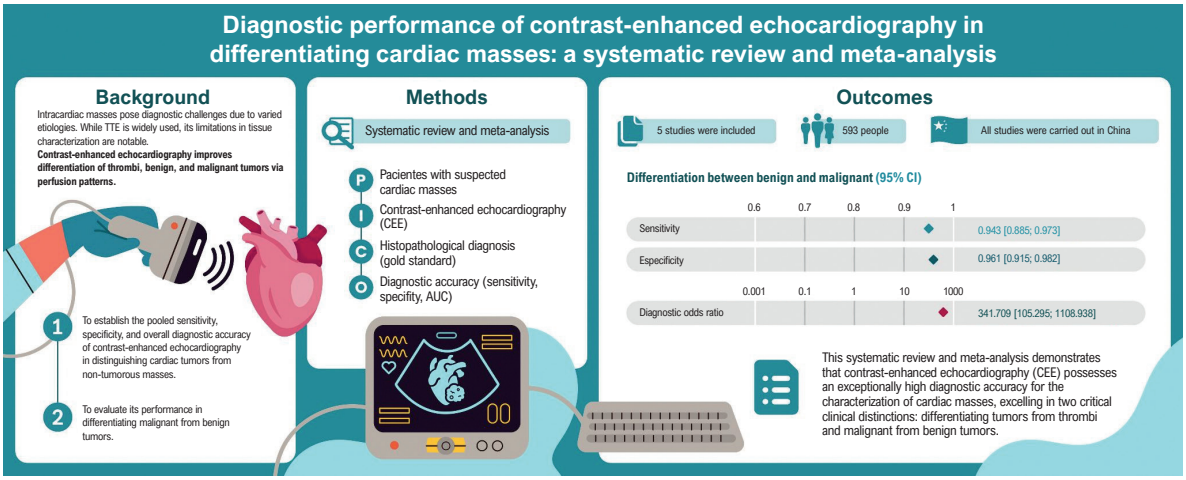

Arq Bras Cardiol: Imagem cardiovasc. 2026;39(1):e20250082

clinical use.[4] Nonetheless, the current evidence base is characterized by small-scale studies, retrospective designs, and case reports, raising concern about generalizability and robustness.[5]

The primary objective of this meta-analysis is to establish the pooled sensitivity, specificity, and overall diagnostic accuracy of CEE in distinguishing cardiac tumors from non-tumorous masses. The secondary objective is to evaluate its performance in differentiating malignant from benign tumors. Ultimately, this study seeks to provide evidence to guide clinical decision-making and highlight priorities for future, large-scale prospective research.

Methods

Protocol and Registration

This systematic review and meta-analysis were developed strictly adhering to the recommendations of the Preferred Reporting Items for Systematic Reviews and Meta-Analyses[6] (PRISMA 2020) statement, its extension for diagnostic test accuracy studies (PRISMA-DTA), and the Cochrane Handbook for Systematic Reviews of Diagnostic Test Accuracy.[7] The study protocol was submitted to the International Prospective Register of Systematic Reviews[8] (PROSPERO) under the registration number CRD420251142676.

Study Design

Diagnostic accuracy studies with a prospective or retrospective design were included. No time restrictions were applied, including articles from the earliest available date in the databases. Reviews, editorials, case reports, and case series with fewer than ten participants were excluded.

Eligibility Criteria

Studies were selected based on eligibility criteria defined by the PICOS framework. The eligible population (P) consisted of adult patients with suspected cardiac masses who underwent CEE. The results of the CEE were compared with the reference standard for a definitive diagnosis (Comparator), which was primarily based on histopathological analysis. However, diagnoses confirmed by other robust imaging modalities (e.g., Cardiac Magnetic Resonance) or by unequivocal therapeutic response (e.g., resolution of a thrombus after anticoagulation therapy) were also considered. The primary outcomes (O) of interest were diagnostic accuracy measures, including Area Under the Curve (AUC), sensitivity, specificity, Positive Predictive Value (PPV), and Negative Predictive Value (NPV).

Target Conditions

The target conditions for this review were the different subtypes of intracardiac masses. The primary condition to be identified was a cardiac tumor (benign or malignant), rather than an intracardiac thrombus.

Additionally, within the spectrum of tumors, a second target was to differentiate benign tumors (e.g., myxoma, fibroma) from malignant tumors (primary, such as sarcomas, or metastatic). The accuracy analyses were organized into subgroups to assess the test's performance for each of these key clinical distinctions.

Index Test

The index test was defined as CEE, performed to characterize a previously identified or suspected cardiac mass. CEE was considered any echocardiogram that involved the intravenous administration of a microbubble

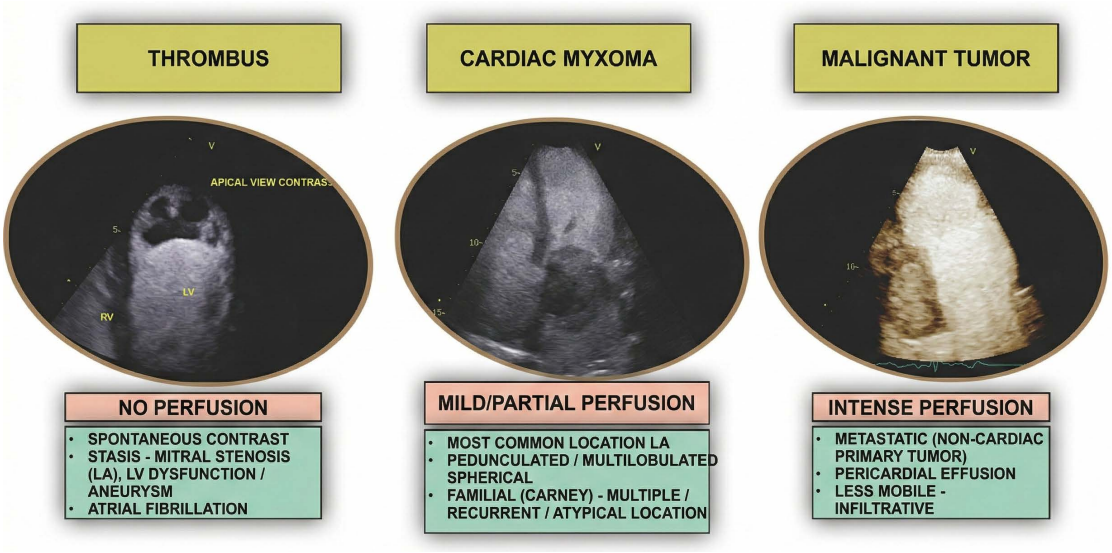

Figure 1 – *Examples of the use of an ultrasound-enhancing agent for the evaluation of mass perfusion.*

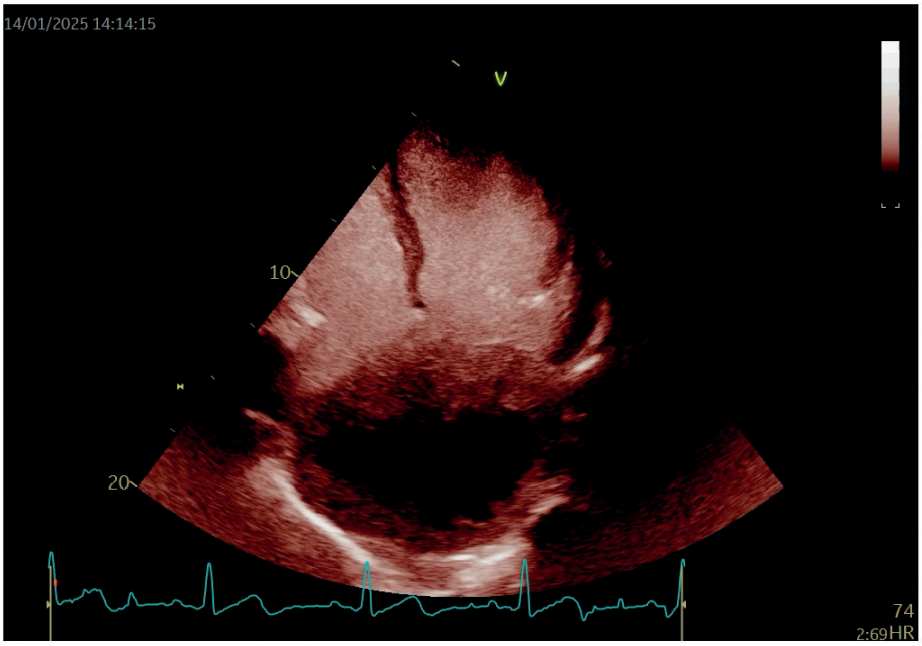

Figure 2 – *Peripheral contrast uptake in a large mass inside the left atrium, without central uptake (necrosis) in a cardiac paraganglioma.*

contrast agent to assess the vascularity and perfusion of the mass. The index test result was not simply dichotomous (positive/negative), but rather a classification of the mass based on its perfusion patterns, with findings compared with the reference standard obtained at approximately the same time.

Information Sources and Search Strategy

A systematic and comprehensive search was conducted in the following electronic databases: PubMed, Embase, Cochrane Library, and Web of Science. The search was completed on August 10, 2025.

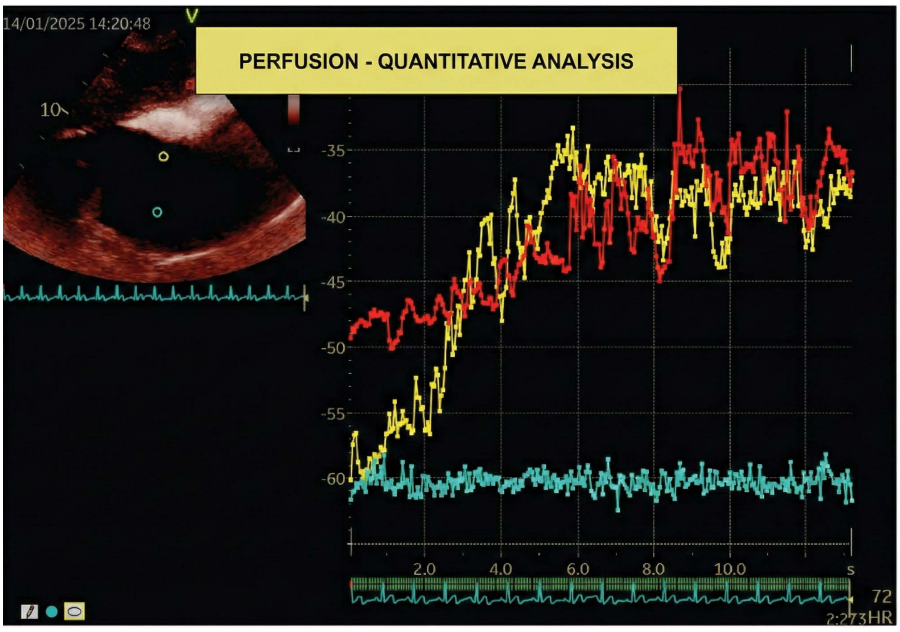

Figure 3 – *Subcostal view. Cardiac paraganglioma. Quantitative analysis of the mass perfusion with an ultrasound-enhancing agent (contrast) - in yellow, the peripheral perfusion of the mass; in red, perfusion of the liver tissue for comparison; in blue, the absence of perfusion in the (necrotic) center of the mass.*

The initial search identified 473 articles (123 in PubMed, 234 in Embase, 8 in the Cochrane Library, and 108 in Web of Science) before removing duplicates. Additionally, the reference lists of included studies were manually searched to identify potentially eligible articles not captured in the initial search.

Study Selection and Data Extraction

The selection process was managed using the Rayyan software.[9] Two independent reviewers (JP and AN) screened titles and abstracts, followed by a full-text assessment. Disagreements were resolved by consensus or through adjudication by a third reviewer. Data were extracted using a standardized form, which included study characteristics, population details, intervention specifics, and raw data for the 2x2 contingency table.

Risk of Bias Assessment

The methodological quality and risk of bias of each included study were independently assessed by two reviewers using the QUADAS-2 tool.[10]

Data Synthesis and Analysis

The accuracy data were synthesized through a meta-analysis using a bivariate random-effects model. From this model, summary estimates with 95% confidence intervals (CIs) for sensitivity and specificity were generated; the Summary Receiver Operating Characteristic (SROC) curve was constructed, and the diagnostic odds ratio was calculated. Heterogeneity was evaluated using I^2 statistics, with $P < 0.05$ from Cochran's Q test or $I^2 > 50\%$ considered indicative of substantial heterogeneity. Statistical significance set at $P < 0.05$. Forest plots were used to illustrate individual and pooled effect sizes. Meta-analyses were performed in RStudio (RStudio 2025.09.0+387) for Windows using the "meta" and "mada" packages for data synthesis and visualization.

Results

Results of the Search

The initial search yielded 473 results. After removing duplicate records and ineligible studies, 13 remained and were fully reviewed against the inclusion criteria. Of these, 5 studies were included. The process is detailed in the PRISMA flow diagram (Figure 4).

The number of participants ranged from 32 to 236; all were adults. The studies varied in design, including prospective observational, cross-sectional, and retrospective approaches, and were conducted across both single and multicenter settings.

All studies employed Contrast-enhanced Echocardiography (CEE) using SonoVue (Bracco, Switzerland) as the contrast agent. The echocardiographic systems used included Philips iE33, in three studies[11-13], and GE Vivid 7 Dimension, in one study[14], with transducers and imaging protocols tailored to each study's objectives. One study[15] did not report the system used in echocardiography.

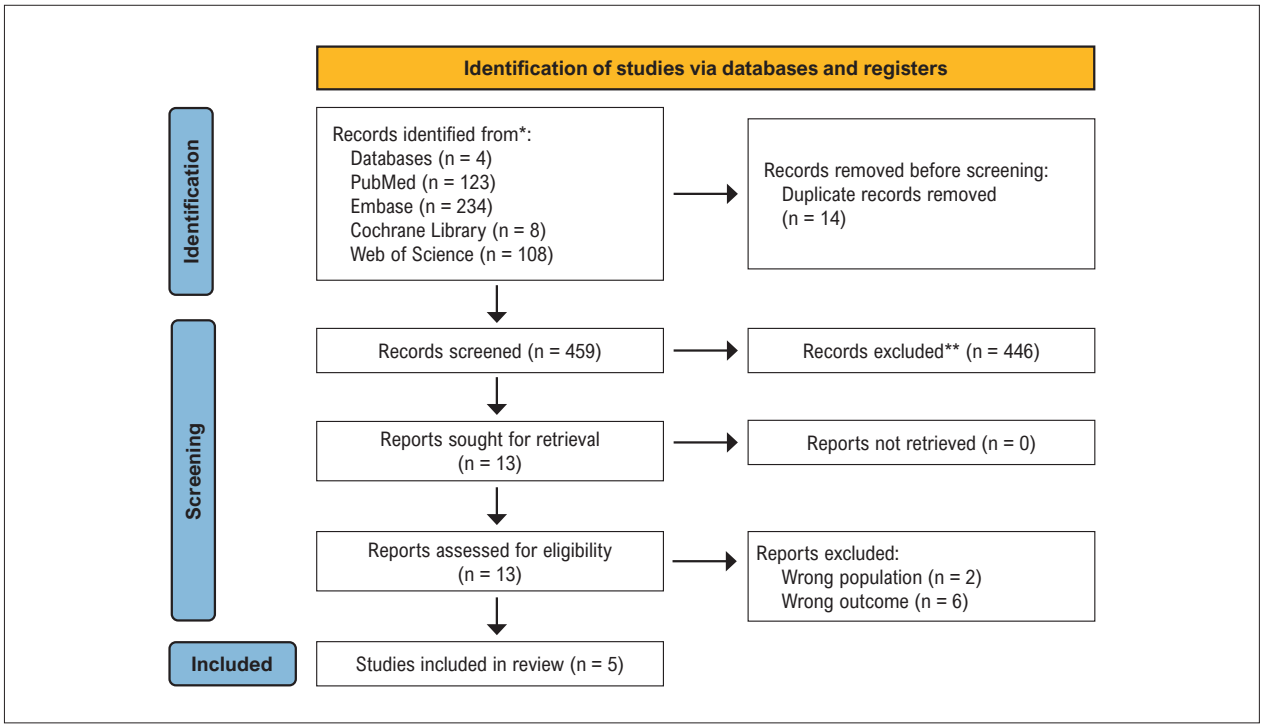

Figure 4 – *PRISMA flow diagram of study screening and selection.*

Quantitative parameters assessed across studies included mass area, peak intensity ratios (e.g., A1/A2, A1/A3), contrast enhancement intensity (A), replenishment rate (β or k), and perfusion ratios between cardiac masses and adjacent myocardium. Qualitative assessments encompassed echogenicity, contour, base morphology, mobility, perfusion characteristics, and presence of pericardial or pleural effusion.

The proportion of male participants ranged from 36.5% to 63.0%, and most studies focused on adult patients presenting with suspected cardiac masses after Transthoracic Echocardiography (TTE). One study[13] included patients undergoing surgical treatment for cardiac masses, while another study[15] targeted patients referred for myocardial contrast echocardiography.

Exclusion criteria were consistent across studies and were severe cardiac or systemic conditions (e.g., NYHA class IV heart failure, arrhythmias, hepatic or renal dysfunction), allergies to contrast agents or blood products, and neuropsychiatric disorders. Some studies also excluded patients lost to follow-up or managed conservatively. Other important characteristics of the studies included in this review are presented in Table 1.

We found no publication bias by visually analyzing the funnel plot (Figure S1), a linear regression for the asymmetry of the funnel plot was made by the Deek's test, which was not statistically significant (Bias = -3.940, SE = 5.283, t = -0.75, p = 0.509), however because of the low number of included studies, the results should be regarded with care and are by themselves not enough to discard publication bias.

Methodological Quality of Included Studies

The methodological quality of the included studies was evaluated using the QUADAS-2 tool, which assesses four domains: patient selection, index test, reference standard, and flow & timing. Each domain was judged to be low risk, with some concerns, or high risk of bias. At the individual study level, two studies[11,12] were rated as having an overall low risk of bias, while two[14,15] raised some concerns, particularly regarding patient selection and flow & timing. One study[13] was considered at high risk of bias due to inappropriate patient selection and concerns regarding the reference standard (Figure S2). In the domain-level analysis, patient selection and flow & timing were the areas with the highest frequency of concerns. At the same time, the index test and reference standard were generally well-conducted. Overall, the methodological quality of the included studies was considered acceptable, with most studies at low risk of bias, although relevant limitations were identified in specific domains (Figure S3).

Findings

To Differentiate Tumor from Thrombi

Every study reported high accuracy in differentiating tumors from thrombi using CEE, resulting in strong diagnostic performance parameters. The estimates for summary sensitivity (Figure 5), specificity (Figure 6), and Diagnostic Odds Ratio (Figure 7) confirm these findings. Due to the 100% accuracy, an SROC curve could not be plotted, but the AUC was 0.989.

Table 1 – Characteristics of the included studies.

Study	Control diagnosis	N	Age	Female	Pseudomass	Thrombi	Malignant tumor	Benign tumor
Wang, 2024	Confirmed by CMR, TEE, CT, surgery, or biopsy, depending on mass type	145	59.4 years (IQR: 51.2–63.9)	55 (38.0%)	4	43	30	66
Li, 2022	Confirmed by CMR, TEE, CT, surgery, or biopsy, depending on mass type	108	61.5 years (IQR: 52.0–67.5)	40 (37.0%)	3	36	36	30
Xia, 2017	Surgical pathology or biopsy (WHO 2015 classification)	236	49.5 years (range: 0.5 to 83)	150 (63.55%)	11	3	29	196
Zhou, 2020	NR	32	NR	NR	0	19	8	5
Tang, 2015	Surgical pathology or resolution after anticoagulation	72	50 ± 15 years (range: 12–85)	30 (40%)	0	16	30	26

Every study adopted a 5% statistical significance level.

To Differentiate Malignant Tumor from Benign

CEE had great results, with high estimates of summary sensitivity (Figure 8) and specificity (Figure 9). The summary Diagnostic Odds Ratio (Figure 10) further supports these findings. Additionally, the SROC curve was plotted (Figure 11).

Discussion

This systematic review and meta-analysis demonstrate that CEE has exceptionally high diagnostic accuracy for characterizing cardiac masses, excelling in two critical clinical distinctions: differentiating tumors from thrombi and malignant from benign tumors.

The first key finding of our analysis was the **great** pooled sensitivity and specificity (100%) of CEE for distinguishing cardiac tumors from thrombi. This result, while remarkable, is biologically plausible. Thrombi are inherently avascular structures, and the intravascular microbubbles used in CEE provide a stark contrast between the complete absence of perfusion within a thrombus and the variable but present vascularization of tumorous tissue, whether benign or malignant. This creates a binary, highly reliable diagnostic feature that is readily identifiable, even to less experienced operators, as suggested by some of the included studies. The near-perfect AUC of 0.989 resulted from model adjustments to prevent infinite values. Even so, these findings warrant cautious interpretation; the limited number of included studies (5) restricts statistical power and may mask potential small-study effects or reporting bias, despite the lack of observed heterogeneity.

The second finding concerns the distinction between benign and malignant tumors. Our pooled analysis yielded a sensitivity of 94.3% (95% CI 88.5% to 97.3%) and a specificity of 96.1% (95% CI 91.5% to 98.2%), with a summary AUC of 0.976. This indicates that CEE is not only excellent at identifying vascularization but also at interpreting its pattern — typically characterized by intense hypervascularity in malignant lesions compared with more moderate, slower perfusion in benign lesions. The high diagnostic odds ratio (DOR = 341.71) signifies a powerful test that can significantly increase or decrease the post-test probability of malignancy, directly informing critical management decisions regarding the urgency of intervention, biopsy planning, or surgical strategy.

Due to concerns of bias and heterogeneity with one study[13] we conducted a *post-hoc* sensitivity analysis by redoing the meta-analysis and leaving the study out; however, it did not significantly alter the results (specificity of 0.952, sensitivity of 0.962, DOR of 374.767), which demonstrates the reliability of the results despite the concerns of bias.

It is the first meta-analysis, to our knowledge, to specifically synthesize the diagnostic performance of CEE for cardiac masses using a rigorous PRISMA-DTA methodology. Secondly, we employed robust statistical models (bivariate and SROC) specifically designed for diagnostic meta-analyses, which account for the potential correlation between sensitivity and specificity and provide more reliable pooled estimates. Thirdly, the included studies were all prospective cohorts, which strengthens the validity of the findings by minimizing selection and recall bias. Finally, the post hoc sensitivity analysis confirmed that the overall results were not unduly influenced by the study judged to be at high risk of bias, thereby enhancing the reliability of our conclusions.

Despite these robust findings, our results must be interpreted in light of several important limitations. The most significant limitation is the small number of included studies (n = 5) and the relatively modest total sample size

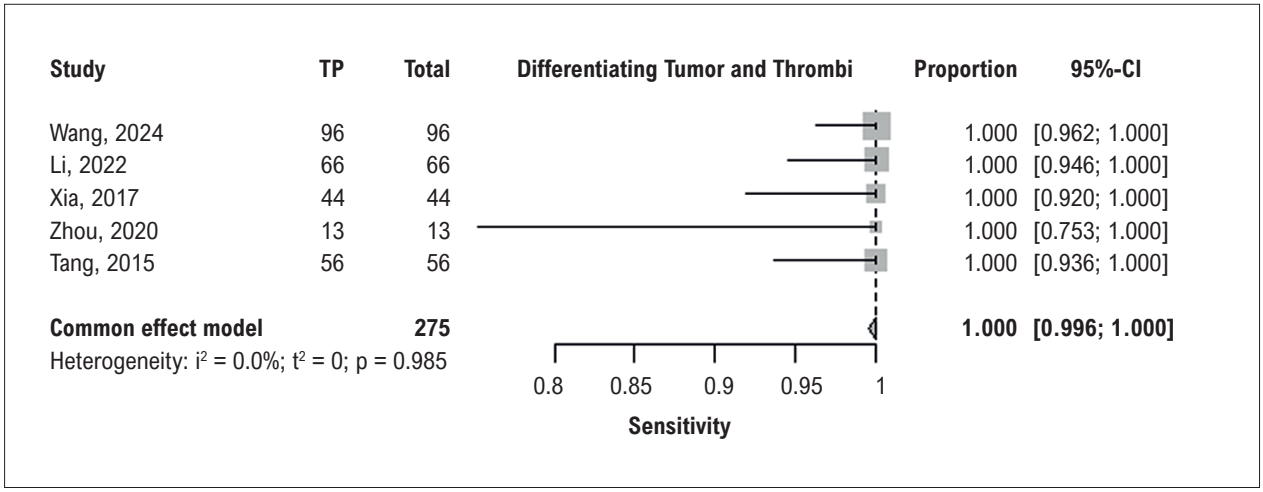

Figure 5 – *Forest plot of sensitivity.*

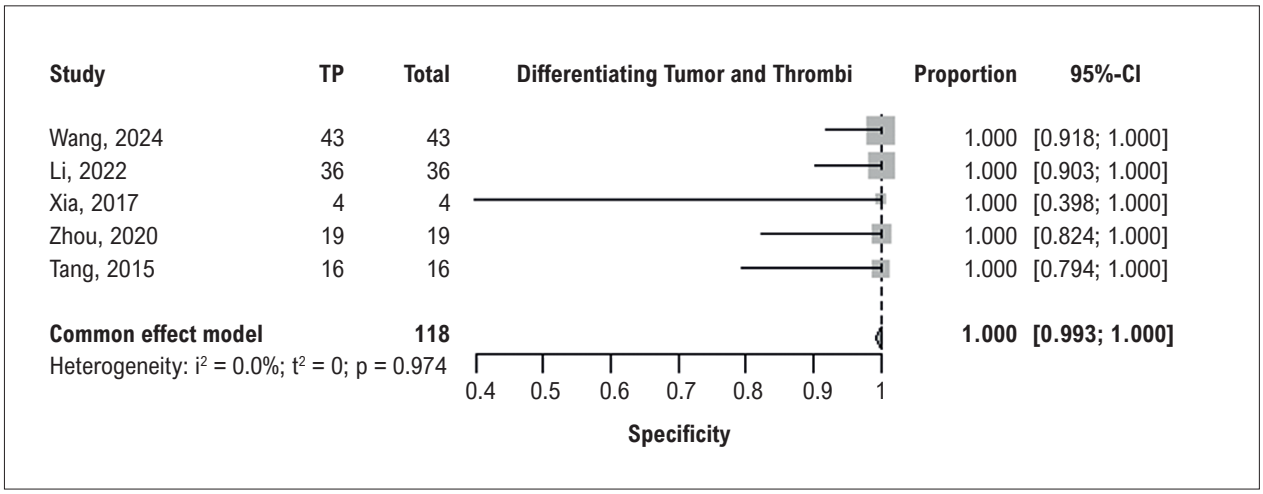

Figure 6 – *Forest plot of specificity.*

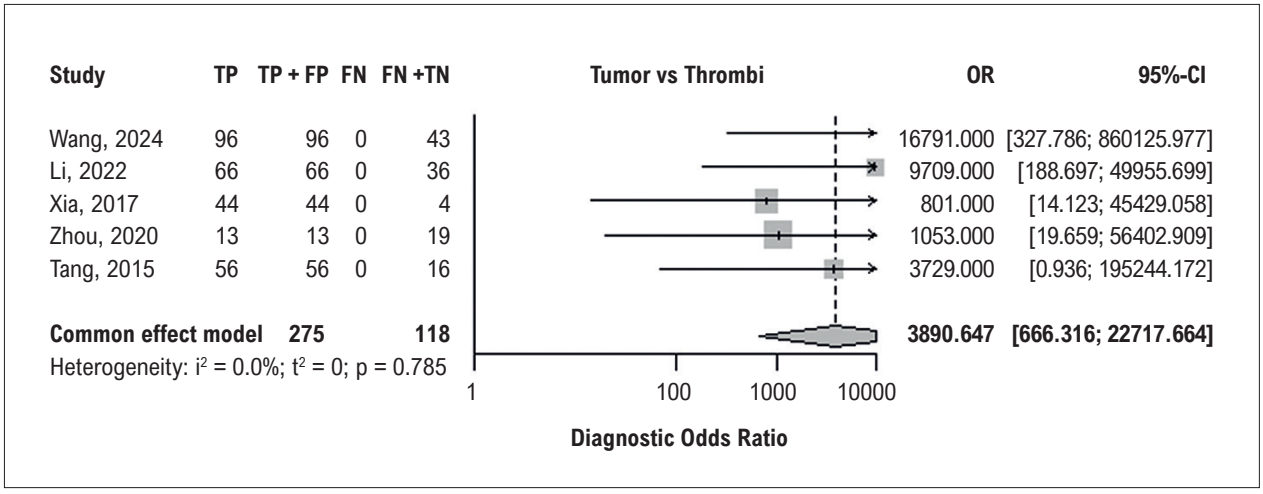

Figure 7 – *Forest plot of DOR.*

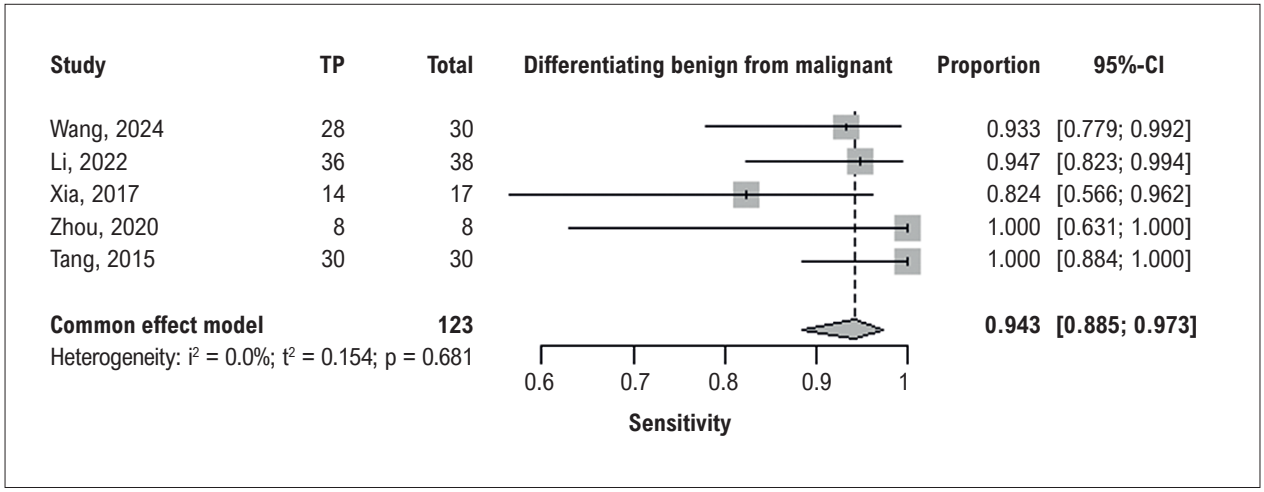

Figure 8 – *Forest plot of sensitivity.*

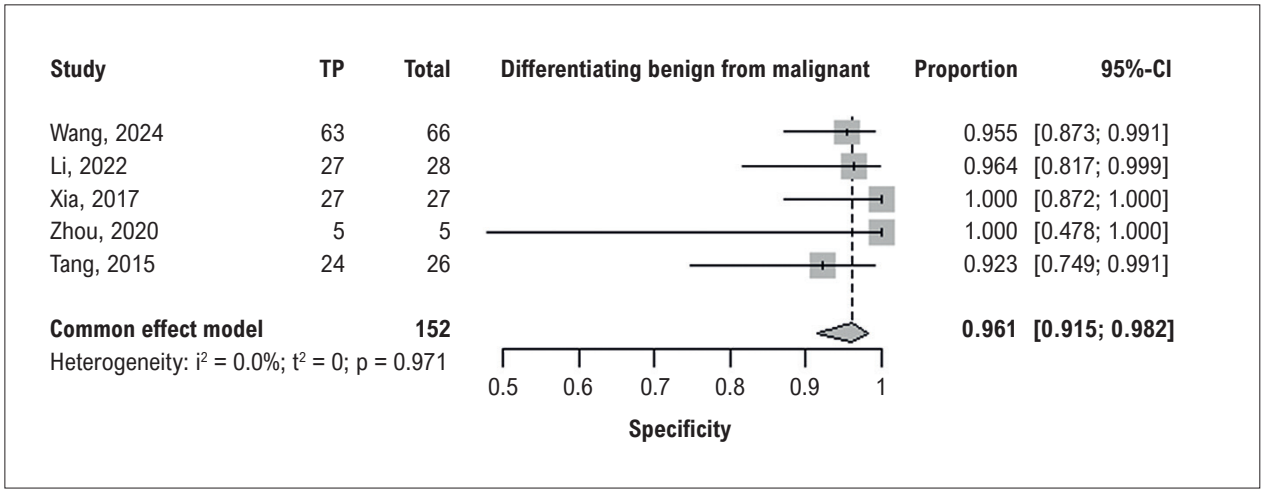

Figure 9 – *Forest plot of specificity.*

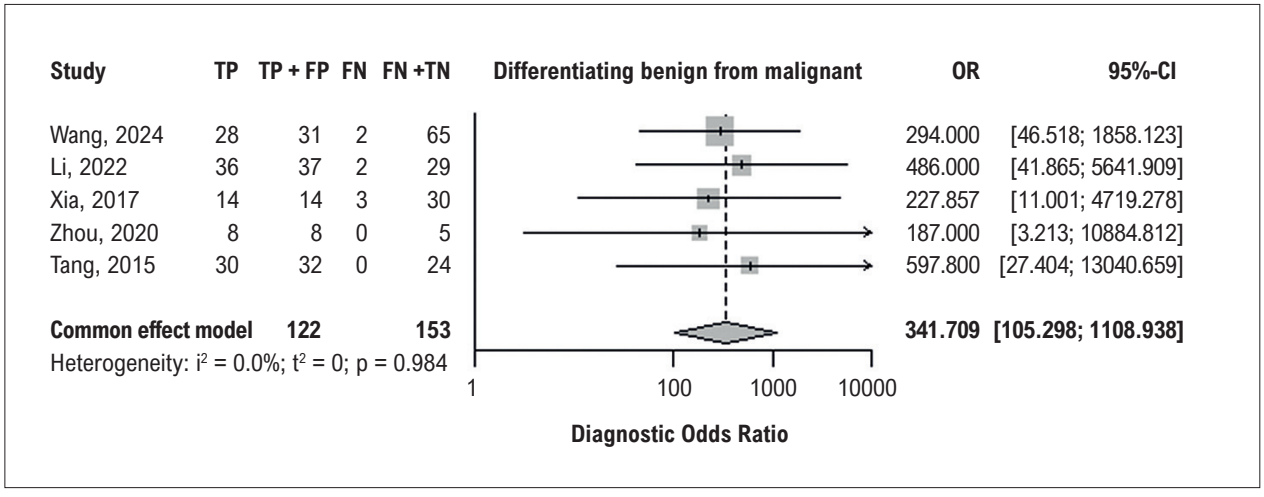

Figure 10 – *Forest plot of DOR.*

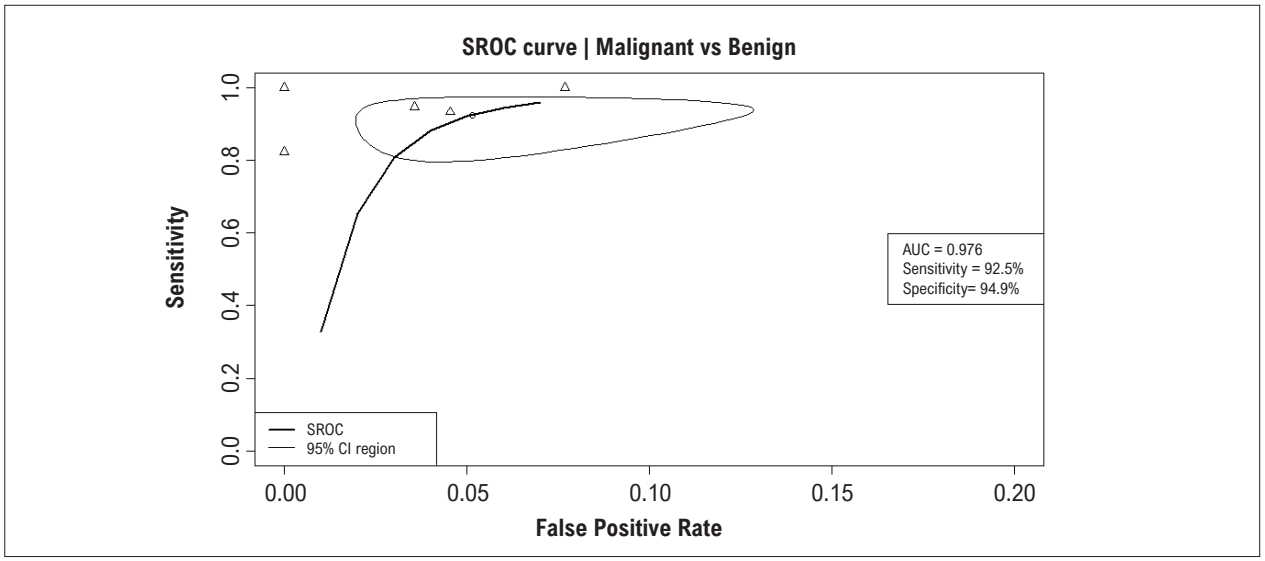

Figure 11 – *SROC curve.*

(n = 381). This was due to most studies failing to report the necessary numbers to calculate the performance metrics. We also may have missed potential studies, as diagnostic accuracy studies are poorly tagged in electronic databases. Regarding publication bias, given the small number of studies, the linear regression Deek's test did not yield the best results, but a visual analysis of the funnel plot showed no publication bias. While the statistical heterogeneity was negligible (I^2 = 0%), the limited number of primary studies constrains the generalizability of our findings and the power to perform more extensive subgroup analyses (e.g., by tumor type, contrast agent generation, or by quantitative or qualitative analyses).

Furthermore, as highlighted by the QUADAS-2 assessment, certain methodological concerns were present in some studies, particularly regarding patient selection and the flow and timing between the index test and the reference standard. The **great** accuracy for thrombus differentiation, while compelling, should be viewed with cautious optimism until confirmed in larger, multi-center settings, as real-world performance can be influenced by image quality, interpreter expertise, and specific contrast protocols.

The clinical implication of our work is substantial. CEE emerges as a highly accurate, accessible, and cost-effective tool that can be integrated into the diagnostic pathway immediately after the initial detection of a mass on conventional echocardiography. It can confidently rule out thrombus, potentially avoiding the need for more expensive and less accessible cross-sectional imaging in many cases. For tumors, it provides a reliable non-invasive indicator of malignancy, helping to triage patients towards urgent intervention or more deliberate planning.

Conclusion

This meta-analysis provides compelling evidence that CEE is a powerful diagnostic tool with excellent accuracy for characterizing cardiac masses. It effectively differentiates tumors from thrombi and is highly proficient at distinguishing malignant from benign tumors. While limitations inherent in the available literature require cautious interpretation, CEE's accessibility, safety, and demonstrated performance support its broader adoption in the standard diagnostic workflow for evaluating intracardiac masses.

Author Contributions

Conception and design of the research: Pedrosa JGG, Tavares M; acquisition of data: Pedrosa JGG, Cavalcanti Neto AL, Stropp RR; analysis and interpretation of the data: Pedrosa JGG, Cavalcanti Neto AL, Stropp RR, Moura GPR, Pontes SLD; statistical analysis: Pedrosa JGG; writing of the manuscript: Pedrosa JGG, Pereira FJL, Stropp RR, Moura GPR, Pontes SLD, Tavares M, Felix AS; critical revision of the manuscript for intellectual content: Pedrosa JGG, Pereira FJL, Moura GPR, Pontes SLD, Tavares M, Felix AS; central illustration: Pontes SLD.

Potential Conflict of Interest

No potential conflict of interest relevant to this article was reported.

Sources of Funding

There were no external funding sources for this study.

Study Association

This study is not associated with any thesis or dissertation work.

Ethics Approval and Consent to Participate

This article does not contain any studies with human participants or animals performed by any of the authors.

Availability of Research Data

The underlying content of the research text is contained within the manuscript.

References

1. L'Angiocola PD, Donati R. Cardiac Masses in Echocardiography: A Pragmatic Review. J Cardiovasc Echogr. 2020;30(1):5-14. doi: 10.4103/jcecho.jcecho_2_20.
2. Kirkpatrick JN, Wong T, Bednarz JE, Spencer KT, Sugeng L, Ward RP, et al. Differential Diagnosis of Cardiac Masses Using Contrast Echocardiographic Perfusion Imaging. J Am Coll Cardiol. 2004;43(8):1412-9. doi: 10.1016/j.jacc.2003.09.065.
3. Uenishi EK, Caldas MA, Tsutsui JM, Abduch MC, Sbano JC, Kalil R Filho, et al. Evaluation of Cardiac Masses by Real-Time Perfusion Imaging Echocardiography. Cardiovasc Ultrasound. 2015;13:23. doi: 10.1186/s12947-015-0018-3.
4. Angeli F, Bodega F, Bergamaschi L, Armillotta M, Amicone S, Canton L, et al. Multimodality Imaging in the Diagnostic Work-Up of Patients with Cardiac Masses: JACC: CardioOncology State-of-the-Art Review. JACC CardioOncol. 2024;6(6):847-62. doi: 10.1016/j.jaccao.2024.09.006.
5. Yang Z, Niu Y, Ma H, Gong W, Yu L, Liu L, et al. Contrast-Enhanced Echocardiographic Diagnosis of Benign and Malignant Cardiac Tumors and its Correlation with Pathology. Front Cardiovasc Med. 2023;10:1182334. doi: 10.3389/fcvm.2023.1182334.
6. Page MJ, McKenzie JE, Bossuyt PM, Boutron I, Hoffmann TC, Mulrow CD, et al. The PRISMA 2020 Statement: An Updated Guideline for Reporting Systematic Reviews. BMJ. 2021;372:n71. doi: 10.1136/bmj.n71.
7. Deeks JJ, Bossuyt PM, Leeflang MMG, Takwoingi Y, editors. Cochrane Handbook for Systematic Reviews of Diagnostic Test Accuracy. Version 2.0 [Internet]. London: The Cochrane Collaboration; 2023 [cited 2025 Feb 08]. Available from: https://training.cochrane.org/handbook-dta.
8. National Institute for Health and Care Research. PROSPERO: International Prospective Register of Systematic Reviews [Internet]. York: University of York; 2025 [cited 2026 Feb 08]. Available from: https://www.crd.york.ac.uk/prospero/.
9. Ouzzani M, Hammady H, Fedorowicz Z, Elmagarmid A. Rayyan-a Web and Mobile App for Systematic Reviews. Syst Rev. 2016;5(1):210. doi: 10.1186/s13643-016-0384-4.
10. Whiting PF, Rutjes AW, Westwood ME, Mallett S, Deeks JJ, Reitsma JB, et al. QUADAS-2: A Revised Tool for the Quality Assessment of Diagnostic Accuracy Studies. Ann Intern Med. 2011;155(8):529-36. doi: 10.7326/0003-4819-155-8-201110180-00009.
11. Wang Q, Wang B, Zhang X, Zhong X, Chang S, Yang J, et al. The Usefulness of Contrast Echocardiography in the Evaluation of Cardiac Masses: A Multicenter Study. BMC Cardiovasc Disord. 2024;24(1):43. doi: 10.1186/s12872-024-03708-2.
12. Li Y, Ren W, Wang X, Xiao Y, Feng Y, Shi P, et al. The Diagnostic Accuracy of Contrast Echocardiography in Patients with Suspected Cardiac Masses: A Preliminary Multicenter, Cross-Sectional Study. Front Cardiovasc Med. 2022;9:1011560. doi: 10.3389/fcvm.2022.1011560.
13. Xia H, Gan L, Jiang Y, Tang Q, Zhang P, Tang X, et al. Use of Transesophageal Echocardiography and Contrast Echocardiography in the Evaluation of Cardiac Masses. Int J Cardiol. 2017;236:466-72. doi: 10.1016/j.ijcard.2017.01.073.
14. Tang QY, Guo LD, Wang WX, Zhou W, Liu YN, Liu HY, et al. Usefulness of Contrast Perfusion Echocardiography for Differential Diagnosis of Cardiac Masses. Ultrasound Med Biol. 2015;41(9):2382-90. doi: 10.1016/j.ultrasmedbio.2015.05.010.
15. Zhou Q, Xiong Y, Zhou Y. Feasibility of Myocardial Contrast Echocardiography Quantitative Analysis in Differentiating Cardiac Masses. JACC. 2020;75(11):1688.

*Supplemental Materials

For additional information, please click here.

Echocardiography with Ultrasound Enhancement Agents and the Diagnostic Challenge of Cardiac Masses: Solid Evidence for a Complex Clinical Problem

Rafael Bonafim Piveta,[1,2] *Miguel Osman Dias Aguiar*[1,2]
BP (Beneficência Portuguesa),[1] *São Paulo, SP – Brazil*
Einstein Hospital Israelita,[2] *São Paulo, SP – Brazil*

Short editorial referring to the article: Diagnostic Performance Of Contrast-Enhanced Echocardiography In Differentiating Cardiac Masses: A Systematic Review And Meta-analysis

The proper characterization of intracardiac masses continues to be one of the most relevant challenges in contemporary cardiovascular imaging. Thrombi, benign tumors, and malignant neoplasms share some similar morphological characteristics in conventional echocardiography, but they entail radically different approaches, prognoses, and therapeutic urgencies. Despite significant advances in cardiovascular imaging diagnostic techniques, critical decisions, such as whether to anticoagulate or operate, investigate or observe, treat urgently or monitor, are still frequently challenging in clinical practice. Echocardiography, although indispensable as an initial method, often fails to differentiate thrombi, benign tumors, and malignant neoplasms in a significant number of patients.[1] Given this scenario, it is legitimate to question: why does echocardiography with ultrasound enhancing agents (UEAs), available for decades, still play a secondary role in many diagnostic algorithms?

The meta-analysis, "Diagnostic performance of contrast-enhanced echocardiography in differentiating cardiac masses", presents important arguments for this context. Using methodological rigor, aligned with PRISMA-DTA and Cochrane Handbook recommendations,[2,3] the authors demonstrate that echocardiography with UEAs has shown exceptional diagnostic performance in two of the most critical dilemmas in clinical practice: differentiating tumors from thrombi and distinguishing benign from malignant tumors.

The results presented are impressive. Echocardiography with UEAs has demonstrated combined sensitivity and specificity of 100% in differentiating between tumors and thrombi, with an AUC close to 1.0. This finding is pathophysiologically consistent, since thrombi are avascular structures, while tumors — whether benign or malignant — have some degree of perfusion detectable by intravascular microbubbles.[4,5] This functional distinction gives echocardiography with UEAs a clear diagnostic advantage over conventional echocardiography, especially in clinical situations in which the decision between anticoagulation and invasive investigation needs to be made quickly and safely.

Even more relevant is the performance of echocardiography with UEAs in differentiating between benign and malignant tumors. The meta-analysis demonstrated a sensitivity of 94.3% and a specificity of 96.1%, with an AUC of 0.976, indicating high discriminatory capacity. These results reinforce previous observations that perfusion patterns, such as intense hyperperfusion, rapid filling, and perfusion heterogeneity, are heavily associated with malignancy.[6,7] Thus, echocardiography with UEAs transcends the merely morphological role and consolidates itself as a functional tool for tissue characterization, a role traditionally reserved for cardiac magnetic resonance imaging.

Given these data, another important question arises: Why do we continue to systematically refer patients to more expensive, less accessible, and often unavailable methods in a timely manner, before fully exploring the potential of echocardiography with UEAs? The answer seems to lie less in scientific evidence and more in cultural, logistical, and training barriers. Echocardiography with UEAs is still underused, often restricted to centers of excellence, despite its excellent safety profile, wide availability, and the possibility of being performed even at bedside in unstable patients or those with contraindications to more complex methods.[5,7]

However, some limitations deserve to be highlighted. The small number of studies included (five prospective cohorts, totaling 381 patients) reflects the scarcity of primary data suitable for diagnostic meta-analyses in this area. In addition, the QUADAS-2 assessment identified methodological concerns in some studies, particularly related to patient selection and the time flow between the index test and the reference standard. These factors limit the unrestricted generalization of the results and reinforce the need for more robust studies, with standardized protocols and greater population diversity.

Despite the significant increase in diagnostic accuracy provided by contrast-enhanced echocardiography in this scenario, the technique presents some pitfalls that require attention when used for this specific purpose. Recent thrombi, although avascular, may show some degree of enhancement with contrast, usually restricted to the periphery of the mass. In the study by Li et al., among the 36 patients diagnosed with thrombi, three showed marked enhancement, all corresponding to recent thrombi.[8] This pattern can make differentiation from cardiac tumors difficult; however, it is important to emphasize that tumors, especially malignant ones, tend to show diffusely

Keywords

Echocardiography; contrast; cardiac masses

Mailling Address: Rafael Bonafim Piveta •
Einstein Hospital Israelita. Rua Albert Einstein, 701. Postal code: 05652-900. Morumbi, São Paulo, SP – Brazil
E-mail: rafael.piveta@einstein.br

DOI: https://doi.org/10.36660/abcimg.20260009i

SUMÁRIO

increased perfusion, involving both the central and peripheral regions of the mass, which helps in diagnostic distinction.

Nevertheless, the findings of this meta-analysis represent an important step in consolidating echocardiography with UEAs as a core method in the evaluation of cardiac masses. The consistency of the findings, the biological plausibility, and the magnitude of the observed effects indicate a solid scientific basis for expanding the use of contrast-enhanced echocardiography in the diagnostic workflow of routine practice. In a scenario where quick and accurate decisions directly impact clinical outcomes, underusing an accessible, safe, and highly accurate method is unreasonable.

In conclusion, the evidence presented in this study reinforces that echocardiography with UEAs not only represents a complementary technique, but also a strategic, accessible tool with high clinical impact. In a scenario where quick and accurate decisions are fundamental, establishing echocardiography with UEAs in the diagnostic algorithms for intracardiac masses, seems not only reasonable, but also necessary.

References

1. L'Angiocola PD, Donati R. Cardiac Masses in Echocardiography: A Pragmatic Review. J Cardiovasc Echogr. 2020;30(1):5-14. doi: 10.4103/jcecho.jcecho_2_20.
2. Page MJ, McKenzie JE, Bossuyt PM, Boutron I, Hoffmann TC, Mulrow CD, et al. The PRISMA 2020 Statement: An Updated Guideline for Reporting Systematic Reviews. BMJ. 2021;372:n71. doi: 10.1136/bmj.n71.
3. Deeks JJ, Bossuyt PM, Leeflang MMG, Takwoingi Y, editors. Cochrane Handbook for Systematic Reviews of Diagnostic Test Accuracy. Version 2.0. London: Cochrane; 2023.
4. Kirkpatrick JN, Wong T, Bednarz JE, Spencer KT, Sugeng L, Ward RP, et al. Differential Diagnosis of Cardiac Masses Using Contrast Echocardiographic Perfusion Imaging. J Am Coll Cardiol. 2004;43(8):1412-9. doi: 10.1016/j.jacc.2003.09.065.
5. Uenishi EK, Caldas MA, Tsutsui JM, Abduch MC, Sbano JC, Kalil R Filho, et al. Evaluation of Cardiac Masses by Real-Time Perfusion Imaging Echocardiography. Cardiovasc Ultrasound. 2015;13:23. doi: 10.1186/s12947-015-0018-3.
6. Yang Z, Niu Y, Ma H, Gong W, Yu L, Liu L, et al. Contrast-Enhanced Echocardiographic Diagnosis of Benign and Malignant Cardiac Tumors and its Correlation with Pathology. Front Cardiovasc Med. 2023;10:1182334. doi: 10.3389/fcvm.2023.1182334.
7. Angeli F, Bodega F, Bergamaschi L, Armillotta M, Amicone S, Canton L, et al. Multimodality Imaging in the Diagnostic Work-Up of Patients with Cardiac Masses: JACC: CardioOncology State-of-the-Art Review. JACC CardioOncol. 2024;6(6):847-62. doi: 10.1016/j.jaccao.2024.09.006.
8. Li Y, Ren W, Wang X, Xiao Y, Feng Y, Shi P, et al. The Diagnostic Accuracy of Contrast Echocardiography in Patients with Suspected Cardiac Masses: A Preliminary Multicenter, Cross-Sectional Study. Front Cardiovasc Med. 2022;9:1011560. doi: 10.3389/fcvm.2022.1011560.

Original Article

Development and Validation of a Predictive Model for Atrial Functional Mitral Regurgitation

Alexandre Costa Souza,[1,2] Bruna de Mattos Ivo Junqueira,[1] Stephanie de Azevedo Drubi,[1] Priscila Pinheiro,[1] Laila Caroline Gomes,[1] Pedro Henrique Correia Filgueiras,[3] Ricardo André Sales Pereira Guedes,[1] Marco André Moraes Sales,[1] Yuri Xavier de Carvalho,[1] Carolina Thé Macêdo[1]

Hospital São Rafael,[1] Salvador, BA – Brazil
Instituto D'Or de Pesquisa e Ensino,[2] Rio de Janeiro, RJ – Brazil
Universidade Federal de São Paulo, Escola Paulista de Medicina,[3] São Paulo, SP – Brazil

Abstract

Background: **Identifying atrial etiology in patients with mitral regurgitation remains challenging because the diagnosis is often established by exclusion. The use of a multivariable model may enhance diagnostic accuracy in the context of atrial functional mitral regurgitation.**

Objective: **To develop and validate a multivariable logistic regression model based on clinical and echocardiographic characteristics to predict atrial functional mitral regurgitation.**

Methods: **This cross-sectional study included patients with significant mitral regurgitation diagnosed by transesophageal echocardiography. The dataset was randomly divided into a training set (70%) and a validation set (30%). Statistical analyses were performed using a significance level of 5%.**

Results: **A total of 203 patients were included. The median age was 79 years in the atrial group and 72 years in the non-atrial group (p = 0.0022). Receiver operating characteristic curve analysis demonstrated good discriminative performance, with an area under the curve of 0.896 (95% CI, 0.845-0.947) in the training set. In the validation set, the model achieved an area under the curve of 0.946 (95% CI, 0.89-1.00), which indicates high predictive accuracy. Model calibration assessed by the Hosmer-Lemeshow test (chi-square test = 5.197; df = 8; p = 0.736) demonstrated good agreement between predicted and observed outcomes.**

Conclusion: **A multivariable model was derived and validated as a useful tool for predicting atrial etiology in patients with mitral regurgitation, potentially reducing diagnostic variability in clinical practice.**

Keywords: **Mitral Valve Insufficiency; Echocardiography; Statistical Models; Logistic Models.**

Introduction

Mitral regurgitation (MR) is one of the most prevalent valvular heart diseases in clinical practice and is associated with substantial cardiovascular morbidity and mortality.[1,2] Atrial functional MR (AFMR) initially arises from mitral annular dilation secondary to atrial remodeling; however, recent evidence suggests the involvement of multiple mechanisms, including alterations in atrial compliance and changes in the geometry of valvular apparatus.[1,3] Large echocardiographic registries estimate that AFMR accounts for approximately 40% of cases of moderate to severe functional MR. Early identification of AFMR facilitates the maintenance of sinus rhythm and the timely implementation of interventions, such as catheter ablation, which may attenuate disease progression.[4] In contrast to ventricular functional MR (VFMR), which is primarily associated with left ventricular dilation and systolic dysfunction, AFMR is characterized by isolated atrial remodeling with preserved left ventricular systolic function.[5]

AFMR is marked by left atrial dysfunction resulting from elevated intracavitary pressure, leading to dilation of the left atrium and the mitral annulus, alterations in leaflet concavity (the so-called "saddle-shaped" configuration), and planar leaflet coaptation. Posterior displacement of the mitral annulus toward the ventricular inflow tract further contributes to the regurgitant mechanism.[1,6] These findings reflect atrial remodeling and dynamic changes of the mitral annulus, commonly observed in clinical settings such as atrial fibrillation (AF) or heart failure with preserved ejection fraction (HFpEF). Despite these characteristic features, the diagnosis of AFMR is frequently established

Mailing Address: Alexandre Costa Souza •
Hospital São Rafael. Avenida São Rafael. Postal code: 41253-190. Salvador, BA – Brazil
E-mail: alexandrecostahsr@gmail.com
Manuscript received October 21, 2025, revised manuscript December 20, 2025, accepted January 26, 2026
Editor responsible for the review: Marcelo Tavares

DOI: https://doi.org/10.36660/abcimg.20250086i

Central Illustration: Development and Validation of a Predictive Model for Atrial Functional Mitral Regurgitation

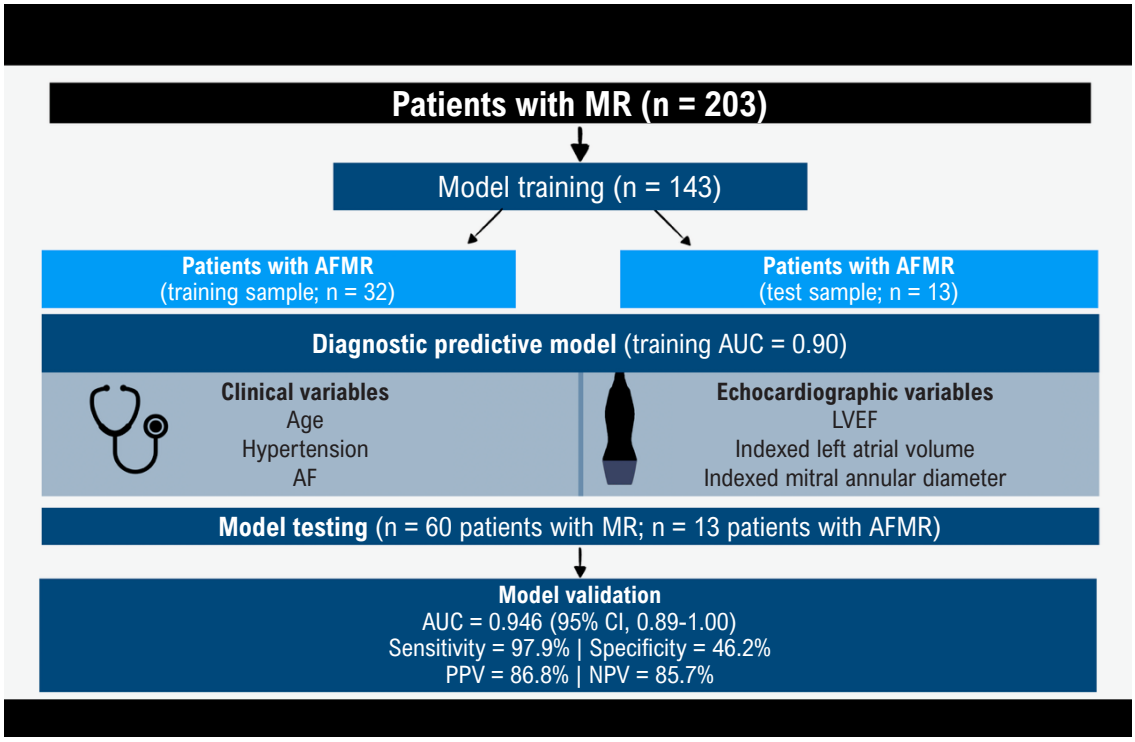

Arq Bras Cardiol: Imagem cardiovasc. 2026;39(1):e20250086

Development and Validation of a Predictive Model for Atrial Functional Mitral Regurgitation. MR: mitral regurgitation; AF: atrial fibrillation; AFMR: atrial functional mitral regurgitation; AUC: area under the curve; LVEF: left ventricular ejection fraction; NPV: negative predictive value; PPV: positive predictive value

by exclusion, owing to its overlap with other forms of functional MR.[1] In this context, the development of more structured diagnostic criteria may enhance etiological classification and improve clinical risk stratification in patients with AFMR.[1,7,8]

The severity of AFMR has been associated with adverse clinical outcomes, including increased mortality, heart failure-related hospitalizations, and the need for valvular interventions.[3,8] Patients with AFMR often present with more pronounced symptoms, greater structural remodeling of the left-sided cardiac chambers, and concomitant tricuspid regurgitation, underscoring the increased clinical complexity of this population.[3,9]

The current study aimed to develop a multivariable logistic regression model that integrates clinical and echocardiographic variables in order to distinguish AFMR from other causes of MR. Internal validation of the model was performed using an independent dataset from the initial derivation cohort, thereby enhancing methodological rigor and offering the potential to reduce diagnostic variability in clinical practice.

Methods

Study design and population

This was a prospective, single-center, observational study conducted between October 2022 and January 2025. The study population consisted of 203 consecutive patients with moderate or severe MR who underwent transesophageal echocardiography (TEE) at a tertiary care hospital in Brazil. Patients were included consecutively and by convenience, reflecting routine clinical practice, and were referred for TEE based on clinical indications for reassessment of MR severity or clarification of its etiology.

Patient selection

Eligible participants were adults (≥ 18 years) with a clinical indication for TEE as determined by the attending cardiologists, either in outpatient or inpatient settings, for diagnostic evaluation of MR. Patients with a mitral valve prosthesis or those whose MR severity was reclassified as mild on TEE were excluded from the study.

Echocardiographic assessment

All patients underwent comprehensive two-dimensional transthoracic echocardiography followed by TEE using a Vivid E95 ultrasound system equipped with a phased-array transducer (M5S) (General Electric, Horten, Norway).

MR severity was quantified in accordance with the recommendations of the American Society of Echocardiography, using vena contracta width, regurgitant volume, and effective regurgitant orifice area as objective diagnostic criteria. Qualitative assessment included the proportion of left atrial area occupied by the regurgitant jet and the presence of Coandă effect.[10]

Etiological classification of MR was independently performed by two experienced echocardiographers based on updated diagnostic criteria for AFMR. AFMR was defined by the presence of moderate or severe left atrial enlargement (> 42 mL/m^2), mitral annular dilation (> 35 mm in the parasternal long-axis view or ≥ 36 mm in the apical four-chamber view during systole on transthoracic echocardiography), and the exclusion of diagnostic criteria for alternative MR etiologies.[1]

Other causes of MR were defined according to established guidelines specific to each etiology, including mitral valve prolapse, chordal rupture, calcific degeneration, mitral cleft, and VFMR. Patients were classified into two main groups: atrial and non-atrial etiology.

Statistical analysis

Statistical analyses were performed using R software (version 4.4.2) within the RStudio environment, using appropriate packages for predictive modeling and model performance assessment. Categorical variables are presented as absolute and relative frequencies (%), while continuous variables are reported as median and interquartile range (IQR), as none demonstrated normal distribution. Normality was assessed using the Shapiro-Wilk test.

Comparisons between the atrial and non-atrial groups were conducted according to variable type. Categorical variables were compared using Pearson's chi-square test or Fisher's exact test, as appropriate based on expected cell frequencies. Continuous variables were compared using the Mann-Whitney *U* test. A two-sided significance level of 5% ($\alpha = 0.05$) was adopted for all analyses.

Predictive model development

A multivariable logistic regression model was constructed using the presence of AFMR as the dependent variable. Independent variables were selected based on clinical relevance, absence of significant collinearity, and statistical performance in univariable analyses.

Collinearity assessment

To ensure model stability, collinearity among continuous variables was assessed using the variance inflation factor (VIF). VIF values < 5 were considered indicative of low collinearity and acceptable for inclusion. Values between 5 and 10 were classified as moderate collinearity and required clinical judgment for retention or exclusion, whereas values > 10 indicated severe collinearity and led to variable removal. This process was conducted iteratively to retain only variables with the greatest clinical and statistical relevance.

Model derivation and validation

To robustly assess predictive performance, the dataset was randomly divided into two independent subsets: 70% of patients were allocated to the training set (n = 143), and the remaining 30% to the test (validation) set (n = 60). The split preserved the proportion of AFMR cases and ensured balanced representation across both datasets.

Model discrimination was evaluated separately in the training and validation samples using receiver operating characteristic (ROC) curve analysis, with calculation of the area under the curve (AUC) and corresponding 95% CIs.

In addition to AUC, diagnostic performance metrics including sensitivity, specificity, positive predictive value (PPV), and negative predictive value (NPV) were assessed across different cutoff points to optimize predictive accuracy.

Model calibration was evaluated using the Hosmer-Lemeshow goodness-of-fit test, assessing agreement between predicted and observed probabilities. Calibration performance was further examined through graphical calibration curves, allowing visualization of the alignment between model predictions and observed outcomes.

Results

A total of 203 patients were included in the study, of whom 45 (22.2%) were classified as having AFMR. The cohort was divided into a training set comprising 143 patients (70%) and a test set comprising 60 patients (30%), preserving the proportion of AFMR cases. In the training cohort, 32 patients (22.4%) had AFMR; in the test cohort, 13 patients (21.7%) had AFMR (Central Illustration).

Baseline demographic characteristics in the training cohort demonstrated a median age of 78 years (IQR, 72-84) in the atrial group and 70 years (IQR, 60-78) in the non-atrial group. Male sex was observed in 43.75% of patients in the atrial group and 63.06% in the non-atrial group, although this difference did not reach statistical significance (p = 0.0799) (Table 1).

To ensure model stability and interpretability, a systematic collinearity analysis was performed using VIF to identify and exclude redundant variables. Variables with VIF > 5 were removed to minimize linear dependencies and improve coefficient stability in the logistic regression model. Among anthropometric variables, height and body surface area (BSA) exhibited strong correlation; therefore, BSA was excluded due to its lower incremental informational value. Similarly, the linear mitral annular diameter was excluded in favor of the mitral annular diameter indexed to BSA, which demonstrated lower collinearity and greater clinical applicability (Tables 1 and 2).

After successive iterations of collinearity assessment, six variables were retained for inclusion in the predictive model: three clinical variables (age, hypertension, and

AF) and three echocardiographic variables (left ventricular ejection fraction [LVEF], indexed left atrial volume, and mitral annular diameter indexed to BSA). All retained variables demonstrated VIF values < 2, indicating negligible collinearity. The most statistically significant predictor was indexed mitral annular diameter ($p = 4.81 \times 10^{-7}$), followed by age ($p = 0.0022$) and LVEF ($p = 0.0067$), underscoring their relevance for etiological differentiation (Table 3).

The selection of these predictors was guided by both clinical relevance and statistical significance, ensuring robustness and accuracy of the predictive model (Table 3). This parsimonious set of variables supports improved discrimination of AFMR and may contribute to reduced diagnostic variability and enhanced clinical decision-making.

In the training cohort, the ROC curve analysis demonstrated an AUC of 0.896 (95% CI, 0.845-0.947), which indicates good discriminative performance (Figure 1). Model calibration assessed by the Hosmer-Lemeshow test yielded $\chi^2 = 5.197$, with 8 degrees of freedom ($p = 0.736$), which indicates good agreement between predicted and observed outcomes (Figure 2).

To compare predictive performance across different variable combinations, ROC curves were constructed for three distinct models: a clinical model (clinical variables only), a structural model (echocardiographic variables only), and a complete model (combined clinical and echocardiographic variables). Corresponding AUC values were 0.7974 (95% CI, 0.7264-0.8685), 0.7922 (95% CI, 0.7214-0.8630), and 0.8961 (95% CI, 0.8454-0.9468), respectively (Figure 3).

In the test cohort, the ROC curve analysis demonstrated an AUC of 0.946 (95% CI, 0.8899-1.0000) (Figure 4). At the selected cutoff point, the model achieved a sensitivity of 97.9%, specificity of 46.2%, PPV of 86.8%, and NPV of 85.7%.

Discussion

Mitral annular diameter is widely used in the evaluation of AFMR; however, its diagnostic specificity is limited in the setting of advanced atrial remodeling.[11-13] Previous studies have demonstrated modest discriminative performance of this isolated parameter, prompting the development of multiparametric approaches.[14] In the current study, we developed a multivariable logistic regression model integrating clinical and echocardiographic variables, which demonstrated high discriminative performance consistently confirmed by statistical testing. The structured combination of readily available variables overcomes the limitations of isolated echocardiographic parameters and improves etiological classification of AFMR.

Multiparametric models combining clinical and echocardiographic data have shown value in different contexts of MR. A notable example is the MIDA score, derived from the Mitral Regurgitation International Database, which integrates clinical and imaging variables

Table 1 – Clinical and demographic characteristics of the atrial and non-atrial groups in the training sample

Variable	Atrial (n = 32)	Non-atrial (n = 111)	p-value
Male sex, n (%)	14 (43.8)	70 (63.1)	0.08
Previous CAD, n (%)	8 (25.0)	41 (36.9)	0.30
PCI, n (%)	6 (18.8)	20 (18.0)	> 0.99
Previous MR, n (%)	1 (3.1)	11 (9.9)	0.30
Previous stroke, n (%)	5 (15.6)	17 (15.3)	> 0.99
Diabetes mellitus, n (%)	10 (31.3)	44 (39.6)	0.51
Hypertension, n (%)	27 (84.4)	67 (60.4)	0.02
Dyslipidemia, n (%)	26 (81.3)	63 (56.8)	0.02
Use of beta-blockers, n (%)	17 (53.1)	61 (54.9)	> 0.99
Use of antiarrhythmic drugs, n (%)	12 (37.5)	29 (26.1)	0.30
CKD, n (%)	8 (25.0)	19 (17.1)	0.45
AF, n (%)	23 (71.9)	49 (44.1)	0.01
Use of anticoagulant, n (%)	22 (68.8)	47 (42.3)	0.15
Pacemaker, n (%)	4 (12.5)	17 (15.3)	0.73
Tricuspid regurgitation, n (%)	13 (40.6)	34 (30.6)	0.40
CKD treated by dialysis, n (%)	1 (3.1)	11 (9.9)	0.30

Values with p < 0.05 indicate statistically significant differences. AF: atrial fibrillation; CAD: coronary artery disease; CKD: chronic kidney disease; MR: mitral regurgitation; PCI: percutaneous coronary intervention.

Table 2 – Continuous characteristics of the atrial and non-atrial groups in the training sample

Variable	Atrial median (P_{25}-P_{75})	Non-atrial median (P_{25}-P_{75})	p-value
Age, years	78.0 (72.0-84.0)	70.0 (60.0-78.0)	< 0.001
HR, bpm	92.0 (74.0-118.0)	79.0 (69.0-90.0)	0.015
Weight, kg	70.0 (60.0-80.0)	72.5 (63.0-82.8)	0.410
BSA, m^2	1.8 (1.64-1.85)	1.8 (1.65-1.99)	0.110
LA diameter, mm	46.0 (44.0-49.0)	45.0 (41.0-49.0)	0.049
Indexed LA volume, mL/m^2	62.0 (51.0-78.0)	53.5 (45.0-68.0)	0.004
LVEF, %	61.0 (56.0-64.0)	48.0 (30.0-64.0)	0.002
E/E′ ratio	16.0 (13.9-18.0)	17.0 (10.0-21.8)	0.950
TAPSE, mm	19.0 (18.0-20.0)	19.0 (18.0-21.0)	0.650
Right ventricular S′, cm/s	11.0 (10.0-11.0)	11.0 (9.5-12.0)	0.830
PASP, mmHg	44.0 (40.0-50.0)	40.0 (33.5-51.0)	0.110
Intercommissural mitral annular diameter, mm	36.0 (34.0-40.0)	34.0 (31.0-36.0)	< 0.001
Indexed mitral annular diameter, mm/m^2	21.2 (20.2-22.4)	18.3 (17.0-20.1)	< 0.001

Values with p < 0.05 indicate statistically significant differences. BSA: body surface area; HR: heart rate; LA: left atrium; LVEF: left ventricular ejection fraction; TAPSE: tricuspid annular plane systolic excursion; PASP: pulmonary artery systolic pressure.

Table 3 – Variables included in the diagnostic predictive model for atrial functional mitral regurgitation

Variable	Atrial	Non-atrial	p-value
Age, years	78.0 (72.0-84.0)	70.0 (60.0-78.0)	< 0.001
Hypertension, n (%)	27 (84.4)	67 (60.4)	0.020
AF, n (%)	23 (71.9)	49 (44.1)	0.010
Indexed mitral annular diameter, mm/m^2	21.2 (20.2-22.4)	18.3 (17.0-20.1)	< 0.001
LVEF, %	61.0 (56.0-64.0)	48.0 (30.0-64.0)	0.002
Indexed LA volume, mL/m^2	62.0 (51.0-78.0)	53.5 (45.0-68.0)	0.004

Values with p < 0.05 indicate statistically significant associations, according to the applied test. AF: atrial fibrillation; LA: left atrium; LVEF: left ventricular ejection fraction.

for prognostic stratification in degenerative MR and has demonstrated consistent performance across multiple internal and external cohorts.[15-17] Although the MIDA score was designed for prognostic assessment in primary mitral disease, the present model focuses on improving diagnostic performance for differentiating AFMR. By incorporating routinely available variables (e.g., age, cardiac rhythm, LVEF, and indexed mitral annular diameter), the proposed model addresses a clinically relevant gap for which no dedicated diagnostic tool currently exists, as highlighted in recent research on AFMR.[1,18] Thus, the multiparametric principle appears applicable to both prognostic and diagnostic purposes when appropriately tailored to the clinical context.

Recent population-based studies further emphasize the importance of early recognition of AFMR. In the National Echocardiography Database Australia (NEDA) cohort, which included more than 5,500 patients with moderate to severe AFMR, atrial etiology accounted for approximately 40% of cases and was associated with slightly lower but still substantial mortality compared with VFMR, with a 5-year mortality rate approaching 50%.[4] Complementarily, a longitudinal analysis of 635 individuals with mild to moderate AFMR demonstrated that, even in the absence of overt hemodynamic progression, this entity confers an annual mortality risk of 5.9% and is associated with diastolic dysfunction and pulmonary hypertension.[3]

In this context, real-time differentiation of AFMR from other forms of MR remains challenging. The proposed score incorporates variables validated in large registries such as NEDA and can be calculated during echocardiographic assessment, thereby standardizing etiological classification and facilitating early referral to electrophysiology or heart team evaluation, particularly in centers lacking advanced three-dimensional imaging or with variable expertise.[4] As

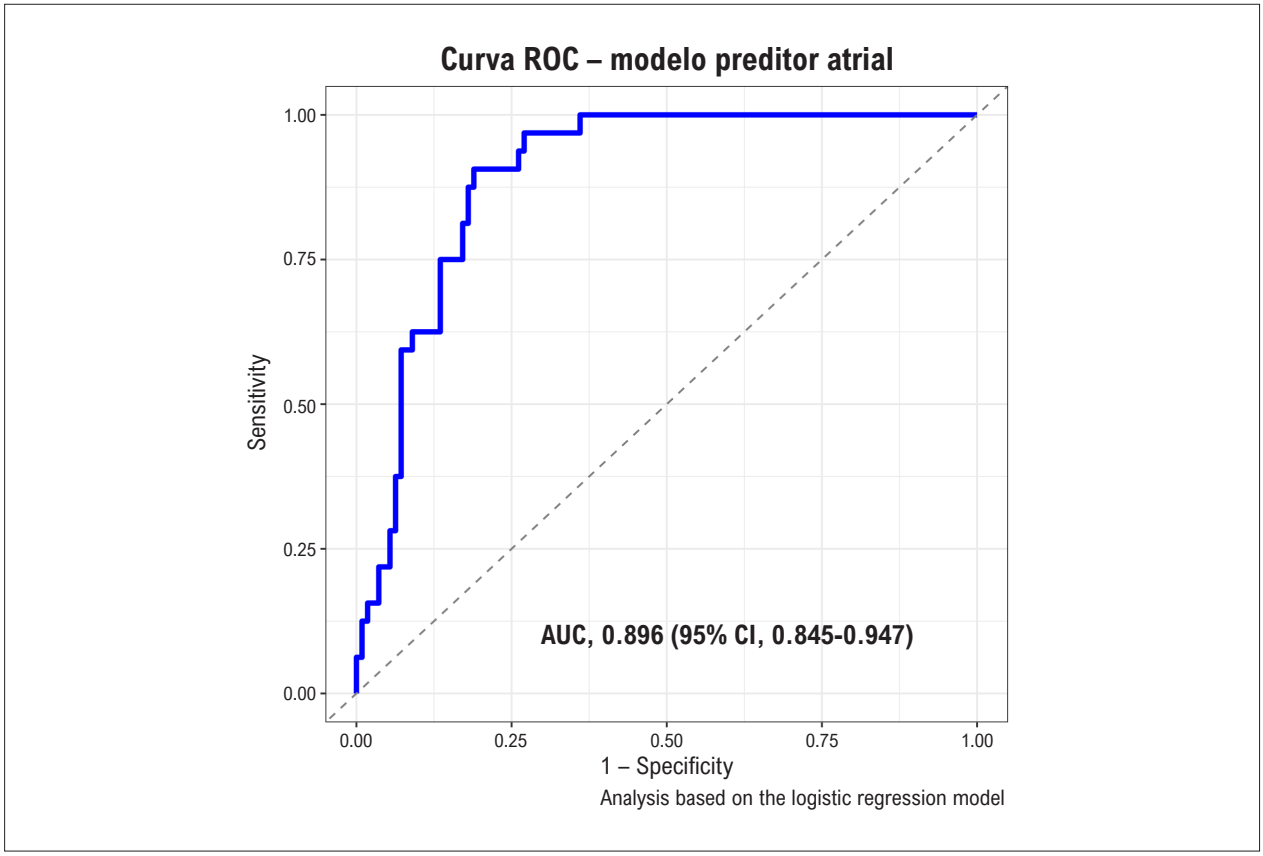

Figure 1 – *Discriminative performance of the atrial etiology predictive model. AUC: area under the curve; ROC: receiver operating characteristic*

a screening tool, the model may assist in identifying AFMR and guiding clinical decisions, including consideration of rhythm control strategies such as catheter ablation or optimization of therapy for HFpEF, with potential implications for follow-up and clinical outcomes.

Internal consistency was assessed using a hold-out validation approach, reserving 30% of the sample for independent testing. This strategy allows evaluation of predictive performance in data not used for model derivation, thereby reducing the risk of overfitting and supporting internal generalizability. Nevertheless, reliance on a single cohort limits assessment of coefficient stability and may underestimate variability across different populations. Additional validation in external cohorts will be required to confirm reliability and expand the clinical applicability of the model.

Study limitations

This study did not incorporate serum biomarkers (e.g., N-terminal pro-B-type natriuretic peptide), atrial strain measurements, electrocardiographic parameters, or three-dimensional quantification of mitral annulus. These additional domains may provide incremental information regarding atrial remodeling and hemodynamic burden, potentially enhancing the discriminative performance of the algorithm. Future studies should evaluate the impact of these markers on diagnostic accuracy and model reproducibility across different clinical settings.[12] Furthermore, international guidelines recommend integrating additional variables in the assessment of valvular regurgitation, which underscores their relevance to clinical practice.[15]

While several multicenter studies have compared AFMR exclusively with VFMR, the present analysis used all non-atrial etiologies, including primary MR, as the reference group.[19,20] This approach was based on two practical considerations: the limited number of isolated VFMR cases, which would have compromised statistical power in both training and test phases, and the intention to evaluate model performance in a real-world scenario characterized by heterogeneous clinical, anatomical, and functional presentations of MR. We acknowledge that such heterogeneity may attenuate the model's ability to distinguish subtle differences between functional subtypes, thereby limiting specific pathophysiological inferences.

From a methodological standpoint, given the number of observed events (45 cases of AFMR) and the number of predictors included in the final model (six variables), the events-per-variable ratio lies at the lower boundary of conventional recommendations for logistic regression, potentially increasing the risk of overfitting. This risk was

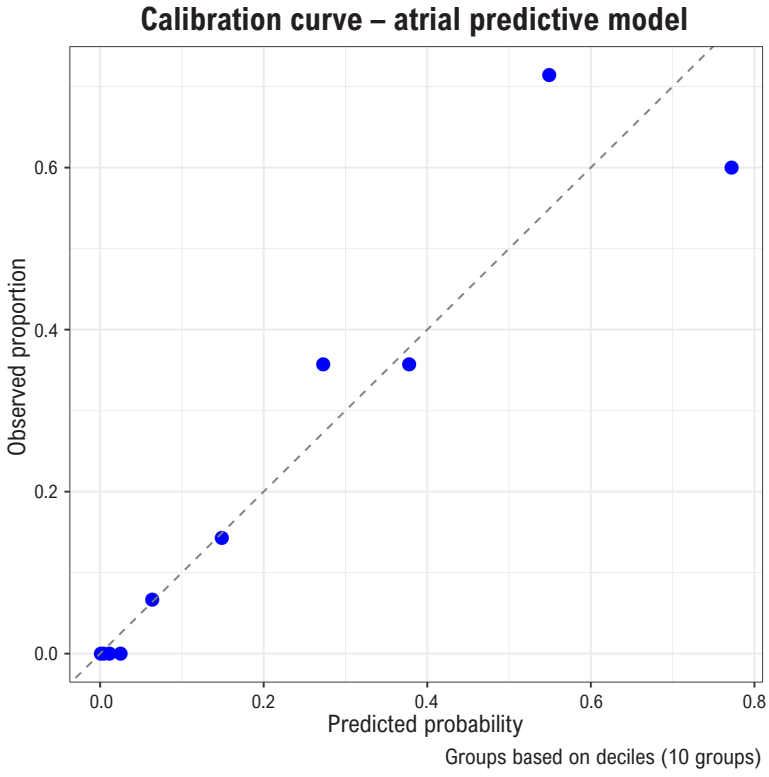

Figura 2 – *Calibration curve of the atrial predictive model.*

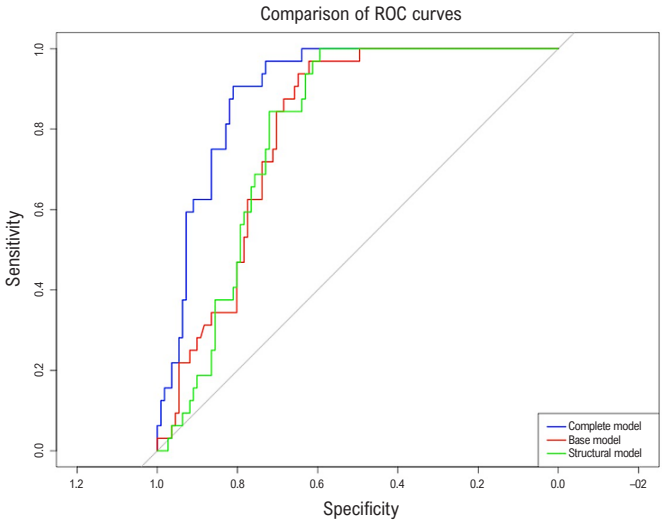

Table – AUC and 95% CI for the three models

Model	AUC (95% CI)
Base (clinical variables)	0,7974 (0,7264–0,8685)
Structural (echocardiographic variables)	0,7922 (0,7214–0,8630)
Complete (clinical + echocardiographic)	0,8961 (0,8454–0,9468)

Figure 3 – *Comparison of ROC curves for clinical, echocardiographic, and combined models. AUC: area under the curve; ROC: receiver operating characteristic*

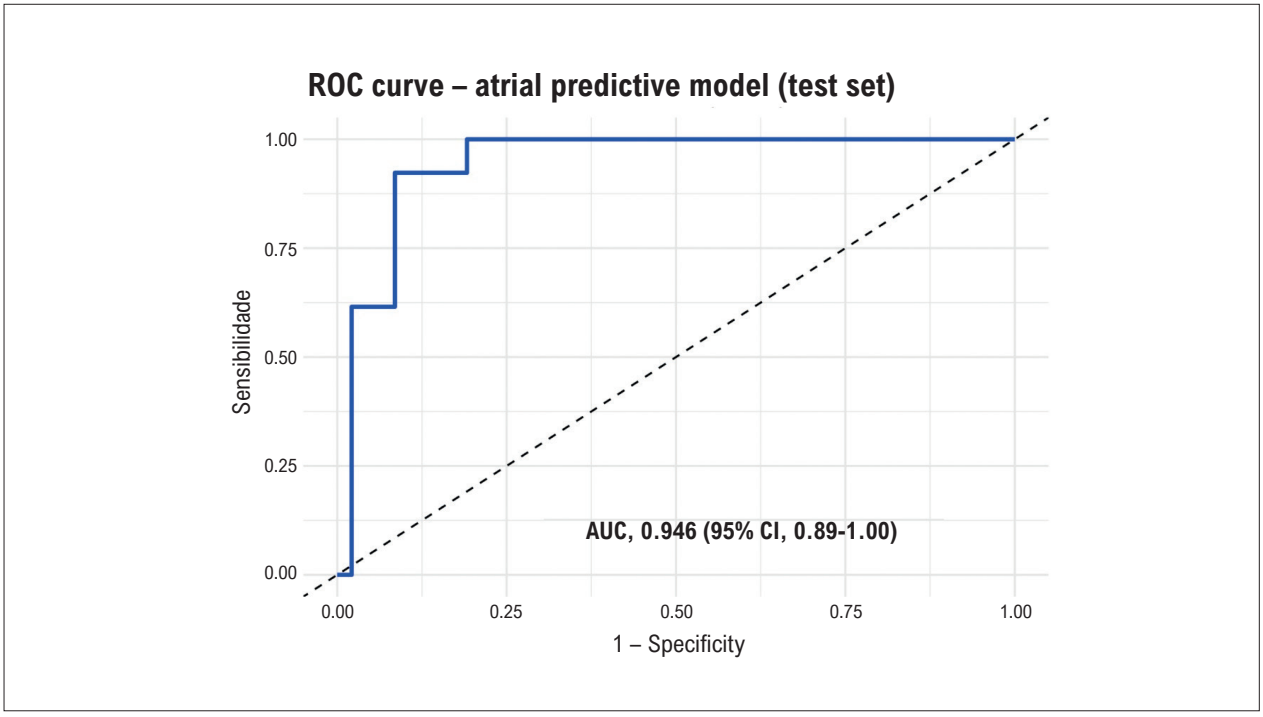

Figure 4 – *ROC curve of the atrial predictive model in the test set. AUC: area under the curve; ROC: receiver operating characteristic*

mitigated through parsimonious selection of predictors with strong clinical and echocardiographic plausibility, as well as systematic collinearity assessment. Additionally, the high AUC observed in the test sample (0.946) should be interpreted with caution since it was derived from a limited number of events in that subset (n = 13), which increases uncertainty and the possibility of performance overestimation. Accordingly, these findings should be regarded as exploratory and require confirmation in independent external cohorts.

Conclusion

The derivation and validation of a multivariable model for predicting AFMR may be clinically useful. Because of the limitations of isolated mitral annular measurements for diagnostic purposes, the integration of echocardiographic and clinical parameters within a unified model demonstrated potential to reduce diagnostic variability, which enables earlier detection and timely interventions that may improve the prognosis and management of patients with AFMR.

Author Contributions

Conception and design of the research and statistical analysis: Souza AC; acquisition of data: Souza AC, Pinheiro P; analysis and interpretation of the data: Souza AC, Filgueiras PHC; writing of the manuscript: Souza AC, Junqueira BMI, Drubi AS, Pinheiro P, Guedes RASP, Gomes LC; critical revision of the manuscript for intellectual content: Junqueira BMI, Sales MAM, Guedes RASP, Macêdo CT; illustration: Filgueiras PHC, Carvalho YX.

Potential Conflict of Interest

No potential conflict of interest relevant to this article was reported.

Sources of Funding

There were no external funding sources for this study.

Study Association

This article is part of the thesis of Doctoral submitted by Alexandre Costa Souza, from Instituto Dor de ensino e pesquisa (I'Dor-RJ).

Ethics Approval and Consent to Participate

This study was approved by the Ethics Committee of the Hospital São Rafael under the protocol number 5722007. All the procedures in this study were in accordance with the 1975 Helsinki Declaration, updated in 2013. Informed consent was obtained from all participants included in the study.

Use of Artificial Intelligence

The authors did not use any artificial intelligence tools in the development of this work.

Availability of Research Data

The underlying content of the research text is contained within the manuscript.

References

1. Zoghbi WA, Levine RA, Flachskampf F, Grayburn P, Gillam L, Leipsic J, et al. Atrial Functional Mitral Regurgitation: A JACC: Cardiovascular Imaging Expert Panel Viewpoint. JACC Cardiovasc Imaging. 2022;15(11):1870-82. doi: 10.1016/j.jcmg.2022.08.016.

2. Dziadzko V, Dziadzko M, Medina-Inojosa JR, Benfari G, Michelena HI, Crestanello JA, et al. Causes and Mechanisms of Isolated Mitral Regurgitation in the Community: Clinical Context and Outcome. Eur Heart J. 2019;40(27):2194-202. doi: 10.1093/eurheartj/ehz314.

3. Naser JA, Alexandrino FB, Harada T, Michelena HI, Borlaug BA, Eleid MF, et al. The Natural History of Atrial Functional Mitral Regurgitation. J Am Coll Cardiol. 2024;83(16):1495-507. doi: 10.1016/j.jacc.2024.02.026.

4. Moonen A, Ng MKC, Playford D, Strange G, Scalia GM, Celermajer DS. Atrial Functional Mitral Regurgitation: Prevalence, Characteristics and Outcomes from the National Echo Database of Australia. Open Heart. 2023;10(1):e002180. doi: 10.1136/openhrt-2022-002180.

5. Danojevic S, De Raffele M, Niro L, Delgado V. Atrial Functional Mitral Regurgitation: Was this New Entity Needed?. REC Interv Cardiol. 2024;6(2):127-9. doi: 10.24875/RECIC.M24000443.

6. Gertz ZM, Raina A, Saghy L, Zado ES, Callans DJ, Marchlinski FE, et al. Evidence of Atrial Functional Mitral Regurgitation due to Atrial Fibrillation: Reversal with Arrhythmia Control. J Am Coll Cardiol. 2011;58(14):1474-81. doi: 10.1016/j.jacc.2011.06.032.

7. Silbiger JJ. Does Left Atrial Enlargement Contribute to Mitral Leaflet Tethering in Patients with Functional mitral Regurgitation? Proposed role of Atriogenic Leaflet Tethering. Echocardiography. 2014;31(10):1310-1. doi: 10.1111/echo.12629.

8. Pretto AS. Insuficiência Mitral Funcional Atrial. Arq Bras Cardiol: Imagem Cardiovasc. 2024;37(1):e20230097. doi: 10.36660/abcimg.20230097.

9. Farhan S, Silbiger JJ, Halperin JL, Zhang L, Dukkipati SR, Vogel B, et al. Pathophysiology, Echocardiographic Diagnosis, and Treatment of Atrial Functional Mitral Regurgitation: JACC State-of-the-Art Review. J Am Coll Cardiol. 2022;80(24):2314-30. doi: 10.1016/j.jacc.2022.09.046.

10. Murata A, Kaneko T, Amano M, Sato Y, Ohno Y, Obokata M, et al. Qualitative and Quantitative Assessment of Atrial Functional Mitral Regurgitation: Analysis from the REVEAL-AFMR Registry. Eur Heart J Cardiovasc Imaging. 2025;26(2):299-306. doi: 10.1093/ehjci/jeae288.

11. Zoghbi WA, Adams D, Bonow RO, Enriquez-Sarano M, Foster E, Grayburn PA, et al. Recommendations for Noninvasive Evaluation of Native Valvular Regurgitation: A Report from the American Society of Echocardiography Developed in Collaboration with the Society for Cardiovascular Magnetic Resonance. J Am Soc Echocardiogr. 2017;30(4):303-71. doi: 10.1016/j.echo.2017.01.007.

12. Deferm S, Bertrand PB, Verbrugge FH, Verhaert D, Rega F, Thomas JD, et al. Atrial Functional Mitral Regurgitation: JACC Review Topic of the Week. J Am Coll Cardiol. 2019;73(19):2465-76. doi: 10.1016/j.jacc.2019.02.061.

13. Kagiyama N, Mondillo S, Yoshida K, Mandoli GE, Cameli M. Subtypes of Atrial Functional Mitral Regurgitation: Imaging Insights Into Their Mechanisms and Therapeutic Implications. JACC Cardiovasc Imaging. 2020;13(3):820-35. doi: 10.1016/j.jcmg.2019.01.040.

14. Souza AC, Junqueira BMI, Drubi SA, Gomes LC, Freire MV, Pinheiro P, et al. Desempenho do Diâmetro do Anel Mitral no Diagnóstico da Etiologia Atrial na Insuficiência Mitral: Uma Análise Comparativa. Arq Bras Cardiol: Imagem Cardiovasc. 2025;38(1):e20240134. doi: 10.36660/abcimg.20240134i.

15. Vahanian A, Beyersdorf F, Praz F, Milojevic M, Baldus S, Bauersachs J, et al. 2021 ESC/EACTS Guidelines for the Management of Valvular Heart Disease. Eur Heart J. 2022;43(7):561-32. doi: 10.1093/eurheartj/ehab395.

16. Mesi O, Gad MM, Crane AD, Ramchand J, Puri R, Layoun H, et al. Severe Atrial Functional Mitral Regurgitation: Clinical and Echocardiographic Characteristics, Management and Outcomes. JACC Cardiovasc Imaging. 2021;14(4):797-808. doi: 10.1016/j.jcmg.2021.02.008.

17. Grigioni F, Clavel MA, Vanoverschelde JL, Tribouilloy C, Pizarro R, Huebner M, et al. The MIDA Mortality Risk Score: Development and External Validation of a Prognostic Model for Early and Late Death in Degenerative Mitral Regurgitation. Eur Heart J. 2018;39(15):1281-91. doi: 10.1093/eurheartj/ehx465.

18. Akamatsu K, Abe Y, Matsumura Y, Shimeno K, Naruko T, Takahashi Y, et al. Etiology of Atrial Functional Mitral Regurgitation: Insights from Transthoracic Echocardiography in 159 Consecutive Patients with Atrial Fibrillation and Preserved Left Ventricular Ejection Fraction. Cardiology. 2020;145(8):511-21. doi: 10.1159/000508279.

19. Kim K, Kitai T, Kaji S, Pak M, Toyota T, Sasaki Y, Ehara N, et al. Outcomes and Predictors of Cardiac Events in Medically Treated Patients with Atrial Functional Mitral Regurgitation. Int J Cardiol. 2020;316:195-202. doi: 10.1016/j.ijcard.2020.06.042.

20. Okamoto C, Okada A, Nishimura K, Moriuchi K, Amano M, Takahama H, et al. Prognostic Comparison of Atrial and Ventricular Functional Mitral Regurgitation. Open Heart. 2021;8(1):e001574. doi: 10.1136/openhrt-2021-001574.

Functional Mitral Regurgitation of Atrial Origin: Search for Diagnostic Criteria

Minna Moreira Dias Romano[1]

Universidade de São Paulo, Faculdade de Medicina de Ribeirão Preto,[1] *Ribeirão Preto, SP – Brazil*

Short editorial referring to the article: Development and Validation of a Predictive Model for Atrial Functional Mitral Regurgitation

Identifying the various mechanisms of Mitral Regurgitation (MR) is essential for understanding the disease, prognosis, and planning structural therapeutic approaches. Recently, several studies on valvular heart disease have recognized functional MR. This condition is associated with the impact of cardiac geometry on mitral valve function, rather than primary valvular injury such as rheumatic, degenerative, infectious (endocarditis), or congenital diseases.

Furthermore, within the group of patients with functional MR, a subgroup has been identified that does not present Left Ventricular (LV) dilation or dysfunction.[1] In this subgroup, the likely mechanism of MR is chronic enlargement of the Left Atrium (LA) and the mitral annulus, commonly associated with atrial fibrillation.[2] Preliminary studies suggest associated left atrial dysfunction, which can be measured through tissue mechanics analysis. These factors likely contribute to the reduction of the coaptation surface of the mitral leaflet edges.

Echocardiographic assessment of valve function, and not only of the pathological characteristics of the mitral valve components and annulus, is essential for suspecting MR, although in some cases the diagnosis remains subjective and based on the exclusion of other causes. Echocardiography (ECHO), even in its two-dimensional form, can evaluate LA dimensions and atrial function using the Speckle Tracking technique.[3] However, a more detailed analysis of valve anatomy, particularly of the annulus, requires more advanced assessments, such as two-dimensional transesophageal ECHO or three-dimensional (3D) imaging.[4,5] Nevertheless, the availability of 3D ECHO is still limited by equipment cost and the need for adequate training of echocardiographers.

The study published in this edition presents a diagnostic proposal for atrial MR using a variable derived from two-dimensional transesophageal ECHO. This variable is not merely the linear diameter of the mitral annulus, but its value indexed to body surface area. Importantly, the researchers did not restrict their evaluation to the diagnostic capacity of a single parameter, but rather to the combination of key parameters, including age, presence of atrial fibrillation, and comorbidities such as systemic arterial hypertension, together with ECHO parameters such as LV ejection fraction and indexed LA volume, associated with the indexed annular diameter. Using multivariate analyses and logistic regression, and comparing model performance with the consensus clinical diagnosis of two observers, the study demonstrated good performance of the model incorporating all variables.

Thus, there is a proposed predictive diagnostic model for atrial MR based on the combination of clinical variables and two-dimensional ECHO parameters. The results presented represent an initial proposal, which may in the future be tested against the performance of validated 3D ECHO variables for this diagnosis. It is necessary to evaluate functional MR using different diagnostic techniques in order to identify this subgroup of atrial MR, which is peculiar when compared with MR of left ventricular origin.

Keywords

Mitral Valve Insufficiency; Atrial Fibrillation; Echocardiography

Mailing Address: Minna Moreira Dias Romano •
Universidade de São Paulo, Faculdade de Medicina de Ribeirão Preto. Rua Carlos Rateb Cury, 697. Postal code: 14110-000. Ribeirão Preto, SP – Brazil
E-mail: minna@fmrp.usp.br

DOI: https://doi.org/10.36660/abcimg.20260008i

References

1. Zoghbi WA, Levine RA, Flachskampf F, Grayburn P, Gillam L, Leipsic J, et al. Atrial Functional Mitral Regurgitation: A JACC: Cardiovascular Imaging Expert Panel Viewpoint. JACC Cardiovasc Imaging. 2022;15(11):1870-82. doi: 10.1016/j.jcmg.2022.08.016.
2. Muraru D, Guta AC, Ochoa-Jimenez RC, Bartos D, Aruta P, Mihaila S, et al. Functional Regurgitation of Atrioventricular Valves and Atrial Fibrillation: An Elusive Pathophysiological Link Deserving Further Attention. J Am Soc Echocardiogr. 2020;33(1):42-53. doi: 10.1016/j.echo.2019.08.016.
3. Tang Z, Fan YT, Wang Y, Jin CN, Kwok KW, Lee AP. Mitral Annular and Left Ventricular Dynamics in Atrial Functional Mitral Regurgitation: A Three-Dimensional and Speckle-Tracking Echocardiographic Study. J Am Soc Echocardiogr. 2019;32(4):503-13. doi: 10.1016/j.echo.2018.11.009.
4. Kagiyama N, Mondillo S, Yoshida K, Mandoli GE, Cameli M. Subtypes of Atrial Functional Mitral Regurgitation: Imaging Insights Into Their Mechanisms and Therapeutic Implications. JACC Cardiovasc Imaging. 2020;13(3):820-35. doi: 10.1016/j.jcmg.2019.01.040.
5. Ito K, Abe Y, Takahashi Y, Shimada Y, Fukumoto H, Matsumura Y, et al. Mechanism of Atrial Functional Mitral Regurgitation in Patients with Atrial Fibrillation: A Study Using Three-Dimensional Transesophageal Echocardiography. J Cardiol. 2017;70(6):584-90. doi: 10.1016/j.jjcc.2017.03.013.

Cardiovascular Complications in Patients with COVID-19 and Their Relationship with Mortality: An Echocardiographic Perspective

João Henrique Andrade de Almeida,[1] Gustavo Miranda de Azevedo Ferreira,[2] Marina de Azevedo Martins Andrade,[3] Heloísa Marceliano Nunes,[4] Igor Brasil Costa[4]

Universidade do Estado do Pará,[1] Belém, PA – Brazil

Centro Universitário do Estado do Pará,[2] Belém, PA – Brazil

FAMAZ,[3] Belém, Pará – Brazil

Instituto Evandro Chagas,[4] Ananindeua, PA – Brazil

Abstract

Background: **Echocardiography plays a fundamental role in the diagnosis of cardiovascular diseases related to SARS-CoV-2 infection. Despite prior investigation in the literature, studies focusing on cardiovascular manifestations among patients from the Brazilian Legal Amazon region remain scarce.**

Objectives: **To identify cardiovascular complications of COVID-19 in patients admitted to a hospital in the North Region of Brazil and their potential association with mortality.**

Methods: **We conducted a retrospective cohort study including 25 medical records of adults diagnosed with COVID-19. These patients were admitted to a hospital in Belém, Pará, in Northern Brazil, between March 2020 and December 2020. Demographic and clinical characteristics, as well as echocardiographic findings, were extracted from the medical records. Statistical analyses were performed adopting a significance level of $\alpha < 0.05$. The project was approved by the Research Ethics Committee (approval number: 5.540.025).**

Results: **Among the 25 patients, 15 (60%) were male, with a mean age of 69.6 ± 14.4 years. Hypertension (n = 23; 92%) was the most prevalent cardiovascular risk factor, followed by diabetes (n = 11; 44%) and obesity (n = 8; 32%). We detected echocardiographic abnormalities in 20 (80%) individuals, with diastolic dysfunction being the most frequent (n = 18; 72%). All 7 patients who died showed abnormal echocardiography ($p > 0.05$). Atrial fibrillation or flutter (n = 5; 20%), decompensated heart failure (n = 3; 12%), and cardiogenic shock (n = 2; 8%) were the most common types of cardiovascular involvement.**

Conclusions: **An increasing trend in COVID-19 mortality was observed among patients with cardiovascular complications. Nevertheless, the statistical power was limited by the small sample size.**

Keywords: **Cardiovascular Diseases; Echocardiography; COVID-19; Mortality.**

Palavras-chave: **Doenças Cardiovasculares; Ecocardiografia; COVID-19; Mortalidade.**

Introduction

SARS-CoV-2 was first reported in Wuhan, China, in December 2019. The virus subsequently spread around the world, leading to the COVID-19 pandemic, which was officially declared in March 11, 2020.1

The COVID-19 pandemic became one of the greatest health crises in modern history. By 2022, the World Health Organization confirmed 526,182,662 cases and 6,286,057 deaths, underscoring the serious consequences of the disease worldwide.[2] In this scenario, Brazil ranked as the country with the third highest number of cases (30,846,602) and the second highest number of deaths (666,037). Initially, the North Region of Brazil recorded high infection and mortality rates, although it was later considered the region with the lowest number of cases and deaths in the country.[3]

A study conducted in China estimated a COVID-19 case fatality rate of 2.3%, reaching as high as 10.5% in patients with cardiovascular comorbidities.[4] Beyond respiratory symptoms, infection with SARS-CoV-2 has been associated with a range of cardiovascular complications, including acute myocardial injury, cardiac arrhythmias, myocarditis, and venous thromboembolism.[5]

Echocardiography has played a central role in the diagnosis of cardiovascular complications in patients with

Mailing Address: João Henrique Andrade de Almeida •
Universidade do Estado do Pará. Tv. Perebebuí, 2623. Postal code: 66087-662. Marco, Belém, PA – Brazil
E-mail: joaohenriqueandrade@hotmail.com
Manuscript received January 15, 2026, revised manuscript February 15, 2026, accepted March 1, 2026
Editor responsible for the review: Marcelo Tavares

DOI: https://doi.org/10.36660/abcimg.20260005i

Original Article

Central Illustration: Cardiovascular Complications in Patients with COVID-19 and Their Relationship with Mortality: An Echocardiographic Perspective

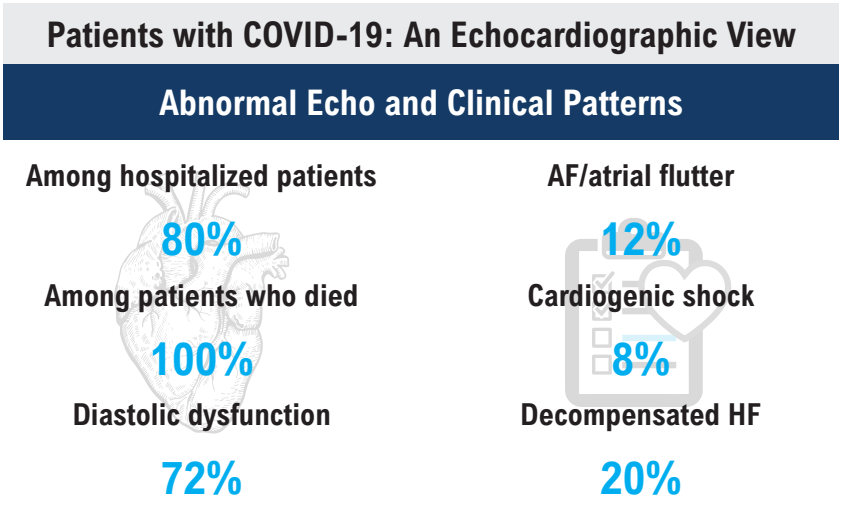

Arq Bras Cardiol: Imagem cardiovasc. 2026;39(1):e20260005

AF: atrial fibrillation; Echo: echocardiogram; HF: heart failure.

COVID-19.[6] During the disease outbreak, echocardiography proved to be an important imaging method, due to its greater portability compared to other imaging modalities, allowing for bedside assessment, especially in critically ill or isolated patients.[6]

While the cardiovascular complications of SARS-CoV-2 infection have already been widely explored by several international scientific studies, there is a significant lack of data from the North Region of Brazil. Accordingly, this study aimed to identify cardiovascular abnormalities among individuals with COVID-19 admitted to a hospital in the Brazilian Legal Amazon, and to assess their relationship with disease-related mortality.

Methods

Ethical considerations

The research team strictly followed Resolution 466/2012, issued by the Brazilian National Health Council. Accordingly, the study received ethical approval from the Research Ethics Committee on Human Beings of the Evandro Chagas Institute (approval number 5.540.025, July 22, 2022).

No direct contact with subjects took place during this retrospective study, which only used anonymized data extracted from medical records. For this reason, the Research Ethics Committee granted a waiver of informed consent.

We committed to using the data exclusively for the study's purposes, maintaining confidentiality and privacy as required by Resolution 466/2012.

Study characterization

This observational epidemiological study adopted a longitudinal and retrospective design to investigate cardiovascular complications associated with COVID-19 in hospitalized patients who underwent transthoracic Doppler echocardiography.

This research report was prepared in accordance with the STROBE recommendations.

Study setting and population

We conducted the research at Hospital Guadalupe, located in the city of Belém, Pará, in the North Region of Brazil. Data were collected from medical records of patients admitted to this facility between March 2020 and December 2020.

Inclusion and exclusion criteria

This research included adults of both sexes, aged 18 years or older, diagnosed with SARS-CoV-2 pulmonary infection, who underwent transthoracic Doppler echocardiography during their hospital stay. Records lacking sufficient data for analysis were excluded.

COVID-19 diagnosis

Participants were tested for SARS-CoV-2 using real-time reverse transcription polymerase chain reaction (RT-PCR), the preferred method for diagnosing COVID-19.

Nevertheless, when RT-PCR results were not recorded, we adopted the Operational Definitions of the Brazilian Ministry of Health (2021) for confirming positive cases.[8]

Cardiovascular involvement

The clinical presentations of COVID-19–related cardiovascular involvement were cardiogenic shock, decompensated heart failure, myocarditis, pericarditis, and cardiac arrhythmias.

Echocardiographic findings

The main echocardiographic findings were identified through exams performed with a CX50 portable ultrasound device (Philips Medical Systems), which was widely employed in similar investigations.

The echocardiographic measurements followed the recommendations of the American Society of Echocardiography and the European Association of Cardiovascular Imaging.[8,9] The median number of days between hospital admission and examination was 6 days.

Data collection

The following variables were collected: previous medical history, cardiovascular risk factors, pre-existing cardiovascular diseases prior to SARS-CoV-2 infection, echocardiographic signs of cardiovascular complications, and clinical outcomes.

As some of the selected medical records lacked electrocardiogram (ECG) results, the identification of cardiac arrhythmias occasionally relied on descriptive diagnoses, without direct interpretation of ECG tracings.

Data analysis

The dataset was organized in a Microsoft Excel spreadsheet. Subsequently, the sample was characterized based on the absolute and relative frequencies of its epidemiological and clinical variables. Continuous variables were expressed as mean ± standard deviation.

We applied Fisher's exact test to explore possible associations among cardiovascular complications, echocardiographic findings, and clinical outcomes. In addition, we performed a statistical analysis using Bioestat software (version 5.3), with a α value < 0.05 considered statistically significant.

Results

We initially analyzed 284 echocardiograms. After removing outpatient procedures, 192 records remained. Among the inpatients, only 25 had a confirmed COVID-19 diagnosis, thus comprising the final study sample.

Data were collected from the medical records of these 25 patients who were hospitalized with COVID-19 and underwent echocardiography during their hospital stay. The most relevant data are summarized in the Central Illustration.

Among the 25 medical records evaluated, 60% (15/25) were from male patients, and 40% (10/25) were female. The mean age of the patients was 69.6 ± 14.4 years. Figure 1 presents the age distribution of study participants.

The cardiovascular risk factors identified at the time of hospital admission are shown in Table 1.

Table 2 details the forms of cardiovascular involvement according to their echocardiographic abnormalities and clinical manifestations, as well as their association with the mortality rate.

Figure 2 illustrates outcomes related to the number of deaths and hospital discharges of the patients.

Table 3 displays clinical presentations of cardiovascular involvement, exploring their link with the echocardiographic findings.

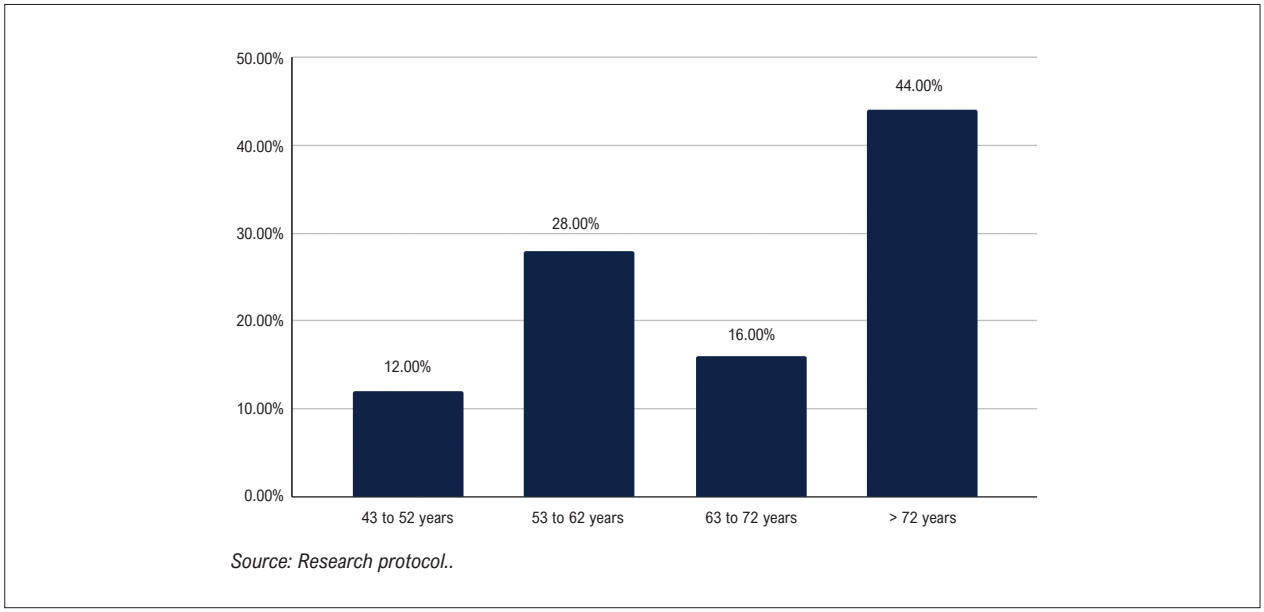

Figure 1 – *Age distribution of the study population hospitalized at Hospital Guadalupe, Belém, Pará, Brazil, between March 2020 and December 2020.*

Table 1 – Cardiovascular risk factors identified in patients hospitalized with COVID-19 at Hospital Guadalupe, in Belém, Pará, Brazil, between March 2020 and December 2020.

Cardiovascular risk factors	N = 25	%
Systemic arterial hypertension	23	92.0
Diabetes mellitus	11	44.0
Obesity	8	32.0
Coronary artery disease	7	28.0
Cardiac arrhythmias	4	16.0
Previous smoking	3	12.0
Heart failure	1	4.0
Alzheimer's disease	1	4.0
Asthma	1	4.0
COPD, pulmonary fibrosis	1	4.0
Chronic kidney disease	1	4.0

Source: Research protocol. COPD: chronic obstructive pulmonary disease. %: Frequency; N: Records analyzed.

Table 2 – Clinical and echocardiographic alterations and their association with the mortality rate of patients hospitalized with COVID-19 at Hospital Guadalupe, in Belém, Pará, Brazil, between March 2020 and December 2020.

Cardiovascular involvement	Discharge (n = 18)	%	Death (n = 7)	%	Total (n = 25)	%	p value
Abnormal echocardiogram							
Yes	13	72.2	7	100.0	20	80.0	0.2743
No	5	27.8	–	–	5	20.0	
AF/atrial flutter							
Yes	2	11.1	3	42.9	5	20.0	0.113
No	16	88.9	4	57.1	20	80.0	
Decompensated HF							
Yes	1	5.6	2	28.6	3	12.0	0.1796
No	17	94.4	5	71.4	22	80.0	
Cardiogenic shock							
Yes	–	–	2	28.6	2	8.0	0.07
No	18	100.0	5	71.4	23	92.0	

*Source: Research protocol. Dashes (–) indicate a value of zero, not resulting from rounding. AF: atrial fibrillation; HF: heart failure. %: Frequency; N: Records analyzed. * Fisher's exact test.*

Lastly, the association between echocardiographic abnormalities and clinical outcomes is displayed in Table 4, offering insights into their prognostic value.

Discussion

Statistical analysis of data from the medical records allowed the characterization of the clinical and epidemiological profile of the patients diagnosed with COVID-19 who underwent echocardiography during hospitalization.

Among the selected patients, 60% were male, and 40% were female, with a mean age of 69.6 ± 14.4 years. The predominance of male patients (71.4%) among the deaths recorded is in agreement with findings from a similar study,[10] suggesting male sex as a possible marker of mortality.

Overall, 92% of study participants had a prior diagnosis of systemic arterial hypertension, 44% showed type 2 diabetes mellitus, and 32% were obese. Notably, the proportion of hypertensive patients was considerably higher than in other investigations, which ranged from 57% to 69%.[11-14] We believe this

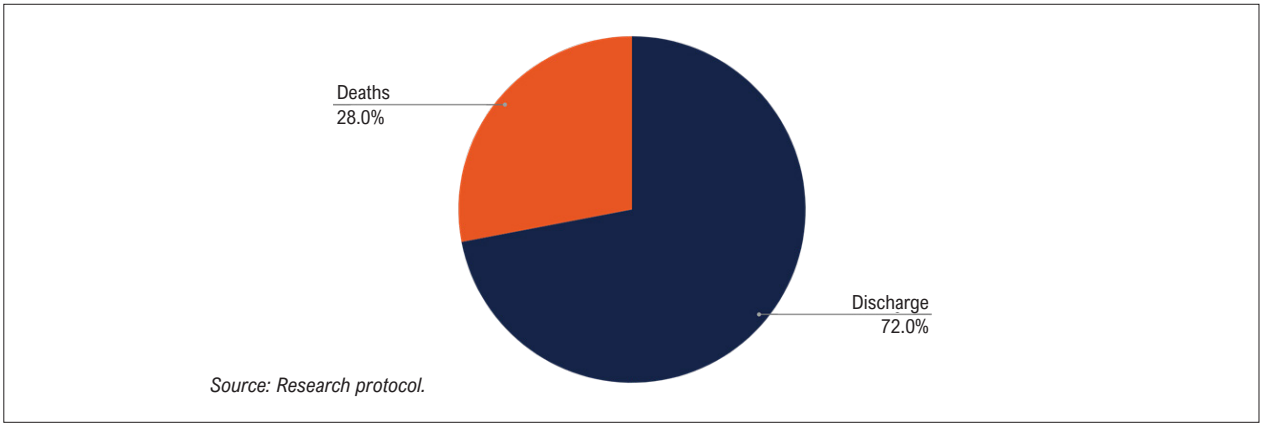

Figure 2 – *Outcomes related to the number of deaths and hospital discharges of patients hospitalized with COVID-19 at Hospital Guadalupe in Belém, Pará, Brazil, between March 2020 and December 2020.*

Table 3 – Cardiovascular involvement and its association with echocardiographic findings in patients hospitalized with COVID-19 at Hospital Guadalupe in Belém, Pará, Brazil, between March 2020 and December 2020.

Cardiovascular involvement	Normal (n = 5)	%	Abnormal (n = 20)	%	Total (n = 25)	%	p value
AF/Atrial flutter							
Yes	–	–	5	25.0	5	20.0	0.544
No	5	100.0	15	75.0	20	80.0	
Decompensated HF							
Yes	–	–	3	15.0	3	12.0	0.587
No	5	100.0	17	85.0	22	88.0	
Cardiogenic shock							
Yes	–	–	2	10.0	2	8.0	1.0
No	5	100.0	18	90.0	23	92.0	

*Source: Research protocol. Dashes (–) indicate a value of zero, not resulting from rounding. AF: atrial fibrillation; HF: heart failure. %: Frequency; N: Records analyzed. * Fisher's exact test.*

may be explained by the higher prevalence of the disease in Belém than in the settings where the referenced studies were performed.

Regarding the cardiovascular abnormalities detected by echocardiography, 80% of the exams revealed alterations. Among them, the main finding was diastolic dysfunction, present in 72% of the participants. This frequency was higher than that reported in a more statistically robust study, in which only 16% of individuals exhibited dysfunction.[11] Conversely, this discrepancy may plausibly be attributed to the higher burden of comorbidities in the current sample, especially hypertension and diabetes.

None of the patients without echocardiographic alterations presented atrial fibrillation, atrial flutter, heart failure, or cardiogenic shock. On the other hand, among individuals with echocardiographic abnormalities, these conditions were diagnosed in 25%, 15%, and 10% of cases, respectively ($p > 0.05$). Although cardiovascular complications were only observed in the group with echocardiographic findings, it was not possible to infer a statistically significant association ($p > 0.05$).

The observed mortality rate was 28%, a value higher than the 20% and 15% reported in similar studies,[15,16] but lower than the 32% and 38% found in other investigations,[14,17] possibly reflecting differences in the severity criteria adopted.

All deaths (100%) occurred in patients with echocardiographic abnormalities, indicating a trend whose validity is limited by the small sample size.

Pericardial effusion has been described as one of the most common pathological findings in SARS-CoV-2 infection, resulting from pericarditis. Interestingly, no cases of pericardial effusion were identified among the study participants, differing from the 30% reported in a similar study.[18] This discrepancy is likely due to the greater severity of that study's sample.

Table 4 – Echocardiographic abnormalities and their association with the outcomes of patients hospitalized for COVID-19 at Hospital Guadalupe, in Belém, Pará, Brazil, between March 2020 and December 2020.

Abnormalities	Discharge n = 18	%	Death n = 7	%	Total n = 25	%	p value
Diastolic dysfunction							
Yes	12	66.67	6	85.7	18	72.0	0.6257
No	6	33.33	1	14.3	7	28.0	
Left atrial dilation							
Yes	5	27.78	3	42.9	8	32.0	0.6395
No	13	72.22	4	57.1	17	68.0	
Hypertrophy							
Yes	5	27.78	2	28.6	7	28.0	0.9931
No	13	72.22	5	71.4	18	72.0	
Aortic root dilatation							
Yes	3	16.67	–	–	3	12.0	0.5343
No	15	83.33	7	100.0	22	88.0	
Segmental dysfunction							
Yes	–	–	2	28.6	2	8.0	0.07
No	18	100	5	71.4	23	92.0	
Elevated PSAP							
Yes	1	5.556	1	14.3	2	8.0	0.49
No	17	94.44	6	85.7	23	92.0	
Systolic dysfunction							
Yes	–	–	1	14.3	1	4.0	0.28
No	18	100	6	85.7	24	96.0	
Right atrial dilation							
Yes	1	5.556	–	–	1	4.0	1.0
No	17	94.44	7	100.0	24	96.0	

*Source: Research protocol. Dashes (–) indicate a value of zero, not resulting from rounding. PSAP: pulmonary artery systolic pressure. %: Frequency; N: Records analyzed. * Fisher's exact test.*

Conclusions

The vast majority of patients hospitalized for COVID-19 analyzed in this study had abnormal echocardiographic findings, with diastolic dysfunction being the most frequent. Among those who died, at least one echocardiographic abnormality was detected.

The cardiovascular complications observed included atrial fibrillation and flutter, decompensated heart failure, and cardiogenic shock. However, these complications were not present in patients with normal echocardiographic findings.

Although a likely trend toward increased mortality from SARS-CoV-2 infection can be inferred among patients who experienced cardiovascular complications, the small sample size of this study limits the statistical strength of the associations. Accordingly, the present study serves an exploratory purpose in depicting the reality of the North Region of Brazil during the COVID-19 pandemic.

Acknowledgements

We thank Hospital Guadalupe for authorizing the data collection on its premises.

Author Contributions

Conception and design of the research: : Almeida JHA, Ferreira GMA, Andrade MAM, Nunes HM, Costa IB; acquisition of data: Almeida JHA, Andrade MAM; analysis and interpretation of the data: Almeida JHA, Ferreira GMA; statistical analysis: Almeida JHA; writing of the manuscript: Almeida JHA, Ferreira GMA, Andrade MAM; critical revision of the manuscript for intellectual content: Ferreira GMA, Nunes HM, Costa IB; manuscript formatting: Ferreira GMA; supervision: Nunes HM; co-supervision: Costa IB.

Potential Conflict of Interest

No potential conflict of interest relevant to this article was reported.

Sources of Funding

There were no external funding sources for this study.

Study Association

This article is part of the thesis of master submitted by João Henrique Andrade de Almeida, from Instituto Evandro Chagas.

Ethics Approval and Consent to Participate

This study was approved by the Ethics Committee of the Instituto Evandro Chagas under the protocol number 5.540.025. All the procedures in this study were in accordance with the 1975 Helsinki Declaration, updated in 2013. Informed consent was obtained from all participants included in the study.

Use of Artificial Intelligence

The authors did not use any artificial intelligence tools in the development of this work.

Availability of Research Data

The underlying content of the research text is contained within the manuscript.

References

1. Dong E, Du H, Gardner L. An Interactive Web-Based Dashboard to Track COVID-19 in Real Time. Lancet Infect Dis. 2020;20(5):533-4. doi: 10.1016/S1473-3099(20)30120-1.
2. World Health Organization. WHO Coronavirus (COVID-19) Dashboard [Internet]. Geneva: WHO; 2025 [cited 2026 Mar 20]. Available from: https://covid19.who.int/.
3. Brasil. Ministério da Saúde. Secretaria de Vigilância em Saúde. Doença pelo Novo Coronavírus – COVID-19: Boletim Epidemiológico Especial. Brasília: Ministério da Saúde; 2022.
4. Wu Z, McGoogan JM. Characteristics of and Important Lessons from the Coronavirus Disease 2019 (COVID-19) Outbreak in China: Summary of a Report of 72 314 Cases from the Chinese Center for Disease Control and Prevention. JAMA. 2020;323(13):1239-42. doi: 10.1001/jama.2020.2648.
5. Driggin E, Madhavan MV, Bikdeli B, Chuich T, Laracy J, Biondi-Zoccai G, et al. Cardiovascular Considerations for Patients, Health Care Workers, and Health Systems during the COVID-19 Pandemic. J Am Coll Cardiol. 2020;75(18):2352-71. doi: 10.1016/j.jacc.2020.03.031.
6. Coelho-Filho OR, PINTO IM, VIEIRA MLC. Cardiovascular Imaging in COVID-19. Rev Soc Cardiol Estado de São Paulo 2020;30(4):490-7. doi: 10.29381/0103-8559/20203004490-7.
7. Brasil. Ministério da Saúde. Secretaria de Vigilância em Saúde. Guia de Vigilância Epidemiológica: Emergência de Saúde Pública de Importância Nacional pela Doença pelo Coronavírus 2019 – COVID-19. Brasília: Ministério da Saúde; 2021.
8. Lang RM, Badano LP, Mor-Avi V, Afilalo J, Armstrong A, Ernande L, et al. Recommendations for Cardiac Chamber Quantification by Echocardiography in Adults: An Update from the American Society of Echocardiography and the European Association of Cardiovascular Imaging. J Am Soc Echocardiogr. 2015;28(1):1-39.e14. doi: 10.1016/j.echo.2014.10.003.
9. Argulian E, Sud K, Vogel B, Bohra C, Garg VP, Talebi S, et al. Right Ventricular Dilation in Hospitalized Patients with COVID-19 Infection. JACC Cardiovasc Imaging. 2020;13(11):2459-61. doi: 10.1016/j.jcmg.2020.05.010.
10. Schröder J, Kahlke V, Staubach KH, Zabel P, Stüber F. Gender Differences in Human Sepsis. Arch Surg. 1998;133(11):1200-5. doi: 10.1001/archsurg.133.11.1200.
11. Churchill TW, Bertrand PB, Bernard S, Namasivayam M, Churchill J, Crousillat D, et al. Echocardiographic Features of COVID-19 Illness and Association with Cardiac Biomarkers. J Am Soc Echocardiogr. 2020;33(8):1053-4. doi: 10.1016/j.echo.2020.05.028.
12. Jain SS, Liu Q, Raikhelkar J, Fried J, Elias P, Poterucha TJ, et al. Indications for and Findings on Transthoracic Echocardiography in COVID-19. J Am Soc Echocardiogr. 2020;33(10):1278-84. doi: 10.1016/j.echo.2020.06.009.
13. Jarori U, Maatman TK, Maatman B, Mastouri R, Sawada SG, Khemka A. Mitral Annular Plane Systolic Excursion: An Early Marker of Mortality in Severe COVID-19. J Am Soc Echocardiogr. 2020;33(11):1411-3. doi: 10.1016/j.echo.2020.08.012.
14. Sud K, Vogel B, Bohra C, Garg V, Talebi S, Lerakis S, et al. Echocardiographic Findings in Patients with COVID-19 with Significant Myocardial Injury. J Am Soc Echocardiogr. 2020;33(8):1054-5. doi: 10.1016/j.echo.2020.05.030.
15. Mahmoud-Elsayed HM, Moody WE, Bradlow WM, Khan-Kheil AM, Senior J, Hudsmith LE, et al. Echocardiographic Findings in Patients with COVID-19 Pneumonia. Can J Cardiol. 2020;36(8):1203-7. doi: 10.1016/j.cjca.2020.05.030.
16. Li Y, Li H, Zhu S, Xie Y, Wang B, He L, et al. Prognostic Value of Right Ventricular Longitudinal Strain in Patients with COVID-19. JACC Cardiovasc Imaging. 2020;13(11):2287-99. doi: 10.1016/j.jcmg.2020.04.014.
17. Szekely Y, Lichter Y, Taieb P, Banai A, Hochstadt A, Merdler I, et al. Spectrum of Cardiac Manifestations in COVID-19: A Systematic Echocardiographic Study. Circulation. 2020;142(4):342-53. doi: 10.1161/CIRCULATIONAHA.120.047971.
18. Santos BMD, Sacilotto L. Cardiac Arrhythmias and COVID-19: Side-by-Side in the Pandemic. Arq Bras Cardiol. 2021;117(5):1016-7. doi: 10.36660/abc.20210810.

Correlation Between Venous Excess Ultrasound and N-Terminal Pro-B-Type Natriuretic Peptide Levels in Patients With Acute Decompensated Heart Failure

Marcella Pereira Flores,[1,2] Alexandre Costa Souza,[1,2] Marcus Vinicius Silva Freire de Carvalho,[1,2] Rodrigo Morel Vieira de Melo,[1,2] Lívia Rodrigues Sampaio Cavalcante,[1,2] Natália Duarte Barroso,[1,2] Yuri Xavier de Carvalho,[1,2] Raisa Mainarte Franco Barros,[1,2] Clara Talita Silva Lobo,[1,2] Adriano Chaves de Almeida Filho[1,2]

Hospital São Rafael,[1] Salvador, BA – Brazil

Instituto D'Or de Pesquisa e Ensino,[2] Rio de Janeiro, RJ – Brazil

Abstract

Background: The Venous Excess Ultrasound (VExUS) score has been proposed as an ultrasonographic method for assessing systemic venous congestion in patients with acute decompensated heart failure (ADHF). However, the relationship between VExUS and the biomarker N-terminal pro-B-type natriuretic peptide (NT-proBNP) remains unclear in literature.

Objectives: To evaluate the correlation between the VExUS score and serum NT-proBNP levels in patients with ADHF.

Methods: This retrospective observational study included 117 patients hospitalized with ADHF. Systemic venous congestion was assessed using the VExUS score, and serum NT-proBNP levels were obtained from laboratory records. Comparisons between groups were performed using the Kruskal-Wallis test, followed by Dunn's test for multiple comparisons. The strength of association between variables was analyzed using Spearman's correlation coefficient.

Results: NT-proBNP levels increased progressively with increasing VExUS severity, with median values of 2,890 pg/mL (VExUS 0), 4,700 pg/mL (VExUS 1), 5,430 pg/mL (VExUS 2), and 13,200 pg/mL (VExUS 3). Statistical analysis demonstrated a significant difference between groups (Kruskal-Wallis: $\chi^2 = 39.18$; $p < 0.0001$). Dunn's test indicated that patients with VExUS 3 had significantly higher NT-proBNP levels compared with the other groups ($p < 0.01$). A moderate positive correlation was observed between the variables (Spearman's coefficient $\rho = 0.567$; $p < 0.0001$).

Conclusion: The results indicate that the VExUS score is associated with NT-proBNP levels and may be integrated into clinical reasoning when assessing venous congestion in patients with ADHF.

Keywords: Heart Failure; Ultrasonics; Inpatients.

Introduction

Heart failure (HF) is a highly prevalent condition worldwide, affecting more than 64 million people and associated with significant impact on morbidity, mortality, and healthcare costs.[1] Over the past decades, a continuous increase has been observed in both the incidence and the clinical complexity of HF, accompanied by a higher number of hospitalizations and worse outcomes across different populations.[2] Recurrent hospitalizations after episodes of decompensation are common, occurring in approximately half of patients during early follow-up, which increases the demand for specialized care.[3]

Early recognition of signs of hypervolemia is essential in the management of acute decompensated HF (ADHF), particularly in emergency departments and specialized cardiology care units. Accurate identification of congestion allows timely therapeutic interventions, reduces the risk of hemodynamic deterioration, and is associated with better clinical outcomes. In the hospital setting, systematic assessment of volume status is crucial to guide decisions related to the use of diuretics, adjustment of perfusion-guided therapies, and the need for advanced support, contributing to greater safety and effectiveness of treatment.[4,5]

Among the complementary tests used in the evaluation of ADHF, the N-terminal fragment of pro-B-type natriuretic peptide (NT-proBNP) plays a relevant role in the characterization of congestion and prognostic stratification. Elevated levels of this biomarker are associated with greater clinical severity, increased risk of adverse events, and higher probability of rehospitalization, which reinforces its usefulness in monitoring patients during hospitalization and at the time of discharge.[6]

Mailing Address: Marcella Pereira Flores •
Hospital São Rafael. Avenida São Rafael, 2152. Postal code: 41253-190. São Marcos, Salvador, BA – Brazil
E-mail: marcellapflavigne@gmail.com
Manuscript received February 13, 2026, revised manuscript February 23, 2026, accepted February 23, 2026
Editor responsible for the review: Marcelo Tavares

DOI: https://doi.org/10.36660/abcimg.20260018i

Central Illustration: Correlation Between Venous Excess Ultrasound and N-Terminal Pro-B-Type Natriuretic Peptide Levels in Patients With Acute Decompensated Heart Failure

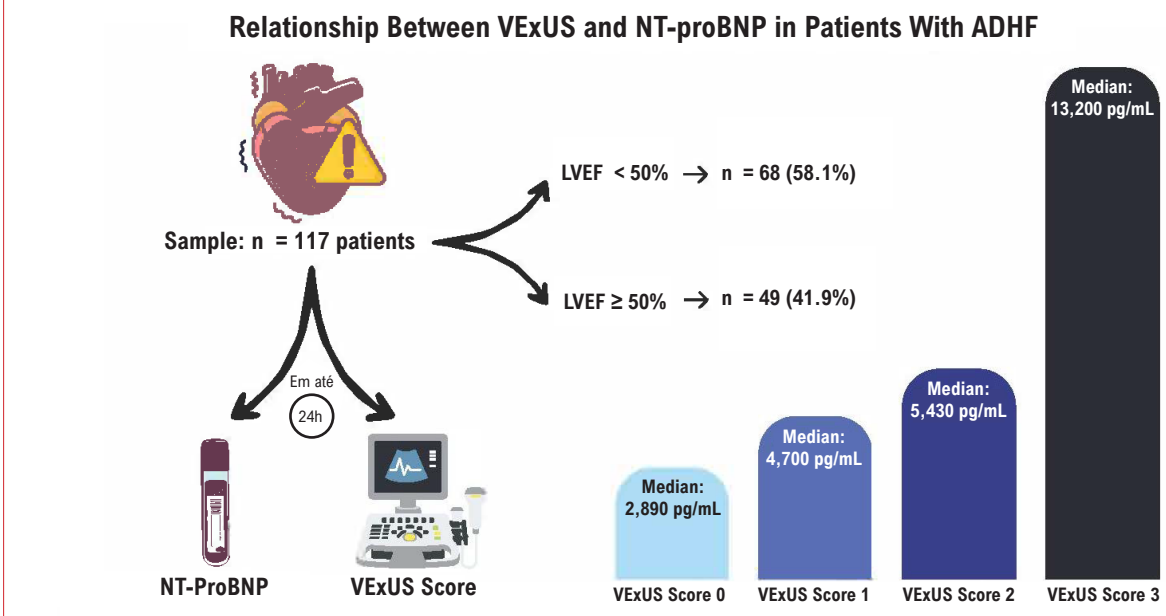

Arq Bras Cardiol: Imagem cardiovasc. 2026;39(1):e20260018

Correlation Between Venous Excess Ultrasound and N-Terminal Pro-B-Type Natriuretic Peptide Levels in Patients With Acute Decompensated Heart Failure. ADHF: acutely decompensated heart failure; LVEF: left ventricular ejection fraction; NT-proBNP: N-terminal pro-B-type natriuretic peptide; VExUS: Venous Excess Ultrasound.

Point-of-care ultrasound (POCUS) has emerged as a complementary tool in the assessment of congestion in patients with ADHF, as it allows direct analysis of venous structures and provides additional information to clinical examination and laboratory markers. The Venous Excess Ultrasound (VExUS) score was proposed as a structured method to quantify systemic venous congestion, integrating findings from the inferior vena cava and patterns of hepatic, portal, and renal venous flow.[7] Recent studies have demonstrated that VExUS may assist in identifying residual congestion and contribute to therapeutic decision-making during hospitalization.[8] In addition, POCUS shows satisfactory interobserver agreement in the evaluation of venous parameters, which reinforces its usefulness in emergency departments and cardiology units.[8]

Despite advances in the use of POCUS and the growing application of the VExUS score in the assessment of systemic venous congestion, the relationship between this method and laboratory markers widely used in clinical practice, such as NT-proBNP, remains poorly explored. Understanding this potential association may contribute to improving the characterization of volume status in patients with ADHF. Therefore, the present study aimed to evaluate the correlation between the VExUS score and serum NT-proBNP levels in patients hospitalized with ADHF.

Methods

Study design and population

This was a cross-sectional observational study conducted with patients admitted with ADHF. The sample included 117 hospitalized patients, all evaluated for systemic venous congestion using the VExUS score and undergoing serum measurement of the NT-proBNP biomarker.

Ultrasound assessment and laboratory sampling were performed within the first 24 hours after admission to the emergency department of a tertiary referral hospital in the city of Salvador, state of Bahia, between November 2023 and December 2024.

Patients without complete records of the ultrasound examination required for VExUS score determination, without available NT-proBNP measurement within the established period, or with a diagnosis of advanced liver disease were excluded because of the potential interference with the venous parameters analyzed. After applying these criteria, the final sample consisted of 117 patients.

Clinical assessment and definition of variables

Clinical data were obtained through review of medical records, including age, sex, left ventricular ejection fraction

(LVEF), and hemodynamic profile at admission according to the Stevenson classification. Other clinical and laboratory variables were used to characterize the sample.

The main exposure variable was the VExUS score, considered in four categories (0, 1, 2, and 3), corresponding to the grading of systemic venous congestion. The main outcome variable was the serum NT-proBNP level (pg/mL), analyzed as a continuous variable.

Ultrasound assessment and Venous Excess Ultrasound score

Systemic venous congestion was assessed by POCUS using a Vivid™ iq Ultrasound System (GE HealthCare, USA). Different transducers were used according to the evaluation window: a sector transducer for cardiac windows and a convex transducer for evaluation of the abdominal and retroperitoneal venous system.

Examinations were performed with the patient in the supine position, with the head of the bed elevated to approximately 30°. During acquisition of venous flow signals, brief periods of apnea were attempted whenever clinically feasible to reduce respiratory artifacts and improve the definition of Doppler waveforms, particularly in smaller vessels such as the renal interlobar veins.

During evaluation of hepatic venous flow, simultaneous electrocardiographic recording was used, allowing more precise identification of the S (systolic) and D (diastolic) waves and ensuring greater uniformity in the interpretation of flow patterns.

The ultrasound windows analyzed included the inferior vena cava, hepatic venous flow, portal flow, and renal venous flow, according to the VExUS score protocol. The diameter of the inferior vena cava and the venous flow patterns in the three abdominal territories were recorded and classified according to the criteria established for the VExUS system. Based on these findings, patients were classified into VExUS scores 0, 1, 2, or 3, representing increasing degrees of systemic venous congestion.

Measurement of N-terminal pro-B-type natriuretic peptide

Serum NT-proBNP levels were obtained from laboratory tests performed during hospitalization for ADHF, according to the institutional routine of the service. Measurements were performed using standardized immunometric methods in the local laboratory.

Values were expressed in pg/mL and used in the statistical analyses without additional transformation in the original protocol.

Statistical analysis

Initially, patients were stratified into four groups according to the VExUS score (0, 1, 2, and 3). Comparison of NT-proBNP levels between groups was performed using the Kruskal-Wallis test, followed by Dunn's test for multiple pairwise comparisons.

The strength of association between the VExUS score and NT-proBNP levels was evaluated using Spearman's correlation coefficient (ρ), considering the ordinal nature of VExUS and the expected asymmetric distribution of NT-proBNP values.

To model the relationship between the VExUS score and NT-proBNP, a Gamma regression model with a logarithmic link function was used, with NT-proBNP as the dependent variable and the VExUS score as the explanatory variable. Model fit was evaluated using McFadden's pseudo R^2.

Continuous variables were assessed for distribution using the Shapiro-Wilk test. Given the asymmetry observed in most variables, results were presented as median and interquartile range. Categorical variables were expressed as absolute frequencies and proportions.

The significance level adopted was 5% ($p < 0.05$). All analyses were performed using R software, version 4.4.3.

Results

Sample characteristics

In the present study, 117 patients hospitalized with ADHF were evaluated. The median age was 79 years. Of the total, 53 patients were female (45.3%) and 64 were male (54.7%).

Regarding left ventricular function, 68 patients had LVEF $< 50\%$, whereas 49 had LVEF $\geq 50\%$. Concerning the hemodynamic profile at admission, profile B (warm and wet) was observed in 110 patients (94.0%), while profile C (cold and wet) was identified in seven patients (6.0%).

All patients included in the study had a complete ultrasound assessment required for VExUS score classification and serum NT-proBNP measurement performed within the first 24 hours after hospital admission.

Distribution of the Venous Excess Ultrasound score

Patients were stratified into four groups according to the VExUS score: VExUS 0 ($n = 21$), VExUS 1 ($n = 35$), VExUS 2 ($n = 31$), and VExUS 3 ($n = 30$). This distribution allowed comparison of serum NT-proBNP levels across different degrees of systemic venous congestion assessed by the score.

N-terminal pro-B-type natriuretic peptide levels according to the Venous Excess Ultrasound score

A progressive increase in the median NT-proBNP levels was observed as the VExUS score increased. The medians were 2,890 pg/mL in the VExUS 0 group, 4,700 pg/mL in the VExUS 1 group, 5,430 pg/mL in the VExUS 2 group, and 13,200 pg/mL in the VExUS 3 group.

Statistical analysis using the Kruskal-Wallis test demonstrated a significant difference between groups ($\chi^2 = 39.18$; $p < 0.0001$). In the multiple comparisons performed with Dunn's test, statistically significant differences were observed in comparisons involving the VExUS 3 group ($p < 0.01$).

Correlation between the Venous Excess Ultrasound score and the N-terminal pro-B-type natriuretic peptide

Correlation analysis between the VExUS score and serum NT-proBNP levels demonstrated a moderate positive correlation, with a Spearman coefficient of 0.567 ($p < 0.0001$).

In the Gamma regression model with a logarithmic link function, the VExUS score showed a β coefficient of 0.584 ($p < 0.0001$). The McFadden pseudo R^2 obtained was 0.024.

Discussion

Using POCUS in the assessment of systemic venous congestion has expanded in the context of cardiovascular diseases, particularly in ADHF. The analysis of hepatic, portal, and renal venous flow patterns, integrated with measurements of the inferior vena cava, has been recognized as an approach that complements clinical examination and provides a more comprehensive assessment of the patient's hemodynamic status.[9] The VExUS score emerged as a structured method to synthesize ultrasound findings related to venous overload, with increasing application in different clinical settings.[10] Recent reviews indicate that this tool provides a standardized and reproducible evaluation of systemic venous congestion, contributing to the understanding of the hemodynamic impact of increased venous pressures in different clinical conditions.[7,11,12]

NT-proBNP values showed progressively higher distribution across the categories of the VExUS score, as illustrated in the boxplot (Figure 1). A gradual increase in medians was observed between groups, accompanied by a greater interquartile range at higher score levels. In the VExUS 3 group, greater variability was observed, with the presence of values higher than those seen in the other categories. This graphical pattern demonstrates an upward trend in the distribution of the biomarker as the degree of systemic venous congestion estimated by VExUS increases, complementing the results obtained in the statistical analyses (Central Illustration).

Graphical analysis also demonstrated an ascending distribution of NT-proBNP values across the categories of the VExUS score. Figure 2 presents the scatter plot with the line fitted by Spearman correlation, showing a positive linear trend consistent with the observed coefficient ($\rho = 0.567$). Figure 3 illustrates the curve estimated by the Gamma regression model with a logarithmic link function, in which a progressive increase in predicted NT-proBNP values is observed across the different levels of the VExUS score.

Using Gamma regression with a logarithmic link function allowed appropriate modeling of the asymmetric distribution of NT-proBNP, characterized by wide dispersion and the presence of extreme values at higher levels of congestion. This model captured the exponential relationship between increasing VExUS score and rising biomarker levels, demonstrating a progressive intensification of NT-proBNP values as systemic venous congestion worsens. This approach complements the Spearman analysis by showing that the observed correlation, of moderate magnitude, accompanies the gradual increase in NT-proBNP levels as the VExUS score increases.[10,13,14]

This pattern suggests that the VExUS score, by quantifying the hemodynamic impact of increased venous pressures, objectively reflects the severity of volume decompensation, which is physiologically translated into the release of NT-proBNP.[15,16]

Consistent with the prognostic value of isolated congestion markers, the VExUS 3 score has been associated in other cohorts with more unfavorable clinical outcomes, including higher risk of worsening renal function, reduced natriuretic response, and resistance to diuretic therapy, in addition to worse overall prognosis. The ability of VExUS to dynamically monitor systemic venous congestion makes it potentially useful for guiding diuretic therapy, particularly in cases of cardiorenal syndrome, in which higher scores may support continuation of the diuretic strategy.[17-19]

NT-proBNP predominantly reflects myocardial stress and increased cardiac filling pressures, whereas the VExUS score expresses the hemodynamic consequences of systemic venous congestion by integrating ultrasound signs related to elevated venous pressure and the risk of organ dysfunction. Thus, both methods assess distinct and complementary pathophysiological dimensions of congestion in heart failure and may contribute to a more comprehensive and individualized clinical approach.[20-22]

Limitations of the study

This study has some limitations. It is a cross-sectional observational study conducted at a single center, with a final sample of 117 patients. The cross-sectional design limits the ability to infer causal relationships or to evaluate dynamic changes in venous congestion and NT-proBNP levels during hospitalization.

Although a strategy was adopted to reduce temporal bias, with both VExUS score assessment and NT-proBNP measurement performed within the first 24 hours after hospital admission, this time window, although short, represents a potential limitation considering the dynamic nature of ADHF and the therapeutic interventions initiated during this period.

The application of the VExUS score also has limitations inherent to its components and the clinical context in which it is used. Interpretation of hepatic vein Doppler may be influenced by the presence of significant tricuspid regurgitation and atrial fibrillation, conditions that may alter the venous flow pattern independently of the degree of congestion. Similarly, pulsatility of portal flow may be observed in young and healthy individuals, whereas its reduction may occur in parenchymal liver diseases. For this reason, patients with relevant structural liver disease were excluded from the analysis. Although integration of different venous territories in the VExUS score reduces dependence on a single parameter, these limitations should be considered when interpreting the findings.[10,22,23]

Future studies, preferably with a longitudinal design, will be necessary to evaluate the dynamic evolution of the

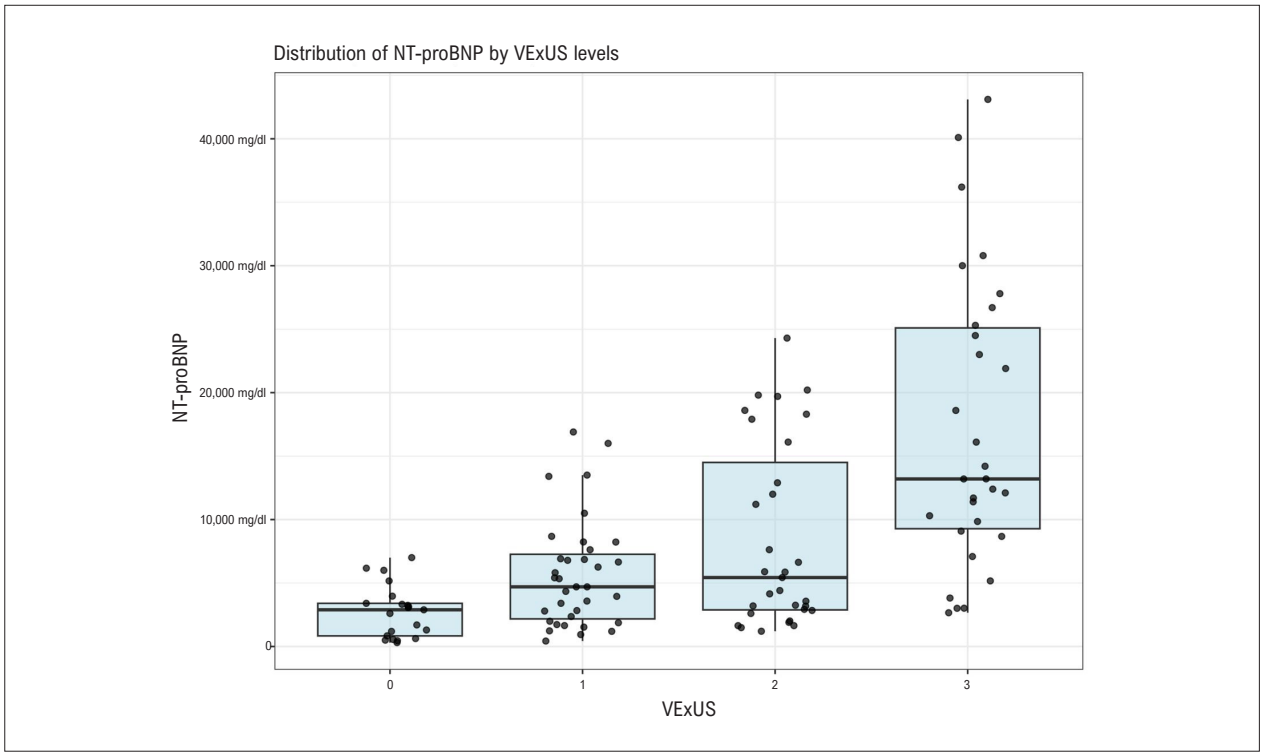

Figure 1 – *Distribution of NT-proBNP levels according to VExUS score categories. NT-proBNP: N-terminal pro-B-type natriuretic peptide; VExUS: Venous Excess Ultrasound.*

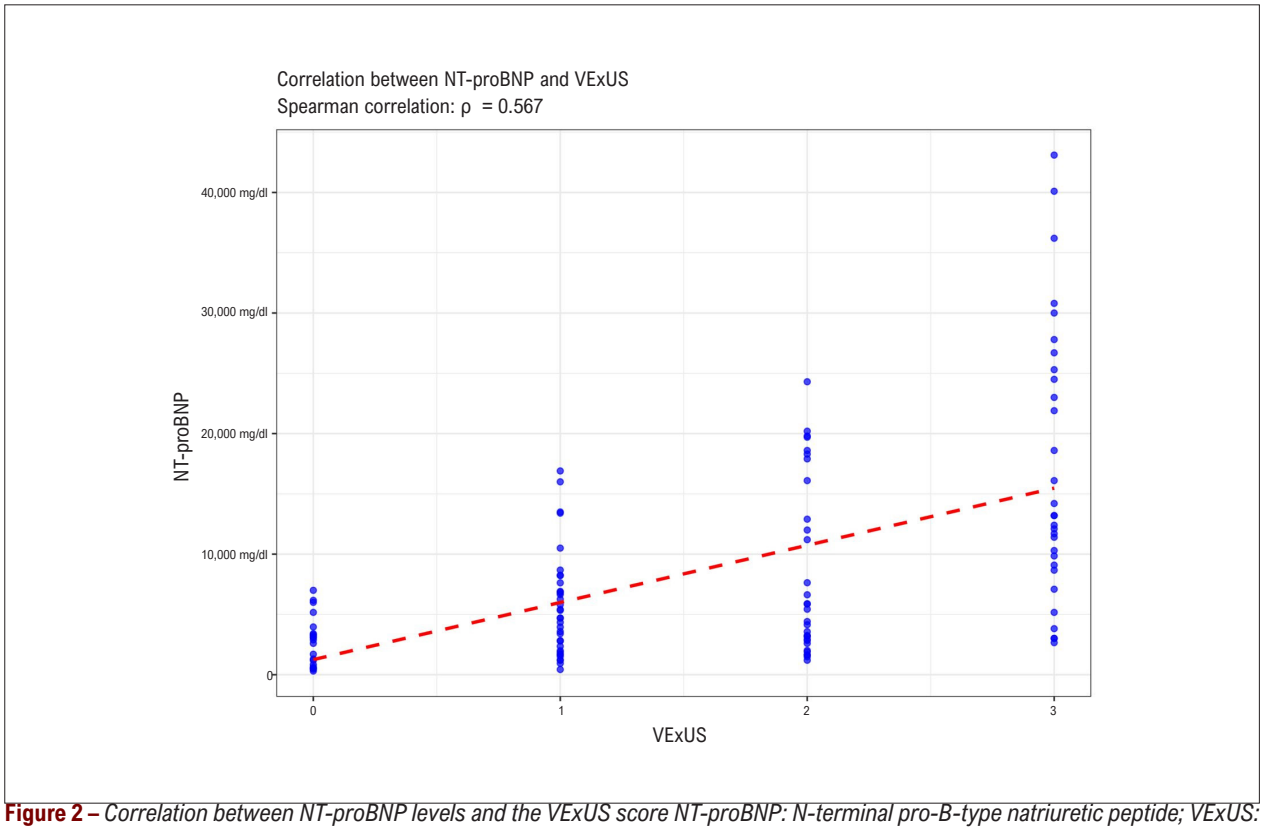

Figure 2 – *Correlation between NT-proBNP levels and the VExUS score NT-proBNP: N-terminal pro-B-type natriuretic peptide; VExUS: Venous Excess Ultrasound.*

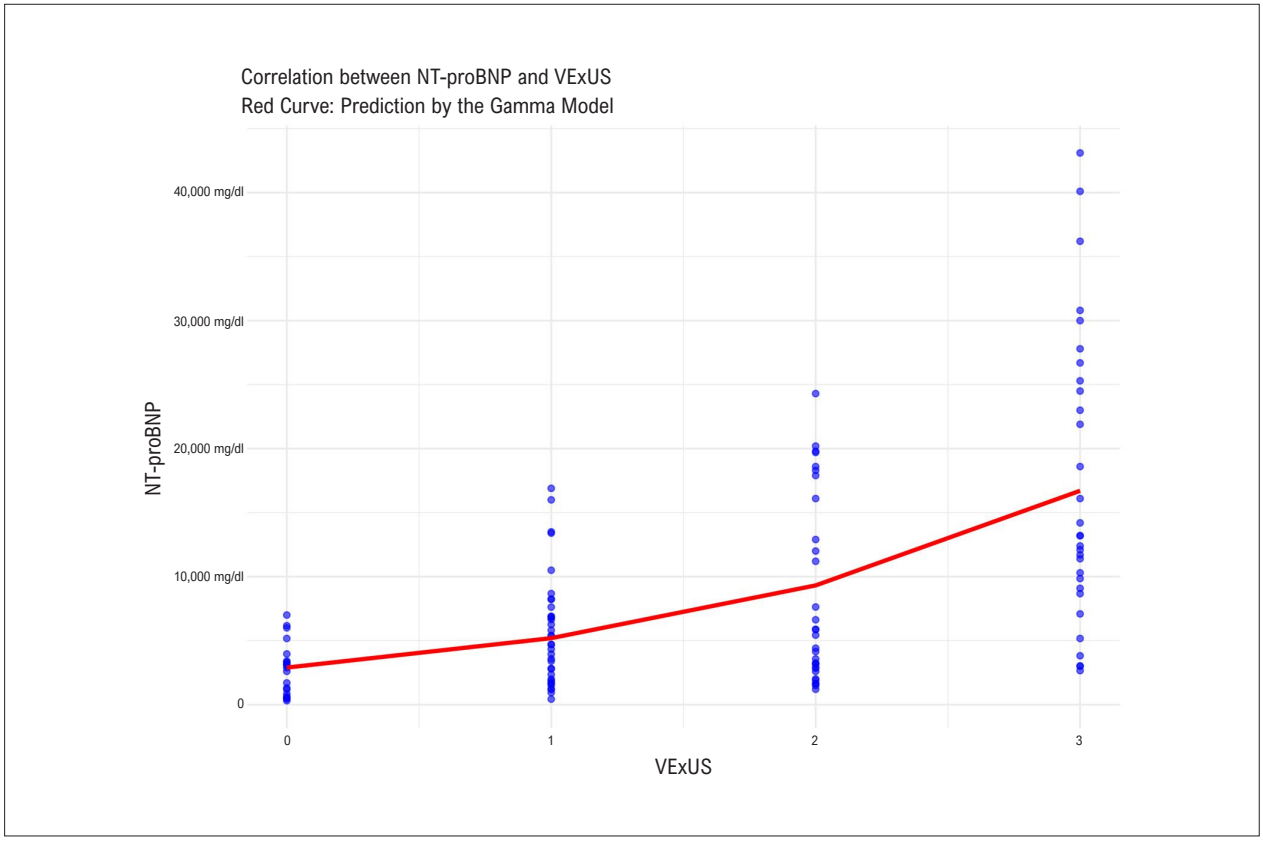

Figure 3 – *Relationship between NT-proBNP and the VExUS score estimated by a Gamma regression model. NT-proBNP: N-terminal pro-B-type natriuretic peptide; VExUS: Venous Excess Ultrasound.*

VExUS score during hospitalization and its relationship with the therapeutic strategies used. This type of approach may provide a more precise understanding of the role of systemic venous congestion assessed by VExUS in the clinical management of patients with ADHF.

Conclusion

The results of this study indicate that the VExUS score is associated with NT-proBNP levels, reinforcing its potential as a complementary tool in the evaluation of systemic venous congestion in patients with ADHF.

The integration of VExUS into clinical reasoning and biomarker interpretation may provide a more comprehensive perspective on volume status, contributing to a more individualized diagnostic and therapeutic approach.

Author Contributions

Conception and design of the research: Almeida Filho AC, Morel RV; acquisition of data: Cavalcante LRS, Carvalho YX, Barros RMF, Lobo CTS; analysis and interpretation of the data and statistical analysis: Souza AC; writing of the manuscript: Flores MP; critical revision of the manuscript for intellectual content: Carvalho MVSF, Barroso ND.

Potential Conflict of Interest

No potential conflict of interest relevant to this article was reported.

Sources of Funding

There were no external funding sources for this study.

Study Association

This study is not associated with any thesis or dissertation work.

Ethics Approval and Consent to Participate

This study was approved by the Ethics Committee on Animal Experiments of CONEP under the protocol number 84674724.7.0000.0048.

Use of Artificial Intelligence

The authors did not use any artificial intelligence tools in the development of this work.

Availability of Research Data

The underlying content of the research text is contained within the manuscript.

References

1. Groenewegen A, Rutten FH, Mosterd A, Hoes AW. Epidemiology of Heart Failure. Eur J Heart Fail. 2020;22(8):1342-56. doi: 10.1002/ejhf.1858.
2. Bragazzi NL, Zhong W, Shu J, Abu Much A, Lotan D, Grupper A, et al. Burden of Heart Failure and Underlying Causes in 195 Countries and Territories from 1990 to 2017. Eur J Prev Cardiol. 2021;28(15):1682-90. doi: 10.1093/eurjpc/zwaa147.
3. Dharmarajan K, Rich MW. Epidemiology, Pathophysiology, and Prognosis of Heart Failure in Older Adults. Heart Fail Clin. 2017;13(3):417-26. doi: 10.1016/j.hfc.2017.02.001.
4. Mullens W, Damman K, Harjola VP, Mebazaa A, Brunner-La Rocca HP, Martens P, Testani JM, et al. The Use of Diuretics in Heart Failure with Congestion - A Position Statement from the Heart Failure Association of the European Society of Cardiology. Eur J Heart Fail. 2019;21(2):137-55. doi: 10.1002/ejhf.1369.
5. McDonagh TA, Metra M, Adamo M, Gardner RS, Baumbach A, Böhm M, et al. 2023 Focused Update of the 2021 ESC Guidelines for the Diagnosis and Treatment of Acute and Chronic Heart Failure. Eur Heart J. 2023;44(37):3627-39. doi: 10.1093/eurheartj/ehad195.
6. Magalhães J, Soares F, Noya M, Neimann G, Andrade L, Correia L. NT-ProBNP at Admission versus NT-ProBNP at Discharge as a Prognostic Predictor in Acute Decompensated Heart Failure. Int J Cardiovasc Sci. 2017;30(6):469-75. doi: 10.5935/2359-4802.20170082.
7. Rinaldi PM, Rihl MF, Boniatti MM. VExUS Score at Discharge as a Predictor of Readmission in Patients with Acute Decompensated Heart Failure: A Cohort Study. Arq Bras Cardiol. 2024;121(5):e20230745. doi: 10.36660/abc.20230745.
8. Saadi MP, Machado GP, Silvano GP, Barbato JPR, Almeida RF, Scolari FL, et al. Assessment of Interrater Reliability in Point-of-Care Ultrasound for Assessing Congestion in Cardiovascular Intensive Care. Arq Bras Cardiol: Imagem cardiovasc. 2025;38(2):e20250022. Doi: 10.36660/abcimg.20250022i.
9. Rola P, Miralles-Aguiar F, Argaiz E, Beaubien-Souligny W, Haycock K, Karimov T, et al. Clinical Applications of the Venous Excess Ultrasound (VExUS) Score: Conceptual Review and Case Series. Ultrasound J. 2021;13(1):32. doi: 10.1186/s13089-021-00232-8.
10. Torres-Arrese M, Mata-Martínez A, Luordo-Tedesco D, García-Casasola G, Alonso-González R, Montero-Hernández E, et al. Usefulness of Systemic Venous Ultrasound Protocols in the Prognosis of Heart Failure Patients: Results from a Prospective Multicentric Study. J Clin Med. 2023;12(4):1281. doi: 10.3390/jcm12041281.
11. Cubo-Romano P, Torres-Macho J, Soni NJ, Reyes LF, Rodríguez-Almodóvar A, Fernández-Alonso JM, et al. Admission Inferior Vena Cava Measurements are Associated with Mortality after Hospitalization for Acute Decompensated Heart Failure. J Hosp Med. 2016;11(11):778-84. doi: 10.1002/jhm.2620.
12. Telo GH, Saadi MP, Silvano GP, Silveira AD, Biolo A. Contribution of Lung Ultrasound and VExUS in the Diagnosis and Monitoring of Patients with Heart Failure. ABC Heart Fail Cardiomyop. 2024;4(1):e20240010. doi: 10.36660/abchf.20240010.
13. Platz E, Lewis EF, Uno H, Peck J, Pivetta E, Merz AA, et al. Detection and Prognostic Value of Pulmonary Congestion by Lung Ultrasound in Ambulatory Heart Failure Patients. Eur Heart J. 2016;37(15):1244-51. doi: 10.1093/eurheartj/ehv745.
14. Ponikowski P, Voors AA, Anker SD, Bueno H, Cleland JGF, Coats AJS, et al. 2016 ESC Guidelines for the Diagnosis and Treatment of Acute and Chronic Heart Failure: The Task Force for the Diagnosis and Treatment of Acute and Chronic Heart Failure of the European Society of Cardiology (ESC) Developed with the Special Contribution of the Heart Failure Association (HFA) of the ESC. Eur Heart J. 2016;37(27):2129-200. doi: 10.1093/eurheartj/ehw128.
15. Guinot PG, Bahr PA, Andrei S, Popescu BA, Caruso V, Mertes PM, et al. Doppler Study of Portal Vein and Renal Venous Velocity Predict the Appropriate Fluid Response to Diuretic in ICU: A Prospective Observational Echocardiographic Evaluation. Crit Care. 2022;26(1):305. doi: 10.1186/s13054-022-04180-0.
16. Kenny JS, Prager R, Rola P, Haycock K, Basmaji J, Hernández G. Unifying Fluid Responsiveness and Tolerance with Physiology: A Dynamic Interpretation of the Diamond-Forrester Classification. Crit Care Explor. 2023;5(12):e1022. doi: 10.1097/CCE.0000000000001022.
17. Andrei S, Bahr PA, Nguyen M, Bouhemad B, Guinot PG. Prevalence of Systemic Venous Congestion Assessed by Venous Excess Ultrasound Grading System (VExUS) and Association with Acute Kidney Injury in a General ICU Cohort: A Prospective Multicentric Study. Crit Care. 2023;27(1):224. doi: 10.1186/s13054-023-04524-4.
18. Beaubien-Souligny W, Rola P, Haycock K, Bouchard J, Lamarche Y, Spiegel R, et al. Quantifying Systemic Congestion with Point-Of-Care Ultrasound: Development of the Venous Excess Ultrasound Grading System. Ultrasound J. 2020;12(1):16. doi: 10.1186/s13089-020-00163-w.
19. Argaiz ER. VExUS Nexus: Bedside Assessment of Venous Congestion. Adv Chronic Kidney Dis. 2021;28(3):252-61. doi: 10.1053/j.ackd.2021.03.004.
20. Maeder MT, Mariani JA, Kaye DM. Hemodynamic Determinants of Myocardial B-Type Natriuretic Peptide Release: Relative Contributions of Systolic and Diastolic Wall Stress. Hypertension. 2010;56(4):682-9. doi: 10.1161/HYPERTENSIONAHA.110.156547.
21. Rola P, Haycock K, Spiegel R, Beaubien-Souligny W, Denault A. VExUS: Common Misconceptions, Clinical Use and Future Directions. Ultrasound J. 2024;16(1):49. doi: 10.1186/s13089-024-00395-0.
22. Salgado AA, Bernardo MPL, Melo FM Netto. My Approach to Evaluate Systemic Venous Congestion: VExUS Protocol. Arq Bras Cardiol: Imagem Cardiovasc. 2024;37(2):e20240026. doi: 10.36660/abcimg.20240026.
23. Putz FJ, Kranert PC, Banas MC, Schierling W, Jung EM, Bergler T, et al. Renal Vein Blood Flow Patterns Identify Patients at Risk for Early Kidney Allograft Loss Due to Cardiac Postrenal Vein Congestion. J Clin Med. 2025;14(14):4897. doi: 10.3390/jcm14144897.

Phenotyping of Congestion in Decompensated Heart Failure: Life-Saving Accuracy

Amanda Fernandes[1]

Hospital Nossa Senhora das Neves,[1] *João Pessoa, PB – Brazil*

Short editorial related to the article: Correlation Between Venous Excess Ultrasound and N-Terminal Pro-B-Type Natriuretic Peptide Levels in Patients With Acute Decompensated Heart Failure

Diagnosing heart failure (HF) in patients with multiple comorbidities continues to pose a challenge, especially when overlaps with pulmonary disease, obesity, or atypical clinical presentation. In this context, complementary diagnostic tools, such as NT-proBNP and venous excess ultrasound (VExUS) score, enable earlier and more accurate assessment of congestion, reducing adverse effects and fostering timely implementation of guideline-directed medical therapy.[1]

Management of decompensated HF becomes even more complex when there is subclinical fluid retention, a frequently underestimated condition that is associated with higher rates of hospital readmission and a comparable mortality risk to that observed in patients with clinically evident edema.[2,3] In these scenarios, VExUS has become a central tool in the diagnostic and therapeutic arsenal, both in differentiating the etiology of dyspnea and in managing patients with overt congestion and cardiorenal syndrome, by allowing for safer and more individualized management of diuresis, minimizing the risk of kidney injury.[4]

A growing body of evidence has supported this role. Anastasiou et al.[5] demonstrated that the VExUS score outperformed other isolated markers of congestion, such as the inferior vena cava diameter, in predicting in-hospital mortality, reinforcing its prognostic value. Furthermore, a randomized clinical trial showed that VExUS-guided diuresis doubled the likelihood of achieving euvolemia in only 2 days when compared to standard care,[6] consolidating bedside ultrasound not only as a diagnostic tool, but as a natural extension of contemporary physical examination.

The role of natriuretic peptides, especially BNP and NT-proBNP, has been well established since the early 2000s. Values within the normal range have sensitivity greater than 90% for excluding HF diagnosis, whereas elevated levels have consistently been associated with worse cardiovascular outcomes and higher mortality.[7] The integration of biomarkers and ultrasound assessment of congestion, therefore, achieves strategic relevance by adding objectivity to risk stratification and allowing for earlier and more informed clinical decisions.

That notwithstanding, regional disparities and the need for specific training in VExUS still represent challenges to the widespread dissemination of this technology. In contrast, NT-proBNP is a widely available biomarker that is financially viable in the Brazilian Unified Health System (SUS) and relatively simple to interpret. Nevertheless, studies directly correlating NT-proBNP levels with VExUS scores remain scarce, and this gap limits a truly integrated approach to congestion.

The pioneering study by Flores et al.[8] stands out by correlating NT-proBNP levels with VExUS score during the first 24 hours of hospitalization for decompensated HF. The majority of the sample was composed of elderly patients (median age of 79 years), and the proportion of female patients was greater than 45%, thus reflecting a population that is frequently underrepresented in clinical studies. They observed that patients with moderate to severe venous congestion (VExUS 2 to 3) had median NT-proBNP levels between 5,430 and 13,200 pg/mL, suggesting that values above 5,430 pg/mL in elderly patients are associated with significant systemic congestion and require immediate clinical attention.

Future studies that stratify these findings by age group, sex, and specific comorbidities, such as chronic kidney disease, congenital heart disease, pulmonary hypertension, and valvular disease, are needed to further refine this approach. In a setting where early decisions directly impact the morbidity, mortality, and quality of life of patients with HF, the integration of biomarkers and functional imaging is not merely a diagnostic innovation, but a clinical imperative.

In patients with HF, identifying congestion before its clinical expression does not mean merely anticipating diagnosis; it involves intervening while it is still possible to alter the outcome.

Keywords

Heart Failure; Natriuretic Peptides; Ultrasound.

Mailing Address: Amanda Fernandes •
Hospital Nossa Senhora das Neves. Rua Etelvina Macedo de Mendonça, 531. Postal code: 58040-530. João Pessoa, PB – Brazil
E-mail: amandadantasff@gmail.com

DOI: https://doi.org/10.36660/abcimg.20260019i

References

1. Santos J, Nobre JP, Ferreira JP, Marques MIM, Henriques M, Cardim N, et al. PRIMARY-HF: Heart Failure Screening in Primary Care using Point-of-Care. Acta Med Port. 2025;38(4):237-244. doi: 10.20344/amp.22463.
2. Lozano-Jiménez S, Sebastian CG, Martín PV, Magallón BG, Centellas AM, Castro D, et al. Prevalence and Prognostic Impact of Subclinical Venous Congestion in Patients Hospitalized for Acute Heart Failure. Eur Heart J Acute Cardiovasc Care. 2026;14(12):749-53. doi: 10.1093/ehjacc/zuaf097.
3. Malagón SV, Acosta-Gutiérrez E, Ramos JAN, Salinas S, Pabón GM. Subclinical Congestion Evaluated by Point of Care Ultrasound (POCUS) at Discharge Predicts Readmission in Patients with Acute Heart Failure: Prognostic Cohort Study. POCUS J. 2024;9(2):125-32. doi: 10.24908/pocus.v9i2.17709.
4. Koratala A, Romero-González G, Soliman-Aboumarie H, Kazory A. Unlocking the Potential of VExUS in Assessing Venous Congestion: The Art of Doing It Right. Cardiorenal Med. 2024;14(1):350-74. doi: 10.1159/000539469.
5. Anastasiou V, Peteinidou E, Moysidis DV, Daios S, Gogos C, Liatsos AC, et al. Multiorgan Congestion Assessment by Venous Excess Ultrasound Score in Acute Heart Failure. J Am Soc Echocardiogr. 2024;37(10):923-33. doi: 10.1016/j.echo.2024.05.011.
6. Islas-Rodríguez JP, Miranda-Aquino T, Romero-González G, Hernández-Del Rio J, Camacho-Guerrero JR, Covarrubias-Villa S, et al. Effect on Kidney Function Recovery Guiding Decongestion with VExUS in Patients with Cardiorenal Syndrome 1: A Randomized Control Trial. Cardiorenal Med. 2024;14(1):1-11. doi: 10.1159/000535641.
7. Chow SL, Maisel AS, Anand I, Bozkurt B, de Boer RA, Felker GM, et al. Role of Biomarkers for the Prevention, Assessment, and Management of Heart Failure: A Scientific Statement from the American Heart Association. Circulation. 2017;135(22):e1054-91. doi: 10.1161/CIR.0000000000000490.
8. Flores MP, Souza AC, Carvalho MVSF, Morel RV, Cavalcante LRS, Barroso ND, et al. Correlação Entre o Venous Excess Ultrasound e os Níveis de Fragmento N-terminal do Pró-Peptídeo Natriurético Tipo B em Pacientes Com Insuficiência Cardíaca Agudamente Descompensada. Arq Bras Cardiol: Imagem Cardiovasc. 2026;39(1):e20260018. doi: 10.36660/abcimg.20260018.

Three-Dimensional Echocardiographic Assessment of the Right Ventricle: Why Should We Use It

Tiago R. Politi,[1,2] Rodrigo B.M. Barretto,[1] João Cesar Nunes Sbano,[1,2] David Costa de Souza Le Bihan,[1,2] Wilson Mathias Jr.[1,2]

Universidade de São Paulo, Instituto do Coração,[1] São Paulo, SP – Brazil

Fleury Group,[2] São Paulo, SP – Brazil

Central Illustration: Three-Dimensional Echocardiographic Assessment of the Right Ventricle: Why Should We Use It

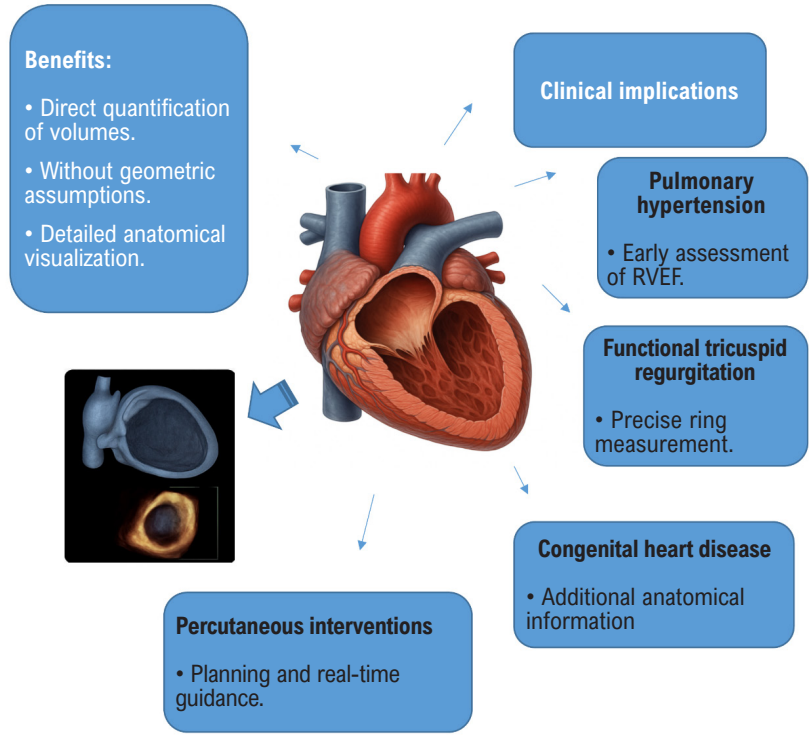

Arq Bras Cardiol: Imagem cardiovasc. 2026; 39(1):e20250096

Advantages and clinical implications of three-dimensional echocardiography in the evaluation of the right ventricle. RVEF: right ventricular ejection fraction.

Keywords

Three-dimensional Echocardiography; Right Ventricle; Ejection Fraction; Cardiac Magnetic Resonance Imaging

Mailing Address: Tiago Politi •
INCOR HC-FMUSP Echocardiography Service – University of São Paulo. Avenida Dr. Eneas de Carvalho Aguiar, 44. Postal code: 05508-900. São Paulo, SP – Brazil
E-mail: politi.cardiol@gmail.com
Manuscript received November 20, 2025; revised November 27, 2025; accepted November 28, 2025
Editor responsible for the review: Marcelo Tavares

DOI: https://doi.org/10.36660/abcimg.20250096i

Abstract

Right ventricular (RV) assessment using two-dimensional (2D) echocardiography has historically faced significant challenges due to the chamber's complex and unique geometry and its thoracic orientation. In this context, three-dimensional (3D) echocardiography has emerged as a promising tool to overcome and illuminate these limitations, enabling accurate quantification of volumes and ejection fraction without relying on geometric assumptions. As a result, the routine incorporation of 3D echocardiography into RV evaluation may redefine diagnostic and prognostic

paradigms, fostering a more precise and personalized approach in modern cardiology. To consolidate and highlight this technique, this review article explores the technical principles of 3D echocardiography for RV assessment, discusses its advantages over conventional 2D imaging, examines its validation against cardiac magnetic resonance (CMR), and reviews key clinical applications, including pulmonary hypertension, functional tricuspid regurgitation, congenital heart disease, and right-sided heart failure. Additionally, the article outlines current limitations of the technique, future perspectives, and practical recommendations based on contemporary literature.

Introduction

The shape of the right ventricle (RV) is complex, and therefore any image obtained using the Two-dimensional (2D) method cannot accurately represent it. In the apical 2D echocardiographic view, the RV appears triangular, while in the transverse view and under normal conditions, it has a crescent shape. Its architecture is composed of three main components: the inlet tract, which consists of the tricuspid valve (TV), chordae tendineae, and papillary muscle; the apical trabecular myocardium; and the infundibulum or cone, which refers to the smooth region of the ventricular myocardial outflow tract. The latter represents 25% to 30% of its volume.[1,2]

The three parts of the right ventricle are not in the same plane, as seen in a 3D echocardiogram of a normal individual (Figure 1). The inlet tract contracts earlier than the infundibulum, and the response of these three segments to medication, sympathetic stimulation, volume overload, and pressure may differ. For example, studies in animals and humans have suggested that the inotropic response of the infundibulum may be greater than that of the inlet tract.[3]

Furthermore, myofibrils exhibit a circumferential arrangement in the subepicardial tissue and a longitudinal arrangement in the subendocardial tissue, with contraction occurring primarily in a longitudinal direction. This partly explains why longitudinal strain analysis has shown greater predictive value and why many studies on RV strain and strain rate focus on longitudinal strains, rather than radial or circumferential strains. Furthermore, longitudinal deformation of the right ventricular free wall showed a stronger correlation with right ventricular ejection fraction (RVEF), determined by magnetic resonance imaging (MRI), than with changes in Fractional Area Change (FAC) and the S´ wave of the lateral tricuspid annulus, in a heterogeneous group of patients.[4]

In the clinical setting, accurate assessment of the right ventricle (RV), when available, is essential in several cardiovascular conditions, including pulmonary diseases, congenital heart disease, right heart failure, and after valve interventions. As previously described, due to its

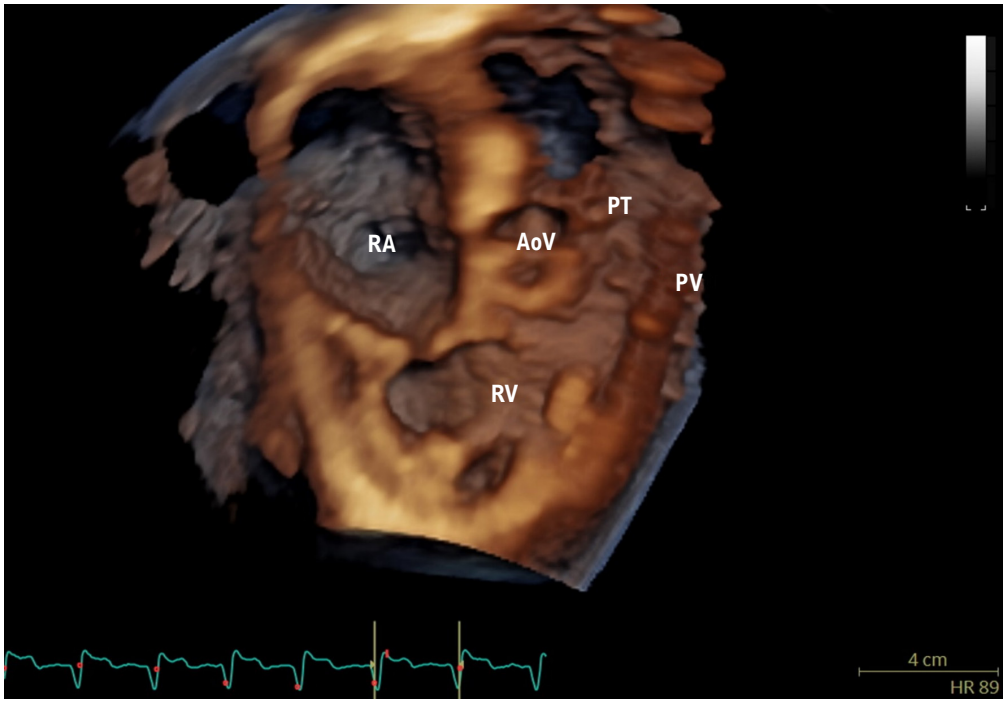

Figure 1 – *3D image showing parts of the right ventricle in different planes. The image shows the inlet tract, trabecular portion, and infundibulum in three-dimensional section, highlighting the anatomical structures.*
TV: tricuspid valve; PV: pulmonary valve; RV: right ventricle; AO: aorta; PT: pulmonary trunk; RA: right atrium.

asymmetrical anatomy, pyramidal shape, and longitudinal peristaltic contraction pattern, its analysis is made difficult by conventional two-dimensional (2D) echocardiographic methods.[5,6] Furthermore, interobserver variability and dependence on orthogonal planes limit the reproducibility and accuracy of 2D echocardiography in quantifying RV function.[7]

Therefore, three-dimensional (3D) echocardiography emerges as a fundamental tool in understanding this complex cardiac chamber, representing a significant advance in this context, offering direct volumetric measurements and a better characterization of its contractile mechanics. With the development of dedicated software and transducers with higher temporal and spatial resolution, it has become possible to integrate RV assessment more robustly and reliably into clinical practice (Central Illustration).[1,8]

Next, we present the technical principles of 3D echocardiography in Right Ventricular (RV) analysis, review its most relevant clinical applications, and discuss its limitations, according to current literature recommendations.[9,10]

Technical Fundamentals of 3D Right Ventricular Echocardiography

A proper 3D dataset of the right ventricle requires special attention to specific technical aspects:

- Full-volume acquisition: ideally with breath-holding, over four or six cardiac cycles for greater temporal resolution, using matrix-array transducers, in the focused apical window of the right ventricle or in the parasternal inlet window.
- Volume rate: a balance should be sought between high temporal resolution (>20 volumes/s) and complete anatomical coverage.
- Optimized visualization of the tricuspid valve: it is crucial to align the planes to include the tricuspid annulus, the apex of the RV, and the entire cavity.

For three-dimensional visualization of the tricuspid valve via transesophageal imaging, images with three-dimensional zoom in the distal esophagus should be obtained, so as to position the valve more perpendicular to the emitting source, thus optimizing spatial resolution.

Modern software uses machine learning-based auto-contouring algorithms to quantify end-diastolic volume (EDV), end-systolic volume (ESV), and RVEF as seen in Figure 2.[3,11,12]

Evaluation of Right Ventricular Volumes and Ejection Fraction

The clinical validation for determining ventricular volumes and right ventricular ejection fraction (RVEF) by magnetic resonance imaging is well established.[13] In three-dimensional echocardiography, experimental data *in vitro* and in initial clinical studies confirm good accuracy in quantifying RV volume and EF.[1] However, RV volumes derived from 3D echocardiography showed consistent underestimation compared to CMR, including a mean RV EF difference that can reach −0.9%.[13] Therefore, some authors recommend a cutoff point for right ventricular systolic dysfunction when the 3D right ventricular ejection fraction (RVEF) is less than 45%.[14,15]

When calculating right ventricular volumes and ejection fraction using 3D echocardiography, studies have shown significant differences in relation to gender: the absolute end-diastolic volume was greater in men (129 ± 25 mL vs. 102 ± 33 mL in women; $P < 0.01$). However, when indexing by lean body mass (but not by body surface area or height), this difference disappeared (2.1 ± 0.5 vs. 2,2 ± 0.4 mL/kg; p = NS)(8). The normal range of values for men is 87 mL/m² for EDV; 44 mL/m² for ESV and for women 74 mL/m² for EDV; 36 mL/m² for ESV.[15]

Advantages of 3D Echocardiography Compared to 2D in Right Ventricular Assessment

Due to the complex geometry of the right ventricle (RV), the accuracy of 2D echocardiography is limited for volume measurements, leading to underestimation of volumes and significant dependence on the orientation of the slice planes.[5] On the other hand, 3D echocardiography allows complete volumetric acquisition of the RV, true anatomical reconstruction, and quantification without geometric assumptions, with excellent correlation with CMR ($r \approx 0.80$–0.92) and less systematic bias compared to 2D.[16]

From a clinical standpoint, the superiority of 3D echocardiography over 2D echocardiography is most evident in situations of marked right ventricular remodeling (e.g., pulmonary hypertension, severe functional tricuspid regurgitation, and congenital heart disease), where anatomical distortion makes the geometric model of 2D echocardiography even less representative (Table 1).[17,18] However, 3D echocardiography still requires a higher quality acoustic window and can be limited by arrhythmias and low frame rate, especially in unstable patients.[14]

3D Echocardiography vs. VD CMR: Accuracy, Clinical Applicability, and the Role of AI

As previously mentioned, cardiac magnetic resonance (CMR) is widely recognized as the gold standard for quantifying right ventricular volumes and ejection fraction due to its high reproducibility and independence from the acoustic window.[13] However, 3D echocardiography has emerged as a promising alternative, especially in contexts where CMR is unavailable, contraindicated, or impractical.

Despite the superiority of CMR in terms of absolute accuracy, 3D echocardiography offers practical advantages that make it ideal for bedside use, in critically ill patients, and in serial assessments. In conditions such as right heart failure, pulmonary hypertension, or during follow-up of valve therapies, 3D echocardiography allows for the rapid acquisition of prognostic parameters, such as volumes and RVEF, and tricuspid annulus area in real time.[19,20]

Furthermore, software with artificial intelligence has been improving the accuracy of 3D echocardiography by reducing interobserver variability, shortening post-processing time, and improving the consistency of measurements, bringing its results even closer to those of CMR[19] (Table 2).

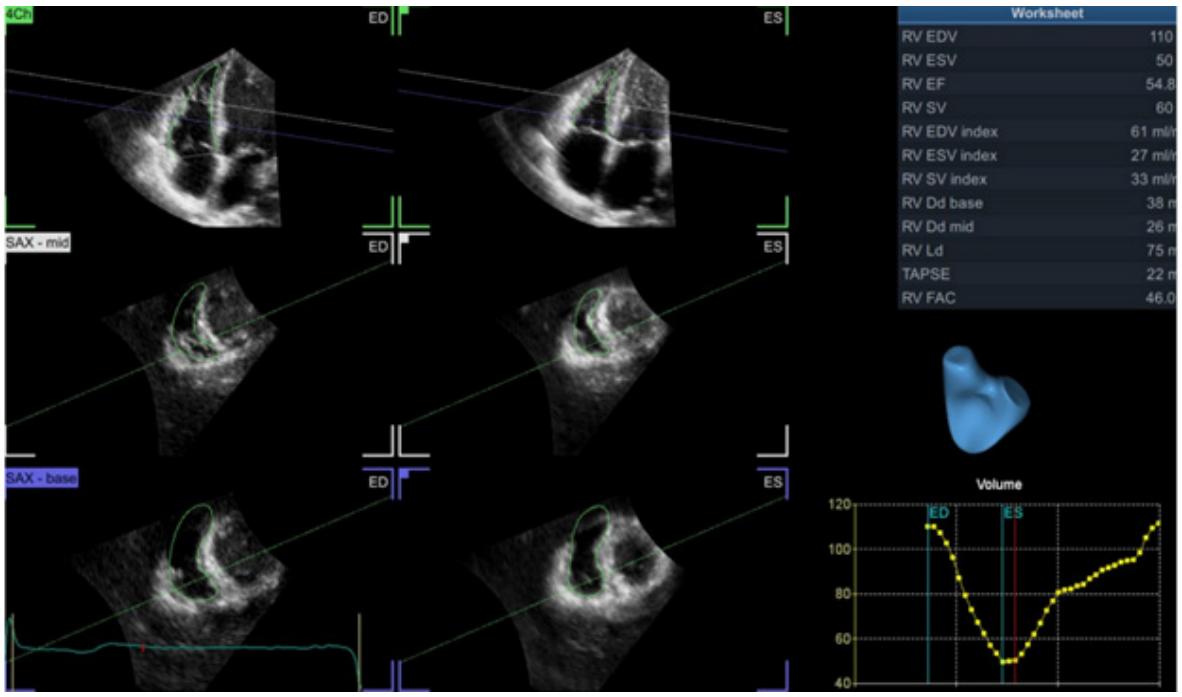

Figure 2 – *Real-time acquisition and three-dimensional reconstruction of the right ventricle. The top panel shows the total volume obtained from the apical window. The lower panel displays the orthogonal multiplanar reconstruction, with automatic endocardial border delineation for volume and ejection fraction calculation.*

Table 1 – Comparison between 2D and 3D echocardiography in right ventricular assessment

Characteristic	2D Echocardiography	3D Echocardiography
Assumed geometry	Yes (ellipsoid or pyramid shape)	No (actual volume captured)
Dependence on anatomical planes	High	Low
Reproducibility	Moderate	High
Acquisition time	Short	Requires multibeat acquisition (several cardiac cycles)
tricuspid annulus assessment	Uniplanar	Multiplanar and volumetric
Use in pulmonary hypertension	Limited	High prognostic accuracy
Post-processing time	Rapid	Moderate to long duration (depends on the workstation)
Accuracy in RVEF calculation	Low-moderate	High (good) correlation with CMR)
Limitations	Angle dependence and acoustic window	Artifacts and lower temporal resolution

Source: Adapted from Shiota T. 3D Echocardiography, 3rd ed. Springer; 2021. RVEF: right ventricular ejection fraction; CMR: cardiac magnetic resonance imaging.

Prognostic comparison of RV systolic function: analysis of RVEF by 3D echocardiography, longitudinal strain of the RV free wall by 2D echocardiography, and CMR

Determining prognosis based on the assessment of right ventricular systolic function traditionally used conventional parameters derived from 2D echocardiography, such as

Table 2 – Comparison between three-dimensional echocardiography and cardiac magnetic resonance (CMR) for right ventricular assessment

Characteristic	3D Echocardiography	CMR
Volumetric acquisition method	Real-time (direct 3D volumetry)	Manual contouring of multiple planes
Assumed geometry	No	No
Reproducibility	Moderate to high	Very High
Correlation between RVEF and CMR	r = 0.80–0.92	Reference standard
Underestimation of volumes	Yes, light (depending on the window).	No
Assessment of late gadolinium enhancement (fibrosis)	No	Yes
Valvular functional assessment	Yes (three-dimensional)	Yes (with lower temporal resolution)
Temporal resolution	Moderate (>20 volumes/s)	Moderate (30–50 ms per frame)
Spatial resolution	Moderate	High
Cost and availability	Low, widely available	High, limited availability
Contraindications	None relevant	Metal implants, claustrophobia, dialysis-dependent chronic kidney disease.
Exam time	Quick (5–10 min)	Extended (30–60 min)
Applicability in ICU/bedside setting	Yes	No

Source: Adapted from Shiota T. 3D Echocardiography, 3rd ed. Springer; 2021, Lang RM et al.[14] Maffessanti F et al.[8]. RVEF: right ventricular ejection fraction; CMR: Cardiac magnetic resonance imaging; CKD: chronic kidney disease.

tricuspid annular excursion (TAPSE) and area variation (FAC). However, modern techniques such as 3D echocardiography, 2D right ventricle free-wall longitudinal strain (2D-RVFWLS) and Cardiac Magnetic Resonance imaging (CMR) demonstrate greater accuracy and prognostic power.

A. Validation and Prognosis: EF 3D vs. 2D-RVFWLS vs. CMR

In patients with dilated cardiomyopathy, 3D EF showed a strong association with adverse cardiac events, surpassing the prognostic relevance of 2D-RVFWLS in multivariate analysis; 3D EF remained the only independent predictor after adjustment for clinical and echocardiographic variables (cut-off 43.4%, AUC = 0.76).[21,22]

Other evidence suggests that 3D EF may offer additional and incremental prognostic value over 2D strain and other conventional parameters, including in populations such as patients with severe COVID-19.[21]

In Heart Failure with preserved Ejection Fraction (HFpEF), longitudinal strain of the right ventricular free wall, measured using 3D speckle tracking, showed prognostic value equivalent to 3D EF and superior to 2D-RVFWLS (HR 5.73 vs. 3.17 and 3.47).[21]

B. CMR and Prognostic Correlation

Although CMR remains the gold standard for right ventricular volume quantification, comparative studies show that 3D EF correlates well with ejection fraction measured by CMR, with excellent reproducibility, and can be used as an alternative for prognostic determination in many clinical contexts[23,24] (Table 3).

Relevant Clinical Applications of 3D Right Ventricular Echocardiography

The main clinical applications of 3D RV echocardiography are described below (Tables 4 and 5).

A. Pulmonary Hypertension

In Pulmonary Hypertension (PH), RV function is the main prognostic determinant. 3D echocardiography allows for more precise quantification of the Right Ventricular Ejection Fraction (RVEF). An RVEF < 45% for 3D is associated with a higher risk of decompensation and mortality.[17,25,19]

B. Functional Tricuspid Regurgitation

3D echocardiography allows for the evaluation of the exact mechanism of Tricuspid Regurgitation (TR), including dilation and geometry of the tricuspid annulus and papillary muscles (Figures 3 and 4). 3D reconstruction allows for more accurate measurement of the Effective Regurgitant Orifice Area (EROA) than the 2D PISA method. Data important for planning percutaneous interventions, such as the separation between the cusps, the height of the valve tenting, and electrode interference in valve function, can also be determined more accurately through three-dimensional reconstructions.[19]

Table 3 – Summary comparative table

Method	Main advantage	Limitation	Comparative prognostic value
FE 3D (Eco 3D)	Precise volumetry, complete geometry	Requires good image quality and advanced software	Elevated (independent, higher than 2D)
2D-RVFWLS	Easy to obtain, high temporal resolution	Dependent on the acoustic window and geometry	Moderate, low value compared to FE 3D.
CMR	Reference standard	Limited access, high cost, and time	High – reference for objective and prognostic assessment.

Source: Adapted from Meng et al.[21].CMR: cardiac magnetic resonance; EF: ejection fraction.

Table 4 – Main Clinical Applications of 3D Right Ventricular Echocardiography

Clinical scenario	3D echocardiography application of the RV	Clinical impact
Pulmonary hypertension	RVEF assessment and RV remodeling	Better risk stratification
Functional tricuspid regurgitation	Analysis of the tricuspid ring and regurgitation mechanism	Assists in planning percutaneous intervention
Congenital heart disease	Quantification of volumes and geometry of the RV	Longitudinal monitoring in pathologies such as T4F, systemic RV, and Ebstein's anomaly
Heart failure	Early identification of right ventricular dysfunction	Provides an independent prognosis
Structural interventions	Anatomical information for treatment planning. Real-time device guidance (e.g. TriClip)	Support for the success of the procedure

Source: Adapted from Grapsa, J et al.[17], Prihadi, E et al.[19], Dragulescu, A et al.[27], Agricola et al.[29]. RVEF: right ventricular ejection fraction; RV: right ventricle.

Table 5 – 3D parameters of the right ventricle and their interpretation

3D Parameter	Cutoff point	Interpretation
RVEF	<45%	Strong predictor of mortality in heart failure and pulmonary hypertension
ESV	> 90 mL	Indicates adverse remodeling
Tricuspid annulus area	> 12 cm²/m²	Progression of tricuspid regurgitation
EROA	> 0.4 cm²	Severe tricuspid regurgitation
Longitudinal strain of the RV	<16%	Subclinical dysfunction, worse prognosis

Source: Adapted from Grapsa, J et al.[17], Molnar A, A et al.[28], Agricola, E et al.[29], Ishizu et al.[30] RVEF: right ventricular ejection fraction; RV: right ventricle; ESV: End-systolic volume; EROA: Effective regurgitant orifice

C. Congenital Heart Diseases

In congenital heart diseases such as tetralogy of Fallot, ventricular septal defect, or Ebstein's anomaly, 3D echocardiography provides accurate volumetric assessment in atypical geometries where 2D echocardiography fails. This is fundamental in surgical planning and longitudinal follow-up.[26,27]

D. Heart Failure with RV Dysfunction

Right ventricular dysfunction in Heart Failure with preserved Ejection Fraction (HFpEF) or reduced Ejection Fraction (HFrEF) is associated with a worse prognosis. 3D echocardiography allows for the early detection of RVEF reduction, even before significant changes in TAPSE or tricuspid annulus S' wave velocity.[28]

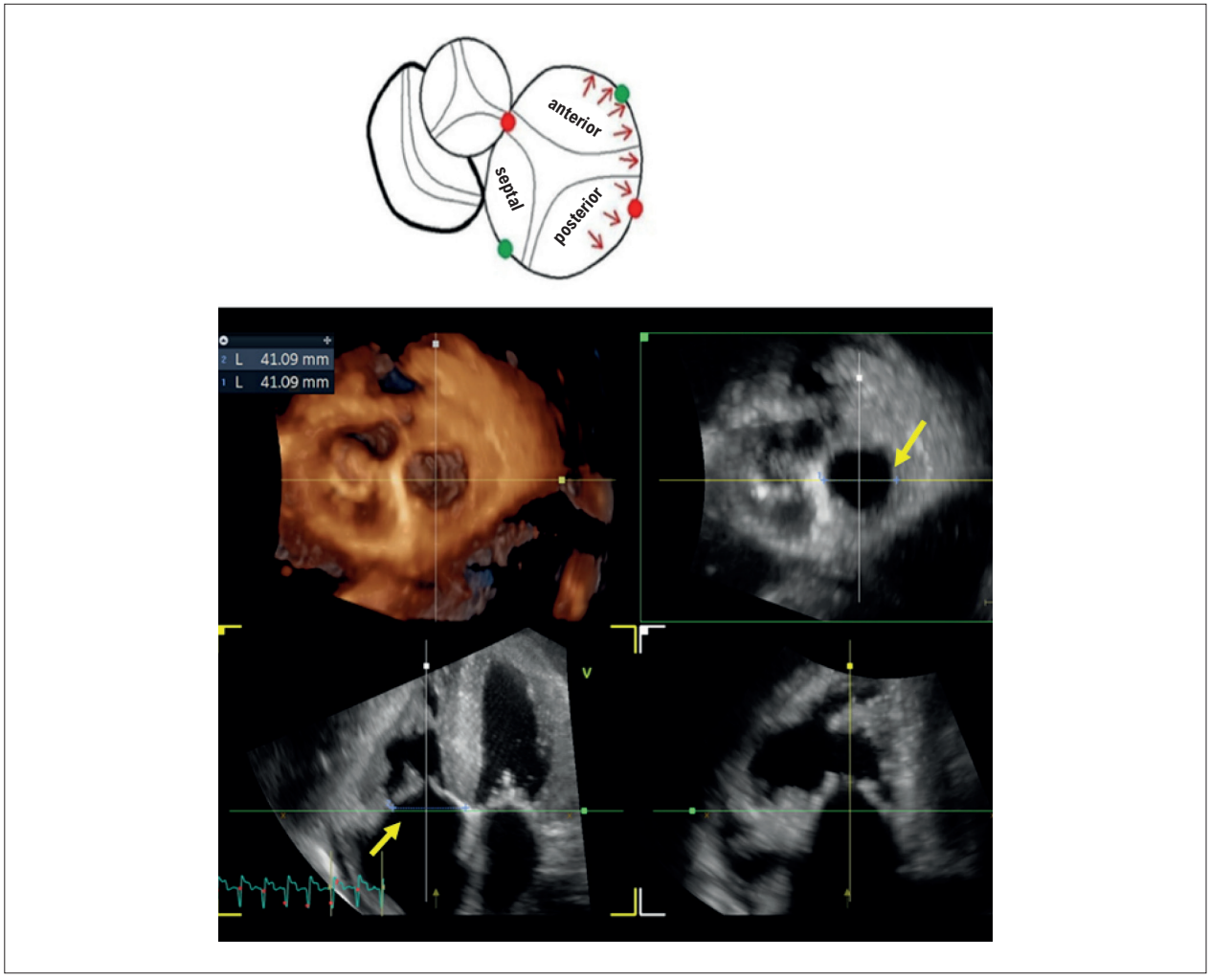

Figure 3 – *Image showing anteroposterior dilation of the tricuspid annulus seen on two-dimensional and three-dimensional echocardiography (yellow arrows). The illustration above shows the anatomical arrangement of the annulus.*

E. Structural Interventions and Post-Procedure Monitoring

Procedures such as percutaneous pulmonary valve implantation, tricuspid clipping, and percutaneous tricuspid valve implantation, and occlusion of interatrial septal defects require pre- and post-procedure evaluation of the right ventricle, tricuspid valve, and septal defect diameters, which is performed with greater accuracy by real-time 3D echocardiography.[29]

Furthermore, during procedures for treating tricuspid regurgitation, an adequate anatomical demonstration of the valve, as well as the interaction between the prostheses and the valve tissue, is essential, making the use of three-dimensional transesophageal echocardiography crucial.

Technical Limitations and Future Perspectives

Despite significant advances, 3D echocardiography still faces technical challenges that limit its routine application in all clinical settings. However, the development of new technologies and artificial intelligence algorithms has driven its continuous evolution.

A. Temporal and Spatial Resolution

One of the most recognized limitations of 3D echocardiography compared to 2D is its lower temporal resolution. Multibeat acquisition is necessary to improve temporal resolution, especially when acquiring large volumes. However, this type of acquisition can introduce artifacts in uncooperative patients, those with hemodynamic instability, tachyarrhythmias, or irregular respiratory patterns.[14] Furthermore, the spatial resolution is still inferior to that of magnetic resonance imaging, which may make endocardial delimitation difficult in the right ventricle with intense trabeculations or distorted anatomy.[30,31]

B. Dependence on the Acoustic Window

Three-dimensional echocardiography remains limited by the quality of the acoustic window. In patients with COPD, obesity, or on mechanical ventilation, the image obtained may be inadequate for accurate reconstruction of right ventricular volumes. In these cases, even with advanced software, the analysis may be unfeasible or inaccurate.[7,32]

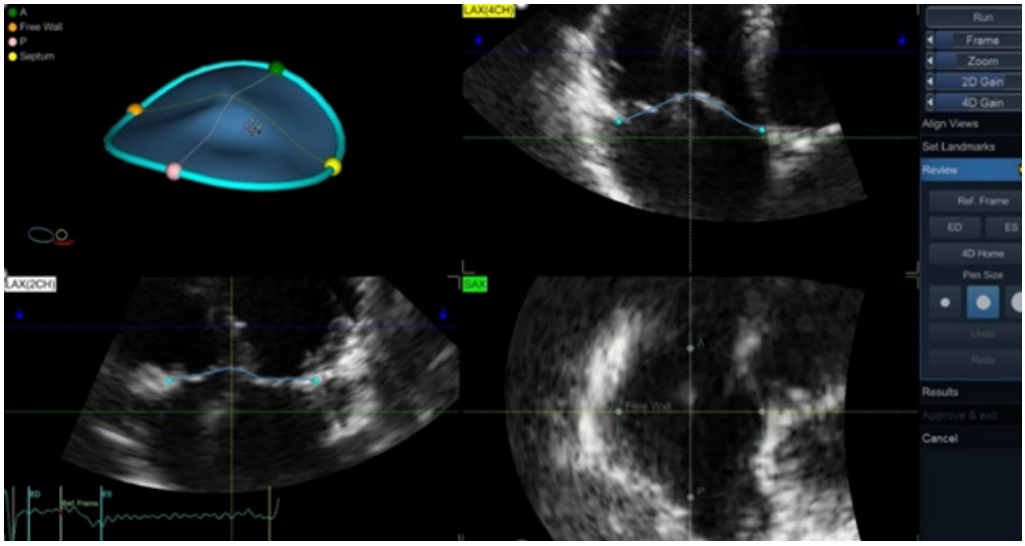

Figure 4 – *Three-dimensional multiplanar reconstruction of the tricuspid valve by 3D echocardiography, showing the spatial model of the annulus with anatomical reference points (apex, septum, free wall, and commissures). Orthogonal cuts (LAX 4-chamber, LAX 2-chamber, and SAX transverse) allow for precise contour adjustment and detailed analysis of valve geometry.*

C. Variability and Learning Curve

Although the accuracy of 3D echocardiography has been demonstrated in multicenter studies, significant interobserver variability still exists in centers with less experience. The learning curve for acquisition, reconstruction, and interpretation is longer than that of 2D echocardiography, requiring specific training.[33]

D. Processing Time and Workflow

Post-processing time, although reduced with modern software, still represents a practical barrier. In high-traffic environments such as ICUs or outpatient clinics, routine use can be hampered by the need for specific workstations and trained operators.[16]

E. Future Perspectives

The most promising innovations in the field include:

- **Integration with artificial intelligence (AI):** The integration of AI in echocardiography has accelerated the 3D quantification of the right ventricle: Genovese et al. demonstrated that machine learning-based software automates the contouring of the right ventricle (RV), reducing interobserver variability and accelerating analysis time to 15 seconds, without manual editing, in approximately 32% of cases, with excellent reproducibility.[11] A recent review showed that AI impacts all stages of the workflow — from the automatic acquisition of standardized slices to automated functional interpretation, promoting greater clinical efficiency.[34]
- **Portable 3D echocardiography** (handheld ultrasound devices - HUDs): Although most studies with wearable devices focus on the left ventricle, the results support the feasibility of automated volumetric quantification of the right ventricle using artificial intelligence or algorithms integrated into wearable devices. This reinforces the discussion about the use of 3D echocardiography in the clinical context of emergency bedside and ICU settings.[35]
- **Multimodal fusion with MR and CT:** 3D echocardiography has advanced beyond the isolated quantification of the right ventricle, acting as a multimodal integration platform with Cardiac Magnetic Resonance imaging (CMR) and Computed Tomography (CT), especially in complex scenarios of congenital heart disease and percutaneous interventions. A recent review highlights this emerging clinical utility, emphasizing the combination of anatomical and functional data from multiple modalities for planning and follow-up.[36]
- **Three-dimensional deformation (3D strain) assessment**: Three-dimensional speckle tracking, a relatively recent technology in 3D echocardiography, was developed to allow the simultaneous analysis of myocardial deformation and the quantification of right ventricular (RV) volumes and ejection fraction in a single volumetric dataset.[30] In addition to global quantification, 3D strain allows for the assessment of regional RV wall motion, revealing heterogeneous segmental deformation patterns—findings that may have prognostic relevance and aid in understanding ventricular mechanics in different clinical contexts. This approach, therefore, represents a potentially useful advancement to

complement the functional analysis of the RV, especially in diseases that involve complex remodeling.[30]

- **Three-dimensional modeling of the right ventricle: technical integration and advanced:** Three-dimensional (3D) modeling of the right ventricle (RV), based on 3D echocardiography, represents a technological leap in cardiac morphofunctional assessment. With segmentation and volumetric reconstruction algorithms, it is possible to build accurate anatomical models of the RV — including its inlet, body, and outlet regions — without relying on two-dimensional geometric assumptions. These reconstructions have high fidelity, with excellent accuracy for volumes and right ventricular ejection fraction (RVEF).[37,16] In addition to reproducing anatomy with high precision, these models allow the generation of segmental strain maps, enabling the analysis of regional myocardial behavior and the identification of dyskinesias or areas with contractile alterations typical of congenital heart disease or valvular dysfunction.[38] The use of these methods in patients with volume or pressure overload—for example, in pulmonary hypertension or valvular regurgitation—has already demonstrated utility in geometric and functional characterization, with a direct impact on risk stratification and therapeutic planning.[39] In the field of medical education and surgical planning, 3D models have been integrated into augmented reality tools and 3D printing systems, enabling personalized anatomical simulation for training and to support interprofessional decision-making in complex cases.[40]
- **Assistance in the implantation of ventricular assist devices**: In a recent publication, three-dimensional echocardiographic assessment of LV and RV volumes and shape is reported as useful for describing the impact of Left Ventricular Assist Device (LVAD) on the heart.[25] RVEF and RV free wall deformation derived from three-dimensional echocardiography were associated with RV failure and long-term outcome in patients undergoing LVAD implantation. These parameters have the potential to be predictors of right heart failure in LVAD surgery.[41]

Conclusions

Three-dimensional (3D) echocardiography represents one of the most relevant innovations in the functional and anatomical evaluation of the right ventricle (RV) in modern clinical practice. By overcoming limitations inherent in two-dimensional echocardiography, especially those related to the geometric complexity of the RV, the method offers direct, reproducible volumetric quantification with excellent correlation to cardiac magnetic resonance imaging—the gold standard for assessing ventricular function and volume.

Its clinical application ranges from the early diagnosis of right ventricular dysfunction to the monitoring of structural therapies and risk stratification in various heart diseases, with parameters such as ejection fraction, end-systolic volume, and tricuspid annulus area demonstrating consistent prognostic value.

Despite remaining technical limitations, such as lower temporal resolution, dependence on acoustic windows, and the need for a learning curve, advances in artificial intelligence, analysis automation, and transducer miniaturization open promising prospects for expanding their use on a large scale.

Therefore, the progressive incorporation of 3D echocardiography into the routine of cardiovascular imaging laboratories is strongly recommended, especially in the evaluation of the right ventricle, as a first-line diagnostic and prognostic tool. In the coming years, technical and interpretative mastery of this method will be an important differentiating factor in the practice of the modern echocardiographer.

Acknowledgment

The authors thank the teams at the Three-Dimensional Echocardiography Laboratory and the Cardiovascular Imaging Department for their technical and scientific support during the development of this work. They also thank their colleagues who contributed suggestions and critical reviews that improved the quality of the manuscript.

This study did not receive direct financial support from public or private funding agencies.

Author Contributions

Conception and design of the research and critical revision of the manuscript for intellectual content: Politi TR, Barretto RBM, Sbano JCN, Le Bihan DCS, Mathias Jr. W; acquisition of data: Politi TR, Barretto RBM, Le Bihan DCS, Mathias Jr. W; analysis and interpretation of the data: Politi TR, Sbano JCN, Le Bihan DCS, Mathias Jr. W; writing of the manuscript: Politi TR.

Potential Conflict of Interest

No potential conflict of interest relevant to this article was reported.

Sources of Funding

There were no external funding sources for this study.

Study Association

This study is not associated with any thesis or dissertation work.

Ethics Approval and Consent to Participate

This article does not contain any studies with human participants or animals performed by any of the authors.

Use of Artificial Intelligence

The authors did not use any artificial intelligence tools in the development of this work.

Availability of Research Data

The underlying content of the research text is contained within the manuscript.

References

1. Shiota T, Jones M, Chikada M, Fleishman CE, Castellucci JB, Cotter B, et al. Real-Time Three-Dimensional Echocardiography for Determining Right Ventricular Stroke Volume in an Animal Model of Chronic Right Ventricular Volume Overload. Circulation. 1998;97(19):1897-900. doi: 10.1161/01.cir.97.19.1897.
2. Nesser HJ, Tkalec W, Patel AR, Masani ND, Niel J, Markt B, et al. Quantitation of Right Ventricular Volumes and Ejection Fraction by Three-Dimensional Echocardiography in Patients: Comparison with Magnetic Resonance Imaging and Radionuclide Ventriculography. Echocardiography. 2006;23(8):666-80. doi: 10.1111/j.1540-8175.2006.00286.x.
3. Shiota T. 3D Echocardiography. 3rd ed. Philadelphia: Elsevier; 2021.
4. Focardi M, Cameli M, Carbone SF, Massoni A, De Vito R, Lisi M, et al. Traditional and Innovative Echocardiographic Parameters for the Analysis of Right Ventricular Performance in Comparison with Cardiac Magnetic Resonance. Eur Heart J Cardiovasc Imaging. 2015;16(1):47-52. doi: 10.1093/ehjci/jeu156.
5. Rudski LG, Lai WW, Afilalo J, Hua L, Handschumacher MD, Chandrasekaran K, et al. Guidelines for the Echocardiographic Assessment of the Right Heart in Adults: A Report from the American Society of Echocardiography Endorsed by the European Association of Echocardiography, a Registered Branch of the European Society of Cardiology, and the Canadian Society of Echocardiography. J Am Soc Echocardiogr. 2010;23(7):685-713. doi: 10.1016/j.echo.2010.05.010.
6. Haddad F, Hunt SA, Rosenthal DN, Murphy DJ. Right Ventricular Function in Cardiovascular Disease, Part I: Anatomy, Physiology, Aging, and Functional Assessment of the Right Ventricle. Circulation. 2008;117(11):1436-48. doi: 10.1161/CIRCULATIONAHA.107.653576.
7. Lang RM, Badano LP, Mor-Avi V, Afilalo J, Armstrong A, Ernande L, et al. Recommendations for Cardiac Chamber Quantification by Echocardiography in Adults: An Update from the American Society of Echocardiography and the European Association of Cardiovascular Imaging. Eur Heart J Cardiovasc Imaging. 2015;16(3):233-70. doi: 10.1093/ehjci/jev014.
8. Maffessanti F, Muraru D, Esposito R, Gripari P, Ermacora D, Santoro C, et al. Age-, Body Size-, and Sex-Specific Reference Values for Right Ventricular Volumes and Ejection Fraction by Three-Dimensional Echocardiography: A Multicenter Echocardiographic Study in 507 Healthy Volunteers. Circ Cardiovasc Imaging. 2013;6(5):700-10. doi: 10.1161/CIRCIMAGING.113.000706.
9. Mukherjee M, Rudski LG, Addetia K, Afilalo J, D'Alto M, Freed BH, et al. Guidelines for the Echocardiographic Assessment of the Right Heart in Adults and Special Considerations in Pulmonary Hypertension: Recommendations from the American Society of Echocardiography. J Am Soc Echocardiogr. 2025;38(3):141-86. doi: 10.1016/j.echo.2025.01.006.
10. Soliman-Aboumarie H, Joshi SS, Cameli M, Michalski B, Manka R, Haugaa K, et al. EACVI Survey on the Multi-Modality Imaging Assessment of the Right Heart. Eur Heart J Cardiovasc Imaging. 2022;23(11):1417-22. doi: 10.1093/ehjci/jeac183.
11. Genovese D, Rashedi N, Weinert L, Narang A, Addetia K, Patel AR, et al. Machine Learning-Based Three-Dimensional Echocardiographic Quantification of Right Ventricular Size and Function: Validation Against Cardiac Magnetic Resonance. J Am Soc Echocardiogr. 2019;32(8):969-77. doi: 10.1016/j.echo.2019.04.001.
12. Tamborini G, Marsan NA, Gripari P, Maffessanti F, Brusoni D, Muratori M, et al. Reference Values for Right Ventricular Volumes and Ejection Fraction with Real-Time Three-Dimensional Echocardiography: Evaluation in a Large Series of Normal Subjects. J Am Soc Echocardiogr. 2010;23(2):109-15. doi: 10.1016/j.echo.2009.11.026.
13. Maceira AM, Prasad SK, Khan M, Pennell DJ. Reference Right Ventricular Systolic and Diastolic Function Normalized to Age, Gender and Body Surface Area from Steady-State Free Precession Cardiovascular Magnetic Resonance. Eur Heart J. 2006;27(23):2879-88. doi: 10.1093/eurheartj/ehl336.
14. Lang RM, Badano LP, Tsang W, Adams DH, Agricola E, Buck T, et al. EAE/ASE Recommendations for Image Acquisition and Display Using Three-Dimensional Echocardiography. Eur Heart J Cardiovasc Imaging. 2012;13(1):1-46. doi: 10.1093/ehjci/jer316.
15. Wang S, Wang S, Zhu Q, Wang Y, Li G, Kong F, et al. Reference Values of Right Ventricular Volumes and Ejection Fraction by Three-Dimensional Echocardiography in Adults: A Systematic Review and Meta-Analysis. Front Cardiovasc Med. 2021;8:709863. doi: 10.3389/fcvm.2021.709863.
16. Muraru D, Spadotto V, Cecchetto A, Romeo G, Aruta P, Ermacora D, et al. New Speckle-Tracking Algorithm for Right Ventricular Volume Analysis from Three-Dimensional Echocardiographic Data Sets: Validation with Cardiac Magnetic Resonance and Comparison with the Previous Analysis Tool. Eur Heart J Cardiovasc Imaging. 2016;17(11):1279-89. doi: 10.1093/ehjci/jev309.
17. Grapsa J, O'Regan DP, Pavlopoulos H, Durighel G, Dawson D, Nihoyannopoulos P. Right Ventricular Remodelling in Pulmonary Arterial Hypertension with Three-Dimensional Echocardiography: Comparison with Cardiac Magnetic Resonance Imaging. Eur J Echocardiogr. 2010;11(1):64-73. doi: 10.1093/ejechocard/jep169.
18. Jenkins C, Chan J, Bricknell K, Strudwick M, Marwick TH. Reproducibility of Right Ventricular Volumes and Ejection Fraction Using Real-Time Three-Dimensional Echocardiography: Comparison with Cardiac MRI. Chest. 2007;131(6):1844-51. doi: 10.1378/chest.06-2143.
19. Prihadi EA, van der Bijl P, Dietz M, Abou R, Vollema EM, Marsan NA, et al. Prognostic Implications of Right Ventricular Free Wall Longitudinal Strain in Patients with Significant Functional Tricuspid Regurgitation. Circ Cardiovasc Imaging. 2019;12(3):e008666. doi: 10.1161/CIRCIMAGING.118.008666.
20. Kitano T, Kovács A, Nabeshima Y, Tokodi M, Fábián A, Lakatos BK, et al. Prognostic Value of Right Ventricular Strains Using Novel Three-Dimensional Analytical Software in Patients with Cardiac Disease. Front Cardiovasc Med. 2022;9:837584. doi: 10.3389/fcvm.2022.837584.
21. Meng Y, Zhu S, Xie Y, Zhang Y, Qian M, Gao L, et al. Prognostic Value of Right Ventricular 3D Speckle-Tracking Strain and Ejection Fraction in Patients with HFpEF. Front Cardiovasc Med. 2021;8:694365. doi: 10.3389/fcvm.2021.694365.
22. Vîjîiac A, Onciul S, Guzu C, Verinceanu V, Bătăilă V, Deaconu S, et al. The Prognostic Value of Right Ventricular Longitudinal Strain and 3D Ejection Fraction in Patients with Dilated Cardiomyopathy. Int J Cardiovasc Imaging. 2021;37(11):3233-44. doi: 10.1007/s10554-021-02322-z.
23. Li Y, Wang T, Haines P, Li M, Wu W, Liu M, et al. Prognostic Value of Right Ventricular Two-Dimensional and Three-Dimensional Speckle-Tracking Strain in Pulmonary Arterial Hypertension: Superiority of Longitudinal Strain Over Circumferential and Radial Strain. J Am Soc Echocardiogr. 2020;33(8):985-94.e1. doi: 10.1016/j.echo.2020.03.015.
24. Erley J, Tanacli R, Genovese D, Tapaskar N, Rashedi N, Bucius P, et al. Myocardial Strain Analysis of the Right Ventricle: Comparison of Different Cardiovascular Magnetic Resonance and Echocardiographic Techniques. J Cardiovasc Magn Reson. 2020;22(1):51. doi: 10.1186/s12968-020-00647-7.
25. Addetia K, Uriel N, Maffessanti F, Sayer G, Adatya S, Kim GH, et al. 3D Morphological Changes in LV and RV during LVAD Ramp Studies. JACC Cardiovasc Imaging. 2018;11(2 Pt 1):159-69. doi: 10.1016/j.jcmg.2016.12.019.
26. van der Zwaan HB, Helbing WA, McGhie JS, Geleijnse ML, Luijnenburg SE, Roos-Hesselink JW, et al. Clinical Value of Real-Time Three-Dimensional Echocardiography for Right Ventricular Quantification in Congenital Heart Disease: Validation with Cardiac Magnetic Resonance Imaging. J Am Soc Echocardiogr. 2010;23(2):134-40. doi: 10.1016/j.echo.2009.12.001.

27. Dragulescu A, Grosse-Wortmann L, Fackoury C, Riffle S, Waiss M, Jaeggi E, et al. Echocardiographic Assessment of Right Ventricular Volumes after Surgical Repair of Tetralogy of Fallot: Clinical Validation of a New Echocardiographic Method. J Am Soc Echocardiogr. 2011;24(11):1191-8. doi: 10.1016/j.echo.2011.08.006.

28. Molnár AÁ, Sánta A, Merkely B. Echocardiography Imaging of the Right Ventricle: Focus on Three-Dimensional Echocardiography. Diagnostics. 2023;13(15):2470. doi: 10.3390/diagnostics13152470.

29. Agricola E, Asmarats L, Maisano F, Cavalcante JL, Liu S, Milla F, et al. Imaging for Tricuspid Valve Repair and Replacement. JACC Cardiovasc Imaging. 2021;14(1):61-111. doi: 10.1016/j.jcmg.2020.01.031.

30. Ishizu T, Seo Y, Atsumi A, Tanaka YO, Yamamoto M, Machino-Ohtsuka T, et al. Global and Regional Right Ventricular Function Assessed by Novel Three-Dimensional Speckle-Tracking Echocardiography. J Am Soc Echocardiogr. 2017;30(12):1203-13. doi: 10.1016/j.echo.2017.08.007.

31. Wu VC, Takeuchi M. Three-Dimensional Echocardiography: Current Status and Real-Life Applications. Acta Cardiol Sin. 2017;33(2):107-18. doi: 10.6515/acs20160818a.

32. Herberg U, Smit F, Winkler C, Dalla-Pozza R, Breuer J, Laser KT. Real-Time 3D-Echocardiography of the Right Ventricle-Paediatric Reference Values for Right Ventricular Volumes Using Knowledge-Based Reconstruction: A Multicentre Study. Quant Imaging Med Surg. 2021;11(7):2905-17. doi: 10.21037/qims-20-1155.

33. Pinedo M, Villacorta E, Tapia C, Arnold R, López J, Revilla A, et al. Inter- and Intra-Observer Variability in the Echocardiographic Evaluation of Right Ventricular Function. Rev Esp Cardiol. 2010;63(7):802-9. doi: 10.1016/s1885-5857(10)70165-1.

34. Zhou J, Du M, Chang S, Chen Z. Artificial Intelligence in Echocardiography: Detection, Functional Evaluation, and Disease Diagnosis. Cardiovasc Ultrasound. 2021;19(1):29. doi: 10.1186/s12947-021-00261-2.

35. de Raat FM, van Houte J, Montenij LJ, Bouwmeester S, Felix SEA, Bingley P, et al. Evaluation of the Image Quality and Validity of Handheld Echocardiography for Stroke Volume and Left Ventricular Ejection Fraction Quantification: A Method Comparison Study. Int J Cardiovasc Imaging. 2024;40(1):15-25. doi: 10.1007/s10554-023-02942-7.

36. Randazzo M, Maffessanti F, Kotta A, Grapsa J, Lang RM, Addetia K. Added Value of 3D Echocardiography in the Diagnosis and Prognostication of Patients with Right Ventricular Dysfunction. Front Cardiovasc Med. 2023;10:1263864. doi: 10.3389/fcvm.2023.1263864.

37. Hameed A, Condliffe R, Swift AJ, Alabed S, Kiely DG, Charalampopoulos A. Assessment of Right Ventricular Function-a State of the Art. Curr Heart Fail Rep. 2023;20(3):194-207. doi: 10.1007/s11897-023-00600-6.

38. Addetia K, Lang RM. Decoding the Right Ventricle in 3 Dimensions. JAMA Cardiol. 2018;3(10):910-1. doi: 10.1001/jamacardio.2018.2452.

39. Otani K, Nabeshima Y, Kitano T, Takeuchi M. Accuracy of Fully Automated Right Ventricular Quantification Software with 3D Echocardiography: Direct Comparison with Cardiac Magnetic Resonance and Semi-Automated Quantification Software. Eur Heart J Cardiovasc Imaging. 2020;21(7):787-95. doi: 10.1093/ehjci/jez236.

40. Muraru D. 22nd Annual Feigenbaum Lecture: Right Heart, Right Now: The Role of Three-Dimensional Echocardiography. J Am Soc Echocardiogr. 2022;35(9):893-909. doi: 10.1016/j.echo.2022.05.011.

41. Magunia H, Dietrich C, Langer HF, Schibilsky D, Schlensak C, Rosenberger P, et al. 3D Echocardiography Derived Right Ventricular Function is Associated with Right Ventricular Failure and Mid-Term Survival after Left Ventricular Assist Device Implantation. Int J Cardiol. 2018;272:348-55. doi: 10.1016/j.ijcard.2018.06.026.

Cardiac Sarcoidosis: The Role of Multimodal Imaging

Lara Cristiane Terra Ferreira Carreira,[1] Lívia Carreira,[2] Adriana Soares Xavier de Brito[3,4]
Cardiologia Nuclear de Curitiba (CNC),[1] Curitiba, PR – Brazil
PUC Paraná,[2] Curitiba, PR – Brazil
Instituto Nacional de Cardiologia,[3] Rio de Janeiro, RJ – Brazil
Rede D'Or São Luiz,[4] Rio de Janeiro, RJ – Brazil

Central Illustration: Cardiac Sarcoidosis: The Role of Multimodal Imaging

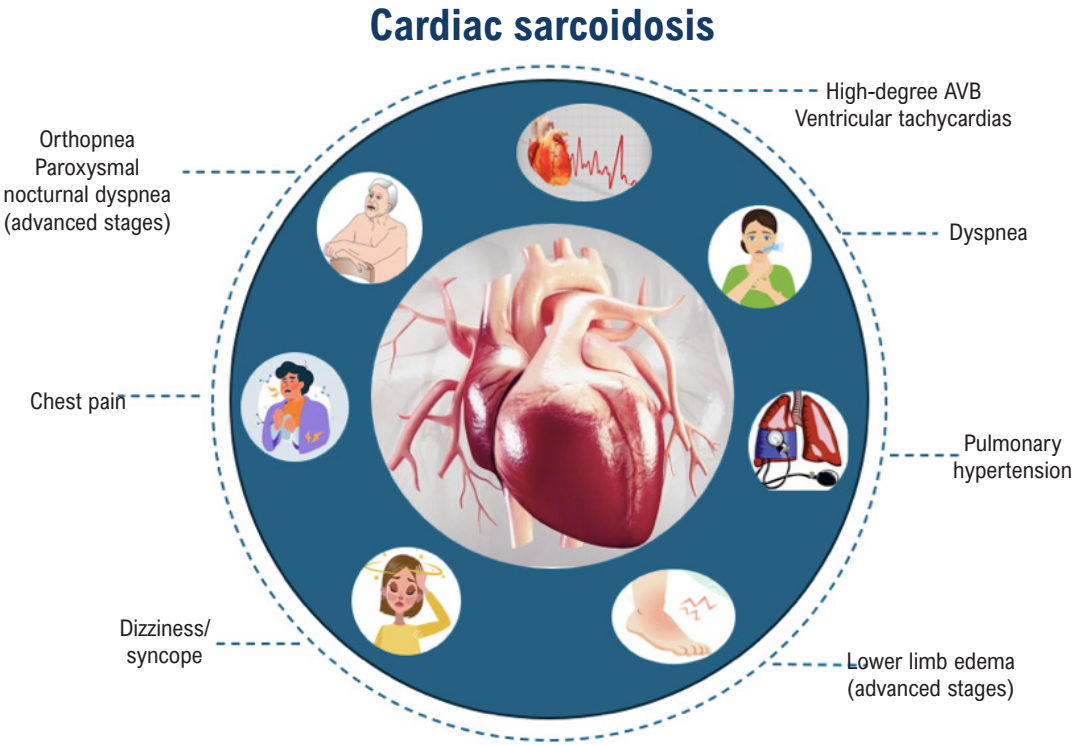

Arq Bras Cardiol: Imagem cardiovasc. 2026; 39(1):e20250038

Central Illustration: Clinical manifestations of cardiac sarcoidosis. AVB: atrioventricular block.

Keywords

Sarcoidosis; Positron-Emission Tomography; Fluorodeoxyglucose F18; Magnetic Resonance Imaging; Multimodal Imaging.

Mailing Address: Adriana Soares Xavier de Brito •
Instituto Nacional de Cardiologia. Rua das Laranjeiras, 374. Postal code: 22240-006. Rio de Janeiro, RJ – Brazil
E-mail: adrijsoares@hotmail.com
Manuscript received February 8, 2026; revised February 9, 2026; accepted February 9, 2026
Editor responsible for the review: Marcelo Tavares

DOI: https://doi.org/10.36660/abcimg.20250038i

Abstract

Cardiac sarcoidosis (CS) is a potentially severe manifestation of systemic sarcoidosis, associated with advanced atrioventricular block, ventricular arrhythmias, heart failure, and sudden death. Diagnosis remains challenging due to phenotypic variability and the limitations of conventional diagnostic methods. Advances in imaging techniques, especially the combination of positron emission tomography/computed tomography (PET/CT) using ^{18}F-FDG and cardiac magnetic resonance imaging (CMR), have revolutionized the diagnostic

approach and therapeutic monitoring of CS. This article reviews current concepts of CS and its diagnosis, with a focus on the role of PET/CT, the importance of appropriate patient preparation, and integration with CMR.

Introduction

Sarcoidosis is an inflammatory granulomatous disease of unknown etiology, characterized by non-caseating granulomas that can affect multiple organs.[1,2]

The disease affects the lungs and thoracic lymph nodes in approximately 90% of cases, but it can also involve the heart, liver, spleen, skin, eyes, parotid glands, among other organs and tissues. It is estimated that 20% to 25% of patients with pulmonary and/or systemic sarcoidosis have asymptomatic cardiac involvement (clinically silent disease),[2] whereas approximately 5% have clinically manifest cardiac involvement. This involvement is associated with increased morbidity and mortality, resulting from infiltrative heart disease with intense myocardial inflammation.

Approximately half of cardiac sarcoidosis (CS) cases occur in isolation, without evidence of systemic sarcoidosis.[1]

The pathophysiology of CS involves an exaggerated immune response to environmental antigens in individuals who are genetically predisposed. This response culminates in the activation of T cells and the formation of granulomas, with subsequent progression to myocardial fibrosis. The disease most frequently affects individuals between 25 and 55 years of age, with higher prevalence among women, Black individuals, and Japanese populations. It is also responsible for a significant proportion of sudden death in young adults.[3]

CS can manifest as arrhythmias, atrioventricular blocks, dilated cardiomyopathy, or sudden death. Cardiac symptoms are usually dominant, as patients often present only with low-grade pulmonary involvement and no other organ involvement.[2] The high morbidity and mortality make early and accurate diagnosis essential (Central Illustration).

The prevalence of CS has increased during the last two decades, probably due to the use of advanced cardiac imaging. At the same time, it is remains a reversible cause of cardiomyopathy and arrhythmias that is frequently underdiagnosed.

Clinical diagnosis and current criteria

Investigation for CS should be performed in individuals with known systemic sarcoidosis, especially when other organs are involved. In addition, CS should be suspected in patients under 55 years of age who present with atrioventricular block (AVB), ventricular arrhythmias, or heart failure of unclear etiology.

Diagnosis of CS remains challenging due to the limited sensitivity and specificity of any single diagnostic modality, highlighting the importance of high clinical suspicion, the use of multimodal imaging to guide diagnosis and treatment, and histological findings.

Endomyocardial biopsy remains the gold standard for CS diagnosis, but, due to the irregular and predominantly mesocardial pattern of involvement, it has a diagnostic yield of around 25% to 30%, with a high rate of false negatives. There is, therefore, an ongoing debate regarding the real need for histological confirmation for definitive diagnosis.[4]

The main diagnostic criteria for CS have been established by the Heart Rhythm Society (HRS)[5] and the Japanese Circulation Society (JCS).[6] According to the HRS, definitive diagnosis requires histological confirmation of non-caseating granulomas in the myocardium, whereas probable diagnosis can be established in the presence of confirmed extracardiac sarcoidosis and typical evidence of cardiac involvement, either by imaging or characteristic clinical manifestations. On the other hand, the JCS admits the diagnosis of isolated CS even in the absence of histological confirmation, provided that there are compatible clinical and imaging findings, allowing greater sensitivity in detecting cases without apparent systemic sarcoidosis.

Even though these criteria are still widely used, especially in regional contexts, no set of criteria is perfect or universally applicable.

The current trend is to abandon the rigid and binary use of these criteria (positive/negative) and adopt an integrated probabilistic approach, classifying the diagnosis as:

- Definite
- Highly probable
- Probable
- Possible/low probability

This approach is inspired by the World Association of Sarcoidosis and Other Granulomatous Disorders (WASOG) classification and has been adopted by multiple authors to incorporate the relative weight of clinical, laboratory, and advanced imaging findings (CMR and PET, Figure 1) in the final probability of CS.[3]

Sarcoidosis is often called "the great mimicker," due to its diverse manifestations and must be differentiated from other cardiac syndromes with a similar phenotype, such as acute myocarditis, chronic inflammatory cardiomyopathies (including those related to autoimmune, hereditary and infiltrative diseases) and other granulomatous diseases. Clinical context and cardiac imaging are often insufficient to differentiate sarcoidosis from other forms of cardiac pathology that cause hereditary arrhythmogenic cardiomyopathies or myocarditis. The wide spectrum of clinical presentations and the limitations in obtaining histopathological confirmation, especially in cases of clinically isolated CS, are additional challenges in distinguishing it from alternative diagnoses. To address this complexity, a multidisciplinary team is needed, composed of specialists in systemic sarcoidosis, heart failure, electrophysiology, advanced cardiac imaging, cardiovascular genetics, and cardiac pathology.[3]

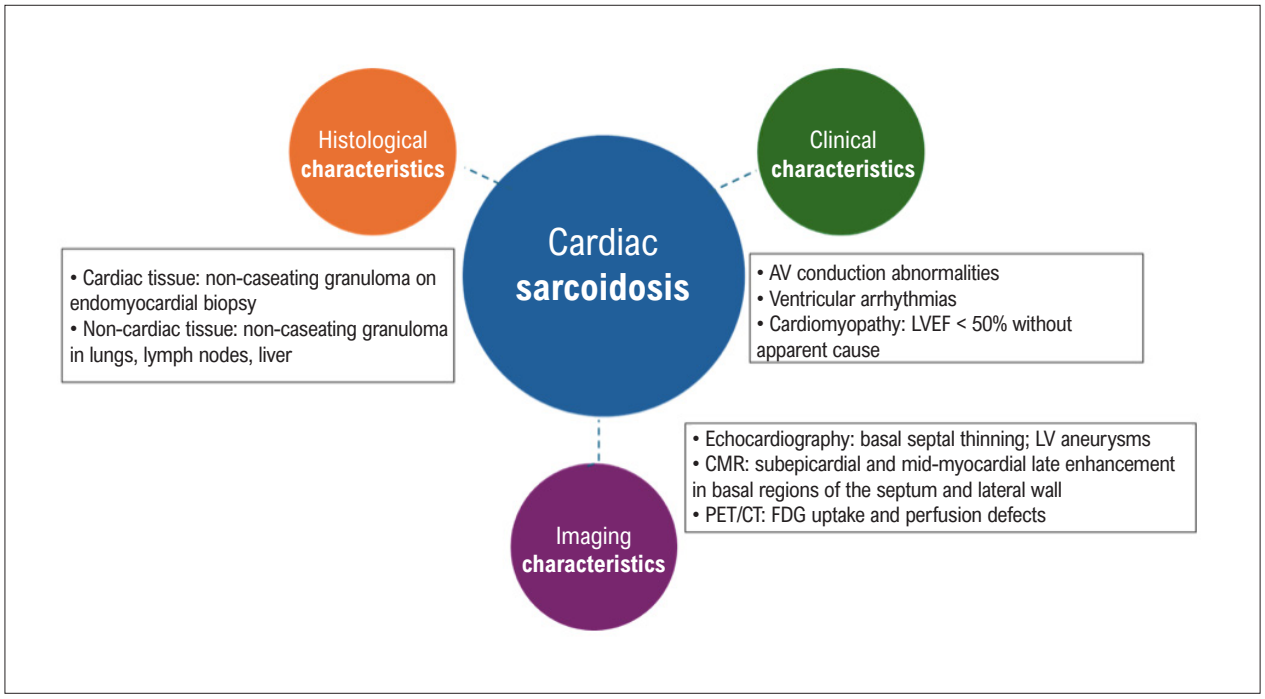

Figure 1 – *Diagnosis of cardiac sarcoidosis. AV: atrioventricular; CMR: cardiac magnetic resonance imaging; FDG: fluorodeoxyglucose; LV: left ventricle; LVEF: left ventricular ejection fraction; PET/CT: positron emission tomography/computed tomography.*

Diagnostic modalities

Electrocardiography

Although widely available, electrocardiography (ECG) has limited sensitivity and specificity for the diagnosis of CS.[7] Nevertheless, diagnostic guidelines have incorporated some ECG abnormalities as criteria, including conduction disturbances, AVB, frequent or multifocal ventricular extrasystoles, right or left bundle branch blocks, and abnormal Q waves.[5,6]

Holter ECG can increase suspicion for CS in the presence of frequent ventricular extrasystoles, high-grade conduction abnormalities, or ventricular arrhythmias such as ventricular tachycardia.[3]

Echocardiography

Transthoracic echocardiography is widely available and can be used as an initial tool to detect structural and functional abnormalities in the heart, although it does not provide detailed tissue characterization.[7] Although abnormal echocardiography is useful for determining cardiac involvement in patients with suspected CS (low to moderate sensitivity), a normal echocardiogram does not rule out the presence of cardiac involvement (low specificity). Abnormal findings that support diagnosis of CS include septal thinning, abnormal ventricular wall anatomy (ventricular aneurysm or regional ventricular wall thickening), unexplained left ventricular (LV) systolic dysfunction, or LV dilation.[8] When combined with clinical symptoms, ECG or Holter abnormalities, echocardiography increases the sensitivity for detecting CS. Furthermore, more recent echocardiographic approaches, including global longitudinal strain measurements, can assist in accurately identifying patients with CS who have preserved left ventricular ejection fraction (LVEF).[9]

Despite its limited sensitivity and specificity, echocardiography remains useful for initial screening and serial monitoring of CS due to its wide availability and low cost.

Myocardial perfusion imaging

Myocardial perfusion scintigraphy generally shows segmental areas of reduced tracer uptake in the ventricular myocardium of patients with CS, making it useful in resting assessment of scars resulting from microvascular compression and/or fibrogranulomatous replacement of myocardial tissue, which can generate perfusion defects. Generally, these defects do not follow the typical vascular distribution pattern of coronary artery disease, except in cases of very extensive involvement. Therefore, they are nonspecific findings and can be observed in ischemic dilated cardiomyopathies or cardiomyopathies of other etiologies. Thus, myocardial perfusion imaging alone is not sufficient to confidently establish the diagnosis of CS, especially in the absence of cardiac symptoms.

On the other hand, positron emission tomography/computed tomography (PET/CT) using ^{18}F-fluorodeoxyglucose (^{18}F-FDG) for assessment of myocardial metabolism, associated with perfusion imaging

performed with ^{13}N-ammonia, ^{82}Rb or, alternatively, single-photon emission computed tomography (SPECT) using ^{99m}Tc-sestamibi, has emerged as a valuable tool in the diagnosis and staging of CS. This hybrid approach allows simultaneous identification of active inflammation and areas of fibrosis, contributing to improved stratification of disease activity and chronicity.[10]

Cardiac magnetic resonance imaging

Cardiac magnetic resonance imaging (CMR) is a high-spatial-resolution modality that, in addition to providing detailed assessment of biventricular function, identifies and quantifies areas of myocardial injury, including edema and fibrosis, primarily through late gadolinium enhancement (LGE).

Gadolinium is an extracellular contrast agent with rapid elimination from normal myocardium, but slow elimination from areas of fibrosis and inflammation, resulting in delayed enhancement in expanded extracellular space.

CMR allows for precise, non-invasive evaluation of the entire heart with high accuracy in detecting focal myocardial changes typical of CS, in both the acute (edema) and chronic (fibrosis) phases. Furthermore, it provides detailed information on cardiac structure and function, also enabling the identification of mediastinal and hilar lymphadenopathy, hepatosplenic changes, and pulmonary nodules that may suggest extracardiac sarcoidosis. The technique is also capable of detecting other cardiomyopathies and ischemic disease, which reinforces its value in differential diagnosis.

CMR has become a fundamental tool in the diagnostic assessment of CS, and it is routinely recommended in patients with clinical suspicion of the disease, especially given the well-recognized limited sensitivity of echocardiography.[10]

Using clinical criteria as a reference standard and non-ischemic LGE patterns as a definition of positivity, CMR demonstrated high sensitivity (95%) and specificity (85%) for diagnosis of CS, according to a meta-analysis of 17 studies involving 1,031 individuals.[11]

The presence of LGE is the strongest predictor of all-cause mortality and sustained ventricular arrhythmias in individuals with known or suspected CS.[12]

A systematic review and meta-analysis of macroscopic pathological images of hearts with histologically confirmed CS identified common sites of myocardial involvement. LV subepicardial, interventricular septum, LV multifocal, and right ventricular free wall involvement were observed in more than 90% of cases (frequent pathological features).[13]

In many cases, however, the LGE pattern may be nonspecific, making it difficult to differentiate between CS, myocarditis, and other cardiomyopathies. Therefore, no single LGE pattern is sufficient to establish the diagnosis of CS. It is thus recommended that CMR findings be analyzed by a multidisciplinary team within a multimodal framework.

CMR also provides a high negative predictive value, both to rule out the disease and to identify patients with a low event rate, and it may be useful in assessing other differential diagnoses (e.g., arrhythmogenic right ventricular cardiomyopathy, myocarditis, prior myocardial infarction).

Positron emission tomography/computed tomography using ^{18}F-fluorodeoxyglucose

FDG, a glucose analogue, is sequestered in activated inflammatory cells, such as macrophages and lymphocytes, via insulin-independent glucose transporter proteins (GLUT1 and GLUT3) and, therefore, accumulates in areas of regulated glucose metabolism, including hypermetabolic sites of myocardial sarcoid infiltration. Thus, it detects metabolically active inflammatory lesions.

Reviews have reported a diagnostic sensitivity of 91% and specificity of 75.5% for ^{18}F-FDG-PET/CT in the diagnosis of CS. The main cause of the limited specificity and high variability seems to be associated with physiological FDG uptake in normal myocardium. Therefore, adequate preparation for the study is essential to accurately diagnose CS using ^{18}F-FDG-PET/CT.

Cardiac ^{18}F-FDG-PET/CT provides useful anatomical and morphological information to assess the location, extent, activity, and stage of the disease. As a complementary modality to CMR, it enables non-invasive image-guided diagnosis and identifies extracardiac sites suitable for biopsy, contributing to histological confirmation of systemic sarcoidosis.

Furthermore, it is applied for monitoring therapeutic response, longitudinal follow-up, risk stratification, and prognosis.[14]

The most characteristic pattern of CS on ^{18}F-FDG-PET/CT is multifocal radiopharmaceutical uptake, particularly when associated with resting perfusion defects (metabolic-perfusion mismatch pattern), reflecting disruption between perfusion and metabolism (Figure 2B). In some cases, focal FDG uptake restricted to the interventricular septum (even in the absence of late enhancement on CMR) may be the only imaging sign of sarcoid involvement, especially in patients with heart block (Figure 2A). When active inflammatory tissue is replaced by fibrosis, FDG uptake is not observed at the LGE sites (match pattern), i.e., metabolically inactive disease (Figure 2C). Findings of FDG uptake that can lead to false positives result from inadequate physiological suppression or increased glucose uptake in conditions such as hibernating myocardium, inflammatory or genetic dilated cardiomyopathies, recent infarction, and inflammatory responses following recent cardiac procedures such as ventricular ablation (Figure 2D).[3]

The extent of FDG uptake has been correlated with the risk of adverse events such as death, ventricular arrhythmias, and hospitalizations for heart failure, although CMR with LGE has shown superior prognostic capacity in some studies.[15]

Although there is still not enough data to justify the exclusive use of FDG-PET for risk stratification of sudden cardiac death, its association with CMR and clinical data may be valuable for prognostic assessment.

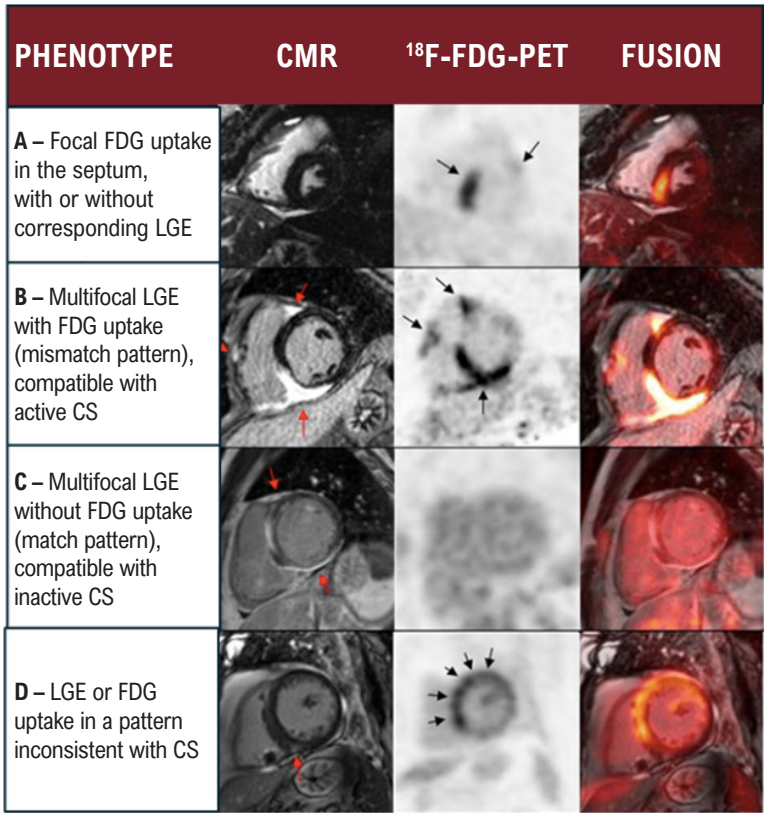

Figure 2 – *Findings on cardiac magnetic resonance and ^{18}F-FDG-PET according to disease phenotype (adapted from Cheng et al.3). CMR: cardiac magnetic resonance imaging; CS: cardiac sarcoidosis; FDG: fluorodeoxyglucose; LGE: late gadolinium enhancement; PET: positron emission tomography.*

Patient preparation for ^{18}F-FDG-PET with: suppression of physiological FDG uptake in normal myocardium

It is important to emphasize that glucose is a common energy source in healthy myocardial cells; however, unlike inflammatory cells, cardiomyocytes absorb glucose via an insulin-dependent mechanism (GLUT4) regulated by fasting and dietary composition. During fasting, more than 90% of myocardial energy metabolism is derived from fatty acid metabolism. Most of the remaining 10% involves other substances, including glucose. However, myocardial glucose metabolism during fasting varies among individuals, and in some cases, FDG uptake is observed in the myocardium even under fasting conditions. This variability can compromise ^{18}F-FDG-PET images of myocardial inflammation and affect diagnostic accuracy. Consequently, inducing a metabolic shift in the heart, defined as the transition from glucose utilization to fatty acids and fatty acid-derived ketones, can lead to the suppression of normal FDG uptake in the heart (through inhibition of GLUT4 translocation) and the identification of FDG-avid inflammatory cells.

The goal is to suppress physiological uptake of glucose by the myocardium. To this end, a high-fat, low-carbohydrate diet is recommended for 12 to 24 hours, followed by prolonged fasting for 12 to 18 hours before the examination. Intravenous administration of unfractionated heparin (50 IU/kg), 15 minutes before FDG injection, has also been considered and performed by some centers. Physical activity should be avoided for 24 hours before the examination (at least 12 hours), as it increases myocardial FDG uptake. Adequate sleep the night before the examination is also recommended (Figure 3).

In the case of insulin-dependent patients with diabetes, insulin use is not permitted on the day of the examination. Serum glucose level must be below 180 mg/dL.[16]

Images are acquired approximately 60 to 90 minutes after FDG injection.

Interpretation of cardiac ^{18}F-FDG-PET/CT

Interpretation of ^{18}F-FDG-PET/CT images in CS is based on the identification of FDG uptake patterns, such as focal or focal-over-diffuse uptake, which are indicative of active inflammation.

Semiquantitative analysis, using the standardized uptake value (SUV), can help quantify inflammatory activity and assess treatment response,[17] although there is no evidence relating specific SUV values to clinical outcomes, nor is there a validated SUV threshold that differentiates CS from normal myocardium.

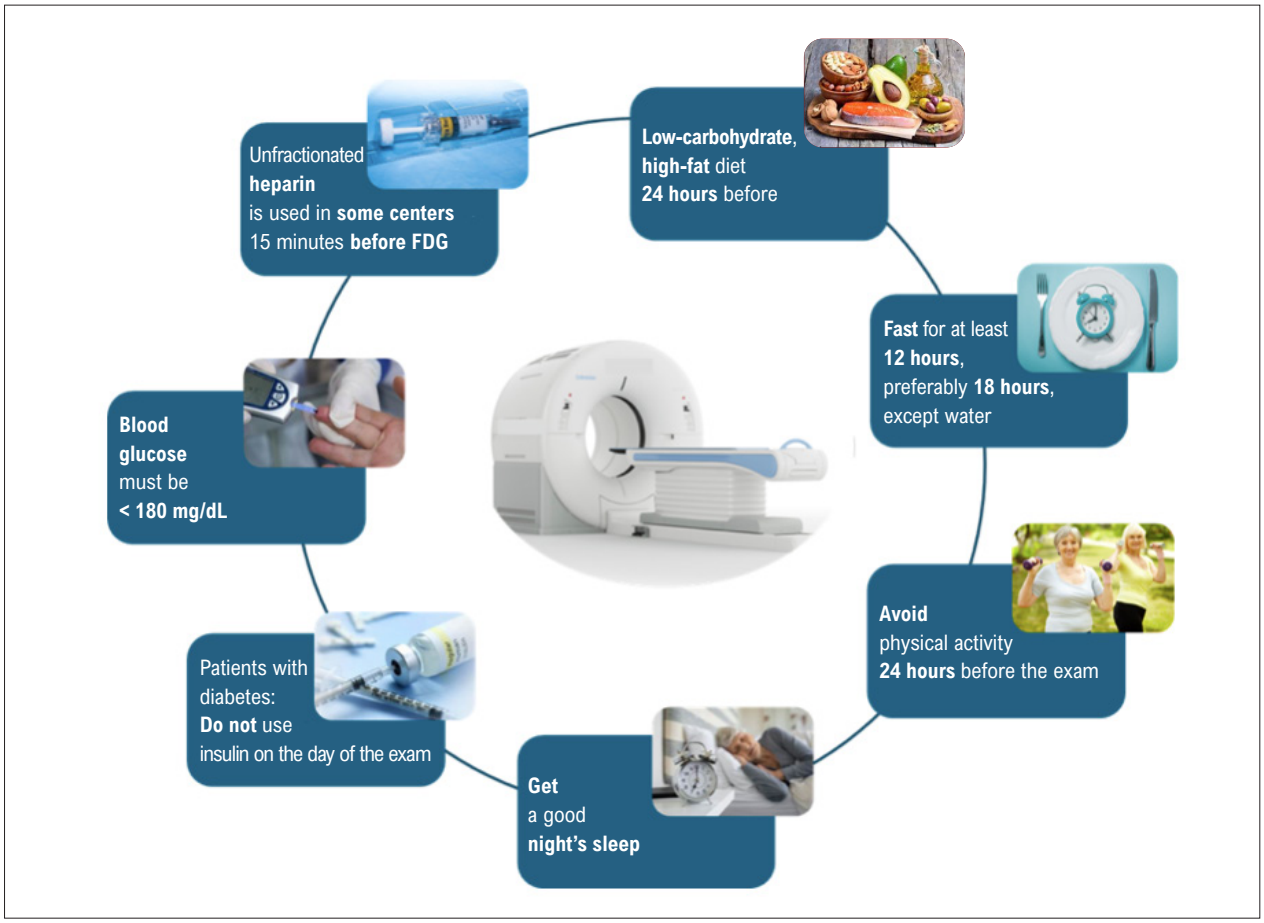

Figure 3 – *Patient preparation for 18F-FDG-PET/CT. FDG: fluorodeoxyglucose; PET/CT: positron emission tomography/computed tomography.*

In the context of monitoring treatment response, FDG-PET is used to assess changes in inflammatory activity after the introduction of immunosuppressive therapies, such as corticosteroids. A reduction in FDG uptake after treatment is associated with a favorable response.[17]

Combined analysis of CMR and FDG-PET

Studies have demonstrated that the hybrid CMR/FDG-PET approach improves diagnostic and prognostic accuracy in patients with CS. The simultaneous presence of LGE and FDG uptake is a strong indicator of active CS, associated with an increased risk of adverse cardiac events, such as cardiac arrest and ventricular tachycardia.[18]

Furthermore, the combination of these modalities enhances risk stratification and monitoring of treatment response, especially in patients with suspected or confirmed cardiac involvement.[19]

The hybrid approach is also useful in complex cases, for example, patients with prior myocardial infarction, where differentiating between post-infarction fibrosis and sarcoid inflammation may be challenging.

Therefore, the combination of FDG-PET and CMR provides a more comprehensive view of cardiac pathology, supporting clinical decision-making and therapeutic management of CS.

Final considerations

In patients with clinical suspicion of sarcoidosis with cardiac involvement, CMR represents an excellent screening modality, as the absence of LGE is associated with a high negative predictive value, as well as excellent prognosis. In patients with contraindications to CMR and symptoms suggestive of active disease, FDG-PET combined with resting myocardial perfusion scintigraphy can also be used for the diagnosis of cardiac and extracardiac disease. In addition, serial assessment of inflammation using FDG-PET has been recommended to monitor response to therapy, thus guiding the duration and choice of medications. Despite growing recognition that CMR and FDG-PET imaging can identify patients at higher risk of adverse events, randomized multicenter trials are lacking to guide and standardize follow-up. Future studies are needed to determine the benefits of image-guided therapies, with the aim of improving these patients' prognosis.

Illustrative clinical cases

Case 1 – A 68-year-old female patient with hypertension presented to the emergency department due to tachycardia and dyspnea at rest. ECG revealed sustained ventricular tachyarrhythmia and clinical signs of decompensated heart failure. Immediate electrical cardioversion was performed, and intravenous amiodarone was administered. Invasive coronary angiography revealed nonobstructive coronary arteries, severe LV systolic dysfunction, and diffuse hypokinesia. CMR revealed moderate left atrial enlargement, LV with global systolic dysfunction (LVEF = 40%). A moderate amount of multifocal LGE was present, unrelated to coronary topography. Enhancement was transmural in the anterior segments (apical and basal); heterogeneous and mid-myocardial to subepicardial in the inferior and anterolateral (medial and basal) segments, with endocardial sparing; and heterogeneous along the right ventricular side of the interventricular septum. The pattern was thus compatible with CS (Figure 4A). Pulse therapy with intravenous corticosteroids was indicated, followed by implantation of a cardioverter-defibrillator.

Two months after hospital discharge, with reduced dose of corticosteroids, the patient presented with fatigue on exertion, palpitations, and afternoon fever. There were no other symptoms of infection, and leukogram revealed mild leukocytosis. Recurrence of myocardial inflammation due to active disease was suspected. PET/CT with ^{18}F-FDG associated with resting myocardial perfusion scintigraphy with ^{99m}Tc-sestamibi was requested to assess inflammation and perfusion. Scintigraphy demonstrated anteroseptal, septoapical, and apical hypoperfusion, LVEF of 29%, diffuse hypokinesia, and akinesia of the apical segments (Figure 4B). ^{18}F-FDG-PET/CT revealed abnormal radiopharmaceutical uptake throughout the anterior and septal walls of the LV, sparing the inferolateral wall, corresponding to an active inflammatory process, with a pattern described as "focal-on-diffuse" (Figure 4C).

Prednisone was resumed at a dose of 1 mg/kg/day, and methotrexate was added to the treatment. She showed a good response and significant clinical improvement

Case 2 – A 56-year-old male patient without comorbidities received a diagnosis of myocardial infarction with non-obstructive coronary arteries (MINOCA) after hospital admission for chest pain and dyspnea, with coronary computed tomography angiography and invasive coronary angiography showing no obstructive lesions. CMR demonstrated increased LV volumes, reduced wall thickness, and akinesia of the inferior, inferoseptal, and basal inferolateral segments. The myocardial mass with LGE was estimated at 27% of the LV. Echocardiography confirmed these findings, with akinesia and thinning of the basal segment of the inferior wall, hypokinesia of the remaining walls, more pronounced in the inferior and inferolateral septum, and global LV dysfunction (LVEF = 35%). ECG showed sinus rhythm, first degree AVB, and complete left bundle branch block. He remained on clinical treatment for heart failure and MINOCA.

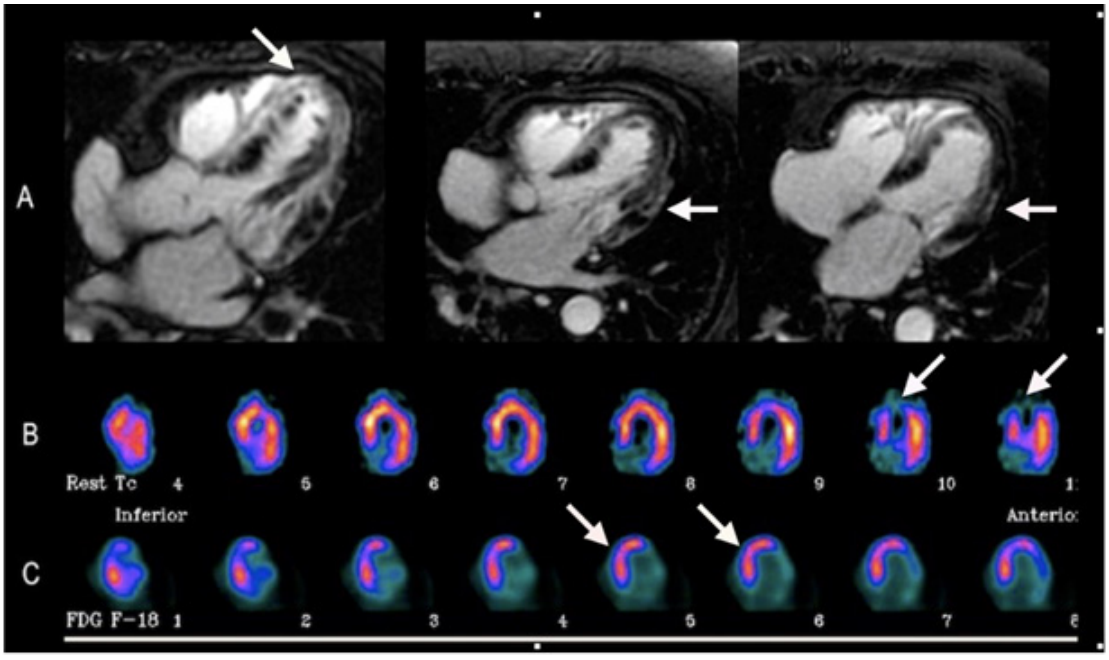

Figure 4 – *(A) Cardiac magnetic resonance imaging with gadolinium demonstrating late enhancement in the septo-apical and lateral regions. (B) Myocardial perfusion scintigraphy with 99mTc-sestamibi – horizontal long axis demonstrating hypoperfusion in the apical segments. (C) 18F-FDG PET/CT with abnormal radiotracer uptake in the left ventricle, sparing the inferolateral wall, representing a focal-on-diffuse pattern. FDG: fluorodeoxyglucose; PET/CT: positron emission tomography/computed tomography.*

Two years later, the patient's functional class worsened, with progressive fatigue during even moderate exertion. A 24-hour Holter ECG demonstrated periods of complete AVB, and the patient was referred for pacemaker implantation, with suspected inflammatory/infiltrative disease. He was also referred for PET/CT with ^{18}F-FDG and resting myocardial perfusion scintigraphy with ^{99m}Tc-sestamibi to assess inflammation and perfusion.

SPECT/CT scintigraphy demonstrated pronounced hypoperfusion throughout the inferior, inferolateral, and basal inferoseptal walls, LVEF of 31%, diffuse hypokinesia and akinesia of the inferior wall, and inferoseptal dyskinesia (Figures 5 and 6, respectively). An ^{18}F-FDG-PET/CT scan revealed abnormal uptake of the radiopharmaceutical in the septal region, inferior region, and throughout the lateral wall, corresponding to an active inflammatory process (Figure 7), demonstrating a metabolic-perfusion mismatch, a pattern described as focal-on-diffuse. In addition, there was increased uptake in subcarinal lymph nodes and pulmonary hila. Lymph node biopsy confirmed the diagnosis of sarcoidosis, and the patient underwent corticosteroid therapy, with a favorable response in terms of functional class and improved LV function.

Author Contributions

Conception and design of the research, acquisition of data, analysis and interpretation of the data, writing of the manuscript and critical revision of the manuscript for intellectual content: Carreira LCTF, Carreira L, Brito ASX.

Potential Conflict of Interest

No potential conflict of interest relevant to this article was reported.

Sources of Funding

There were no external funding sources for this study.

Study Association

This study is not associated with any thesis or dissertation work.

Ethics Approval and Consent to Participate

This article does not contain any studies with human participants or animals performed by any of the authors.

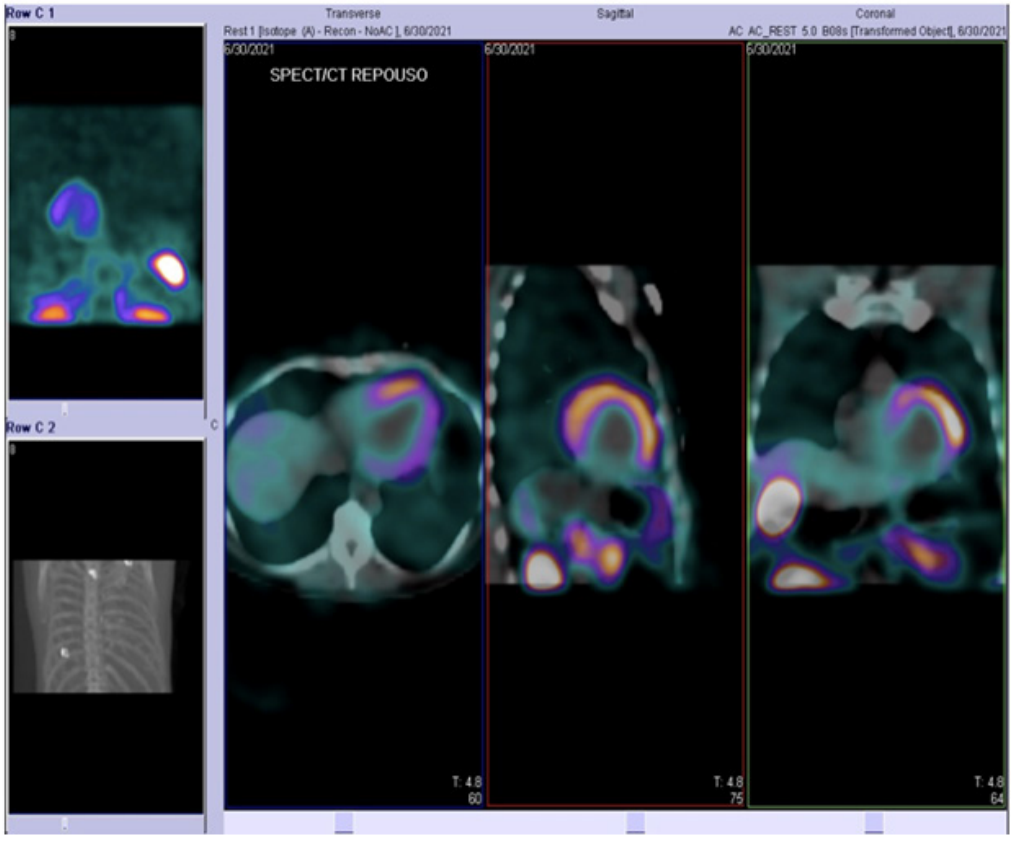

Figure 5 – *SPECT/CT with ^{99m}Tc-sestamibi showing fusion images in the axial, sagittal, and coronal axes demonstrating pronounced hypoperfusion of the radiotracer in the inferior, inferoseptal, and inferolateral walls of the left ventricle. SPECT/CT: single-photon emission computed tomography/computed tomography.*

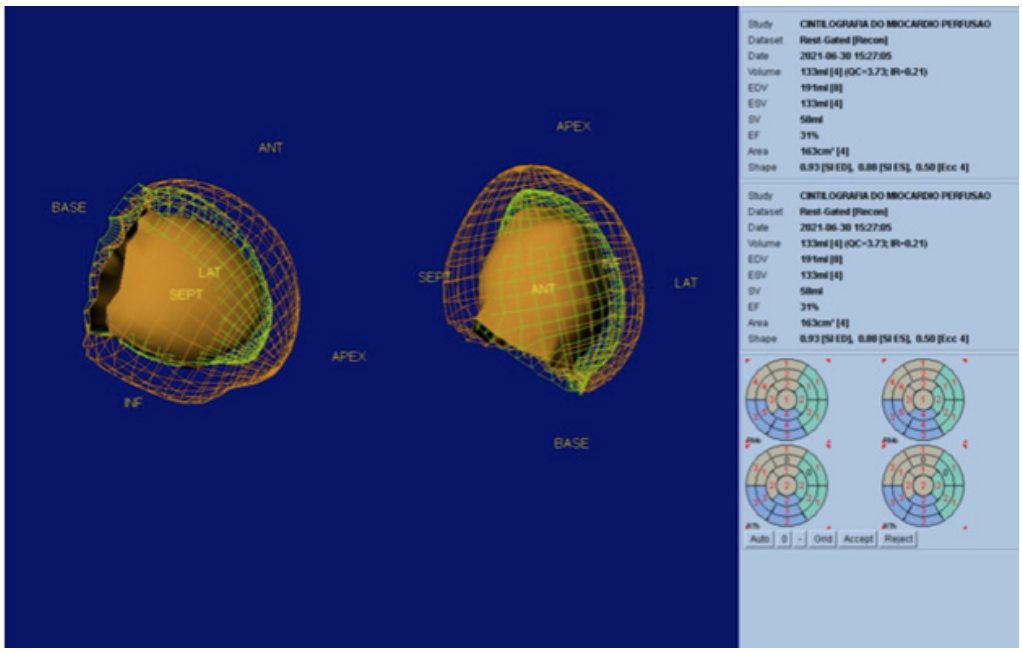

Figure 6 – *Gated-SPECT em repouso com uma reconstrução tridimensional do ventrículo esquerdo demonstrando fração de ejeção de 31%, aumento dos volumes ventriculares, acinesia inferior e discinesia inferosseptal. SPECT: tomografia computadorizada de emissão de fóton único.*

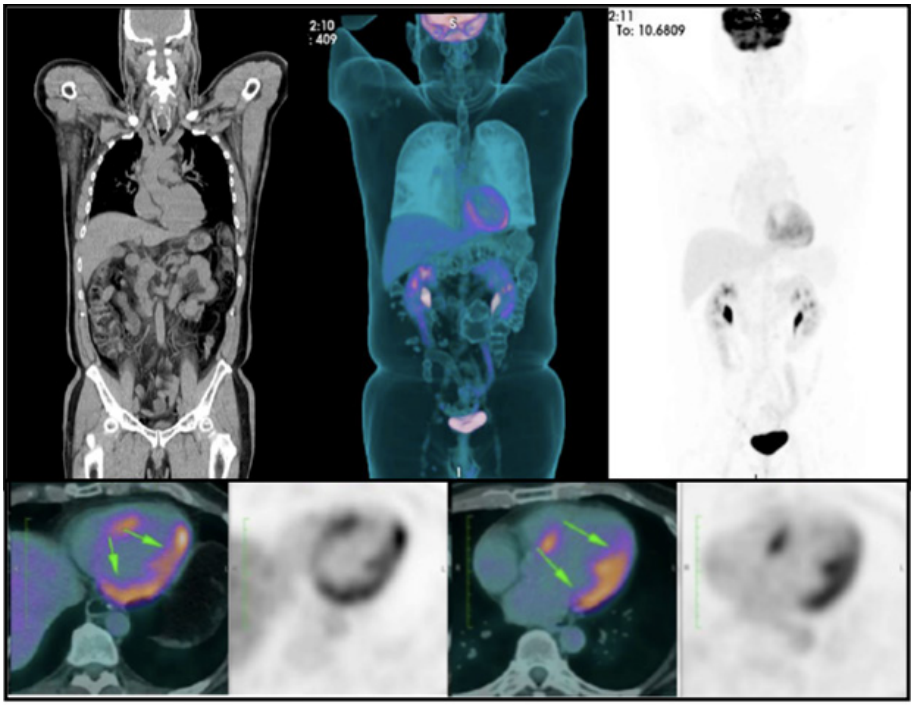

Figura 7 – *Resting gated-SPECT with three-dimensional reconstruction of the left ventricle demonstrating ejection fraction of 31%, increased ventricular volumes, inferior akinesia, and inferoseptal dyskinesia. SPECT: single-photon emission computed tomography.*

Use of Artificial Intelligence

The authors did not use any artificial intelligence tools in the development of this work.

Availability of Research Data

The underlying content of the research text is contained within the manuscript.

References

1. Mathai SV, Patel S, Jorde UP, Rochlani Y. Epidemiology, Pathogenesis, and Diagnosis of Cardiac Sarcoidosis. Methodist Debakey Cardiovasc J. 2022;18(2):78-93. doi: 10.14797/mdcvj.1057.
2. Birnie DH, Nery PB, Ha AC, Beanlands RS. Cardiac Sarcoidosis. J Am Coll Cardiol. 2016;68(4):411-21. doi: 10.1016/j.jacc.2016.03.605.
3. Cheng RK, Kittleson MM, Beavers CJ, Birnie DH, Blankstein R, Bravo PE, et al. Diagnosis and Management of Cardiac Sarcoidosis: A Scientific Statement from the American Heart Association. Circulation. 2024;149(21):e1197-e1216. doi: 10.1161/CIR.0000000000001240.
4. Sharma A, Okada DR, Yacoub H, Chrispin J, Bokhari S. Diagnosis of Cardiac Sarcoidosis: An Era of Paradigm Shift. Ann Nucl Med. 2020;34(2):87-93. doi: 10.1007/s12149-019-01431-z.
5. Birnie DH, Sauer WH, Bogun F, Cooper JM, Culver DA, Duvernoy CS, et al. HRS Expert Consensus Statement on the Diagnosis and Management of Arrhythmias Associated with Cardiac Sarcoidosis. Heart Rhythm. 2014;11(7):1305-23. doi: 10.1016/j.hrthm.2014.03.043.
6. Terasaki F, Azuma A, Anzai T, Ishizaka N, Ishida Y, Isobe M, et al. JCS 2016 Guideline on Diagnosis and Treatment of Cardiac Sarcoidosis - Digest Version. Circ J. 2019;83(11):2329-88. doi: 10.1253/circj.CJ-19-0508.
7. Agrawal T, Saleh Y, Sukkari MH, Alnabelsi TS, Khan M, Kassi M, et al. Diagnosis of Cardiac Sarcoidosis: A Primer for Non-Imagers. Heart Fail Rev. 2022;27(4):1223-33. doi: 10.1007/s10741-021-10126-5.
8. Terasaki F, Yoshinaga K. New Guidelines for the Diagnosis of Cardiac Sarcoidosis in Japan. Ann Nucl Cardiol. 2017;3(1):42-5.
9. Murtagh G, Laffin LJ, Patel KV, Patel AV, Bonham CA, Yu Z, et al. Improved Detection of Myocardial Damage in Sarcoidosis Using Longitudinal Strain in Patients with Preserved Left Ventricular Ejection Fraction. Echocardiography. 2016;33(9):1344-52. doi: 10.1111/echo.13281.
10. Slart RHJA, Glaudemans AWJM, Gheysens O, Lubberink M, Kero T, Dweck MR, et al. Procedural Recommendations of Cardiac PET/CT Imaging: Standardization in Inflammatory-, Infective-, Infiltrative-, and Innervation (4Is)-Related Cardiovascular Diseases: A Joint Collaboration of the EACVI and the EANM. Eur J Nucl Med Mol Imaging. 2021;48(4):1016-39. doi: 10.1007/s00259-020-05066-5.
11. Aitken M, Chan MV, Fresno CU, Farrell A, Islam N, McInnes MDF, et al. Diagnostic Accuracy of Cardiac MRI versus FDG PET for Cardiac Sarcoidosis: A Systematic Review and Meta-Analysis. Radiology. 2022;304(3):566-79. doi: 10.1148/radiol.213170.
12. Stevenson A, Bray JJH, Tregidgo L, Ahmad M, Sharma A, Ng A, et al. Prognostic Value of Late Gadolinium Enhancement Detected on Cardiac Magnetic Resonance in Cardiac Sarcoidosis. JACC Cardiovasc Imaging. 2023;16(3):345-57. doi: 10.1016/j.jcmg.2022.10.018.
13. Okasha O, Kazmirczak F, Chen KA, Farzaneh-Far A, Shenoy C. Myocardial Involvement in Patients with Histologically Diagnosed Cardiac Sarcoidosis: A Systematic Review and Meta-Analysis of Gross Pathological Images from Autopsy or Cardiac Transplantation Cases. J Am Heart Assoc. 2019;8(10):e011253. doi: 10.1161/JAHA.118.011253.
14. Chareonthaitawee P, Beanlands RS, Chen W, Dorbala S, Miller EJ, Murthy VL, et al. Joint SNMMI-ASNC Expert Consensus Document on the Role of 18F-FDG PET/CT in Cardiac Sarcoid Detection and Therapy Monitoring. J Nucl Cardiol. 2017;24(5):1741-58. doi: 10.1007/s12350-017-0978-9.
15. Aitken M, Davidson M, Chan MV, Fresno CU, Vasquez LI, Huo YR, et al. Prognostic Value of Cardiac MRI and FDG PET in Cardiac Sarcoidosis: A Systematic Review and Meta-Analysis. Radiology. 2023;307(2):e222483. doi: 10.1148/radiol.222483.
16. Kumita S, Yoshinaga K, Miyagawa M, Momose M, Kiso K, Kasai T, et al. Recommendations for 18F-Fluorodeoxyglucose Positron Emission Tomography Imaging for Diagnosis of Cardiac Sarcoidosis-2018 Update: Japanese Society of Nuclear Cardiology Recommendations. J Nucl Cardiol. 2019;26(4):1414-33. doi: 10.1007/s12350-019-01755-3.
17. Lee PI, Cheng G, Alavi A. The Role of Serial FDG PET for Assessing Therapeutic Response in Patients with Cardiac Sarcoidosis. J Nucl Cardiol. 2017;24(1):19-28. doi: 10.1007/s12350-016-0682-1.
18. Trivieri MG, Robson PM, Vergani V, LaRocca G, Romero-Daza AM, Abgral R, et al. Hybrid Magnetic Resonance Positron Emission Tomography is Associated with Cardiac-Related Outcomes in Cardiac Sarcoidosis. JACC Cardiovasc Imaging. 2024;17(4):411-24. doi: 10.1016/j.jcmg.2023.11.010.
19. Greulich S, Gatidis S, Gräni C, Blankstein R, Glatthaar A, Mezger K, et al. Hybrid Cardiac Magnetic Resonance/Fluorodeoxyglucose Positron Emission Tomography to Differentiate Active from Chronic Cardiac Sarcoidosis. JACC Cardiovasc Imaging. 2022;15(3):445-56. doi: 10.1016/j.jcmg.2021.08.018.

Step-by-Step Approach to the Evaluation of Constrictive Pericarditis

Aline Travessa,[1] *Paulo Henrique Pereira,*[2] *Louise Moutinho Machado,*[1] *Natalia Sousa Esteves*[1]

Hospital de Aeronáutica de Belém,[1] *Belém, PA – Brazil*

Força Aérea Brasileira, Departamento de Ciência e Tecnologia Aeroespacial,[2] *São José dos Campos, SP – Brazil*

Central Illustration: Step-by-Step Approach to the Evaluation of Constrictive Pericarditis

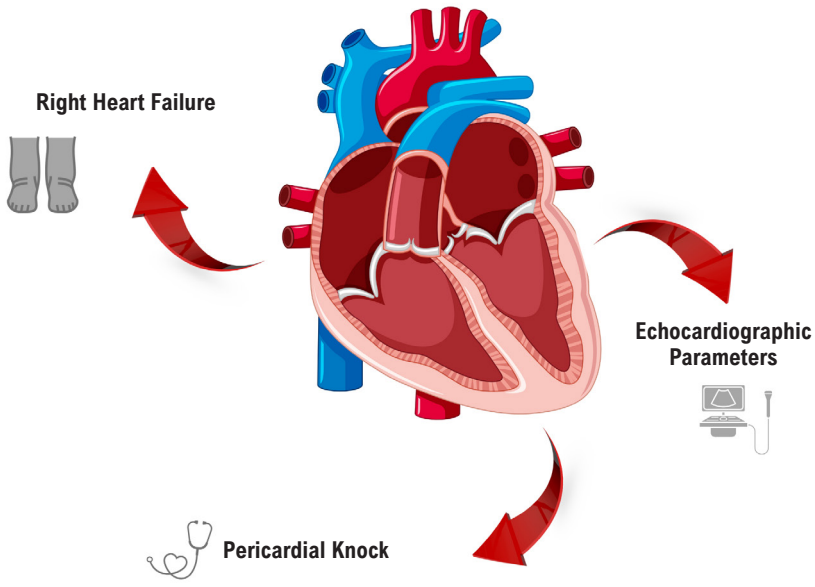

Arq Bras Cardiol: Imagem cardiovasc. 2026;39(1):e20250063

Abstract

Constrictive Pericarditis (CP) is an uncommon but potentially curable condition, typically presenting with right-sided heart failure and impaired ventricular filling. Diagnosis can be challenging and requires a structured approach that integrates various cardiovascular imaging modalities. This article offers a practical guide, based on evidence and clinical experience, for the step-by-step recognition of Constrictive Pericarditis, highlighting echocardiographic findings.

Keywords

Pericarditis; Echocardiography; Doppler Echocardiography

Mailing Address: Aline Travessa •
Hospital de Aeronáutica de Belém. Avenida Almirante Barroso, 3492. Postal code: 66613-710. Belém, PA – Brazil.
E-mail: alinetravessa@cardiol.br
Manuscript received January 19, 2026, revised manuscript January 29, 2026, accepted January 29, 2026
Editor responsible for the review: Marcelo Tavares

DOI: https://doi.org/10.36660/abcimg.20250063i

Introduction

Constrictive pericarditis is a condition resulting from chronic inflammation of the pericardium, which culminates in fibrosis, thickening, and calcification, leading to marked restriction of cardiac chamber filling. Although it may develop as a complication of acute pericarditis, progression to the constrictive form usually occurs over months to years.

Etiologies include systemic infections, prior cardiac surgery, malignancy, radiotherapy, particularly mediastinal irradiation, autoimmune diseases, and idiopathic causes. In endemic countries, tuberculosis is a major cause.[1,2]

Clinical suspicion most often arises in patients with right-sided heart failure, characterized by systemic congestion (hepatic congestion, anasarca, cardiac cirrhosis) and features of low cardiac output, such as fatigue, cardiac cachexia, and muscle weakness. Additional findings may include a pericardial knock on physical examination and electrocardiographic abnormalities, such as low QRS voltage and nonspecific ST- and T-wave changes. In this setting, cardiovascular imaging plays a central role in establishing the diagnosis and guiding management (Center Figure).

This article aims to present a practical, evidence-based diagnostic flowchart for the evaluation of CP, with emphasis on the sequential use of imaging modalities.

Pathophysiology of CP

Following pericardial injury, an inflammatory cascade is triggered, involving innate immune mechanisms with activation of the NLRP3 inflammasome and release of proinflammatory cytokines, particularly those of the IL-1 family. This inflammatory response promotes cellular infiltration, amplifying and sustaining the autoinflammatory process. Over time, persistent inflammation leads to fibroblast proliferation, granulation tissue formation, pathological neovascularization, and progressive pericardial thickening. This process may progress to fibrosis and calcification, ultimately leading to CP.[3,4]

Under physiological conditions, the pericardium has sufficient elasticity to accommodate changes in cardiac volume. In CP, pericardial thickening restricts ventricular expansion during diastole.

From a hemodynamic standpoint, two key mechanisms stand out:

1. Dissociation between intrathoracic and intracardiac pressures, caused by the rigid pericardium, which prevents normal transmission of respiratory variations;
2. Marked ventricular interdependence, in which increased venous return to the right chambers during inspiration results in reduced filling of the left chambers, due to interventricular septal shift toward the Left Ventricle (LV), secondary to the inability of the Right Ventricle (RV) free wall to expand as a result of the restriction imposed by the thickened pericardium.[5]

Thus, ventricular filling during diastole is initially rapid but is abruptly interrupted by pericardial constraint, leading to increased filling pressures in the right chambers, reduced preload in the left chambers, and decreased cardiac output.

Finally, inflammatory and hemodynamic alterations also contribute to sodium and water retention through activation of the sympathetic nervous system and the renin–angiotensin–aldosterone system, perpetuating symptoms and complicating clinical management.

Early recognition of constrictive pericarditis allows appropriate indication of pericardiectomy, which may be curative and restore normal diastolic function in many patients.

Clinical presentation and diagnosis

Loss of normal pericardial compliance restricts diastolic ventricular filling, resulting in a clinical syndrome dominated by right-sided heart failure. In advanced stages, this presentation is frequently misinterpreted as primary hepatic or renal disease.[6]

Exertional dyspnea is among the most common symptoms and often develops insidiously, reflecting elevated pulmonary venous pressures and reduced cardiac output. Fatigue is another frequent complaint and is directly related to decreased peripheral perfusion. Patients commonly present with bilateral, ascending peripheral edema as a sign of systemic congestion. Ascites, in turn, occurs in approximately half of cases and may be disproportionate to the degree of edema, misleadingly suggesting primary liver disease.[7]

Other findings include abdominal fullness, anorexia, and early satiety, frequently related to hepatoesplenic congestion. In advanced cases, cachexia may be present.

Physical examination should focus on characteristic findings such as Kussmaul's sign (paradoxical inspiratory jugular venous distension), pulsus paradoxus (a > 10 mmHg inspiratory decline in systolic blood pressure), and the classic pericardial knock, an early diastolic sound best heard at the mitral or tricuspid area, indicating abrupt cessation of ventricular filling.

When present together, these findings should strongly raise suspicion for CP and prompt comprehensive evaluation using complementary imaging modalities (Figure 1).

CP encompasses subtypes with important diagnostic and therapeutic implications.

- **Transient Constrictive Pericarditis (TCP):** associated with active inflammation and reversible pericardial thickening, characterized by spontaneous resolution or resolution after anti-inflammatory therapy (NSAIDs, colchicine, or corticosteroids); early identification is important to avoid unnecessary pericardiectomy.[6,7]
- **Effusive-Constrictive Pericarditis (ECP):** defined by persistence of constrictive physiology after drainage of a significant pericardial effusion (PEff). The classic hemodynamic finding is the persistence of elevated right atrial pressure after pericardiocentesis. Currently, ECP can be identified by echocardiography through the presence of constrictive features after drainage.[6,7]

CP's main differential diagnosis is restrictive cardiomyopathy, particularly infiltrative diseases such as amyloidosis and sarcoidosis. The distinction is based on clinical presentation, hemodynamic assessment, and imaging studies.

Among imaging diagnostic modalities, the following can be highlighted:

- **Transthoracic Echocardiography (TTE):** first-line examination for anatomical and hemodynamic assessment of CP. Transesophageal and stress echocardiography are generally unnecessary for establishing the diagnosis. Limitations: inability to identify active inflammation or fibrosis.
- **Computed Tomography (CT):** gold standard for the identification of pericardial calcifications and for surgical planning, allowing detailed visualization of the relationship with adjacent structures.
- **Cardiac Magnetic Resonance (CMR):** a complementary modality that assesses pericardial thickening (>3 mm), edema (T2-STIR), inflammation (LGE), and therapeutic response. It is also useful for surgical planning and follow-up of reversible forms.
- **Cardiac Catheterization (CC):** used when noninvasive tests are inconclusive. It demonstrates equalization of diastolic pressures, the square root sign, and respiratory discordance between RV and LV systolic pressures. Although invasive, it remains a reference standard for confirmation in equivocal cases.

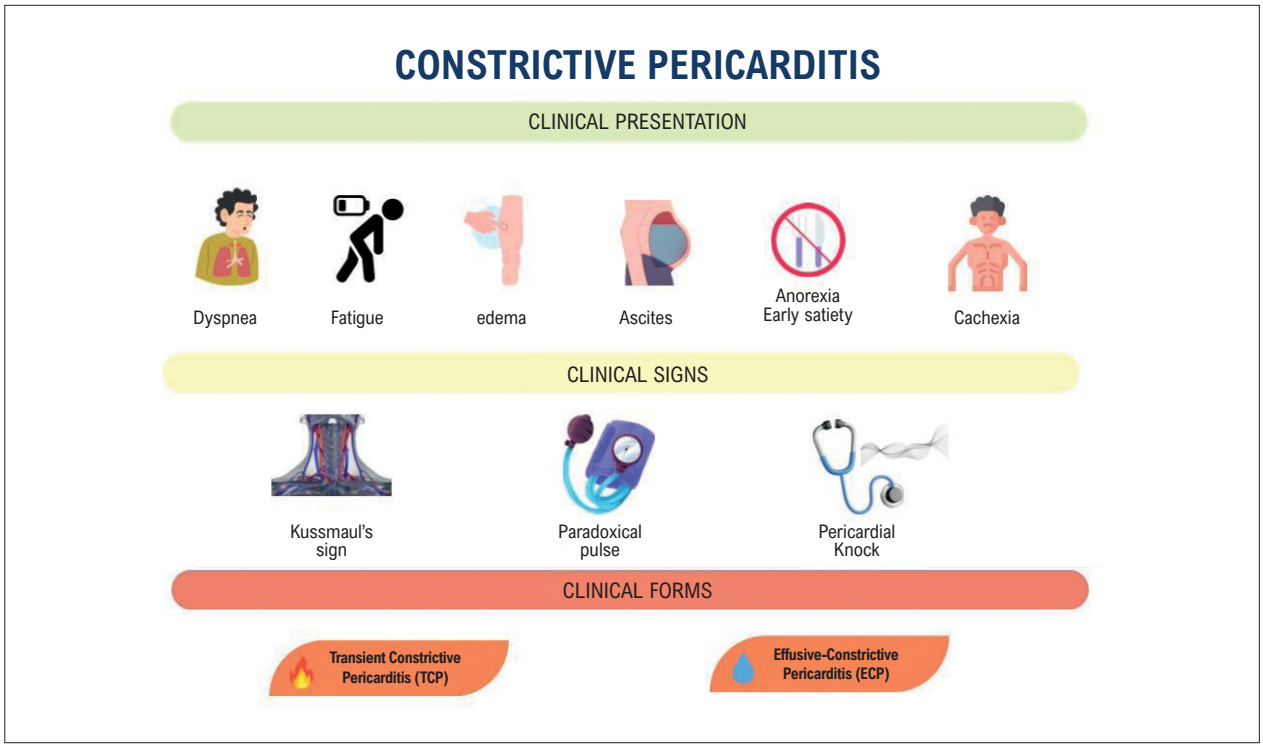

Figure 1 – *Clinical presentation of Constrictive Pericarditis*

Table 1 – Indications for Imaging Modalities in Constrictive Pericarditis

TTE	Initial examination to assess function and hemodynamics; detection of suggestive signs of CP.
CMR	Identification of active inflammation, fibrosis, and pericardial thickening.
TC	Assessment of calcifications and preoperative planning.
CC	Definitive diagnosis in cases with inconclusive findings; detailed hemodynamic assessment.

Table 1 summarizes the main indications for each diagnostic method.

Echocardiographic evaluation: step by step

During echocardiographic evaluation, techniques such as M-mode and Doppler are mandatory. For optimal echocardiographic assessment, a respirometer should always be used, particularly for evaluation of parameters such as septal motion, variation of atrioventricular flows, hepatic vein Doppler, and superior vena cava Doppler.

The main echocardiographic criteria include:

1. **Pericardial thickening:** although not always present, identification of a thickened or calcified pericardium is suggestive, in addition to assessment of pericardial effusion.
2. **Characteristic hemodynamic changes:**
   - **Respiratory-related septal bounce:** abrupt motion of the interventricular septum during diastole, with anterior displacement during inspiration and posterior displacement during expiration (Figure 2), reflecting exaggerated ventricular interdependence.
   - **Respiratory variation of mitral and tricuspid inflow velocities:** inspiratory variation of mitral inflow (E wave) greater than 25% and tricuspid inflow (E wave) greater than 40%.
   - **Restrictive diastolic filling pattern:** E/A ratio greater than 2 and mitral E-wave deceleration time shorter than 140 ms.
   - **End-diastolic expiratory reversal velocity in the hepatic vein:** a ratio between end-diastolic reversed and forward flow velocity ≥ 0.8 is highly specific.
3. **Tissue Doppler findings:**
   - **Preserved or increased medial mitral annular e′ velocity:** medial e′ velocity ≥ 9 cm/s is highly specific for CP.
   - ***"Annulus reversus"*:** medial e′ velocity exceeds lateral e′ velocity, due to the effect of pericardial restriction.
4. **Dilation and lack of collapse of the inferior vena cava and hepatic veins:** indicative of elevated right atrial pressure.

The combination of these findings increases diagnostic accuracy; particularly, the presence of respiratory septal shift associated with medial e′ velocity ≥ 9 cm/s or expiratory diastolic reversal of hepatic venous flow shows high sensitivity and specificity for the diagnosis of CP.[7]

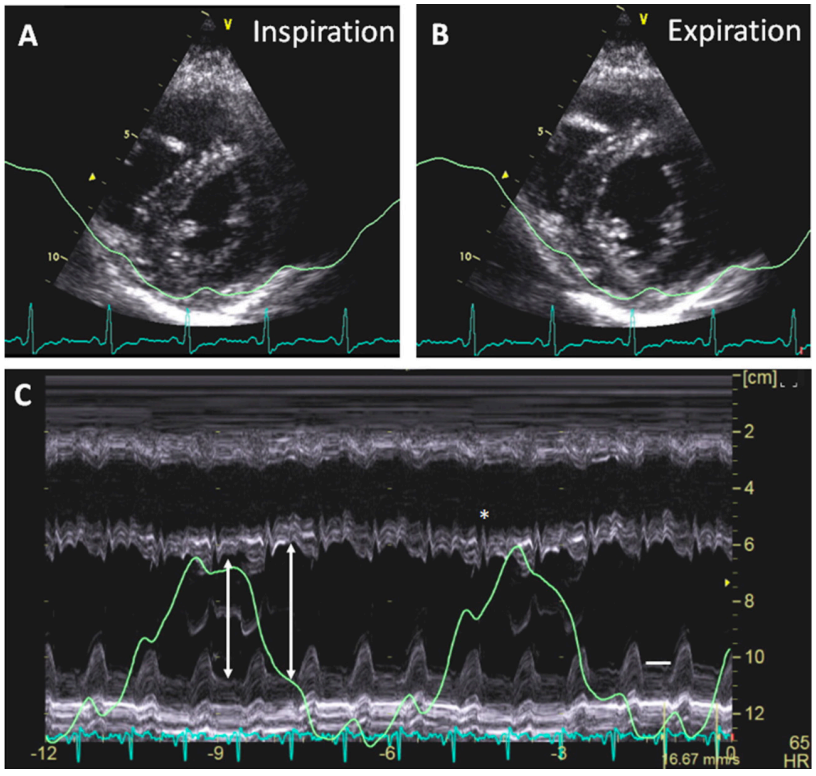

Figure 2 – *Respiratory variation in interventricular septal motion.*

A landmark Mayo Clinic study evaluated 130 patients with surgically confirmed CP and identified five key echocardiographic variables derived from prior investigations: interventricular septal motion abnormalities (including respirophasic septal shift and septal bounce), respiratory variation in mitral inflow E-wave velocity, septal mitral annular e′ velocity, the septal-to-lateral e′ ratio, and expiratory diastolic reversal of hepatic venous flow.[8]

In addition to these variables, the use of global longitudinal strain and three-dimensional echocardiography may provide additional information.

The integrated use of anatomical and functional criteria is essential to differentiate constrictive pericarditis from restrictive cardiomyopathy (Table 2) and other causes of diastolic heart failure.

Figure 3 demonstrates a practical flowchart for the echocardiographic diagnostic approach in suspected constrictive pericarditis.

Differential Diagnosis: Constrictive Pericarditis vs. Restrictive Cardiomyopathy

Constrictive pericarditis and restrictive cardiomyopathy share symptoms of diastolic dysfunction, but there are marked differences, as summarized in Table 3.

Conclusion

Constrictive pericarditis (CP) is a complex but potentially treatable condition; its diagnosis requires a systematic approach that combines clinical signs and imaging tools. While echocardiography remains the cornerstone of initial evaluation, multimodality imaging is essential for identifying active inflammation and fibrosis and guiding therapeutic decision-making. Adoption of a structured diagnostic protocol facilitates early recognition, avoids unnecessary interventions, and ultimately improves patient outcomes.

Author Contributions

Conception and design of the research: Pereira PH; acquisition of data: Travessa A, Pereira PH; analysis and interpretation of the data: Travessa A; writing of the manuscript: Travessa A, Machado LM, Esteves NS, Pereira PH; critical revision of the manuscript for intellectual content: Travessa A.

Potential Conflict of Interest

No potential conflict of interest relevant to this article was reported.

Sources of Funding

There were no external funding sources for this study.

Study Association

This study is not associated with any thesis or dissertation work.

Table 2 – Main clinical, echocardiographic, and laboratory characteristics for differential diagnosis

Characteristic	Constrictive pericarditis	Restrictive cardiomyopathy
Paradoxical pulse	Present in 1/3 of cases	Rarely
Pericardial knock	Frequently	Absent
ECG with low QRS voltage	Frequently	Rarely
Respiratory variation in mitral/tricuspid flows	Marked	Absent or slight
Septal bounce	Present	Absent
Ventricular wall thickness	Normal	Increased
Dip-plateau pattern on catheterization	Present	Variable
BNP	Normal or slightly high	Elevated

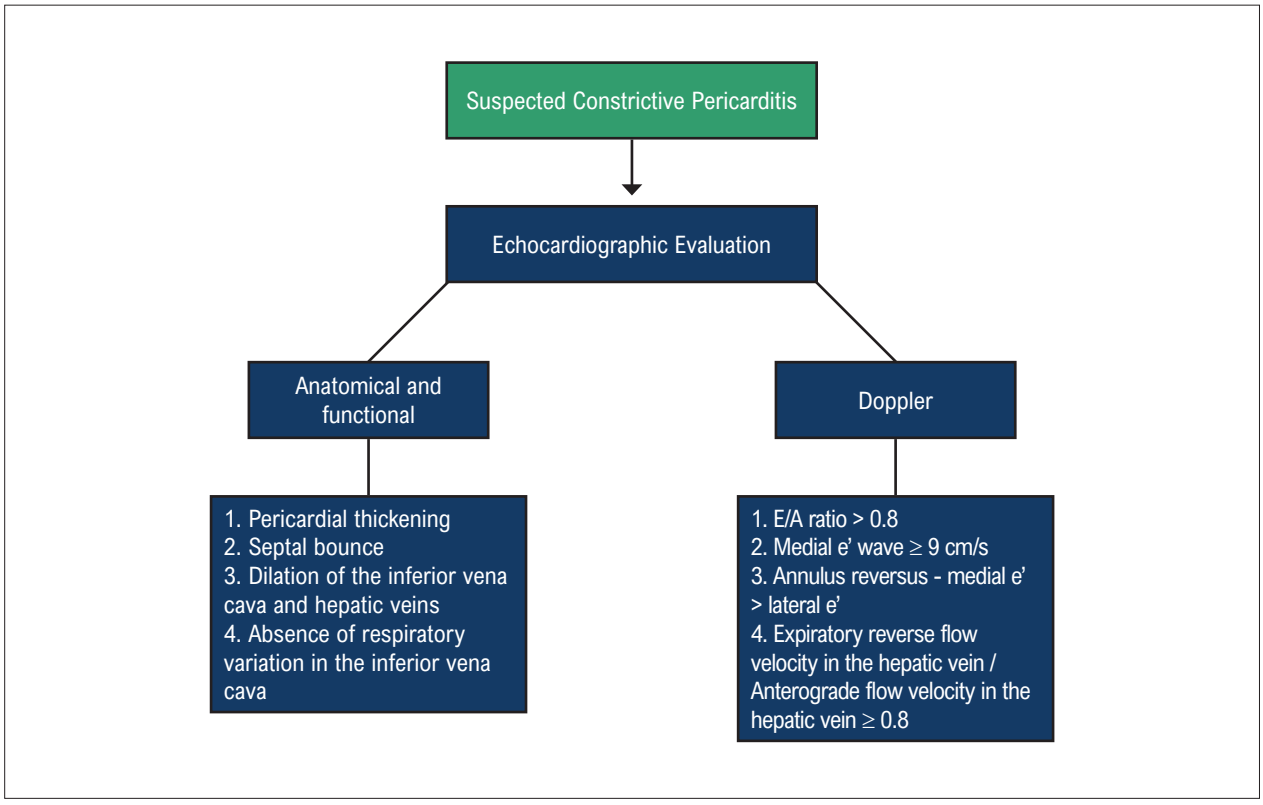

Figure 3 – *Echocardiographic evaluation in Constrictive Pericarditis.*

Table 3 – Imaging parameters for differential diagnosis

Characteristic	Constrictive pericarditis	Restrictive cardiomyopathy
Pericardial thickening	Frequently	Absent
lateral (tissue Doppler)	Preserved or increased	Reduced
Late pericardial enhancement (MRI)	Frequently	Absent
Septal bounce	Present	Absent
Ventricular interdependence	Pronounced	Minimum

Ethics Approval and Consent to Participate

This article does not contain any studies with human participants or animals performed by any of the authors.

Use of Artificial Intelligence

During the preparation of this work, the author(s) used Canva for creation of the central figure of the manuscript. After using this tool/service, the author(s) reviewed and edited the content as needed and take full responsibility for the content of the published article.

Availability of Research Data

The underlying content of the research text is contained within the manuscript.

References

1. Tzani A, Doulamis IP, Tzoumas A, Avgerinos DV, Koudoumas D, Siasos G, et al. Meta-Analysis of Population Characteristics and Outcomes of Patients Undergoing Pericardiectomy for Constrictive Pericarditis. Am J Cardiol. 2021;146:120-7. doi: 10.1016/j.amjcard.2021.01.033.
2. Cremer PC, Klein AL, Imazio M. Diagnosis, Risk Stratification, and Treatment of Pericarditis: A Review. JAMA. 2024;332(13):1090-100. doi: 10.1001/jama.2024.12935.
3. Del Buono MG, Bonaventura A, Vecchié A, Moroni F, Golino M, Bressi E, et al. Pathogenic Pathways and Therapeutic Targets of Inflammation in Heart Diseases: A Focus on Interleukin-1. Eur J Clin Invest. 2024;54(2):e14110. doi: 10.1111/eci.14110.
4. Bonaventura A, Montecucco F. Inflammation and Pericarditis: Are Neutrophils Actors Behind the Scenes? J Cell Physiol. 2019;234(5):5390-5398. doi: 10.1002/jcp.27436.
5. Marta L, Alves M, Peres M, Ferreira R, Ferreira H, Leal M, et al. Effusive-Constrictive Pericarditis as the Manifestation of an Unexpected Diagnosis. Rev Port Cardiol. 2015;34(1):69.e1-6. doi: 10.1016/j.repc.2014.08.013.
6. Klein AL, Wang TKM, Cremer PC, Abbate A, Adler Y, Asher C, et al. Pericardial Diseases: International Position Statement on New Concepts and Advances in Multimodality Cardiac Imaging. JACC Cardiovasc Imaging. 2024;17(8):937-88. doi: 10.1016/j.jcmg.2024.04.010.
7. Wang TKM, Klein AL, Cremer PC, Imazio M, Kohnstamm S, Luis SA, et al. 2025 Concise Clinical Guidance: An ACC Expert Consensus Statement on the Diagnosis and Management of Pericarditis: A Report of the American College of Cardiology Solution Set Oversight Committee. J Am Coll Cardiol. 2025;86(25):2691-719. doi: 10.1016/j.jacc.2025.05.023.
8. Welch TD, Ling LH, Espinosa RE, Anavekar NS, Wiste HJ, Lahr BD, et al. Echocardiographic Diagnosis of Constrictive Pericarditis: Mayo Clinic criteria. Circ Cardiovasc Imaging. 2014;7(3):526-34. doi: 10.1161/CIRCIMAGING.113.001613.
9. Welch TD. Constrictive Pericarditis: Diagnosis, Management and Clinical Outcomes. Heart. 2018;104(9):725-31. doi: 10.1136/heartjnl-2017-311683.
10. Nishimura RA. Constrictive Pericarditis in the Modern Era: A Diagnostic Dilemma. Heart. 2001;86(6):619-23. doi: 10.1136/heart.86.6.619.
11. Bogaert J, Francone M. Cardiovascular Magnetic Resonance in Pericardial Diseases. J Cardiovasc Magn Reson. 2009;11(1):14. doi: 10.1186/1532-429X-11-14.
12. Bogaert J, Dymarkowski S. Clinical Cardiac MRI. Berlim: Springer; 2020.
13. Talreja DR, Nishimura RA, Oh JK, Holmes DR. Constrictive Pericarditis in the Modern Era: Novel Criteria for Diagnosis in the Cardiac Catheterization Laboratory. J Am Coll Cardiol. 2008;51(3):315-9. doi: 10.1016/j.jacc.2007.09.039.
14. Syed FF, Schaff HV, Oh JK. Constrictive Pericarditis--A Curable Diastolic Heart Failure. Nat Rev Cardiol. 2014;11(9):530-44. doi: 10.1038/nrcardio.2014.100.
15. Welch TD, Oh JK. Constrictive Pericarditis: Old Disease, New Approaches. Curr Cardiol Rep. 2015;17(4):20. doi: 10.1007/s11886-015-0576-x.
16. Miranda WR, Oh JK. Constrictive Pericarditis: A Practical Clinical Approach. Prog Cardiovasc Dis. 2017;59(4):369-79. doi: 10.1016/j.pcad.2016.12.008.
17. Ha JW, Ommen SR, Tajik AJ, Barnes ME, Ammash NM, Gertz MA, et al. Differentiation of Constrictive Pericarditis from Restrictive Cardiomyopathy Using Mitral Annular Velocity by Tissue Doppler Echocardiography. Am J Cardiol. 2004;94(3):316-9. doi: 10.1016/j.amjcard.2004.04.026.
18. Hurrell DG, Nishimura RA, Higano ST, Appleton CP, Danielson GK, Holmes DR Jr, et al. Value of Dynamic Respiratory Changes in Left and Right Ventricular Pressures for the Diagnosis of Constrictive Pericarditis. Circulation. 1996;93(11):2007-13. doi: 10.1161/01.cir.93.11.2007.
19. Lloyd JW, Anavekar NS, Oh JK, Miranda WR. Multimodality Imaging in Differentiating Constrictive Pericarditis From Restrictive Cardiomyopathy: A Comprehensive Overview for Clinicians and Imagers. J Am Soc Echocardiogr. 2023;36(12):1254-65. doi: 10.1016/j.echo.2023.08.016.

Review Article

The Use of Artificial Intelligence in the Diagnosis of Cardiac Amyloidosis: Integrative Review

Nilson Batista Lemos,[1] *Gabriela Aparecida Moreira Araújo,*[1] *Marcelo Dantas Tavares de Melo*[1]

Universidade Federal da Paraíba,[1] *João Pessoa, PB – Brazil*

Resumo

Fundamento: Cardiac amyloidosis is a rare form of infiltrative cardiomyopathy characterized by the deposition of proteins in the myocardium, resulting in increased wall thickness, impaired ventricular function, and possible progression to heart failure. Diagnosis is challenging due to the low prevalence of the disease and the nonspecific nature of its clinical manifestations. The application of artificial intelligence (AI) to the analysis of medical tests emerges as a promising strategy for early detection, more accurate diagnosis, and timely initiation of treatment.

Methods: An integrative literature review was conducted on the use of AI in the diagnosis of cardiac amyloidosis. Articles published between 2019 and 2024 were searched in the PubMed, Scopus, Web of Science, Embase, and Cochrane Library databases.

Results: Of the 420 articles initially identified, 21 met the eligibility criteria and were included in the final analysis. A predominance of retrospective observational studies applying machine learning models was observed. Among the diagnostic modalities evaluated in association with AI, electrocardiography and echocardiography were the most frequently studied tests.

Conclusion: AI demonstrates high potential to improve the screening and diagnosis of cardiac amyloidosis when applied to the analysis of clinical and imaging tests. The findings of this review indicate that AI may accelerate the diagnostic process, reduce the need for invasive procedures, and optimize the use of health care resources. However, to expand its integration into clinical practice and enhance its generalizability, further model refinement and validation in more diverse populations are required.

Keywords: Amyloidosis; Artificial Intelligence; Diagnosis.

Introduction

Amyloidosis is a generic term used to describe the extracellular deposition of fibrils formed by low-molecular-weight protein subunits derived from different precursor proteins. Amyloid deposits may result in a wide variety of clinical manifestations, which vary according to the type of protein involved, the amount deposited, and the tissue location. In the genesis of these deposits, initially soluble peptides undergo conformational changes, predominantly acquiring an antiparallel beta-pleated sheet structure, which favors their stacking into twisted fibrils.[1]

There are dozens of systemic and localized forms of amyloidosis. Among them, four precursor proteins may give rise to both localized and systemic deposits. The main systemic forms are immunoglobulin light-chain (AL) amyloidosis and (ATTR) transthyretin amyloidosis. These forms are named according to the precursor protein of the amyloid deposit (AL or ATTR) and account for approximately 95% of cases of cardiac amyloidosis. The remaining forms correspond to other subtypes of amyloidosis, which are also clinically relevant.[2,3]

ATTR amyloidosis is characterized by the misfolding and subsequent deposition of transthyretin, a protein responsible for the transport of thyroid hormone and vitamin A. It may present in wild-type or hereditary form.[2-4] Similarly, AL amyloidosis results from the accumulation of misfolded immunoglobulin light chains produced by plasma cells associated with dyscrasias.[2,3]

In cardiac amyloidosis, it is a rare form of progressive cardiomyopathy whose population prevalence has not yet been well established.[5] The disease is caused by myocardial deposition of misfolded amyloid proteins, resulting in restrictive cardiomyopathy, with possible progression to heart failure, conduction system disorders, and cardiac death.[3,5,6] It may present with cardiovascular signs and symptoms or be diagnosed during the investigation of extracardiac manifestations of the disease.[3,6,7] Due to its heterogeneous clinical phenotype and frequently nonspecific manifestations, diagnosis and management tend to occur late.[3,6]

Correspondência: Nilson Batista Lemos •
Universidade Federal da Paraíba. Campus I Lot., Cidade Universitaria. CEP: 58051-900. João Pessoa, PB – Brasil
E-mail: nilsonlemos18@gmail.com
Artigo recebido em 08/02/2026; revisado em 09/02/2026; aceito em 09/02/2026.
Editor responsável pela revisão: Marcelo Tavares

DOI: https://doi.org/10.36660/abcimg.20260016i

Central Illustration: The Use of Artificial Intelligence in the Diagnosis of Cardiac Amyloidosis: Integrative Review

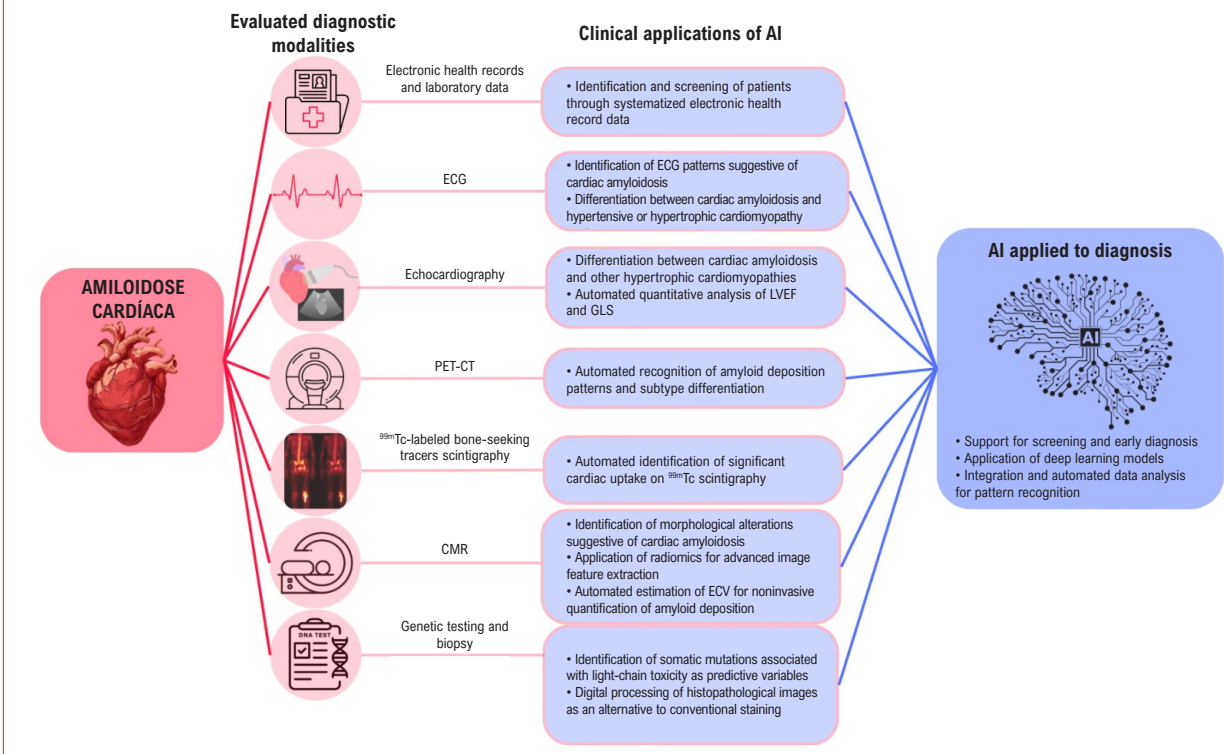

Arq Bras Cardiol: Imagem cardiovasc. 2026;39(1):e20260016

With regard to the diagnostic approach to cardiac amyloidosis, it is essential to recognize clinical scenarios and abnormalities in complementary tests that indicate the need for investigation. However, diagnosis is challenging, especially because it is often an indolent disease whose symptoms may overlap with those of more prevalent heart diseases.[3,5] Depending on the clinical context and resource availability, various tools may be employed, including electrocardiography (ECG), echocardiography, cardiac magnetic resonance (CMR), bone-seeking tracers scintigraphy, monoclonal protein screening by immunofixation, and biopsy of the affected tissue. Each method has its own characteristics and different levels of diagnostic accuracy (Central Illustration).

Some findings may increase clinical suspicion of cardiac amyloidosis, such as discordance between increased left ventricular (LV) wall thickness and low QRS voltage, unexplained LV hypertrophy, low-flow, low-gradient aortic stenosis, relative apical sparing of longitudinal strain, a diffuse circumferential subendocardial late gadolinium enhancement pattern of the LV on CMR, and myocardial uptake of bone tracers on bone-seeking tracers scintigraphy.

Despite the diversity of available diagnostic methods, cardiac amyloidosis remains underdiagnosed,[3,5-7] which has important repercussions for patients' quality of life. At the same time, the development of therapies capable of improving clinical outcomes has driven the search for strategies to increase diagnostic rates. These interventions may reduce or stabilize protein deposition, with a consequent reduction in the relative risk of hospitalizations, morbidity, and mortality associated with the disease.

Because of the need for early detection of cardiac amyloidosis, the development of mechanisms that optimize screening and diagnosis with lower costs and risks is essential.[3] This review aims to present the main advances in disease detection, with emphasis on promising technological tools in diagnostic medicine, especially artificial intelligence (AI).

AI is a branch of computer science dedicated to the development of systems capable of performing tasks that simulate human cognitive functions, such as decision-making and complex reasoning. In the field of medical diagnosis, these systems are trained using machine learning techniques, in which large volumes of data, often images, are used for pattern recognition. Among the most commonly employed approaches are convolutional neural networks (CNNs), which consist of multiple layers that extract progressively more complex features from the analyzed data, enabling automated identification of patterns in images and other types of information. In general, the larger and more representative the dataset used for training, the greater the model's accuracy tends to be.

Incorporating AI into medical practice enables the more effective screening of rare diseases and improves diagnostic accuracy. AI appears particularly promising for rare diseases that are often underrecognized in clinical practice. Automated systems can integrate multiple signs, symptoms, and complementary findings, helping to guide clinical reasoning. Thus, core skills in medicine, such as pattern recognition, are increasingly being incorporated into computational models with the aim of enhancing diagnostic reliability and supporting decision-making in everyday medical practice.

Several studies have investigated the applicability of AI in the early diagnosis of cardiac amyloidosis. Among the most recent approaches are the integration of AI with imaging methods, such as positron emission tomography (PET-CT), bone-seeking tracers scintigraphy, and CMR as well as its application to the automated analysis of ECGs, genetic data, and phenotypic profiles of cardiac abnormalities. These aspects will be discussed throughout this review.

Methods

The present study is characterized as an integrative literature review aimed at critically analyzing the use of AI in the diagnosis of cardiac amyloidosis. The review was conducted following six methodological steps: i) definition of the research question; ii) establishment of inclusion criteria and sample selection; iii) identification of preselected and selected studies; iv) organization and representation of the included studies; v) critical analysis of the data; and vi) synthesis of the available knowledge.

Searches were conducted in the PubMed, Scopus, Web of Science, Embase, and Cochrane Library databases. The search strategy was developed using the descriptors "artificial intelligence," "amyloidosis," and "diagnosis," included in the Medical Subject Headings and Embase Subject Headings, combined using the Boolean operator AND.

Original studies and meta-analyses published between 2019 and 2024 that evaluated the application of AI in the diagnosis of cardiac amyloidosis were included. Articles that did not meet the inclusion criteria were excluded, as well as narrative reviews, case reports, editorials, and studies with methodology considered inadequate.

After article selection, methodological quality was assessed to ensure greater rigor in the interpretation of findings and robustness of the conclusions. For this step, the JBI critical appraisal tool was used, which includes specific criteria according to study design, covering aspects related to the sample, methodology, data analysis, bias control, and ethical considerations. Quality classification is based on the proportion of affirmative responses to the evaluated criteria, allowing comparison across studies and critical analysis of their results.

Results

The search strategy yielded 420 articles, distributed as follows: 124 identified in PubMed, 61 in Web of Science, 84 in Scopus, 147 in Embase, and 4 in the Cochrane Library. After removal of 192 duplicate studies, 228 articles remained for screening.

Title and abstract screening resulted in the selection of 43 studies for full-text evaluation. After application of the eligibility criteria, 21 articles were included in the final analysis (Figure 1).

Regarding methodological assessment according to the JBI criteria, most studies were classified as having good to excellent methodological quality, with scores ranging from 6 to 8 points. The main factors contributing to this classification included the use of robust statistical metrics and the application of cross-validation in the developed AI models.

As limitations, the absence of gold-standard diagnostic confirmation of cardiac amyloidosis in part of the studies was observed, as well as the lack of external validation of the proposed models, which limits the generalizability of the findings. The detailed results of the methodological assessment are presented in Table 1.

Discussion

The use of AI as a supportive tool in the diagnosis of rare diseases, such as cardiac amyloidosis, has been considered promising, especially in the context of conditions with high clinical heterogeneity and that are frequently underrecognized by general practitioners. Early identification of the disease may modify its natural history and improve prognosis. This review sought to emphasize the potential of already established diagnostic tools for the evaluation of cardiac amyloidosis when combined with machine learning-based systems, an approach addressed in all included studies.

To organize the analysis of the findings, AI performance will be discussed according to the different diagnostic modalities used in the screening and evaluation of cardiac amyloidosis.

Performance of artificial intelligence in the evaluation of medical record data and laboratory tests

Among the screening strategies for amyloid cardiomyopathy, the use of data extracted from electronic health records of patients with heart failure (HF) with preserved ejection fraction (HFpEF) stands out. To differentiate amyloid etiology, especially wild-type ATTR amyloidosis (ATTRwt), from non-amyloid etiology, Huda et al.[8] collected electronic health record data and developed an AI model capable of screening and identifying patients with ATTRwt amyloidosis. The system achieved an area under the receiver operating characteristic curve (AUC) of 0.80. Performance was supported by the identification of comorbidities more prevalent in the amyloid etiology group, such as atrial fibrillation and chronic kidney disease, and in the non-amyloid group, such as hypertension, diabetes mellitus, obesity, and coronary artery disease, which were used as predictive variables.

Subsequently, Castaño et al.[9] refined the model by focusing the analysis on 11 main phenotypes associated with cardiac amyloidosis, including carpal tunnel syndrome and arrhythmias. The model demonstrated accuracy (74%), sensitivity (77%), and specificity (72%), with an AUC of 0.82. Although there was a slight reduction in some

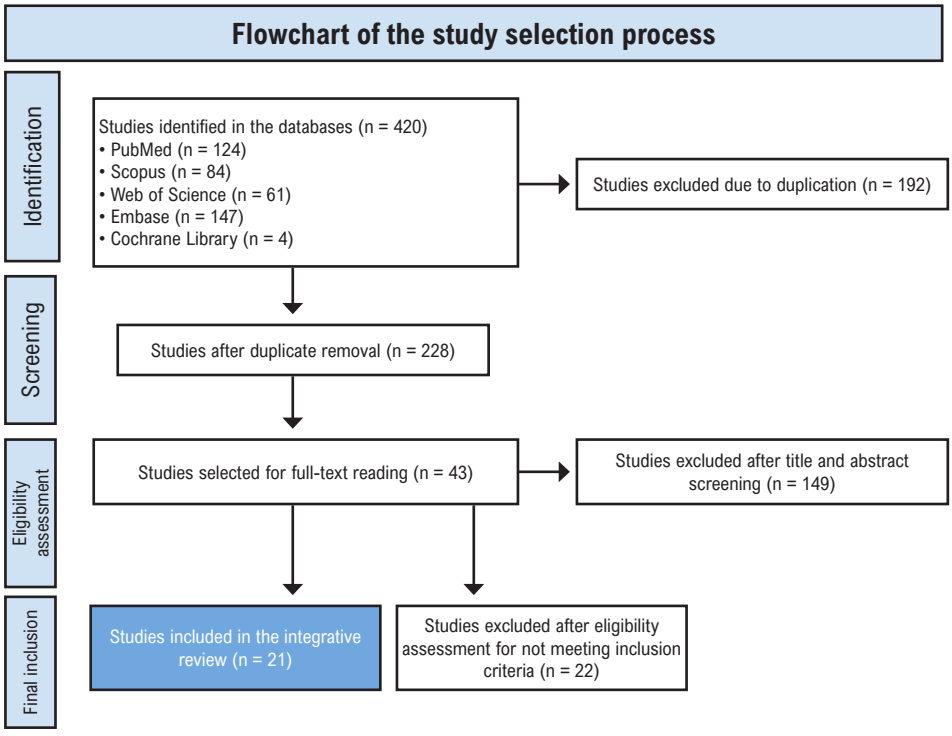

Figure 1 – *Flowchart of the study selection process for the studies included in the integrative review.*

performance parameters, the model was simplified in terms of programming, facilitating its implementation in hospital settings and expanding its potential for population screening.

The studies by Huda et al.[8] and Castaño et al.[9] demonstrate the feasibility of automated screening through systematic extraction of clinical data, a process that would be costly and operationally complex if performed manually. Although such models are limited by the quality of records coded according to the International Classification of Diseases and by the documented phenotypes, without direct integration of laboratory or imaging tests for definitive typing, they represent relevant tools for large-scale screening, directing patients with higher probability toward further investigation.

Additionally, phenotypes recognized by the model, such as carpal tunnel syndrome, may precede the development of HF, which suggests a potential application of AI in preclinical stages, with implications for early identification of ATTR amyloidosis.

Performance of artificial intelligence in electrocardiographic evaluation

The application of AI in ECG analysis has emerged as a screening strategy, considering that ECG is a widely available, low-cost, noninvasive test.[3,5] Model validation represents a fundamental step in the development of these tools, as it involves testing multiple variables across different populations.[5,6]

Harmon et al.[10] developed an algorithm applicable to diverse populations, including different races and sexes. The model achieved an AUC of 0.84 (95% CI: 0.82-0.86), maintaining consistent performance across subgroups, except in the Hispanic population, possibly underrepresented in the sample. The algorithm performed better in ECGs with low voltage and patterns compatible with prior infarction, and showed lower performance in left bundle branch block and LV hypertrophy. These findings suggest the need for greater sample diversity, without invalidating the use of the tool as a screening method.

Vrudhula et al.[5] evaluated approximately 1.3 million ECGs from 341,989 patients. The different tested models showed AUC values ranging from 0.660 (95% CI: 0.642-0.736) to 0.898 (95% CI: 0.868-0.924), demonstrating relevant potential for screening and referral for further investigation. However, because of the rarity and underdiagnosis of cardiac amyloidosis, models are often trained with a limited number of confirmed cases.

Similarly, Goto et al.[3] reported strong performance, with a C-statistic of 0.91 (95% CI: 0.90-0.93) in the Brigham and Women's Hospital test set, 0.85 (0.82-0.87) at Massachusetts General Hospital, and 0.86 (0.83-0.88) at the University of California, San Francisco. However, the authors emphasize that isolated ECG features do not provide sufficient sensitivity or specificity to be used as independent heuristics, and their integration with other clinical and diagnostic variables is recommended to optimize model performance.

Table 1 – Methodological characteristics and quality assessment of the included studies

No.	Study (author/ year)	Design	Score (JBI/8)	Methodological assessment
1	Agibetov et al. (2021)	Retrospective observational study with cardiac magnetic resonance and application of machine learning	7	High quality
2	Barbieri et al. (2024)	Study with automated three-dimensional transthoracic echocardiography associated with machine learning	7	High quality
3	Castaño et al. (2024)	Retrospective case-control observational study with application of machine learning	7	High quality
4	Cotella et al. (2023)	Retrospective observational study with echocardiography and application of machine learning	7	High quality
5	Delbarre et al. (2023)	Multicenter retrospective observational study with bone-seeking tracers scintigraphy analyzed by machine learning	8	Excellent
6	Eckstein et al. (2022)	Observational cohort study with echocardiography and use of machine learning	6	Good quality
7	Garofalo et al. (2021)	Predictive computational study with experimental validation focused on genetic assessment using machine learning	6	Good quality
8	Goto et al. (2021)	Multicenter observational study using electrocardiography and echocardiography	8	Excellent
9	Harmon et al. (2023)	Retrospective observational study with electrocardiography and application of machine learning	7	High quality
10	Huda et al. (2021)	Retrospective observational study with application of machine learning	7	High quality
11	Ma et al. (2024)	Retrospective observational study with non-contrast cardiac magnetic resonance and use of machine learning	7	High quality
12	Martini et al. (2020)	Prospective observational study with cardiac magnetic resonance and application of machine learning	8	Excellent
13	Miller et al. (2024)	Retrospective observational study with positron emission tomography and automated segmentation	8	Excellent
14	Nowak et al. (2024)	Retrospective observational study with cardiac magnetic resonance, T1 mapping, and use of machine learning	7	High quality
15	Santarelli et al. (2020)	Prospective observational study with positron emission tomography and application of machine learning	7	High quality
16	Schrutka et al. (2021)	Prospective case-control observational study with application of machine learning	6	Good quality
17	Shiri et al. (2024)	Prospective single-cohort observational study with application of machine learning	7	High quality
18	Spielvogel et al. (2024)	Multicenter retrospective observational study with bone-seeking tracers scintigraphy and use of machine learning	8	Excellent
19	Vrudhula et al. (2024)	Retrospective observational study with application of machine learning	6	Good quality
20	Yang et al. (2024)	Observational study with digital histopathological analysis using a neural network and autofluorescence	7	High quality
21	Zhang et al. (2023)	Retrospective observational study with echocardiography and application of machine learning	6	Good quality

Schrutka et al.[6] also reinforce that the proposed model may assist in raising suspicion of cardiac amyloidosis even in the absence of advanced imaging methods. In that study, 20 patients with transthyretin cardiac amyloidosis, 11 with HFpEF, 30 with cardiac amyloidosis, and 50 with other HF etiologies were evaluated. The presence of a low-voltage ECG pattern associated with increased LV wall thickness was highly suggestive of cardiac amyloidosis, allowing differentiation from hypertensive or hypertrophic cardiomyopathy. In the analysis of ECG patterns, pattern 1 was present in 78% of patients with AL amyloidosis and in 58% of those with ATTR amyloidosis ($p = 0.009$), whereas pattern 2 was identified in 7% of AL amyloidosis cases and in 23% of ATTR amyloidosis cases ($p = 0.006$). The absence of a specific pattern was observed in 16% of patients with AL amyloidosis and in 18% of patients with ATTR amyloidosis ($p = 0.620$).

Performance of artificial intelligence in echocardiographic evaluation

Considering the versatility of echocardiography and its central role in the diagnostic investigation of cardiac amyloidosis, the development of AI models capable of reducing operational variability and improving diagnostic accuracy is highly relevant.

Xiaofeng Zhang et al.[1] observed that there are still few studies on echocardiography-based myocardial texture analysis and that human visual assessment has limitations in characterizing these alterations. Based on transthoracic echocardiograms, the authors developed four machine learning algorithms to differentiate cardiac amyloidosis from other cardiomyopathies: random forest (RF), support vector machine (SVM), logistic regression (LR), and gradient boosting decision trees (GBDT).

In the analyzed population, all models were able to effectively distinguish cases of cardiac amyloidosis from non-amyloid diseases. The LR model demonstrated the best diagnostic performance, outperforming the traditional ultrasonographic method (AUC: RF 0.77; SVM 0.81; LR 0.81; GBDT 0.71). The authors therefore proposed the application of this tool as a noninvasive diagnostic method for myocardial amyloidosis. However, the relatively small number of cardiac amyloidosis cases may have limited the model's sensitivity for discrimination between groups.

Cotella et al.[2] developed an AI model focused on the automated assessment of LV ejection fraction (LVEF) and global longitudinal strain (GLS), central parameters in the diagnosis of cardiac amyloidosis. The authors justified the incorporation of AI based on the fact that manual measurements are time-consuming and show significant inter- and intraobserver variability, which may compromise diagnostic accuracy and influence therapeutic decisions. The study demonstrated that automated and quantitative measurements of LVEF and GLS showed high accuracy and enabled sensitive and specific detection of abnormalities when compared with conventional manual analysis, both in examinations performed before the diagnosis of cardiac amyloidosis and at the time of diagnosis. No statistically significant differences were observed between values obtained by the two methods in the prediagnostic period (LVEF: $p = 0.791$; GLS: $p = 0.105$) or at the time of diagnosis (LVEF: $p = 0.463$; GLS: $p = 0.722$). In addition, a strong correlation was observed between automated and manual measurements in echocardiograms performed before diagnosis ($r = 0.78$ for LVEF; $r = 0.83$ for GLS) and at established diagnosis ($r = 0.74$ for LVEF; $r = 0.80$ for GLS).

Goto et al.,[3] although acknowledging that ECG-based models show encouraging results, emphasize that their performance may not be sufficient for diagnosing low-prevalence diseases. The echocardiographic model developed by the authors demonstrated greater predictive accuracy compared with the ECG-based model. C-statistics ranged from 0.85-0.91 for ECG and from 0.89-1.00 for echocardiography. Moreover, in subtype analysis, the model showed superior performance in identifying ATTR amyloidosis.

In a more specific population, Shiri et al.[4] evaluated the use of machine learning for detecting ATTR amyloidosis in patients with severe aortic stenosis. Although different diagnostic modalities are useful in the initial assessment of these patients, they are not specific for ATTR amyloidosis. Frequently, definitive diagnosis of ATTR cardiomyopathy depends on histopathological confirmation or identification of a mutation in the *TTR* gene associated with evidence of significant myocardial uptake on bone-seeking tracers scintigraphy. Considering the high cost of genetic testing and bone-seeking tracers scintigraphy, especially in this patient group, the authors developed a noninvasive and potentially cost-effective model based on routine clinical and echocardiographic data. Performance was satisfactory when compared with clinical, laboratory, and interventional imaging variables, with an AUC of 0.79, sensitivity of 0.80, and specificity of 0.78.

Based on evidence that myocardial deformation analysis provides discriminatory value across multiple cardiac chambers, Eckstein et al.[7] developed a supervised model capable of differentiating cardiac amyloidosis from hypertrophic cardiomyopathy and from healthy individuals. The system showed excellent performance (AUC = 0.996; accuracy = 94%; sensitivity = 100%; F1-score = 97%), indicating that automated analysis of multichamber cardiac deformation and function may serve as a clinical decision support tool, even without the need for contrast administration.

With the technological advancement of cardiovascular imaging methods, new approaches have been proposed for screening infiltrative cardiomyopathies. Barbieri et al.[11] developed a model based on three-dimensional transthoracic echocardiography (3D-TTE) combined with AI, aiming to differentiate various phenotypes of cardiac hypertrophy, including cardiac amyloidosis. The method proposes a reformulation of ejection fraction analysis, traditionally based on CMR, through the use of 3D-TTE integrated with an AI system. Three-dimensional acquisition allowed a more detailed and accurate analysis of LV volume, enabling a more precise calculation of ejection fraction, defined as the ratio between stroke volume and end-diastolic volume, reflecting myocardial contractile capacity. This approach provides more accurate information regarding myocardial shortening and wall thickness, key aspects in recognizing infiltrative cardiomyopathies. In conventional two-dimensional

echocardiography, increased wall thickness may mask reduced myocardial shortening, resulting in an apparently preserved ejection fraction. In the context of etiological investigation of HFpEF, the model proved promising, showing higher ejection fraction in patients with hypertrophic cardiomyopathy and cardiac amyloidosis, with the latter exhibiting proportionally even higher values. Diagnostic performance was consistent, with sensitivity of 87%, specificity of 100%, and AUC of 0.959, reinforcing the potential of integrating 3D-TTE and AI in the phenotypic differentiation of myocardial hypertrophy.

Artificial intelligence in positron emission tomography evaluation

Similarly to other imaging modalities, PET-CT has been refined with the aim of making the diagnostic process of cardiac amyloidosis less invasive and more accurate. Deep learning-based models focused on the automated recognition of imaging patterns related to amyloid deposition stand out.

Santarelli et al.[12] developed a model aimed at rapidly, early, and specifically identifying the presence of cardiac amyloidosis and its subtypes. The system demonstrated superior performance compared with analysis performed by a specialist with more than 10 years of experience, showing sensitivity greater than 0.8 and specificity greater than 0.89. The model was able to estimate the probability of correlation between the analyzed image and each subtype of cardiac amyloidosis. The authors also highlighted the risk of overfitting, especially in scenarios with a limited number of images available for training. In such cases, the algorithm may show high performance on training data but fail to generalize to external datasets. To mitigate this risk, strategies such as artificial data augmentation and cross-validation were employed, contributing to greater model robustness.

In the study by Miller et al.,[13] it is recognized that visual interpretation of single-photon emission computed tomography constitutes the standard approach in the diagnostic evaluation of ATTR amyloidosis, although it is inherently subjective. The authors assessed a deep learning approach for automated volumetric quantification of technetium-99m (^{99m}Tc)-pyrophosphate, using segmentation of anatomical structures co-registered on computed tomography attenuation maps in patients with suspected ATTR amyloidosis. The results demonstrated that deep learning-based segmentation was not influenced by the radiotracer uptake pattern and allowed automated quantification of focal uptake images, such as those obtained with ^{99m}Tc-pyrophosphate. The model showed excellent performance (AUC = 0.989; 95% CI: 0.974-1.00), indicating potential for accurate identification of patients with ATTR amyloidosis. Therefore, this approach shows potential for precise identification of patients with ATTR amyloidosis.

Performance of artificial intelligence in the evaluation of bone-seeking tracers scintigraphy

In the context of diagnosing cardiac amyloidosis through the application of AI to imaging analysis, it is possible to structure systems integrated into electronic health records, similar to the model described by Huda et al.,[8] but directed toward the automated interpretation of scintigraphy images.

Delbarre et al.[14] proposed a deep learning model for automated analysis of whole-body ^{99m}Tc bone-seeking tracers scintigraphy, based on the premise that significant cardiac uptake on these examinations is strongly suggestive of ATTR amyloidosis. The model demonstrated sensitivity of 98.9% and specificity of 99.5% in cross-validation. In external validation, a slight reduction in sensitivity to 96.1% was observed, while specificity remained at 99.5%, with an AUC of 0.999 in both stages.

For system development, cardiac uptake ≥ 2 according to the Perugini grading scale was used as a predictive variable. The algorithm was trained using CNNs with image-level labels extracted from examinations recorded in electronic health records, enabling automated identification of patterns suggestive of cardiac amyloidosis. As also emphasized by Castaño et al.,[9] integration between AI and electronic record systems supports efficient screening of frequently underrecognized conditions, such as the association between increased cardiac uptake on whole-body bone-seeking tracers scintigraphy and ATTR amyloidosis, contributing to identification at earlier stages.

Although bone-seeking tracers scintigraphy does not fully replace all diagnostic methods, Delbarre et al.[14] highlighted that when the examination is positive and there is no evidence of monoclonal gammopathy, it may allow definitive noninvasive diagnosis of ATTR cardiomyopathy, particularly in elderly or frail patients in whom myocardial biopsy carries greater risk.

Considering that the diagnosis of cardiac amyloidosis can be established noninvasively through bone-seeking tracers scintigraphy and that visual assessment is inherently subjective and may result in misinterpretation, Spielvogel et al.[15] developed an AI system for standardized and reproducible disease screening. The model was trained using a multinational database of ^{99m}Tc-labeled bone-seeking tracers scintigraphy, encompassing different tracers and scanners. In the Austrian cohort, cross-validation demonstrated an AUC of 1.00 (95% CI: 1.00-1.00). In external validation, results remained high, with an AUC of 0.997 (95% CI: 0.993-0.999) in the United Kingdom, 0.925 (95% CI: 0.871-0.971) in China, and 1.00 (95% CI: 0.999-1.000) in the Italian cohorts. Approximately one decade ago, myocardial biopsy represented the only definitive modality for diagnosing cardiac amyloidosis. The consolidation of bone-seeking tracers scintigraphy constituted a significant advance in this scenario, particularly in the diagnosis of ATTR amyloidosis. The incorporation of AI into this modality further expands its potential by reducing interpretative subjectivity and increasing diagnostic standardization and reliability.

In the aforementioned multicenter study, intense cardiac uptake was automatically and consistently identified across all tracers used in the investigation of cardiac amyloidosis. Additionally, AI-based screening for detection of uptake suggestive of cardiac amyloidosis in patients undergoing whole-body bone-seeking tracers scintigraphy represents a potentially valuable tool for early disease identification and optimization of care pathways. Implementing this strategy may support timely referral for specialized evaluation and enable earlier initiation of disease-modifying therapies, with potential impact on mortality reduction.

Artificial intelligence in cardiac magnetic resonance evaluation

CMR with late gadolinium enhancement (LGE) is a fundamental method in the investigation of cardiac amyloidosis, given its ability to demonstrate morphological alterations and characteristic enhancement patterns. However, its use may be limited in patients with significant renal impairment, a condition frequently associated with amyloidosis, due to the risks related to contrast administration.

Ma et al.[16] investigated the feasibility of diagnosis using non-contrast CMR with native T1 mapping combined with automated radiomic analysis based on AI. The model was trained to recognize specific patterns of amyloid deposition and to indirectly estimate extracellular volume (ECV), a parameter traditionally calculated from pre- and post-gadolinium contrast sequences. In the proposed approach, ECV was accurately estimated through automated identification of myocardial regions of interest. The model achieved an accuracy of 86%, sensitivity of 94%, specificity of 85%, and an AUC of 0.915 in the test set. Unlike bone-seeking tracers scintigraphy, whose main applicability is concentrated on identifying ATTR amyloidosis, non-contrast CMR demonstrated potential for effective diagnosis of cardiac amyloidosis, particularly AL amyloidosis.

In line with this perspective, Nowak et al.[17] emphasized that the diagnostic value of CMR derives from its ability to integrate multiple sequences for detailed assessment of myocardial function, edema, inflammation, and fibrosis. ECV allows noninvasive quantification of myocardial amyloid deposition and may influence therapeutic decisions.

Considering that CMR is a reference modality for diagnosing cardiac amyloidosis, Agibetov et al.[18] observed that its findings may be nonspecific, especially in centers with lower case volumes. To minimize this risk, they developed a CNN-based algorithm applied to a cohort of 502 patients. Regardless of the deep learning technique employed, models trained with LGE images showed better performance. Fine-tuning of the model resulted in an AUC of 0.96, sensitivity of 94%, and specificity of 90%. Automated classification demonstrated performance comparable to that of human specialists. However, as this was a single-center study, generalization of the results requires caution.

Martini et al.[19] also used deep learning for automated analysis of CMR images and estimation of the probability of cardiac amyloidosis. Among the most specific findings, they highlighted the pattern of biventricular pseudo-hypertrophy associated with diffuse transmural LGE. Automated analysis of LGE sequences in the 2C, 4C, and short-axis views was faster and showed accuracy similar to expert assessment, with an AUC of 0.982, positive predictive value of 83%, recall of 95%, and F1-score of 89%.

Performance of artificial intelligence in the evaluation of genetic testing and biopsies

Another promising field in the application of AI to the diagnosis of cardiac amyloidosis, especially in the AL form, involves systematizing the analysis of genetic tests aimed at identifying somatic mutations in immunoglobulin light chains. Garofalo et al.[20] demonstrated, through a machine learning model, an association between somatic mutations acquired during B-cell maturation and the development of cardiac amyloidosis. These mutations affect the structural stability of light chains, favoring protein misfolding and subsequent amyloid deposit formation. The proposed model achieved a sensitivity of 76%, specificity of 82%, and an AUC of 0.87, demonstrating relevant predictive capacity in identifying sequences considered toxic. In addition, the authors highlighted that reversal of these mutations may abolish the toxic phenotype, reinforcing the importance of detailed molecular characterization.

Considering the diversity of pathogenic sequences involved, the use of AI represents an appropriate strategy for organizing and analyzing large volumes of genetic variables, acting as a predictor of toxicity. In this way, the algorithm may identify molecular profiles associated with higher risk of developing cardiac amyloidosis, thereby contributing to risk stratification and potential early diagnosis.

In the field of histopathology, biopsy remains the definitive diagnostic evidence in amyloid cardiomyopathy, despite its invasive nature. In this context, integration between histological techniques and deep learning has also shown promise. Yang et al.[21] proposed a neural network-based approach capable of transforming autofluorescence images into images equivalent to those obtained by bright-field and polarized light microscopy, simulating the effect of Congo red staining.

Currently, the diagnostic gold standard is based on the identification of birefringence under cross-polarized light after Congo red staining. However, this process is influenced by technical variability in staining, slide preparation quality, and availability of appropriate equipment, in addition to involving high costs. The model proposed by Yang et al.[21] demonstrated that digitally generated images showed quality comparable to conventionally stained slides, with potential cost reduction, lower technical dependence, and improved digital storage of samples, considering that specialized scanners for birefringence capture are not always available.

Thus, although there is growing interest in noninvasive diagnostic methods for cardiac amyloidosis, advances in the application of AI to genetic and histopathological analysis also represent a relevant contribution, improving diagnostic accuracy and standardization of laboratory processes.

Barriers to implementing artificial intelligence in the medical workflow

The implementation of AI in medical practice has significant potential to increase diagnostic accuracy, optimize care processes, reduce costs, and support clinical decision-making. However, its incorporation into the workflow faces multifactorial challenges that can be grouped into technical, ethical, organizational, and human dimensions.

From a technical perspective, AI models depend on structured, complete, and standardized datasets. However, many health care systems still operate with fragmented, inconsistent, or incomplete records, which compromises proper training and the generalizability of algorithms. In

addition, historically biased data may perpetuate health care disparities, resulting in inappropriate recommendations for certain population groups. Interoperability among different information systems also represents a relevant challenge, hindering seamless integration of AI into established clinical environments.

From an ethical and legal standpoint, questions arise regarding accountability in cases of clinical error involving algorithmic recommendations. Defining responsibility among developers, institutions, and professionals remains complex. This is compounded by concerns about data privacy, security, and governance, especially when there is interinstitutional data sharing for model training or validation.

At the organizational level, adoption of AI-based tools requires efficient integration into care workflows. Solutions that add steps to the process or disrupt established routines tend to generate resistance and operational burden. In addition, physicians, nurses, and other professionals must be trained to critically interpret the recommendations provided by these systems, using them as support rather than as a substitute for clinical judgment. Implementation also requires investment in technological infrastructure, maintenance, and continuous model updating, which may represent a financial barrier for certain institutions.

Finally, the human dimension involves aspects related to professional acceptance and patient trust. Some professionals may express distrust toward the technology or perceive AI as a threat to their clinical role. The so-called "black box" nature of algorithms, in which the decision-making process is not fully transparent, may reduce trust in the tool and hinder its incorporation into clinical practice. From the patient's perspective, trust in decisions influenced by algorithms is not yet universal. Conversely, there is a risk of excessive reliance on AI by professionals, which may compromise independent clinical reasoning if a critical and reflective stance is not maintained.

Conclusion

Based on the findings of this review, AI emerges as a promising tool for optimizing the screening and diagnosis of cardiac amyloidosis. Its application across different diagnostic modalities demonstrates potential to accelerate disease identification, contribute to greater diagnostic accuracy, and consequently support improved clinical outcomes.

The high capacity for processing and analyzing large volumes of data enables AI to recognize complex patterns, expand its ability to generalize, provided it is trained on robust and representative datasets, and assist in the early detection of cardiac amyloidosis. Furthermore, using automated models may reduce the subjectivity of human interpretation, minimize the need for invasive procedures in certain contexts, and rationalize the use of health care resources.

However, despite the advances observed, the consolidation of AI in clinical practice requires continuous model refinement, external validation in diverse populations, and efficient integration into care workflows. Strategic implementation planning, training of health professionals, ethical governance in data management, and ongoing monitoring of algorithmic performance are equally essential.

Author Contributions

Conception and design of the research, analysis and interpretation of the data, writing of the manuscript and critical revision of the manuscript for intellectual content: Lemos NB, Araújo GAM, Melo MDT; obtaining financing: Lemos NB, Araújo GAM.

Potential Conflict of Interest

No potential conflict of interest relevant to this article was reported.

Sources of Funding

There were no external funding sources for this study.

Study Association

This study is not associated with any thesis or dissertation work.

Ethics Approval and Consent to Participate

This article does not contain any studies with human participants or animals performed by any of the authors.

Use of Artificial Intelligence

The authors did not use any artificial intelligence tools in the development of this work.

Availability of Research Data

The underlying content of the research text is contained within the manuscript.

References

1. Zhang X, Liang T, Su C, Qin S, Li J, Zeng D, et al. Deep Learn-Based Computer-Assisted Transthoracic Echocardiography: Approach to the Diagnosis of Cardiac Amyloidosis. Int J Cardiovasc Imaging. 2023;39(5):955-65. doi: 10.1007/s10554-023-02806-0.
2. Cotella JI, Slivnick JA, Sanderson E, Singulane C, O'Driscoll J, Asch FM, et al. Artificial Intelligence Based Left Ventricular Ejection Fraction and Global Longitudinal Strain in Cardiac Amyloidosis. Echocardiography. 2023;40(3):188-95. doi: 10.1111/echo.15516.
3. Goto S, Mahara K, Beussink-Nelson L, Ikura H, Katsumata Y, Endo J, et al. Artificial Intelligence-Enabled Fully Automated Detection of Cardiac Amyloidosis Using Electrocardiograms and Echocardiograms. Nat Commun. 2021;12(1):2726. doi: 10.1038/s41467-021-22877-8.
4. Shiri I, Balzer S, Baj G, Bernhard B, Hundertmark M, Bakula A, et al. Multi-Modality Artificial Intelligence-Based Transthyretin Amyloid Cardiomyopathy Detection in Patients with Severe Aortic Stenosis. Eur J Nucl Med Mol Imaging. 2025;52(2):485-500. doi: 10.1007/s00259-024-06922-4.

5. Vrudhula A, Stern L, Cheng PC, Ricchiuto P, Daluwatte C, Witteles R, et al. Impact of Case and Control Selection on Training Artificial Intelligence Screening of Cardiac Amyloidosis. JACC Adv. 2024;3(9):100998. doi: 10.1016/j.jacadv.2024.100998.

6. Schrutka L, Anner P, Agibetov A, Seirer B, Dusik F, Rettl R, et al. Machine Learning-Derived Electrocardiographic Algorithm for the Detection of Cardiac Amyloidosis. Heart. 2022;108(14):1137-47. doi: 10.1136/heartjnl-2021-319846.

7. Eckstein J, Moghadasi N, Körperich H, Valdés EW, Sciacca V, Paluszkiewicz L, et al. A Machine Learning Challenge: Detection of Cardiac Amyloidosis Based on Bi-Atrial and Right Ventricular Strain and Cardiac Function. Diagnostics. 2022;12(11):2693. doi: 10.3390/diagnostics12112693.

8. Huda A, Castaño A, Niyogi A, Schumacher J, Stewart M, Bruno M, et al. A Machine Learning Model for Identifying Patients at Risk for Wild-Type Transthyretin Amyloid Cardiomyopathy. Nat Commun. 2021;12(1):2725. doi: 10.1038/s41467-021-22876-9.

9. Castaño A, Heitner SB, Masri A, Huda A, Calambur V, Bruno M, et al. EstimATTR: A Simplified, Machine-Learning-Based Tool to Predict the Risk of Wild-Type Transthyretin Amyloid Cardiomyopathy. J Card Fail. 2024;30(6):778-87. doi: 10.1016/j.cardfail.2023.11.017.

10. Harmon DM, Mangold K, Suarez AB, Scott CG, Murphree DH, Malik A, et al. Postdevelopment Performance and Validation of the Artificial Intelligence-Enhanced Electrocardiogram for Detection of Cardiac Amyloidosis. JACC Adv. 2023;2(8):100612. doi: 10.1016/j.jacadv.2023.100612.

11. Barbieri A, Imberti JF, Bartolomei M, Bonini N, Laus V, Triglia LT, et al. Quantification of Myocardial Contraction Fraction with Three-Dimensional Automated, Machine-Learning-Based Left-Heart-Chamber Metrics: Diagnostic Utility in Hypertrophic Phenotypes and Normal Ejection Fraction. J Clin Med. 2023;12(17):5525. doi: 10.3390/jcm12175525.

12. Santarelli MF, Genovesi D, Positano V, Scipioni M, Vergaro G, Favilli B, et al. Deep-Learning-Based Cardiac Amyloidosis Classification from Early Acquired Pet Images. Int J Cardiovasc Imaging. 2021;37(7):2327-35. doi: 10.1007/s10554-021-02190-7.

13. Miller RJH, Shanbhag A, Michalowska AM, Kavanagh P, Liang JX, Builoff V, et al. Deep Learning-Enabled Quantification of 99mTc-Pyrophosphate SPECT/CT for Cardiac Amyloidosis. J Nucl Med. 2024;65(7):1144-50. doi: 10.2967/jnumed.124.267542.

14. Delbarre MA, Girardon F, Roquette L, Blanc-Durand P, Hubaut MA, Hachulla É, et al. Deep Learning on Bone Scintigraphy to Detect Abnormal Cardiac Uptake at Risk of Cardiac Amyloidosis. JACC Cardiovasc Imaging. 2023;16(8):1085-95. doi: 10.1016/j.jcmg.2023.01.014.

15. Spielvogel CP, Haberl D, Mascherbauer K, Ning J, Kluge K, Traub-Weidinger T, et al. Diagnosis and Prognosis of Abnormal Cardiac Scintigraphy Uptake Suggestive of Cardiac Amyloidosis Using Artificial Intelligence: A Retrospective, International, Multicentre, Cross-Tracer Development and Validation Study. Lancet Digit Health. 2024;6(4):e251-60. doi: 10.1016/S2589-7500(23)00265-0.

16. Ma Q, Chen J, Cao L, Wu X, Tan Z, Liu H. The Incremental Value of Native T1 Mapping-Derived Radiomics for The Diagnosis of Amyloid Light-Chain Cardiac Amyloidosis. Acad Radiol. 2024;31(12):4801-10. doi: 10.1016/j.acra.2024.07.005.

17. Nowak S, Bischoff LM, Pennig L, Kaya K, Isaak A, Theis M, et al. Deep Learning Virtual Contrast-Enhanced T1 Mapping for Contrast-Free Myocardial Extracellular Volume Assessment. J Am Heart Assoc. 2024;13(19):e035599. doi: 10.1161/JAHA.124.035599.

18. Agibetov A, Kammerlander A, Duca F, Nitsche C, Koschutnik M, Donà C, et al. Convolutional Neural Networks for Fully Automated Diagnosis of Cardiac Amyloidosis by Cardiac Magnetic Resonance Imaging. J Pers Med. 2021;11(12):1268. doi: 10.3390/jpm11121268.

19. Martini N, Aimo A, Barison A, Latta DD, Vergaro G, Aquaro GD, et al. Deep Learning to Diagnose Cardiac Amyloidosis from Cardiovascular Magnetic Resonance. J Cardiovasc Magn Reson. 2020;22(1):84. doi: 10.1186/s12968-020-00690-4.

20. Garofalo M, Piccoli L, Romeo M, Barzago MM, Ravasio S, Foglierini M, et al. Machine Learning Analyses of Antibody Somatic Mutations Predict Immunoglobulin Light Chain Toxicity. Nat Commun. 2021;12(1):3532. doi: 10.1038/s41467-021-23880-9.

21. Yang X, Bai B, Zhang Y, Aydin M, Li Y, Selcuk SY, et al. Virtual Birefringence Imaging and Histological Staining of Amyloid Deposits in Label-Free Tissue Using Autofluorescence Microscopy and Deep Learning. Nat Commun. 2024;15(1):7978. doi: 10.1038/s41467-024-52263-z.

Review Article

Neurological Manifestations of Takayasu Arteritis: A Case Report and Literature Review

Amanda Antunes Arantes Rolim,[1] *Tainá Cândida de Almeida Gontijo Carneiro,*[1] *Flávia de Campos,*[1] *Dilson Palhares Ferreira*[1]

Hospital Regional de Sobradinho, Sobradinho,[1] *Brasília, DF – Brazil*

Abstract

Takayasu arteritis (TA) is a rare large-vessel vasculitis that primarily involves the aorta and its major branches and predominantly affects women of reproductive age. We report the case of a woman who experienced an ischemic stroke at age 20 and a transient ischemic attack at age 53, with TA diagnosed only after the second cerebrovascular event. Although ischemic stroke is an uncommon initial manifestation of TA, early recognition and timely management are essential to prevent further complications and improve long-term outcomes.

Introduction

Takayasu arteritis (TA) is a rare, chronic vasculitis affecting large and medium-sized vessels, primarily the aorta and its major branches. TA predominantly affects women of reproductive age.[1] The disease is characterized by progressive arterial inflammation, which may lead to stenosis, occlusion, and aneurysm formation. Although its exact etiology remains unclear, genetic susceptibility and autoimmune mechanisms, particularly involving Th1 and Th17 lymphocyte pathways, have been implicated.[2]

Early manifestations are often nonspecific and may include fever, weight loss, fatigue, and arthralgia.[1] As the disease progresses, vascular findings become more prominent, including diminished or absent upper limb pulses (84%-96%), limb claudication, inter-arm blood pressure discrepancies, systemic hypertension (33%-83%), and arterial bruits (80%-94%).[1] Approximately 10% of patients remain asymptomatic.[3]

Cerebrovascular events, including ischemic stroke and transient ischemic attack (TIA), occur in 10%-20% of patients with TA[1,4,5] and rarely represent the initial manifestation of the disease.[5] In a cohort of 320 patients, 20% experienced cerebrovascular events, of whom 65% had ischemic stroke and 35% had TIA.[4] Identified risk factors included a history of prior ischemic stroke or TIA and delayed diagnosis.

Keywords

Takayasu Arteritis; Stroke; Neurologic Manifestations

Mailing Address: Amanda Antunes Arantes Rolim •
Hospital Regional de Sobradinho (HRS). Quadra 12, Conjunto B, lote 38. Postal code: 73010-120. Sobradinho, DF - Brazil
E-mail: amanda.arantes1412@gmail.com
Manuscript received December 15, 2025, revised manuscript January 31, 2025, accepted February 20, 2026
Editor responsible for the review: Simone Nascimento dos Santos

DOI: https://doi.org/10.36660/abcimg.20250110i

TA should be suspected in young women presenting with cardiovascular symptoms and cerebrovascular manifestations. Early diagnosis and prompt initiation of immunosuppressive therapy are essential to prevent disease progression, reduce complications, and improve prognosis.[1] This study reports a case of TA initially presenting with ischemic stroke.

Case report

A 53-year-old woman presented to the emergency department after a fall from standing height caused by sudden weakness of the right lower limb. The episode was accompanied by leftward deviation of the oral commissure and dysarthria. Her medical history was notable for an ischemic stroke at age 20, resulting in persistent right-sided spastic hemiparesis. She had not received medical follow-up since that event. The patient was sedentary and denied smoking, alcohol consumption, or regular use of medicines.

On physical examination, vital signs were stable, and no additional abnormalities were observed. Laboratory investigations were unremarkable, including a C-reactive protein level of 3.18 mg/L. Initial cranial computed tomography demonstrated sequelae of a lacunar infarction in the left basal ganglia, with no evidence of acute ischemic lesions. Transthoracic echocardiography was normal. Carotid Doppler ultrasonography revealed approximately 31% stenosis of the proximal and mid segments of the left common carotid artery, with wall thickness ranging from 1.2 to 1.4 mm. The right common carotid artery showed 20% stenosis and wall thickness of 1.4 mm. The left vertebral artery was described as hypoplastic.

A repeat cranial computed tomography performed 48 hours later showed no interval changes. Because the neurological deficits resolved within 3 hours, the clinical diagnosis of TIA was established.

Given the suspicion of TA, blood pressure was measured in all four limbs, revealing no significant discrepancies. However, a bruit was auscultated over the left carotid artery. The patient denied prior constitutional or ischemic symptoms.

Cerebral magnetic resonance angiography (MRA) confirmed the previous ischemic stroke sequela in the left cerebral hemisphere. Cervical MRA (Figure 1) demonstrated approximately 60% stenosis of the proximal left common carotid artery, marked narrowing of the left internal and external carotid arteries with filiform flow, and diffuse hypoplasia of the left vertebral artery.

Thoracic MRA (Figure 2) demonstrated a focal fusiform dilation of the descending thoracic aorta.

Figure 1 – *Cervical magnetic resonance angiography. Source: Author's personal archive (2025).*

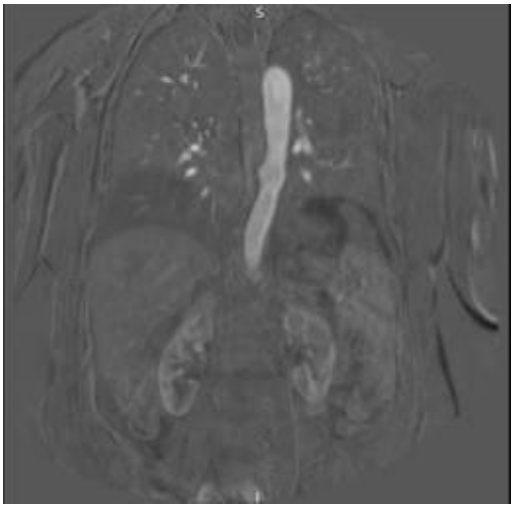

Figure 2 – *Thoracic magnetic resonance angiography. Source: Author's personal archive (2025).*

Abdominal MRA (Figure 3) revealed segmental stenosis of the infrarenal abdominal aorta, beginning at the level of the renal artery origins.

The patient was discharged with referrals to rheumatology, neurology, and cardiology outpatient clinics. However, she did not attend the scheduled appointments and remained without disease-specific treatment despite repeated follow-up attempts.

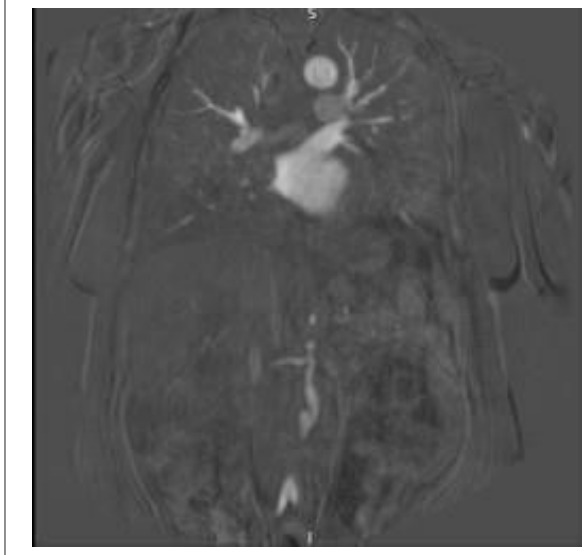

Figure 3 – *Abdominal magnetic resonance angiography. Source: Author's personal archive (2025).*

Discussion

The arteries most commonly affected in TA are large- and medium-caliber supra-aortic vessels, involved in approximately 85% of cases.[6,7] The subclavian (83.73%) and common carotid (73.22%) arteries are the most frequently affected vessels.[7] Renal artery involvement occurs in 24%-68% of cases,[8] and intracranial vessel involvement has been reported in 23.7%, particularly affecting the internal carotid artery.[9] Occlusion of the vertebral and carotid arteries is strongly associated with cerebrovascular ischemic events.

In the present case, the first ischemic event at age 20 likely reflected pre-existing vascular injury. At age 53, the patient presented with a TIA and a left carotid bruit. According to the 2022 American College of Rheumatology/European Alliance of Associations for Rheumatology classification criteria,[10] her clinical and imaging findings were consistent with TA.

Angiographic findings on MRA classified the disease as Type V according to Hata's angiographic classification[11] (Figure 4), which is the most frequent subtype, followed by Type I.[7,11] This classification primarily assists in surgical planning and does not carry established prognostic value.[1]

Risk factors for vascular complications in TA include progressive disease, thoracic aorta involvement, and retinopathy.[12] However, outcomes are influenced by multiple variables, and management must be individualized.

Traditional inflammatory markers, such as C-reactive protein and erythrocyte sedimentation rate, are insufficient to accurately assess disease activity.[13] Additional biomarkers, including matrix metalloproteinases, cytokines, and pentraxins, have been investigated,[13] but they are not routinely available in clinical practice.

Assessment of disease activity remains challenging. Instruments such as the National Institutes of Health criteria,

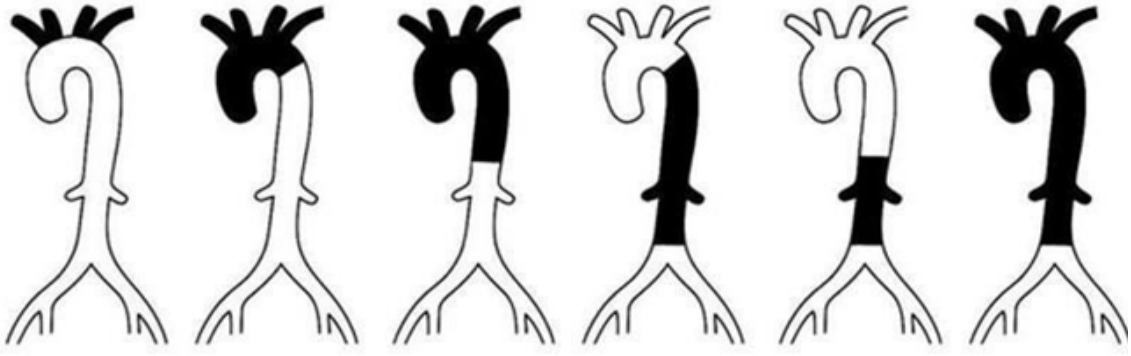

Figure 4 – *Angiographic classification of Takayasu arteritis. The black areas indicate the arteries involved in each type. Source: Adapted from Hata et al.*[11]

the Disease Extent Index for Takayasu Arteritis, and the Indian Takayasu Clinical Activity Score incorporate clinical, laboratory, and imaging parameters, although their accuracy varies.[13] The Takayasu Arteritis Integrated Disease Activity Index has demonstrated high sensitivity and specificity, but further external validation is required.[14] Combining biomarkers with advanced imaging modalities may enhance disease monitoring and therapeutic decision-making.

Treatment strategies depend on disease activity and severity. Active or severe disease requires high-dose glucocorticoids, with intravenous administration reserved for organ-threatening manifestations. In non-severe cases, combination therapy with glucocorticoids and immunosuppressive agents such as methotrexate, tumor necrosis factor inhibitors, or azathioprine has shown improved efficacy. After 6-12 months of sustained remission, gradual glucocorticoid tapering is recommended. In patients with critical cranial or vertebrobasilar involvement, antiplatelet therapy reduces the risk of ischemic events.[15]

Patients without major complications generally have a favorable prognosis.[16] Early initiation of treatment improves long-term outcomes and reduces the risk of accelerated atherosclerosis.[17] Younger patients tend to have lower remission rates, whereas older patients may require less intensive pharmacologic therapy but often exhibit greater functional impairment due to comorbidities.[18]

Conclusions

Although rare, TA may lead to severe neurological events, including stroke. Early recognition, particularly in young women presenting with pulse deficits, blood pressure discrepancies, or limb claudication, is essential. Prompt diagnosis and appropriate treatment improve clinical outcomes and reduce the risk of long-term complications.

Author Contributions

Conception and design of the research and analysis and interpretation of the data: Rolim AAA, Campos F, Carneiro TCAG; acquisition of data and writing of the manuscript: Rolim AAA; critical revision of the manuscript for intellectual content: Campos F, Ferreira DP, Carneiro TCAG.

Potential Conflict of Interest

No potential conflict of interest relevant to this article was reported.

Sources of Funding

There were no external funding sources for this study.

Study Association

This article is part of the Final Course Project by Amanda Antunes Arantes Rolim for Fundação de Ensino e Pesquisa em Ciências da Saúde (FEPECS), conducted at the Hospital Regional de Sobradinho.

Ethics Approval and Consent to Participate

This study was approved by the Ethics Committee of the Fundação de Ensino e Pesquisa em Ciências da Saúde under the protocol number 7.812.420. All the procedures in this study were in accordance with the 1975 Helsinki Declaration, updated in 2013. Informed consent was obtained from all participants included in the study.

Use of Artificial Intelligence

During the preparation of this work, the author(s) used ChatGPT to create Figure 4. After using this tool/service, the author(s) reviewed and edited the content as needed and take full responsibility for the content of the published article.

Availability of Research Data

The data cannot be made publicly available because this is a single case report. The study data correspond to information contained in the patient's medical record and therefore require confidentiality, as established by the Research Ethics Committee for this study.

References

1. Johnston SL, Lock RJ, Gompels MM. Takayasu Arteritis: A Review. J Clin Pathol. 2002;55(7):481-6. doi: 10.1136/jcp.55.7.481.
2. Kermani TA, Warrington KJ. Classification Criteria, Epidemiology and Genetics; and Pathogenesis. In: Salvarani C, Boiardi L, Muratore F, editors. Large and Medium Size Vessel and Single Organ Vasculitis. Cham: Springer; 2021. p. 83-92.
3. Kerr GS, Hallahan CW, Giordano J, Leavitt RY, Fauci AS, Rottem M, et al. Takayasu Arteritis. Ann Intern Med. 1994;120(11):919-29. doi: 10.7326/0003-4819-120-11-199406010-00004.
4. Mirouse A, Deltour S, Leclercq D, Squara PA, Pouchelon C, Comarmond C, et al. Cerebrovascular Ischemic Events in Patients with Takayasu Arteritis. Stroke. 2022;53(5):1550-7. doi: 10.1161/STROKEAHA.121.034445.
5. Duarte MM, Geraldes R, Sousa R, Alarcão J, Costa J. Stroke and Transient Ischemic Attack in Takayasu's Arteritis: A Systematic Review and Meta-Analysis. J Stroke Cerebrovasc Dis. 2016;25(4):781-91. doi: 10.1016/j.jstrokecerebrovasdis.2015.12.005.
6. Mirouse A, Biard L, Comarmond C, Lambert M, Mekinian A, Ferfar Y, et al. Overall Survival and Mortality Risk Factors in Takayasu's Arteritis: A Multicenter Study of 318 Patients. J Autoimmun. 2019;96:35-9. doi: 10.1016/j.jaut.2018.08.001.
7. Wang L, Sun Y, Dai X, Kong X, Ma L, Dai X, et al. Carotid Intima-Media Thickness/Diameter Ratio and Peak Systolic Velocity as Risk Factors for Neurological Severe Ischemic Events in Takayasu Arteritis. J Rheumatol. 2022;49(5):482-8. doi: 10.3899/jrheum.211081.
8. Sharma S, Gupta A. Visceral Artery Interventions in Takayasu's Arteritis. Semin Intervent Radiol. 2009;26(3):233-44. doi: 10.1055/s-0029-1225668.
9. Guo YQ, Du J, Pan LL, Guo X. Clinical Features of Intracranial Vessel Involvement in Takayasu's Arteritis. Zhonghua Yi Xue Za Zhi. 2020;100(23):1789-94. doi: 10.3760/cma.j.cn112137-20200304-00586.
10. Grayson PC, Ponte C, Suppiah R, Robson JC, Gribbons KB, Judge A, et al. 2022 American College of Rheumatology/EULAR Classification Criteria for Takayasu Arteritis. Ann Rheum Dis. 2022;81(12):1654-60. doi: 10.1136/ard-2022-223482.
11. Hata A, Noda M, Moriwaki R, Numano F. Angiographic Findings of Takayasu Arteritis: New Classification. Int J Cardiol. 1996;54(Suppl):S155-63. doi: 10.1016/s0167-5273(96)02813-6.
12. Comarmond C, Biard L, Lambert M, Mekinian A, Ferfar Y, Kahn JE, et al. Long-Term Outcomes and Prognostic Factors of Complications in Takayasu Arteritis: A Multicenter Study of 318 Patients. Circulation. 2017;136(12):1114-22. doi: 10.1161/CIRCULATIONAHA.116.027094.
13. Misra DP, Jain N, Ora M, Singh K, Agarwal V, Sharma A. Outcome Measures and Biomarkers for Disease Assessment in Takayasu Arteritis. Diagnostics. 2022;12(10):2565. doi: 10.3390/diagnostics12102565.
14. Marvisi C, Bolek EC, Ahlman MA, Alessi H, Redmond C, Muratore F, et al. Development of the Takayasu Arteritis Integrated Disease Activity Index. Arthritis Care Res. 2024;76(4):531-40. doi:10.1002/acr.25275.
15. Maz M, Chung SA, Abril A, Langford CA, Gorelik M, Guyatt G, et al. 2021 American College of Rheumatology/Vasculitis Foundation Guideline for the Management of Giant Cell Arteritis and Takayasu Arteritis. Arthritis Care Res. 2021;73(8):1071-87. doi: 10.1002/acr.24632.
16. Ishikawa K, Maetani S. Long-Term Outcome for 120 Japanese Patients with Takayasu's Disease. Clinical and Statistical Analyses of Related Prognostic Factors. Circulation. 1994;90(4):1855-60. doi: 10.1161/01.cir.90.4.1855.
17. Ohigashi H, Haraguchi G, Konishi M, Tezuka D, Kamiishi T, Ishihara T, et al. Improved Prognosis of Takayasu Arteritis Over the Past Decade--Comprehensive Analysis of 106 Patients. Circ J. 2012;76(4):1004-11. doi: 10.1253/circj.cj-11-1108.
18. Oliveira JCS, Santos AMD, Aguiar MF, Gonçalves J Jr, Souza AWS, Pereira RMR, et al. Characteristics of Older Patients with Takayasu's Arteritis: A Two-Center, Cross-Sectional, Retrospective Cohort Study. Arq Bras Cardiol. 2023;120(1):e20220463. doi: 10.36660/abc.20220463.

My Approach to Differentiating Pericardial Effusion with and without Hemodynamic Repercussions

Helder Moura Gomes,[1] Halsted Alarcão Gomes Pereira da Silva[1]
Instituto Dante Pazzanese de Cardiologia,[1] São Paulo, SP – Brazil

Central Illustration: My Approach to Differentiating Pericardial Effusion with and without Hemodynamic Repercussions

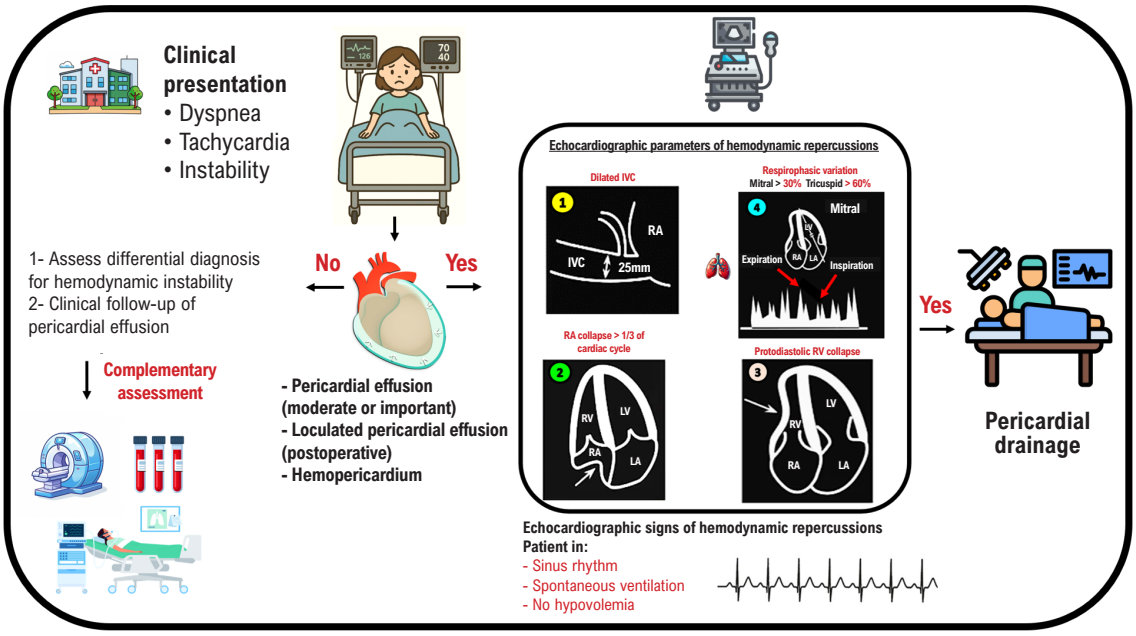

Arq Bras Cardiol: Imagem cardiovasc. 2026; 39(1):e20250105

RA: right atrium; LA: left atrium; RV: right ventricle; LV: left ventricle

Abstract

Pericardial effusion is a common finding in cardiology practice. It is frequently identified in outpatient and inpatient follow-up examinations, especially during the postoperative period of heart surgery. In clinically stable patients, proper assessment can allow for early detection of signs of clinical deterioration. In patients in shock, careful analysis of pericardial effusion can confirm or rule out this condition as the main cause of hemodynamic instability. Precise identification of the location, anatomical characterization of severity, and analysis of hemodynamic repercussions by means of Doppler are essential elements to guide medical management. In addition to technical assessment, precautions when describing findings in imaging reports are equally important. This is because the hemodynamic repercussions observed on echocardiography do not always correspond to the patient's clinical severity.

Keywords

Pericardial Effusion; Echocardiography; Inferior Vena Cava; Cardiac Tamponade.

Mailing Address: Helder Moura Gomes •
Instituto Dante Pazzanese de Cardiologia. Doutor Dante Pazzanese, 500. Postal code: 04.012-180. São Paulo, SP – Brazil
E-mail: heldergomes20@gmail.com
Manuscript received December 12, 2025; revised December 15, 2025; accepted December 15, 2025
Editor responsible for the review: Marcelo Tavares

DOI: https://doi.org/10.36660/abcimg.20250105i

Introduction

Pericardial effusion (PE) occurs due to accumulation of fluid in the pericardial sac. The etiologies include inflammatory, infectious, neoplastic, autoimmune, metabolic, traumatic, and iatrogenic causes.[1] It is not always simple to assess the repercussions of PE, because

SUMÁRIO

factors such as etiology, speed of onset, and hemodynamic conditions can make this assessment a major challenge in clinical practice. Although several methods can assess and quantify PE, given its inherent characteristics, echocardiography is the most widely applied initial method, providing tools for rapid assessment and decision-making, especially in critical patients.

Anatomical and pathophysiological considerations

The pericardium is a sac-like structure that contains the heart and adjacent structures, composed of a fibrous and a serous component. The outer fibrous component is mainly composed of collagen fibers with interspersed short elastic fibrils. The fibrous envelope is continuous superiorly with the adventitia of the great vessels and is attached inferiorly to the diaphragm. The serous component consists of a single layer of mesothelium that forms a parietal layer and a visceral layer, surrounding the pericardial cavity. The parietal layer lines the fibrous pericardium, and together these structures form the parietal pericardium. The visceral layer is also known as the epicardium, which lines the heart.

Between the visceral pericardium and the myocardium, there is a variable amount of epicardial adipose tissue. Epicardial fat is most abundant along the atrioventricular and interventricular sulci and is an important differential diagnosis when assessing PE.

Under physiological conditions, pericardial space normally contains a small amount of fluid, typically ranging from 10 to 50 mL, with an important function related to lubricating the heart, reducing friction during movement between tissues, and allowing the translational and rotational motion of the heart.

Slow increases in this volume tend to have a smaller impact on pericardial pressure and its transmission to the heart chambers, due to the maintenance of pericardial compliance. In rapid increases, this does not occur, and pericardial pressure shows a progressive and rapid increase that will interfere with cardiac hemodynamics (Figure 1).

The right ventricle (RV) wall is thinner than that of the left ventricle (LV). Consequently, more than half of the diastolic pressure in the RV, under physiological conditions, is due to the pericardium, making it a particularly important chamber in assessing the impact of PE, because it is one of the earliest affected.

It is essential to understand the phenomenon of ventricular interdependence inherent to cardiac physiology, in order to grasp the changes that guide the diagnosis of PE with hemodynamic repercussions. The RV and LV are pumps that share a wall, the interventricular septum that separates them, and both are contained within the pericardial sac. Therefore, variations in ventricular volumes and filling pressures can lead to bulging of the septum to one side, depending on the pressure conditions. This occurs under normal conditions, including during physiological inspiration and expiration, but it does not have a significant impact on LV filling (Figure 2).

When there is an increase in pericardial volume and an increase in pressure throughout the heart, RV filling during inspiration can bulge the septum to the left, limiting the

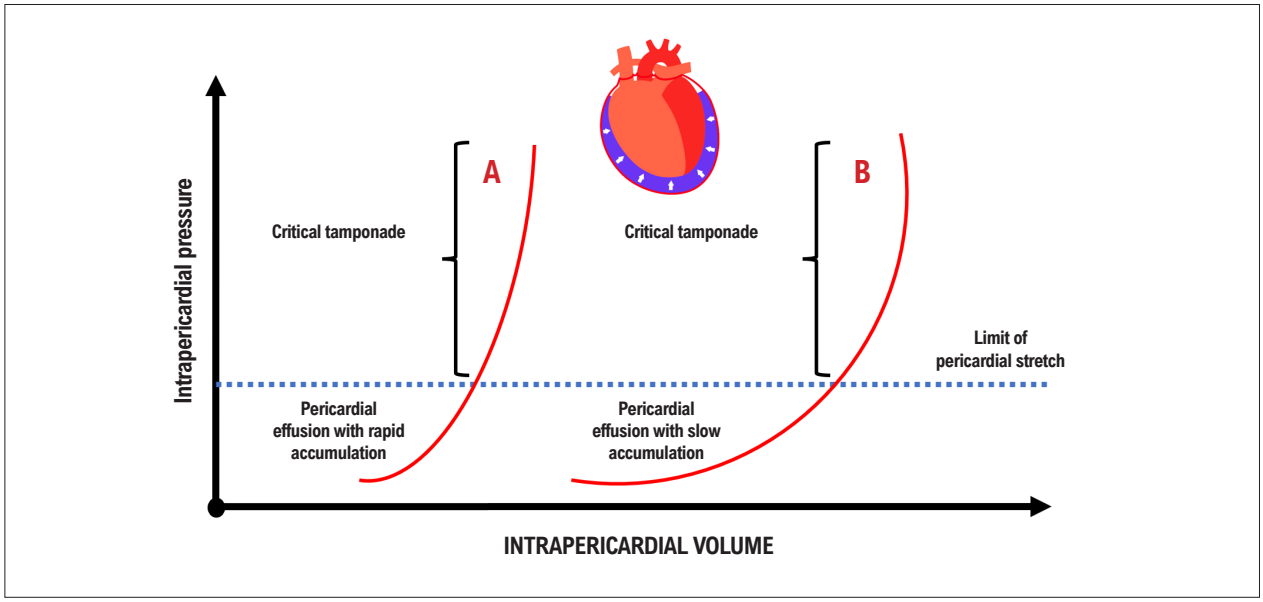

Figure 1 – *Comparative image demonstrating increased pericardial pressures in two possible scenarios. Curve A shows a scenario in which the accumulation of pericardial fluid occurs within a short period of time with a rapid increase in pericardial pressures transmitted to the heart chambers. Curve B shows a scenario in which the accumulation of pericardial fluid occurs over a longer period of time, with a slow and gradual increase in pericardial pressures, and pressure transmission to the heart chambers occurs only after a large accumulation of fluid. Adapted from American Society of Echocardiography guidelines.[2]*

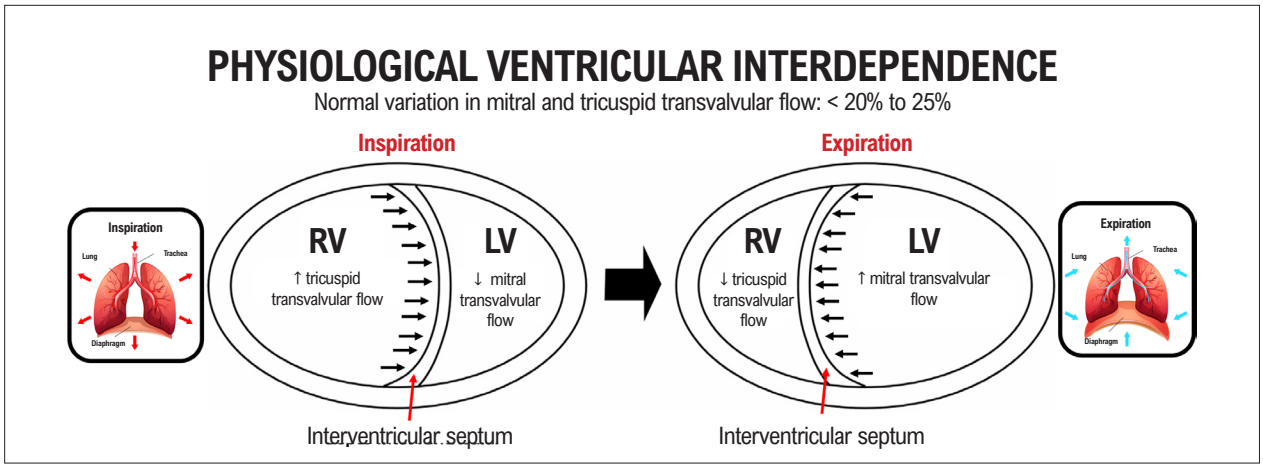

Figure 2 – *Ventricular interdependence demonstrating how the physiological variation of mitral and tricuspid transvalvular flows behaves during inspiration and expiration. Flow variations below 20% are expected in healthy patients. LV: left ventricle; RV: right ventricle.*

volume that fills the left side (reverse Bernheim effect). During expiration, the opposite occurs.[3] In practice, this explains, the paradoxical pulse and the increased variation of mitral and tricuspid flows between inspiration and expiration in extreme cases.

Given that PE can impact cardiac function, leading to low output, it is essential to understand the tools for evaluating PE and its repercussions. Although PE can also be evaluated by magnetic resonance imaging and computed tomography, echocardiography is a fundamental part of this assessment due to its sensitivity for large-volume effusions, portability, and ease of follow-up.

Correct identification of pericardial effusion

The following discussion is based on the fundamental concept that PE must be correctly diagnosed. A simple, yet accurate parameter for analysis is the location of fluid accumulation (anechoic content).

If the fluid is predominantly located anterior to the descending thoracic aorta in longitudinal parasternal view, the most likely diagnosis will be PE. If it is located in retroaortic topography, the diagnosis will be left pleural effusion, considering that the aorta in this segment is anterior and to the left of the vertebral column (Figure 3).

Another finding that can lead to incorrect diagnosis is epicardial fat, which differs from effusion insofar as it is more echogenic than the myocardium, moves along with cardiac motion, and does not naturally generate hemodynamic impact (Figure 4).

Echocardiographic assessment: quantification

By definition, pericardial fluid volume above 50 mL is considered abnormal[2] and should, whenever possible, be described in the final report. Echocardiographic quantification can be performed using size or volume parameters; the former is more commonly used in clinical practice and recommended by the American Society of Echocardiography guidelines, according to their most recent publication. This measurement is performed using two-dimensional echocardiography, and the parameter is described in a semi-quantitative manner, based on the size of the echo-free space seen between the parietal and visceral pericardium at end-diastole. Considering this measurement, we can classify PE as mild (< 10 mm), moderate (10 to 20 mm), and severe (> 20 mm), as described in Table 1.

Figure 5 displays a case of PE of inflammatory etiology, with measurements of the largest diastolic diameters. This assessment should always be performed using multiple echocardiographic windows.

Another parameter described is the volumetric estimate, considering the correlation between diameters and volumes measured on two-dimensional echocardiography. It is inferred that a mild effusion (< 10 mm) would have between 50 and 100 mL of pericardial fluid, a moderate effusion (10 to 20 mm) between 100 and 500 mL, and a significant effusion (> 20 mm) more than 500 mL[2]. There is limited accuracy between this measurement and the actual volume of surgically drained pericardial fluid. Volumetric assessment measured using Simpson's method, preferably in the subcostal window, as published by DeMaria et al. in the *Journal of the American Society of Echocardiography* in 2019,[4] appears to be of greater value. Figure 6 provides an example of how this quantification could be performed in a real-world case.

Uniform and homogeneous effusion suggests the possibility of transudate, whereas findings of asymmetrical distribution and heterogeneous content suggest exudate. Clots and effusions during the postoperative period can be a diagnostic challenge, sometimes requiring assessment using other methods.

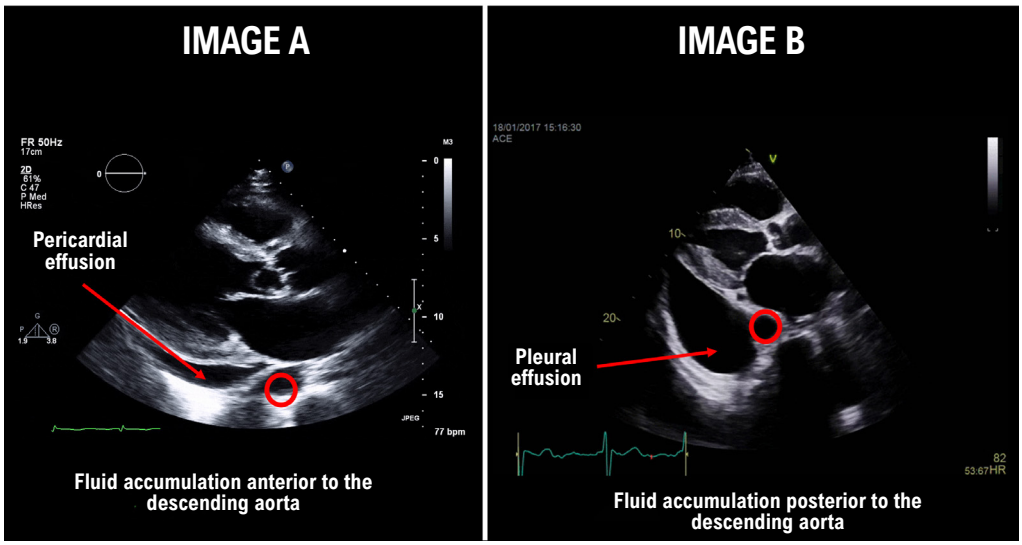

Figure 3 – *Echocardiographic differences between pericardial effusion (Image A) and pleural effusion (Image B), using the descending thoracic aorta as an anatomical reference parameter.*

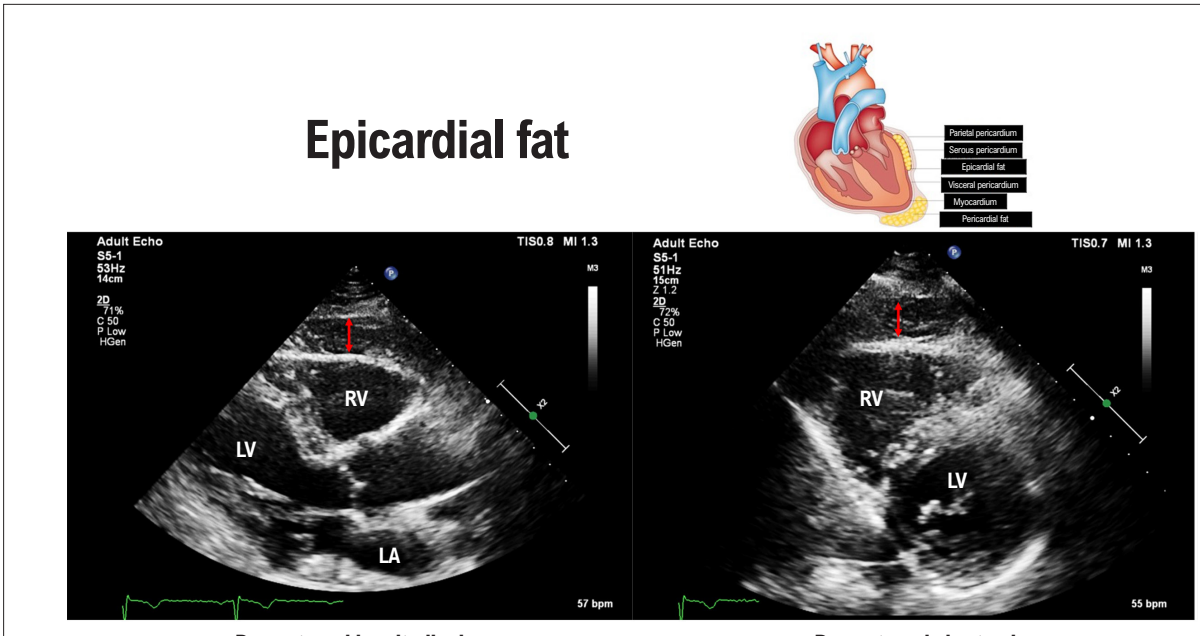

Figure 4 – *Echocardiographic images in the parasternal longitudinal and short-axis window of a patient with metabolic syndrome and extensive epicardial fat layer. Differential diagnosis with pericardial effusion is essential due to the difference in complementary investigation and clinical treatment. LA: left atrium; LV: left ventricle; RV: right ventricle.*

During onset of effusion, hemodynamic repercussions occur when pericardial pressure compresses the cardiac chambers, especially those with lower pressure, and limits chamber filling. To assess the repercussions of effusion, analysis seeks signs of pressure overload in the pericardial space.

Although it is the first-line examination in the assessment of fluid in the pericardial space, it is necessary to take the following limitations into consideration:

• Patients with limited acoustic windows (chronic obstructive pulmonary disease, obesity, postoperative cardiac surgery

Table 1 – Classification of pericardial effusion according to maximum diastolic diameter and estimated volume

ASE/EACVI classification of end-diastolic diameter		
Classification	**Diameter**	**Estimated volume**
• Normal	Seen only in systole	10 to 50 mL
• Minimal	< 5 mm	
• Mild	5 to 9 mm	< 100 mL
• Moderate	10 to 20 mm	100 to 500 mL
• Large	> 20 mm	> 500 mL
• Very large	> 25 mm	> 700 mL

Note: The estimation of pericardial effusion volume should be interpreted only as a reference parameter and not as a scientific dogma. ASE: American Society of Echocardiography; PE: pericardial effusion; EACVI: European Association of Cardiovascular Imaging.

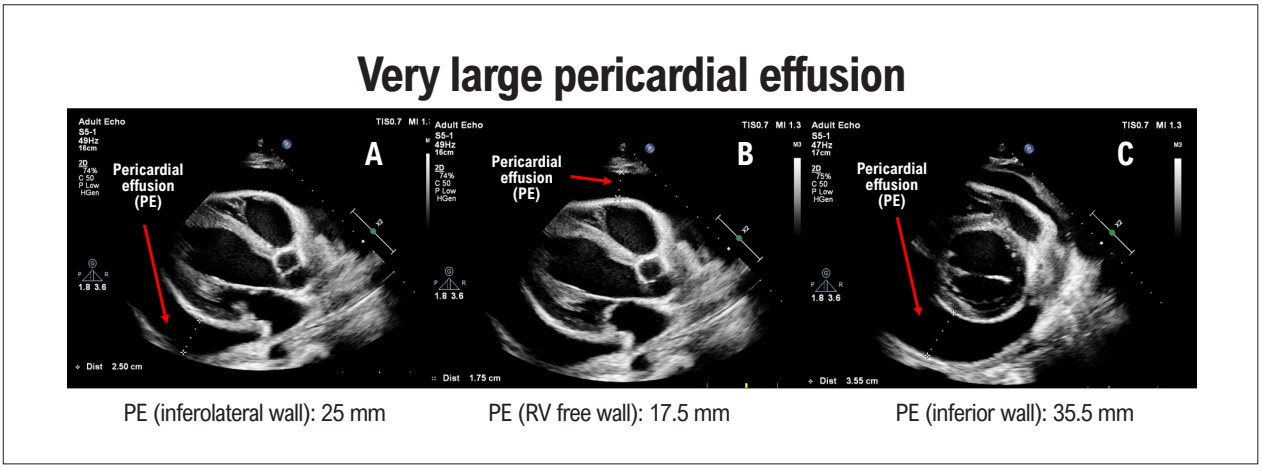

Figure 5 – *Very large pericardial effusion assessed through multiple images (A, B, and C), circumferentially involving the heart, with a maximum diameter of 35.5 mm shown in Image C. PE: pericardial effusion; RV: right ventricle.*

- Operator-dependent
- Low signal-to-noise ratio in pericardial space
- Limited tissue characterization
- Limited assessment in loculated effusions

Echocardiographic assessment: severity (hemodynamic repercussions)

One-dimensional assessment: M mode

Due to its high temporal resolution, this method is still widely used for determining the greatest pericardial fluid diameter, provided that the assessment axis is not oblique in relation to the line of analysis.

- Quantification should be performed following the previously described classification.
- The method more accurately identifies the temporality of right atrial (RA) and RV collapse in relation to the cardiac cycle (Figure 7).
- It allows identification of septal bounce related to increased ventricular interdependence; however, it is necessary to rule out other pathologies that may present the same sign, such as chronic obstructive pulmonary disease.

Two-dimensional assessment: 2D mode

Two-dimensional assessment involves analysis of dynamic anatomical parameters, such as inferior vena cava (IVC) distensibility, and RA and RV collapsibility. It also includes study of cavity flows in order to identify early changes related to hemodynamic repercussions.

Dynamic anatomical assessment of the inferior vena cava and hepatic veins

In PE, right heart chamber pressures are increased due to compression by the effusion. When there are hemodynamic repercussions, IVC plethora is practically a mandatory parameter; diameter greater than 21 mm and variation less than 50% are expected findings. IVC plethora was found in 92% of patients who required pericardial drainage.[5] When it

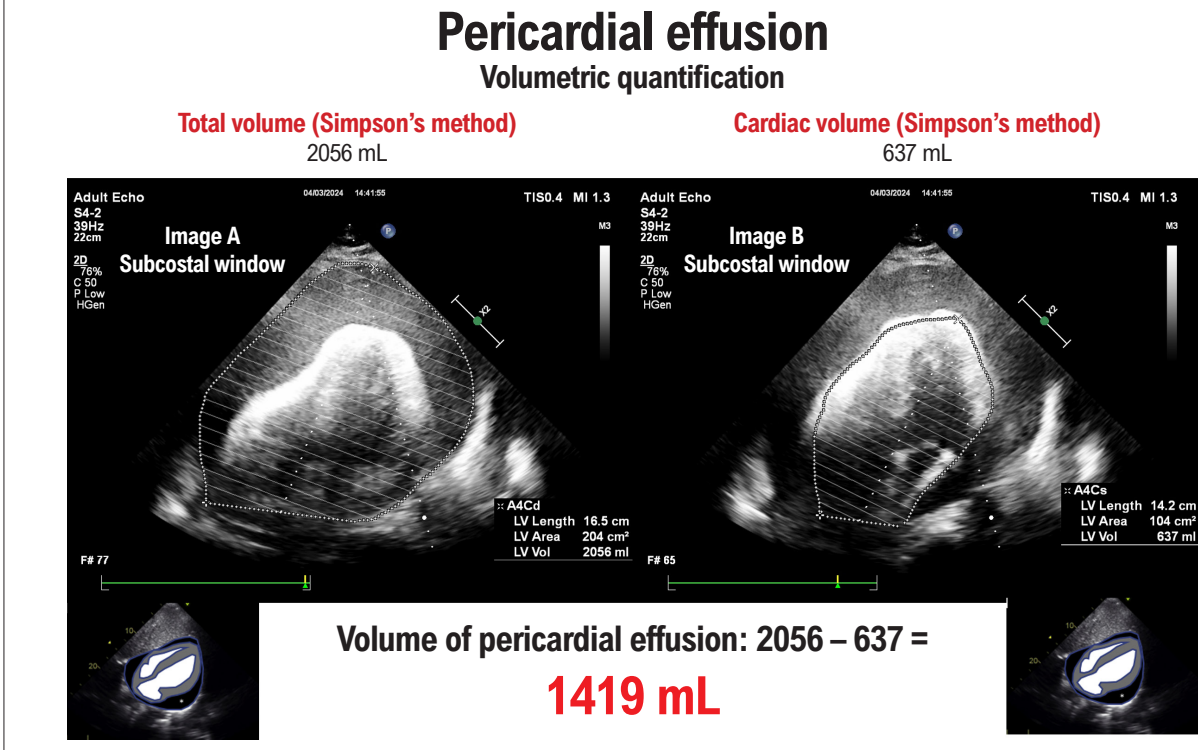

Figure 6 – *Volumetric quantification using Simpson's method. Initially, the pericardium is measured in its outermost component, encompassing all the fluid present, as shown in Image A. In Image B, the cardiac volume is measured during the phase of the cycle in which it presents its largest dimensions and volumes. To obtain the pericardial fluid volume, the simple difference between these two measurements is calculated.*

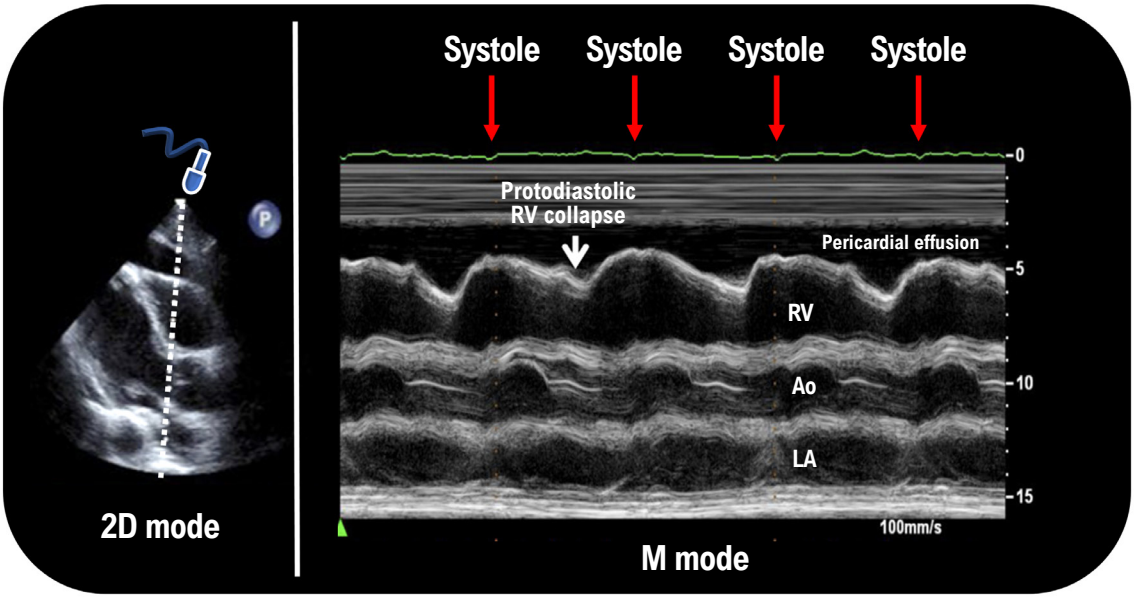

Figure 7 – *Diastolic collapse of the right ventricular free wall assessed by M mode, with easy identification of the systolic and diastolic components. In this case, the one-dimensional slice passing through the aortic valve helped to correlate each period with the electrocardiogram, which showed low voltage due to significant pericardial effusion. Ao: aorta; LA: left atrium; RV: right ventricle.*

is not possible to adequately assess the IVC, the presence of plethora can be inferred based on dilation of the hepatic veins.

Hepatic vein flow is also altered in effusion with repercussions. Normal hepatic venous flow is biphasic, with systolic velocity greater than diastolic velocity (generally around 50 cm/s), and interrupted (or with reverse reflux) during atrial systole. Flows tend to increase during inspiration. When hemodynamic repercussions occur, velocities initially reduce to 20 to 40 cm/s, with diastolic flow progressively decreasing until it appears only during inspiration.[2] When systolic flow occurs only during inspiration, cardiac arrest is imminent. This finding, when associated with cardiac chamber analysis, has high positive and negative predictive value for clinical tamponade (82% and 88%, respectively),[6] as illustrated in Figure 8.

Dynamic anatomical assessment of right heart chambers

With increased pericardial pressure, collapse or indentation of the RA and RV (the heart chambers that are most sensitive to external pressure) reflects the extent to which effusion impacts right chamber filling. This analysis is particularly useful in low-pressure tamponade, a context in which there is no significant IVC plethora.

RA indentation/collapse occurs at the peak of the R wave (atrial diastole). When it lasts for more than one third of the cardiac cycle, it has high sensitivity and specificity for clinical tamponade.[7]

Similarly, RV indentation/collapse occurs after the T wave (ventricular diastole), and its presence indicates that pericardial pressure already exceeds RV pressure. Initially, it occurs only during inspiration, persisting throughout the respiratory cycle as effusion develops. The longer the duration, the greater the repercussion,[8] as illustrated in Figure 9.

Absence of collapse in any chamber has > 90% negative predictive value for effusion with repercussions.[6] On the other hand, the absence of RV collapse can occur in clinical contexts of high RV pressures (RV hypertrophy, severe pulmonary hypertension, or coexisting LV dysfunction).[9,10]

There is a clinical context that deserves even more careful evaluation, namely, when hypovolemia coexists. In these cases, collapse of the right heart chambers and, more rarely, the left chambers occurs earlier due to reduced pressure in the heart chambers. In this scenario, volume expansion and early reassessment of the echocardiographic findings presented are very useful and help guide clinical management, often avoiding surgical intervention.

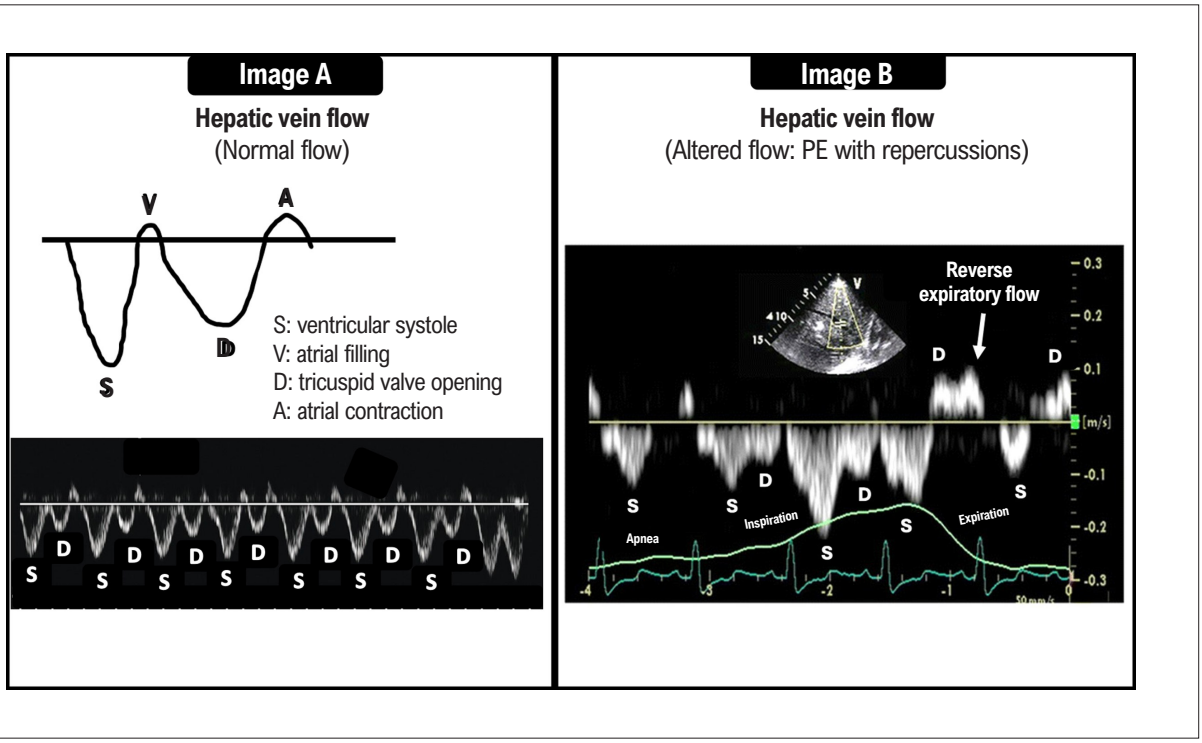

Figure 8 – *Pulsed-wave Doppler of hepatic venous flow velocity in a normal patient (Image A) and in cardiac tamponade (Image B). Velocities below the zero baseline demonstrate flow towards the heart, and those above the baseline represent reverse flow. Reduced anterograde flow reflects decreased venous return. In Image B, during apnea, anterograde flow is only seen during ventricular systole (S). With inspiration, systolic flow predominates, but diastolic flow (D) also exists. In the first flow analysis after expiration, a reversal of diastolic flow (white arrow) occurs, which indirectly equates to exacerbation of ventricular interdependence. PE: pericardial effusion.*

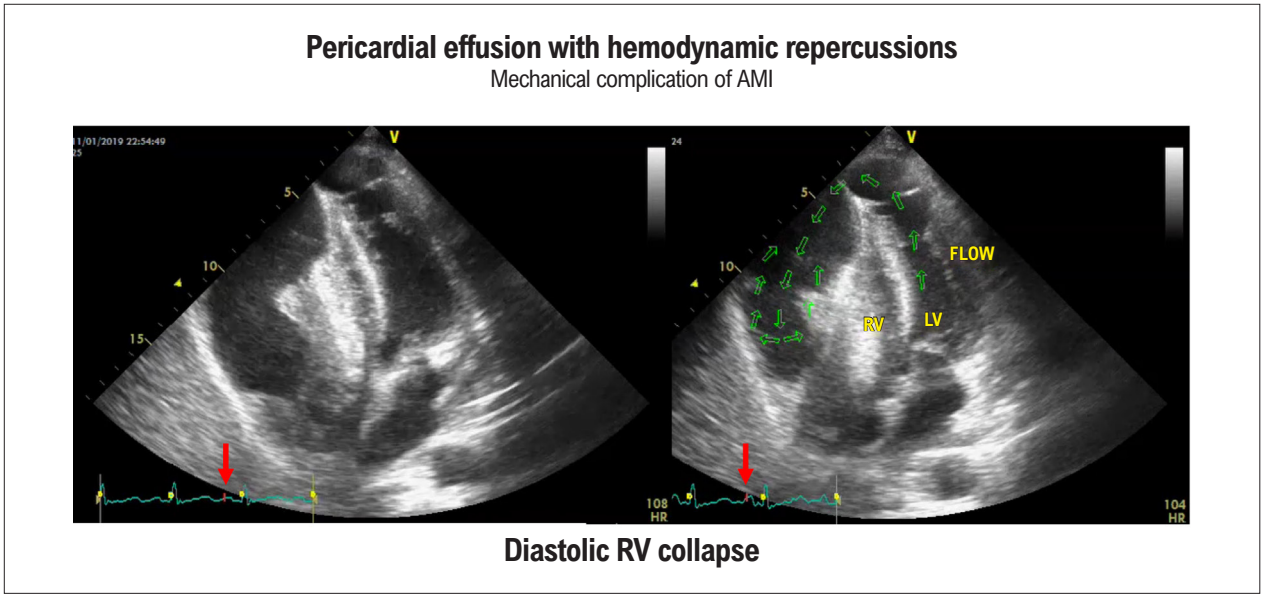

Figure 9 – *Systolic and diastolic collapse of the right ventricle secondary to free wall rupture, a rare mechanical complication associated with extensive anterior wall infarction. AMI: acute myocardial infarction; LV: left ventricle; RV: right ventricle.*

Hemodynamic assessment: Doppler

In the assessment of transvalvular flows, an increase in the variation of mitral and tricuspid E wave velocities is observed, which is related to exacerbation of ventricular interdependence. The following formula is used to calculate:

$$\text{Transvalvular flow variation} = \frac{(\text{expiration} - \text{inspiration})}{\text{expiration}}$$

Transmitral flow during inspiration tends to decrease, whereas tricuspid flow tends to increase during inspiration. Since both are calculated in the same way, the calculation of the variation through the tricuspid valve should result in a negative value. Values above 30% for the mitral valve and 60% for the tricuspid valve are indicative of hemodynamic repercussions[11] (Figures 10 and 11). When analyzing these variations, care should be taken to reduce the spectral Doppler scan rate, which will help to more accurately identify the variations according to the respiratory cycle and, ideally, analyze them together with the respirometer graph.

Even though it is a useful tool, flow assessment should not be applied in the absence of IVC plethora or collapse of any cardiac chamber, as increased variation can also occur in other clinical contexts (atrial fibrillation, mechanical ventilation).

As with the mitral and tricuspid valves, flow variations occur through the LV outflow tract, and it is possible to document the phenomenon that we clinically recognize as paradoxical pulse on echocardiography. Although useful, it occurs in very late stages, guiding immediate intervention to avoid possible circulatory collapse.

Figure 12 summarizes the main echocardiographic parameters that guide identification of possible hemodynamic repercussions.

Precautions when reporting pericardial effusion

When reporting findings of PE, it is important to characterize the effusion in terms of appearance, location, size, and signs of hemodynamic repercussion. This characterization is essential, as it allows for comparison over time and identification of hemodynamic repercussions, assisting the care team in decision-making, given that not every case of effusion with echocardiographic signs of hemodynamic repercussions will imply immediate clinical impact. The term "tamponade" should be avoided, because it is, by definition, a clinical diagnosis.

The following provides a suggested description of PE (hypothetical case):

"...Presence of diffuse pericardial effusion, important degree, with a maximum diameter of 27 mm adjacent to the right chambers. Diastolic collapse of the right atrium observed during more than one third of the cardiac cycle, and increased variation of transmitral E wave velocity of 50% identified.

Taken together, these findings are compatible with important pericardial effusion with echocardiographic signs of hemodynamic repercussions."

Conclusion

Assessment of PE and its repercussions is routine, especially in critically ill patients. Characterizing the size, identifying IVC plethora, and analyzing hemodynamic implications, whether by observing chamber collapse or increased variation in transvalvular flows, always considering the limitations of each parameter, require attention, and the findings should be considered together. Thus, because it provides rapid information and can be performed at the bedside, echocardiography is an excellent

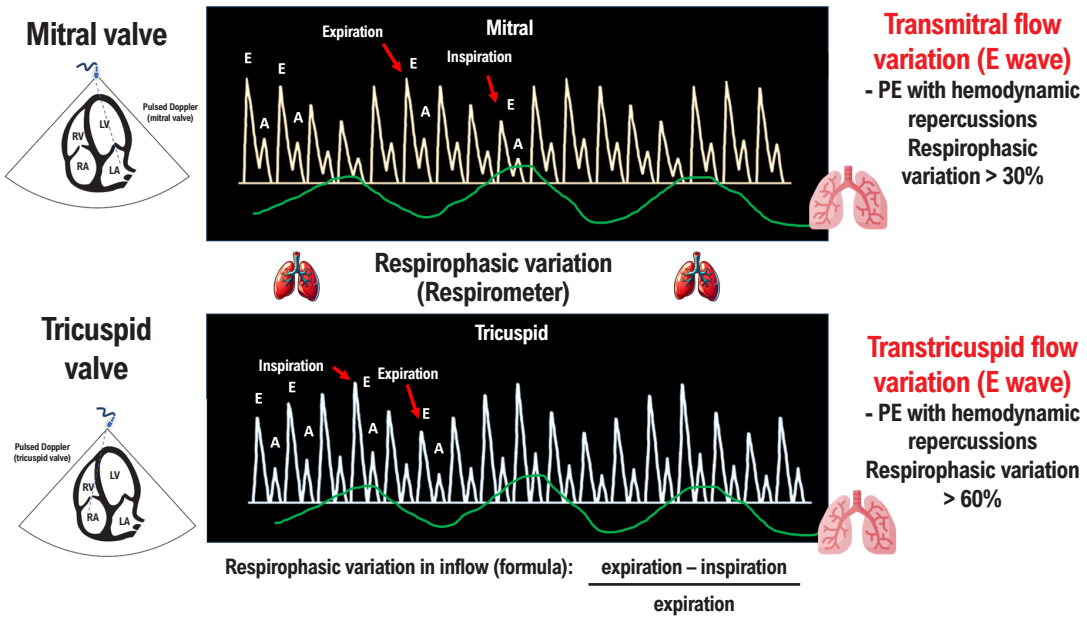

Figure 10 – *Echocardiographic formula and parameters for the correct calculation of transvalvular mitral and tricuspid respiratory variation. As demonstrated in the figure, whenever possible and available, it is of fundamental importance to use a respirometer, with correct identification of respiratory phases associated with the parameter of flow variation. If a respirometer is not available, it is considered that the highest velocity of the E wave through the mitral valve occurs during the expiratory phase, whereas, in the tricuspid valve, it occurs during the inspiratory phase. LA: left atrium; LV: left ventricle; PE: pericardial effusion; RA: right atrium; RV: right ventricle.*

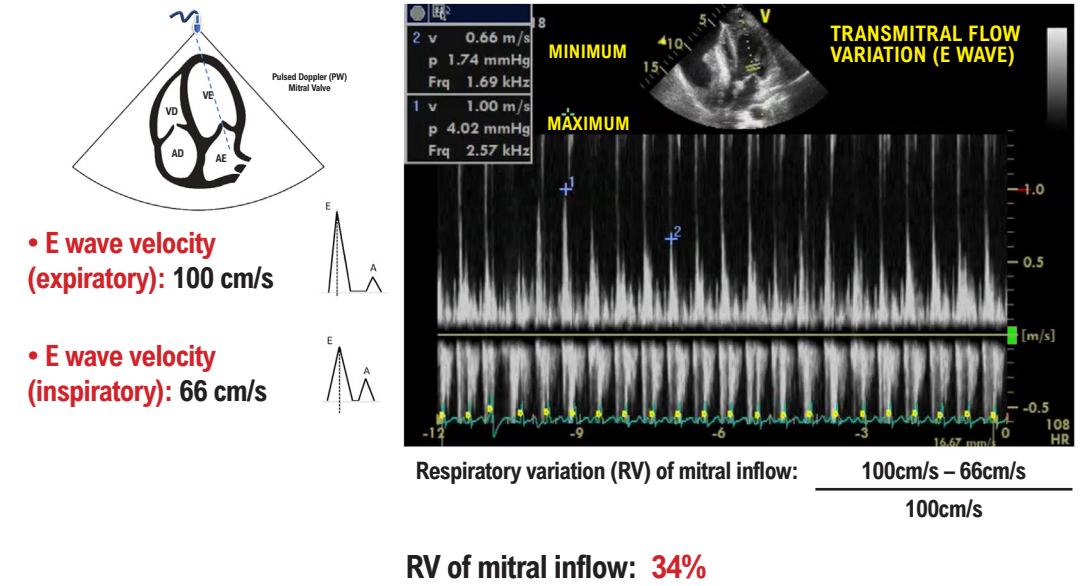

Figure 11 – *Respiratory variation above the normal value observed using transvalvular mitral flow in a patient with tamponade secondary to left ventricular free wall rupture. LA: left atrium; LV: left ventricle; RA: right atrium; RV: right ventricle.*

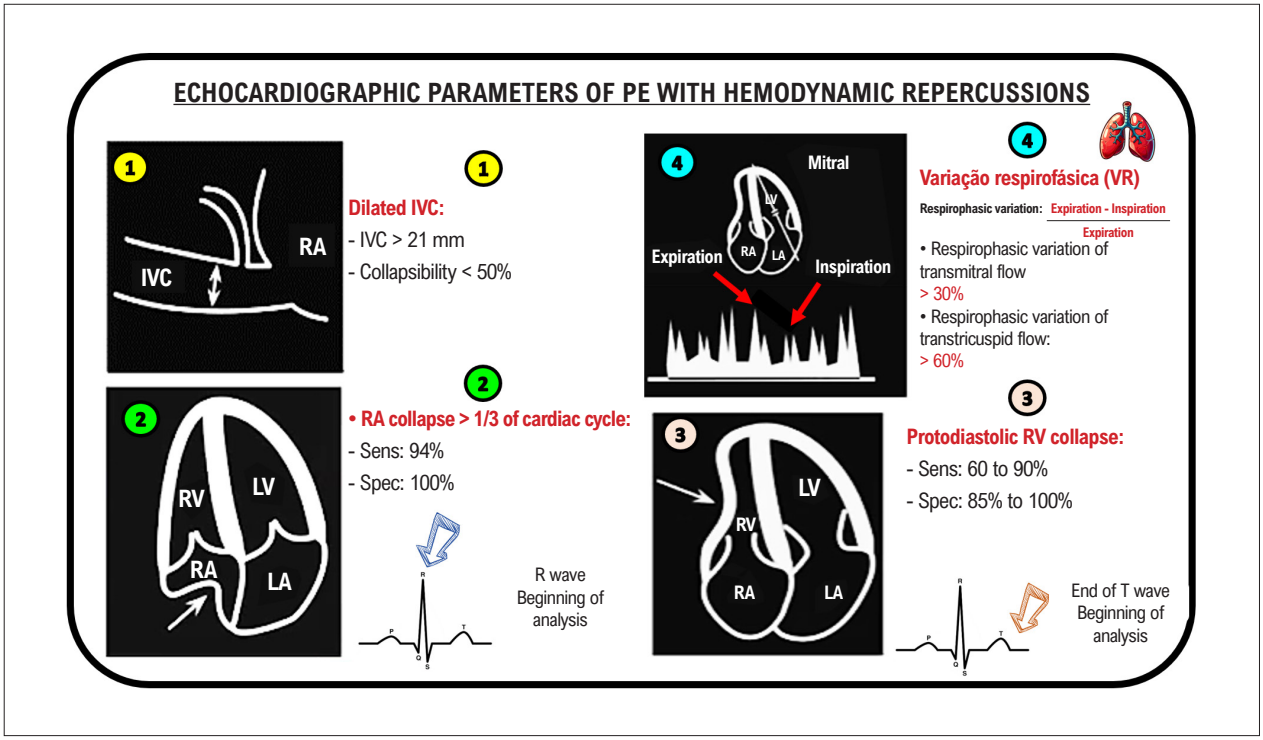

Figure 12 – *Main echocardiographic parameters in the assessment of pericardial effusion with hemodynamic repercussions. IVC: inferior vena cava; LA: left atrium; LV: left ventricle; PE: pericardial effusion; RA: right atrium; RV: right ventricle; Sens: sensitivity; Spec: specificity.*

method for characterizing and assessing the repercussions of PE, making it of fundamental importance to support decision-making by the care team.

Author Contributions

Conception and design of the research and writing of the manuscript: Gomes HM, Silva HAGP.

Potential Conflict of Interest

No potential conflict of interest relevant to this article was reported.

Sources of Funding

There were no external funding sources for this study.

Study Association

This study is not associated with any thesis or dissertation work.

Ethics Approval and Consent to Participate

This article does not contain any studies with human participants or animals performed by any of the authors.

Use of Artificial Intelligence

The authors did not use any artificial intelligence tools in the development of this work.

Availability of Research Data

The underlying content of the research text is contained within the manuscript.

References

1. Adler Y, Charron P, Imazio M, Badano L, Barón-Esquivias G, Bogaert J, et al. 2015 ESC Guidelines for the Diagnosis and Management of Pericardial Diseases: The Task Force for the Diagnosis and Management of Pericardial Diseases of the European Society of Cardiology (ESC)Endorsed by: The European Association for Cardio-Thoracic Surgery (EACTS). Eur Heart J. 2015;36(42):2921-64. doi: 10.1093/eurheartj/ehv318.
2. Klein AL, Abbara S, Agler DA, Appleton CP, Asher CR, Hoit B, et al. American Society of Echocardiography Clinical Recommendations for Multimodality Cardiovascular Imaging of Patients with Pericardial Disease: Endorsed by the Society for Cardiovascular Magnetic Resonance and Society of Cardiovascular Computed Tomography. J Am Soc Echocardiogr. 2013;26(9):965-1012.e15. doi: 10.1016/j.echo.2013.06.023.
3. Settle HP, Adolph RJ, Fowler NO, Engel P, Agruss NS, Levenson NI. Echocardiographic Study of Cardiac Tamponade. Circulation. 1977;56(6):951-9. doi: 10.1161/01.cir.56.6.951.

4. DeMaria DM, Waring AA, Gregg DE, Litwin SE. Echocardiographic Assessment of Pericardial Effusion Size: Time for a Quantitative Approach. J Am Soc Echocardiogr. 2019;32(12):1615-7.e1. doi: 10.1016/j.echo.2019.08.019.

5. Himelman RB, Kircher B, Rockey DC, Schiller NB. Inferior Vena Cava Plethora with Blunted Respiratory Response: A Sensitive Echocardiographic Sign of Cardiac Tamponade. J Am Coll Cardiol. 1988;12(6):1470-7. doi: 10.1016/s0735-1097(88)80011-1.

6. Mercé J, Sagristà-Sauleda J, Permanyer-Miralda G, Evangelista A, Soler-Soler J. Correlation between Clinical and Doppler Echocardiographic Findings in Patients with Moderate and Large Pericardial Effusion: Implications for the Diagnosis of Cardiac Tamponade. Am Heart J. 1999;138(4 Pt 1):759-64. doi: 10.1016/s0002-8703(99)70193-6.

7. Gillam LD, Guyer DE, Gibson TC, King ME, Marshall JE, Weyman AE. Hydrodynamic Compression of the Right Atrium: A New Echocardiographic Sign of Cardiac Tamponade. Circulation. 1983;68(2):294-301. doi: 10.1161/01.cir.68.2.294.

8. Leimgruber PP, Klopfenstein HS, Wann LS, Brooks HL. The Hemodynamic Derangement Associated with Right Ventricular Diastolic Collapse in Cardiac Tamponade: An Experimental Echocardiographic Study. Circulation. 1983;68(3):612-20. doi: 10.1161/01.cir.68.3.612.

9. Hoit BD, Gabel M, Fowler NO. Cardiac Tamponade in Left Ventricular Dysfunction. Circulation. 1990;82(4):1370-6. doi: 10.1161/01.cir.82.4.1370.

10. Hoit BD, Fowler NO. Influence of Acute Right Ventricular Dysfunction on Cardiac Tamponade. J Am Coll Cardiol. 1991;18(7):1787-93. doi: 10.1016/0735-1097(91)90522-b.

11. Appleton CP, Hatle LK, Popp RL. Cardiac Tamponade and Pericardial Effusion: Respiratory Variation in Transvalvular Flow Velocities Studied by Doppler Echocardiography. J Am Coll Cardiol. 1988;11(5):1020-30. doi: 10.1016/s0735-1097(98)90060-2.

Review Article

My Approach to Coronary Flow Assessment With Transthoracic Echocardiography

José Maria Del Castillo,[1] *Issam Shehadeh*[1,2]
Escola de Ecografia de Pernambuco,[1] *Recife, PE – Brazil*
Cardiovision,[2] *Esteio, RS – Brazil*

Abstract

The assessment of coronary flow reserve is an extremely important step in stress echocardiography, both within and outside the context of coronary artery disease. For some, it is seen as an impossible parameter; for others, it is essential. In any case, everything begins with the proper visualization of the coronary arteries at rest. In this article, we will address theoretical and practical concepts for incorporating coronary flow study into the routine of the echocardiographer.

Introduction

The study of coronary flow by echocardiography is still considered, by many authors, a utopia. Practically speaking, we learn that coronary assessment is limited to the visualization of their ostia, often only through transesophageal study. However, identification of the flow in the Left Anterior Descending artery (LAD) at rest, in the mid-distal third, is possible in more than 90% of patients.[1] The incorporation of Coronary Flow Reserve (CFR) assessment into stress echocardiography adds important diagnostic and prognostic information.[2] Furthermore, coronary flow patterns, even at rest, can be very useful in diagnosing not only Coronary Artery Disease (CAD) but also other diseases.

Pathophysiology of Coronary Flow

Coronary flow is biphasic, due to changes in resistance that the myocardial vascular system undergoes during the cardiac cycle. Coronary flow (Q) is regulated by the relationship between perfusion pressure (P) and the resistance offered by extramural arteries (R1), intramural arterioles R2), and compression of subendocardial arterioles caused by ventricular contraction on the blood inside the left ventricle. Since these resistances are lower during diastole, coronary flow is predominantly diastolic in the left coronary artery and more balanced in the right coronary artery, where subendocardial compression is less (Central Illustration).

Keywords

Coronary Artery Disease; Doppler Ultrasonography; Ecocardiografia sob Estresse.

Mailling Address: Issam Shehadeh •
ECOPE. Rua Solidônio Leite, 200. Postal code: 51111-130. Recife, PE – Brazil
E-mail: issam05@gmail.com
Manuscript received January 30, 2026; revised February 9, 2026; accepted February 9, 2026
Editor responsible for the review: Marcelo Tavares

DOI: https://doi.org/10.36660/abcimg.20260006i

Thus, two components of coronary flow can be distinguished: capacitance flow, which depends on the ventricular wall decompression of the left ventricle and the dilation of intramural arterioles (vascular tone), and conductance flow, which depends on the resistance to blood passage through the arteriolar-capillary system (vascular resistance). The more compliant the vascular bed, the greater the acceleration of conductance flow; and the lower the resistance to flow passage, the faster the deceleration of the conductance component (Figure 1).

Coronary flow supplies oxygen to the myocardium according to demand. When oxygen demand increases – for example, during exercise – the coronary arteries increase flow through vasodilation, which leads to increased velocity, especially in epicardial and intramural arteries. The difference in velocity between the resting state and hyperemia (caused by the increased oxygen supply to the myocardium) allows estimation of the so-called CFR. The methods used to measure it, either through hemodynamic study or by obtaining coronary flow via ultrasound, are physical exercise or pharmacologically induced vasodilation (dipyridamole, adenosine, papaverine).

Absence of a specific preset

Undoubtedly, the main limitation for the study of coronary flow is the absence of a specific preset. Some equipment already provides it by default. However, additional adjustments are often required. Since the coronary artery in the mid-distal third is a very subtle structure and the flow is of low velocity, in general, the following adjustments should be made to color and pulsed Doppler:

Color Doppler	Pulsed Doppler
Frequency in the range of 2.5 to 2.9 MHz	Frequency in the range of 2.5 to 2.9 MHz
PRF around 20 cm/s	Velocity scale around 50 cm/s
High gain	Reduced low-velocity filter
High persistence	Sample volume between 2 to 4 mm
High low-velocity filter	Low PRF deactivated
High frame rate	Side-by-side" layout
Sample volume about 1 mm	
Low tissue prioritization	

Central Illustration: My Approach to Coronary Flow Assessment With Transthoracic Echocardiography

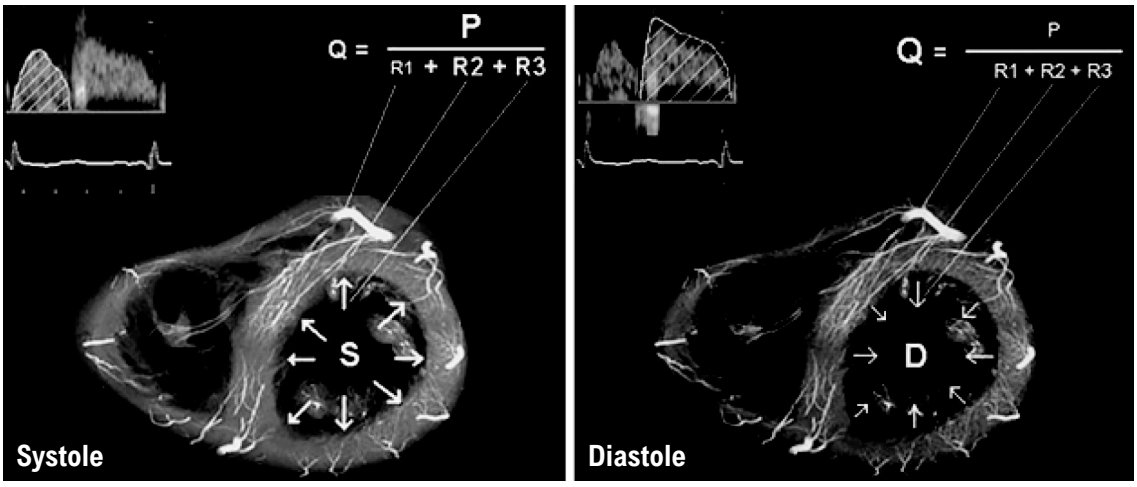

Arq Bras Cardiol: Imagem cardiovasc. 2026;39(1):e20260006

Coronary flow (Q) is regulated by the relationship between perfusion pressure (P) and the resistance offered by the extramural arteries (R1), intramural arterioles (R2), and the compression exerted on the subendocardial arterioles caused by ventricular contraction on the blood inside the LV (R3). Since these resistances are lower during diastole, coronary flow is predominantly diastolic for the left coronary artery and balanced for the right coronary artery, where subendocardial compression is less pronounced

Although there are variations in these parameters among different devices, this is generally the conceptual approach. It is not mandatory to use a pediatric transducer, since current adult transducers operate across a wide frequency range. If available, the use of a higher-frequency transducer may facilitate coronary visualization.

Technique

Left Anterior Descending artery in the mid-distal third

The key point for visualizing the LAD is to identify the anterior interventricular groove. For this purpose, two approaches can be used:

1. Modified short-axis view

Starting from the parasternal short-axis view, approximately at the level of the papillary muscles, one should attempt to visualize the anterior interventricular groove, at the transition between the RV and LV, in the subepicardial region of the junction between the anteroseptal and anterior walls, where the mid portion of the LAD passes. Once the flow – predominantly diastolic —has been detected, the transducer can be slowly rotated clockwise to better align the ultrasound beam with the anterior interventricular groove, thereby allowing detection of larger segments of the artery.

2. Modified parasternal long-axis view

From the traditional parasternal long-axis view, the transducer is slid one or two intercostal spaces lower. Next, the ultrasound beam is angled anteriorly, pointing the transducer toward the patient's left shoulder. This maneuver is crucial to remove part of the right ventricle from the image and expose the interventricular groove. If any portion of the right ventricle remains visible in this view, the transducer should be rotated clockwise until this chamber disappears. The resulting image will be a transitional view between the parasternal long-axis and the short-axis. The interventricular groove will then be exposed. Its location is quite superficial in the patient's chest, which increases the success rate for visualizing the LAD compared with other coronary arteries.

After this step, color Doppler should be activated. The LAD is visualized as a small tubular, pulsatile structure, with upward flow (red) and predominantly diastolic. If a circular structure with the same characteristics is identified, the transducer should be subtly rotated clockwise to open the vessel longitudinally (Video 1). It is extremely important, when studying coronary flow, to activate electrocardiographic monitoring.

It is often possible to perform a sweep of the LAD over a wide extension, both proximally and distally, which allows the study of flow at different points. It is not uncommon to find areas of aliasing on color Doppler, which may correspond to a stenotic segment.

On pulsed Doppler, a biphasic flow is identified, with a predominant diastolic component and a trapezoidal appearance. Diastolic velocity is usually approximately twice the systolic velocity. Some authors, instead of evaluating only velocities, study the Velocity–Time Integral (VTI). From a practical standpoint, velocity analysis appears much simpler and faster, especially when used during stress echocardiography.

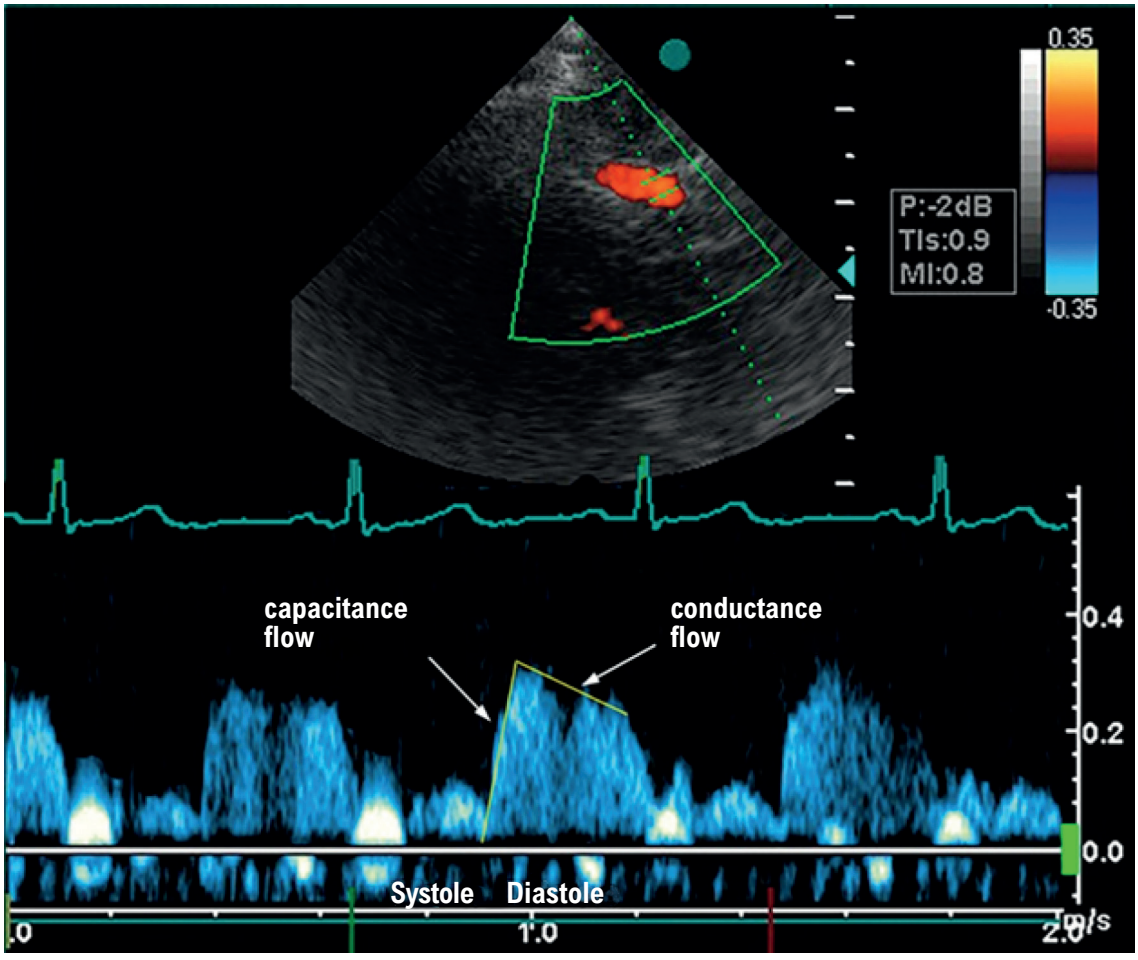

Figure 1 – *Transthoracic Doppler of coronary flow showing a normal systo-diastolic pattern.*

Posterior Descending Branch of the Right Coronary Artery

The success rate for visualizing the Posterior Descending branch (PD) is between 60% and 70%.[3] The view used is the modified apical two-chamber. From this plane, the transducer is rotated slightly counterclockwise and the ultrasound beam is directed posteriorly. This produces a transitional view between the two-chamber and three-chamber planes. Along the inferior wall, one should look for a pulsatile, diastolic, upward (red) flow. This flow can be visualized both at the basal level and more apically along the inferior wall. Therefore, it is important to carefully scan the wall in search of this vessel (Video 2). The pulsed Doppler characteristics are similar to those of the LAD, as previously described.

Marginal Branch of the Circumflex Artery

Among the three coronary arteries, this is technically the most difficult to study, with feasibility below 60%.[4] The examination begins from the apical four-chamber view, rotating the transducer slightly clockwise to adequately expose the lateral wall. A practical tip is to keep the right ventricle widely open on the screen. Then, the ultrasound beam is directed posteriorly, as if studying the coronary sinus. The lateral wall should remain well exposed, even if the image appears out of plane (Video 3). It should be emphasized that these views are specific for studying the coronary arteries and not the left ventricle, which may initially seem unusual.

Color Doppler will demonstrate one or more small vessels in the lateral wall, pulsatile, upward (red), and diastolic. Again, it is important to highlight that the study should always be performed with electrocardiographic monitoring. The pulsed Doppler characteristics are similar to those of the other coronary arteries, as previously described.

Pitfalls

During coronary flow assessment, some structures may mimic the LAD. A vessel commonly found in a similar topographic location is the internal thoracic artery. However, its Doppler flow pattern is distinct: predominantly systolic and with higher velocity. Small pericardial effusions

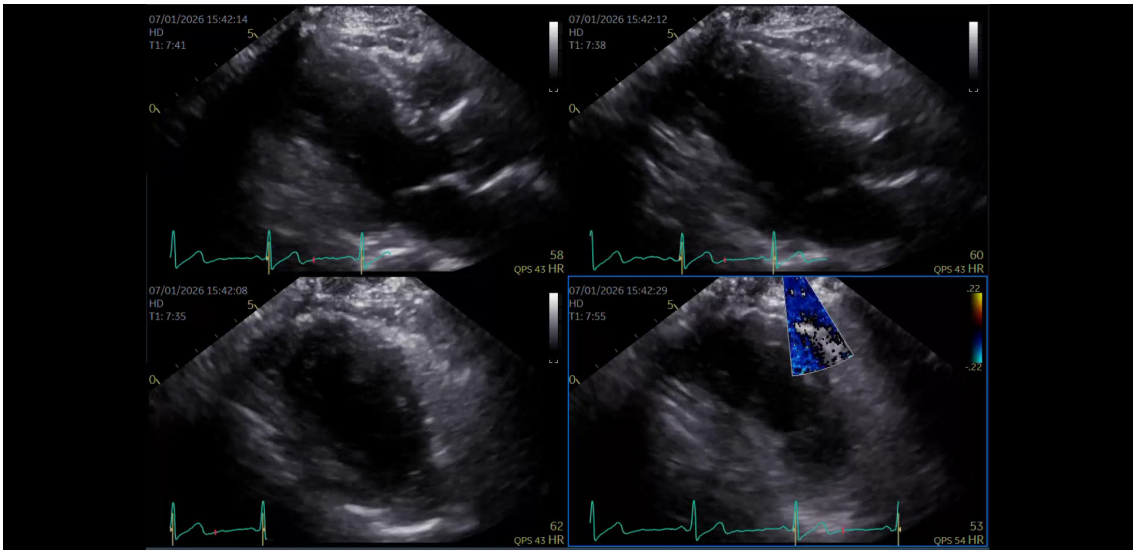

Video 1 – *Step-by-step visualization of the LAD. 1.Low parasternal view. 2. Direct the ultrasound beam toward the patient's left shoulder. 3. Clockwise rotation to remove the RV from the image and identify the interventricular sulcus. 4. Color Doppler demonstrating a small vessel with diastolic flow.*
Link: http://abcimaging.org/supplementary-material/2026/3901/2026-0006_video_01.mp4

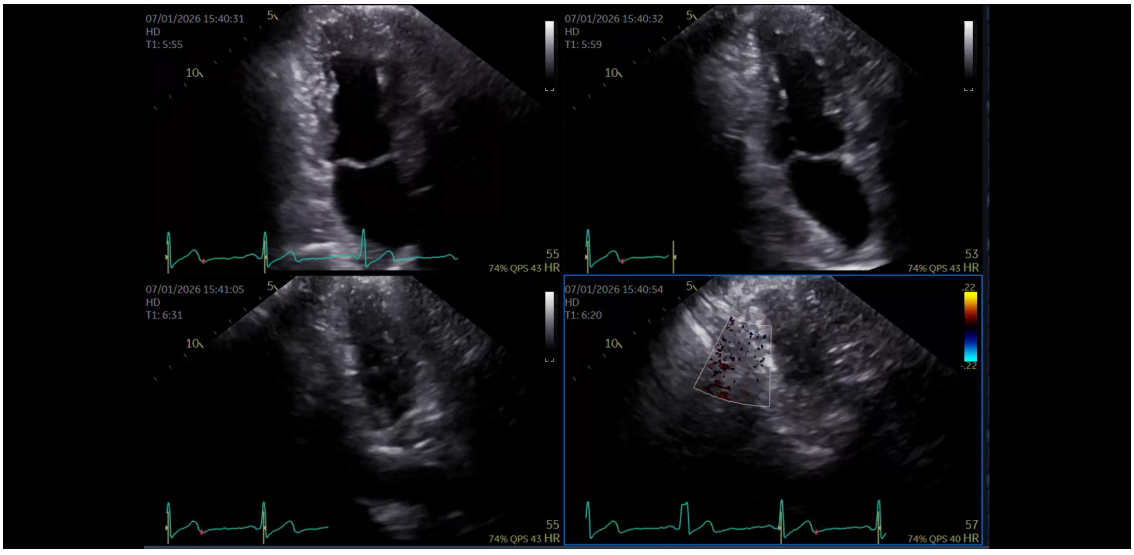

Video 2 – *Step-by-step visualization of the PDA. 1. Standard two-chamber view. 2. Intermediate view between the two- and three-chamber views. 3. Posteriorly direct the ultrasound beam. 4. Color Doppler demonstrating a small vessel with diastolic flow in the inferior wall.*
Link: http://abcimaging.org/supplementary-material/2026/3901/2026-0006_video_02.mp4

may present with a flow resembling that seen on color Doppler; however, pulsed Doppler does not reveal the predominant diastolic pattern. In certain situations, a blue (downward) flow may be identified in the interventricular groove, in contrast to the usual red flow. This may indicate LAD occlusion with retrograde flow or the presence of a septal branch of the LAD itself. The PD flow may be confused with the inflow tract of the right ventricle. Nevertheless, the pulsed Doppler pattern is quite different from the characteristic coronary flow.

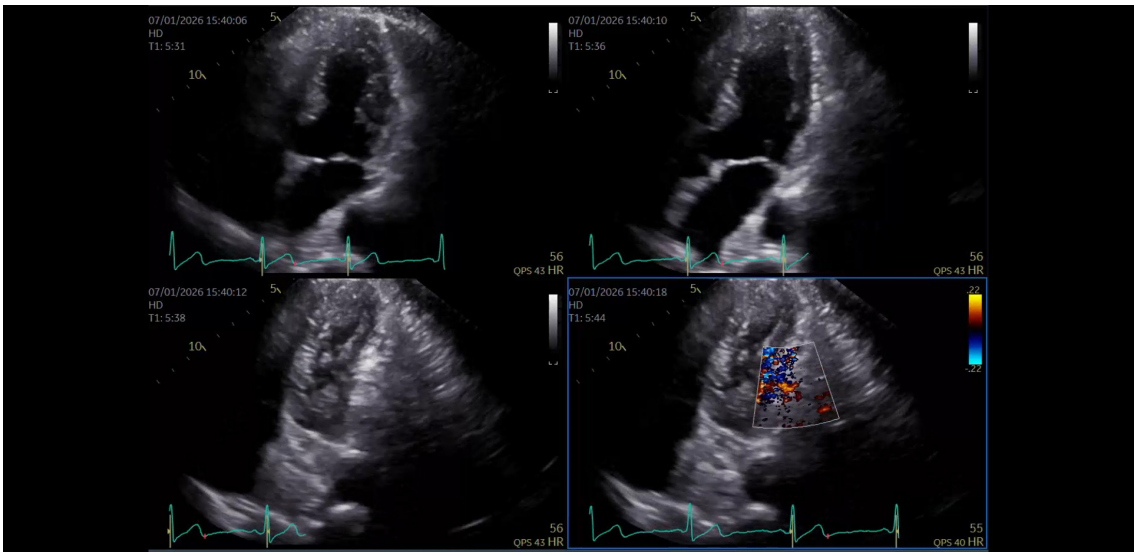

Video 3 – *Step-by-step visualization of the Mg. 1. Standard four-chamber view. 2. Counterclockwise rotation to "open" the RV. 3. Posteriorly direct the ultrasound beam. 4. Color Doppler demonstrating small vessels with diastolic flow in the lateral wall. Link: http://abcimaging.org/supplementary-material/2026/3901/2026-0006_video_03.mp4*

Clinical Applications

Rest

In general, the diastolic velocity of coronary flow is below 40 cm/s. Obviously, this velocity is influenced by several factors. Hyperkinesia, tachycardia, hypertension, and anemia, for example, may increase it even in the absence of stenosis. The systolic component usually does not exceed 60% of the diastolic velocity.

According to a recent study by Cortigiani et al.,[5] in patients with chronic coronary syndromes and preserved left ventricular ejection fraction, a resting coronary flow velocity in the LAD equal to or greater than 32 cm/s was independently associated with worse survival.[5] The combination of this resting velocity with a reduced CFR represented the scenario with the poorest prognosis.

In coronary artery disease, the simple identification of a patent distal LAD flow in a patient with wall motion abnormalities in the same territory adds important clinical information. It is not uncommon to directly visualize points of turbulent, high-velocity flow on Doppler. Some authors suggest a cutoff above 80 cm/s, while others propose above 1 m/s, for the detection of significant obstruction.[6,7]

The identification of a "velocity jump" is an interesting parameter that raises the possibility of significant LAD stenosis. This occurs when the diastolic velocity doubles in different regions of the vessel under study (for example, proximal vs. distal). In addition, an increase in the systolic component of coronary flow velocity is another relevant finding. A diastolic-to-systolic velocity ratio below 1.5 shows a sensitivity of 81.8% and a specificity of 85.7% for the diagnosis of coronary stenosis[7] (Video 4).

The coronary flow pattern with rapid diastolic deceleration, often accompanied by reversed systolic flow, is a strong indicator of the no-reflow phenomenon in patients with acute coronary syndrome undergoing percutaneous coronary intervention. Its pathophysiology lies in damage to the coronary microcirculation, such as endothelial injury and distal embolization, which prevent adequate filling of the vascular bed, increase distal pressure, and accelerate flow deceleration. Studies have shown that the deceleration timeis significantly shorter in these patients (152 ± 109 ms) compared with those without the phenomenon (395 ± 128 ms), indicating severe impairment of myocardial perfusion.[8]

Similarly, in patients with hypertrophic cardiomyopathy, coronary Doppler also reveals an atypical flow pattern, characterized by reduction, absence, or inversion of systolic flow.[9] (Figure 2). This similarity to the pattern observed in no-reflow is attributed to the abnormal increase in intramyocardial pressure during systole, which results in compression of the small intramural vessels and elevation of coronary resistance. In addition, the detection of flow in the septal communicating arteries represents another relevant pattern, being a common finding and particularly prevalent in apical and mixed morphologies,[10] conferring significant auxiliary value in the differential diagnosis of conditions that may mimic apical hypertrophic cardiomyopathy (Video 5).

Coronary Flow Reserve

The incorporation of multiple parameters, in addition to wall motion assessment, transforms stress echocardiography into a powerful and highly versatile clinical tool.[11] Beyond enhancing its diagnostic power, it also provides relevant and non-redundant prognostic information.[12] Several publications have demonstrated the importance of CFR evaluation in different clinical scenarios,[13-15] and the European Society of Cardiology has recommended its routine use since the 2008 stress echocardiography guidelines.[16,17]

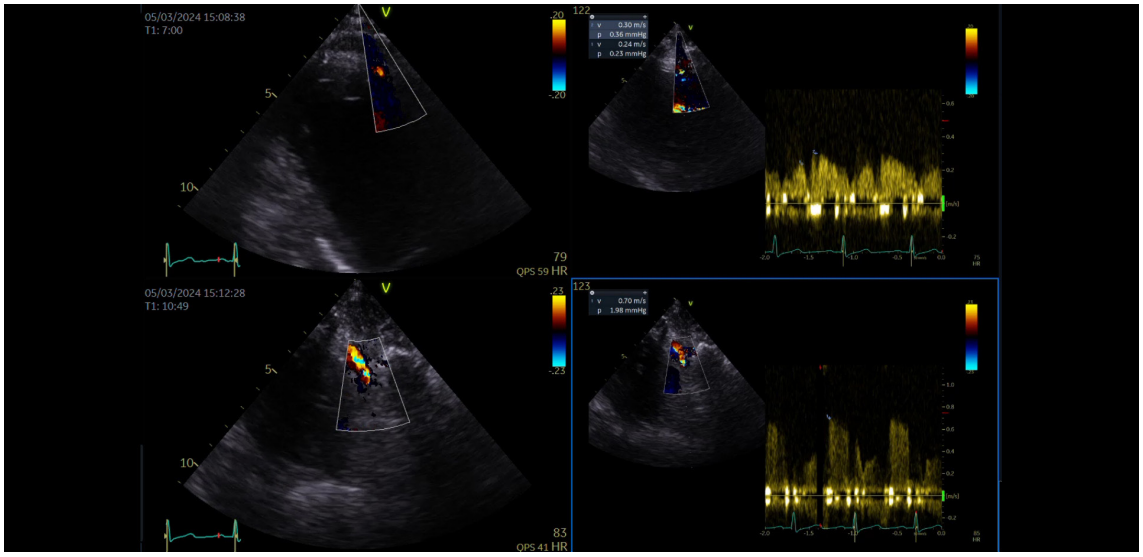

Video 4 – *Identification of pathological LAD flow at rest and velocity step-up. 1. Laminar flow in the mid-distal segment of the LAD. 2. PW Doppler recording showing a diastolic velocity of 30 cm/s and systolic velocity of 24 cm/s, with a ratio of 1.25 (suggestive of stenosis). 3. Turbulent LAD flow when scanning the vessel more proximally. 4. PW Doppler recording showing a velocity of 70 cm/s (2.3-fold increase). Coronary angiography revealed a significant lesion in the left main coronary artery and proximal LAD.*
Link: http://abcimaging.org/supplementary-material/2026/3901/2026-0006_video_04.mp4

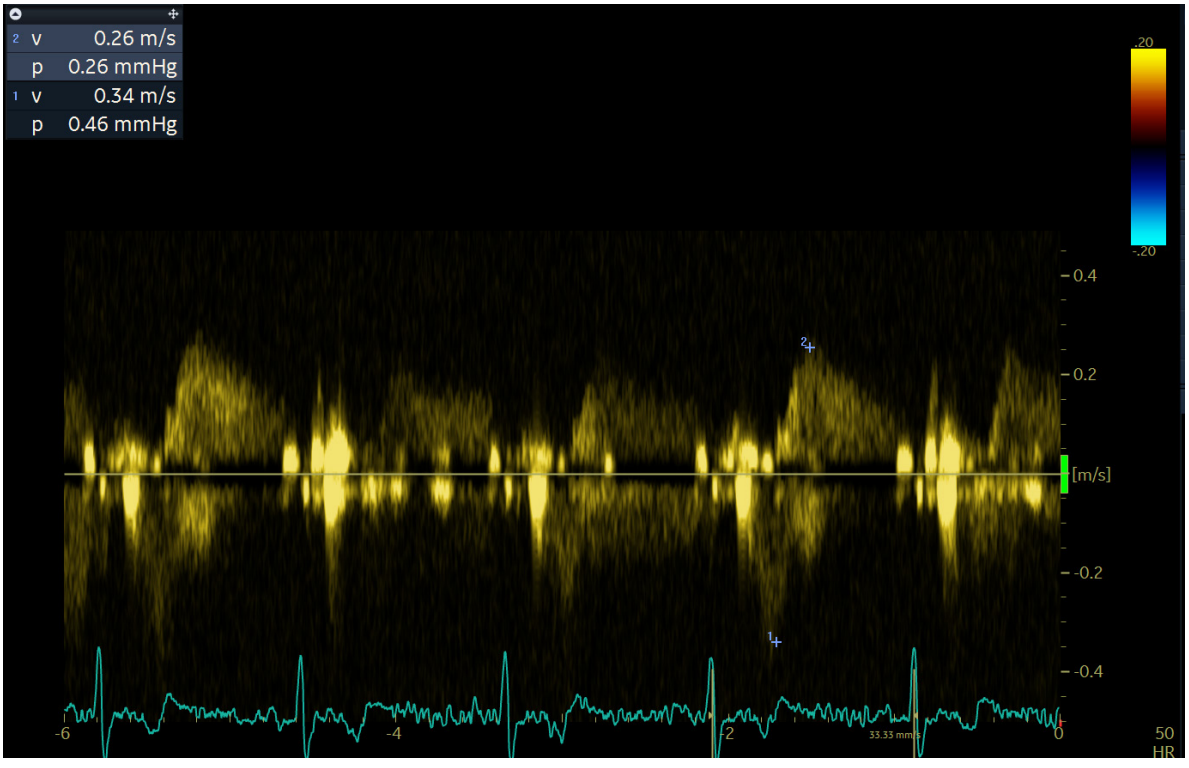

Figure 2 – *LAD flow in a patient with HCM. Inversion of the systolic component is observed*

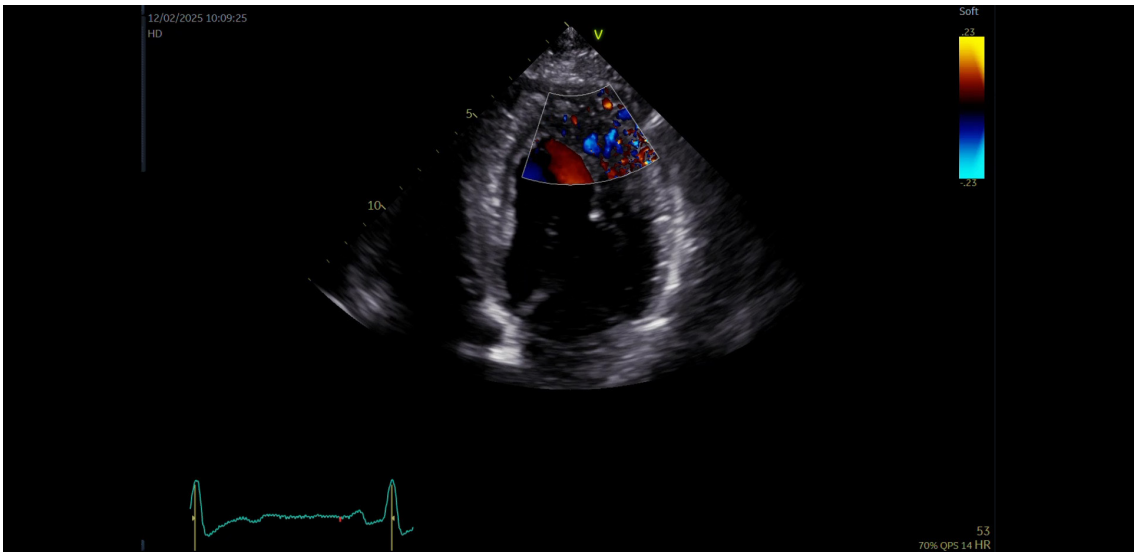

Video 5 – *Flow in apical communicating branches (blue) in a patient with apical hypertrophic cardiomyopathy. Link: http://abcimaging.org/supplementary-material/2026/3901/2026-0006_video_05.mp4*

The addition of coronary flow assessment to stress echocardiography, after adequate training, does not significantly increase the examination time. Its interpretation takes only a few seconds and is based on the ratio between coronary velocity during stress and at rest. The discriminatory value of 2.0 separates normal from pathological. All stress modalities allow CFR evaluation. The success rate is highest in studies with vasodilators (above 90%), followed by dobutamine (around 80%) and bicycle exercise (about 70%).[18]

Methodology with vasodilator

After acquiring all the baseline images, the diastolic velocity of the distal LAD is recorded as far as possible. Without removing the transducer from the patient's chest, and maintaining continuous visualization of the coronary artery at the same point and angle, dipyridamole is administered at a dose of 0.84 mg/kg over four minutes. The maximum velocity is then recorded up to one minute after the end of the infusion (fifth minute of the test). Under normal conditions, the LAD velocity doubles within a few minutes after the start of the test.

Methodology with dobutamine

Unlike the dipyridamole protocol, in which the LAD is continuously monitored, in the dobutamine test the LAD velocity is measured at rest and again after an increment of 50 beats compared with baseline heart rate and/or when 75% of the predicted maximum heart rate is reached, which usually occurs during the high-dose stages of the drug.[19]

zMethodology with supine bicycle exercise

The evaluation of CFR during exercise is more challenging. As workload increases, trunk movement and hyperventilation impair the acoustic window and make visualization of the LAD more difficult.

For less experienced operators, we recommend a strategy similar to the dipyridamole protocol: locate the LAD at rest with color Doppler and ensure its continuous visualization in the imaging sector from the beginning of the test. This approach favors velocity measurement always at the same point and with the same angulation. However, the main limitation of this strategy is the loss of two-dimensional recordings at low workload, which are particularly useful in studies performed with a cycle ergometer.

Another approach, technically more demanding, is to begin LAD monitoring during exercise immediately after acquiring two-dimensional images at low workload, ensuring that velocity is measured at the same point and with the same angulation used at rest (Video 6).

In healthy individuals, coronary velocity doubles already in the early stages of exercise (up to 75 watts). The same concepts applied in the dobutamine protocol regarding heart rate are used for CFR evaluation if this doubling does not occur promptly.

It is worth noting that, although CFR assessment in the LAD is the most commonly used, it can also be performed in the other coronary arteries; however, the success rate tends to be lower.

Conclusion

Coronary flow assessment by echocardiography is no longer a utopia and has already become a reality capable of transforming echocardiography laboratories. At rest or under stress, with vasodilators or during exercise, the possibilities are broad and the information obtained is highly relevant. It is possible to detect significant coronary obstructions at rest and anticipate stress-echo results even before ischemia appears.

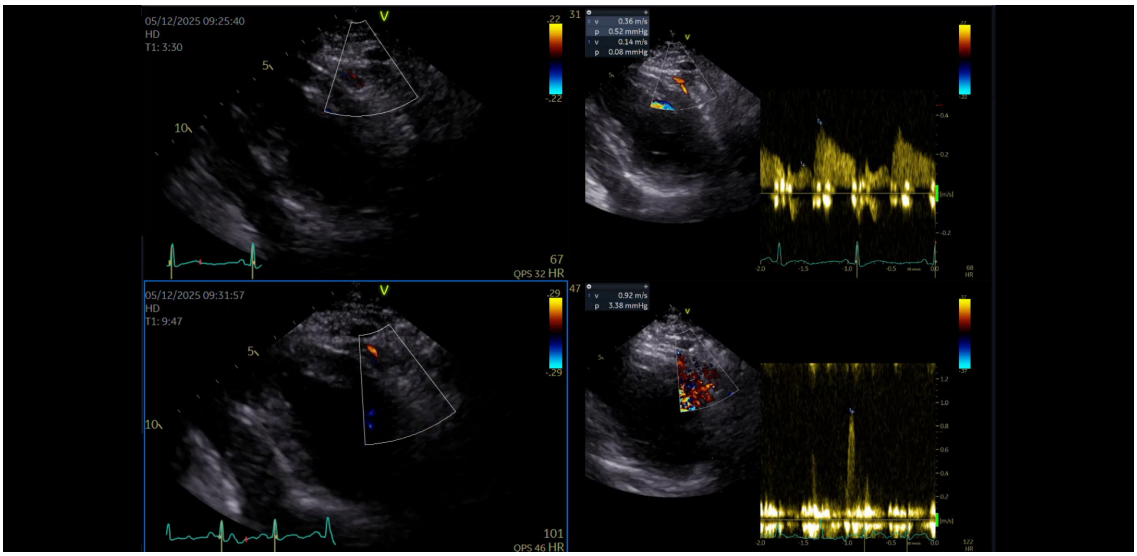

Video 6 – *LAD CFR during exercise. 1. Flow at rest. 2. Diastolic velocity of 36 cm/s. 3. Flow during exercise (75 W). 4. Diastolic velocity of 92 cm/s. CFR of 2.55 (normal > 2).*
Link: http://abcimaging.org/supplementary-material/2026/3901/2026-0006_video_06.mp4

Identifying higher risk in patients with normal segmental wall motion but reduced CFR has a direct clinical impact. Echocardiography, therefore, should not be regarded as a mere adjunct, but rather as the main player.

Author Contributions

Conception and design of the research, writing of the manuscript and critical revision of the manuscript for intellectual content: Del Castillo JM, Shehadeh I.

Potential Conflict of Interest

No potential conflict of interest relevant to this article was reported.

Sources of Funding

There were no external funding sources for this study.

Study Association

This study is not associated with any thesis or dissertation work.

Ethics Approval and Consent to Participate

This article does not contain any studies with human participants or animals performed by any of the authors.

Use of Artificial Intelligence

The authors did not use any artificial intelligence tools in the development of this work.

Availability of Research Data

The underlying content of the research text is contained within the manuscript.

References

1. Zagatina A, Zhuravskaya N, Caprnda M, Shiwani HA, Gazdikova K, Rodrigo L, et al. Should we Routinely Assess Coronary Artery Doppler in Daily Echocardiography Practice? Acta Cardiol. 2022;77(7):573-9. doi: 10.1080/00015385.2021.1973771.
2. Ciampi Q, Zagatina A, Cortigiani L, Gaibazzi N, Daros CB, Zhuravskaya N, et al. Functional, Anatomical, and Prognostic Correlates of Coronary Flow Velocity Reserve During Stress Echocardiography. J Am Coll Cardiol. 2019;74(18):2278-91. doi: 10.1016/j.jacc.2019.08.1046.
3. Rigo F, Murer B, Ossena G, Favaretto E. Transthoracic Echocardiographic Imaging of Coronary Arteries: Tips, Traps, and Pitfalls. Cardiovasc Ultrasound. 2008;6:7. doi: 10.1186/1476-7120-6-7.
4. Vegsundvåg J, Holte E, Wiseth R, Hegbom K, Hole T. Transthoracic Echocardiography for Imaging of the Different Coronary Artery Segments: A Feasibility Study. Cardiovasc Ultrasound. 2009;7:58. doi: 10.1186/1476-7120-7-58.
5. Cortigiani L, Gaibazzi N, Ciampi Q, Rigo F, Rodríguez-Zanella H, Wierzbowska-Drabik K, et al. High Resting Coronary Flow Velocity by Echocardiography Is Associated with Worse Survival in Patients with Chronic Coronary Syndromes. J Am Heart Assoc. 2024;13(4):e031270. doi: 10.1161/JAHA.123.031270.
6. Rigo F, Picano E. Coronary Flow Reserve. In: Picano E, editor. Stress Echocardiography. Cham: Springer; 2015. doi:10.1007/978-3-319-20958-6_9.

7. Lowenstein J. Padrões de Fluxo Coronariano Normal e Determinação da Reserva Coronariana pelo Ecodopplertranstorácico. In: Mathias W Jr, Tsutsui JM, editors. Ecocardiografia. Barueri: Manole; 2012, p. 109-29.

8. Youn HJ, Foster E. Demonstration of Coronary Artery Flow Using Transthoracic Doppler Echocardiography. J Am Soc Echocardiogr. 2004;17(2):178-85. doi: 10.1016/j.echo.2003.08.017.

9. Ferreiro DE, Cianciulli TF, Saccheri MC, Lax JA, Celano L, Beck MA, et al. Assessment of Coronary Flow with Transthoracic Color Doppler Echocardiography in Patients with Hypertrophic Cardiomyopathy. Echocardiography. 2013;30(10):1156-63. doi: 10.1111/echo.12242.

10. Sousa CG, Castillo JMD, Mazzarollo C, Albuquerque ES, Sena ADM, Brindeiro D Filho, et al. Comparative Analysis of the Coronary Arteries Flow Pattern in Secondary Myocardial Hypertrophies and by Sarcomeric Mutation. Arq Bras Cardiol: Imagem Cardiovasc. 2021;34(1):eabc131. doi: 10.47593/2675-312X/20213401eabc131.

11. Picano E, Ciampi Q, Wierzbowska-Drabik K, Urluescu ML, Morrone D, Carpeggiani C. The New Clinical Standard of Integrated Quadruple Stress Echocardiography with ABCD Protocol. Cardiovasc Ultrasound. 2018;16(1):22. doi: 10.1186/s12947-018-0141-z.

12. Ciampi Q, Zagatina A, Cortigiani L, Wierzbowska-Drabik K, Kasprzak JD, Haberka M, et al. Prognostic Value of Stress Echocardiography Assessed by the ABCDE Protocol. Eur Heart J. 2021;42(37):3869-78. doi: 10.1093/eurheartj/ehab493.

13. Lowenstein JA, Caniggia C, Rousse G, Amor M, Sánchez ME, Alasia D, et al. Coronary Flow Velocity Reserve during Pharmacologic Stress Echocardiography with Normal Contractility Adds Important Prognostic Value in Diabetic and Nondiabetic Patients. J Am Soc Echocardiogr. 2014;27(10):1113-9. doi: 10.1016/j.echo.2014.05.009.

14. Cortigiani L, Gaibazzi N, Ciampi Q, Tuttolomondo D, Navacchi R, Bovenzi F, et al. Prognostic Significance of Coronary Flow Velocity Reserve in Patients with Peripheral Arterial Disease. Int J Cardiovasc Imaging. 2025;41(7):1287-95. doi: 10.1007/s10554-025-03411-z.

15. Ciampi Q, Olivotto I, Gardini C, Mori F, Peteiro J, Monserrat L, et al. Prognostic Role of Stress Echocardiography in Hypertrophic Cardiomyopathy: The International Stress Echo Registry. Int J Cardiol. 2016;219:331-8. doi: 10.1016/j.ijcard.2016.06.044.

16. Sicari R, Nihoyannopoulos P, Evangelista A, Kasprzak J, Lancellotti P, Poldermans D, et al. Stress Echocardiography Expert Consensus Statement: European Association of Echocardiography (EAE) (A Registered Branch of the ESC). Eur J Echocardiogr. 2008;9(4):415-37. doi: 10.1093/ejechocard/jen175.

17. Picano E, Pierard L, Peteiro J, Djordjevic-Dikic A, Sade LE, Cortigiani L, et al. The Clinical Use of Stress Echocardiography in Chronic Coronary Syndromes and Beyond Coronary Artery Disease: A Clinical Consensus Statement from the European Association of Cardiovascular Imaging of the ESC. Eur Heart J Cardiovasc Imaging. 2024;25(2):e65-e90. doi: 10.1093/ehjci/jead250.

18. Rigo F, Picano E. Step D for Doppler-Based Coronary Flow Velocity Reserve in Stress Echocardiography. In: Picano E, editors. Stress Echocardiography. Cham: Springer; 2023. p. 55-77. doi: 10.1007/978-3-031-31062-1_4.

19. Forte EH, Rousse MG, Lowenstein JA. Target Heart Rate to Determine the Normal Value of Coronary Flow Reserve during Dobutamine Stress Echocardiography. Cardiovasc Ultrasound. 2011;9:10. doi: 10.1186/1476-7120-9-10.

Review Article

My Approach to VExUS Assessment Using Transesophageal Echocardiography: A Step-by-Step Performance Guide

Angelo Antunes Salgado,[1,2,3] *Marcos Paulo Lacerda Bernardo,*[1,4] *Marcelo Ramalho Fernandes*[4,5]

Universidade do Estado do Rio de Janeiro,[1] *Rio de Janeiro, RJ – Brazil*
Instituto Nacional de Cardiologia,[2] *Rio de Janeiro, RJ – Brazil*
Hospital Pró-Cardíaco,[3] *Rio de Janeiro, RJ – Brazil*
Hospital CopaStar,[4] *Rio de Janeiro, RJ – Brazil*
Hospital Copa D´Or,[5] *Rio de Janeiro, RJ – Brazil*

Abstract

Monitoring systemic venous congestion has become essential in the management of critically ill patients, enabling accurate diagnosis, severity grading, and prognostic stratification. Literature shows that congestion is strongly associated with the development of acute kidney injury and increased mortality when compared with optimized volume states.

In this setting, intraoperative Transesophageal Echocardiography (TEE) has emerged as an advanced and versatile tool. In addition to allowing detailed assessment of cardiac function, TEE is effective in assessing intravascular volume status and predicting fluid responsiveness through dynamic measurement of stroke volume and the degree of systemic congestion. TEE also enables direct visualization of abdominal vessels, such as the hepatic, portal, and intrarenal veins, thereby facilitating the identification of pathological pulsatile flow patterns even in patients with limited transthoracic acoustic windows.

The integration of protocols such as VExUS (or its modified version, mVExUS) allows for a personalized approach focused on "perfusion without congestion." This review outlines the practical application of VExUS assessment using TEE, its technical limitations, and how to use it to guide hemodynamic resuscitation, minimizing organ injury and optimizing clinical outcomes.

Introduction

For decades, perioperative and critical care hemodynamic monitoring has been centered almost exclusively on macrocirculatory parameters related to forward flow, such as mean arterial pressure, cardiac output, and stroke volume.

Keywords

Transesophageal Echocardiography; Prognosis; Operative Surgical Procedures.

Mailing Address: Angelo Antunes Salgado •
Universidade do Estado do Rio de Janeiro. Avenida 28 de Setembro, 77. Postal code: 20550-900. Rio de Janeiro, RJ – Brazil
E-mail: angeloasalgado@gmail.com
Manuscript received February 9, 2026, revised manuscript February 20, 2026, accepted February 21, 2026
Editor responsible for the review: Marcelo Tavares

DOI: https://doi.org/10.36660/abcimg.20260012i

At the same time, the systemic venous system has remained largely neglected. In this context, central venous pressure was used as the primary — and often the sole — marker of the venous compartment, inappropriately guiding fluid therapy despite consistent evidence of its limited ability to predict fluid responsiveness and its association with systemic venous congestion, target-organ dysfunction, and worse clinical outcomes.[1] The contemporary understanding of circulatory pathophysiology integrates the assessment of fluid responsiveness and fluid tolerance, restoring the fundamental role of the venous system in comprehensive hemodynamic monitoring. This paradigm supports personalized interventions informed by microcirculatory markers, such as Capillary Refill Time (CRT) and Near-Infrared Spectroscopy (NIRS), aiming to preserve macro-microcirculatory coherence (hemodynamic coherence) and optimize tissue perfusion.

Evaluation of systemic venous congestion has advanced substantially with the incorporation of ultrasound assessment of visceral vessels, enabling an integrated understanding of the coupling between the venous system and the right heart, including interaction among volume status, right ventricular function, and conditions that impair cardiac filling, such as pericardial disease. In this context, analysis of flow patterns in the inferior vena cava, hepatic veins, portal vein, and intrarenal veins has come to provide direct physiological information regarding the transmission of elevated venous pressure to target organs.[2] As early as 2014,[3] Transesophageal Echocardiography (TEE) was being used to assess the venous system in hemodynamic instability, and subsequent studies published in 2017[4] and 2018[5] demonstrated its relevant prognostic value for cardiovascular surgery outcomes, preceding the formal description of the VExUS score in 2020 (Venous Excess UltraSound) by the Canadian group led by Beaubien-Souligny *et al,*[6] who systematized this evaluation by integrating multiple venous territories into a graded congestion score. Initially intended for patients undergoing cardiac surgery, this tool quickly gained relevance in the management of acute Heart Failure (HF) and in the intensive care setting as a method for quantifying systemic venous congestion, and has been associated with clinically relevant outcomes such as acute kidney injury, need for renal replacement therapy, delirium, prolonged length of stay, and mortality. Operationally, patients with an inferior vena cava diameter < 2 cm are classified as VExUS 0, whereas those with an IVC ≥ 2 cm

SUMÁRIO

Central Illustration: VExUS Assessment Using Transesophageal Echocardiography: A Step-by-Step Performance Guide

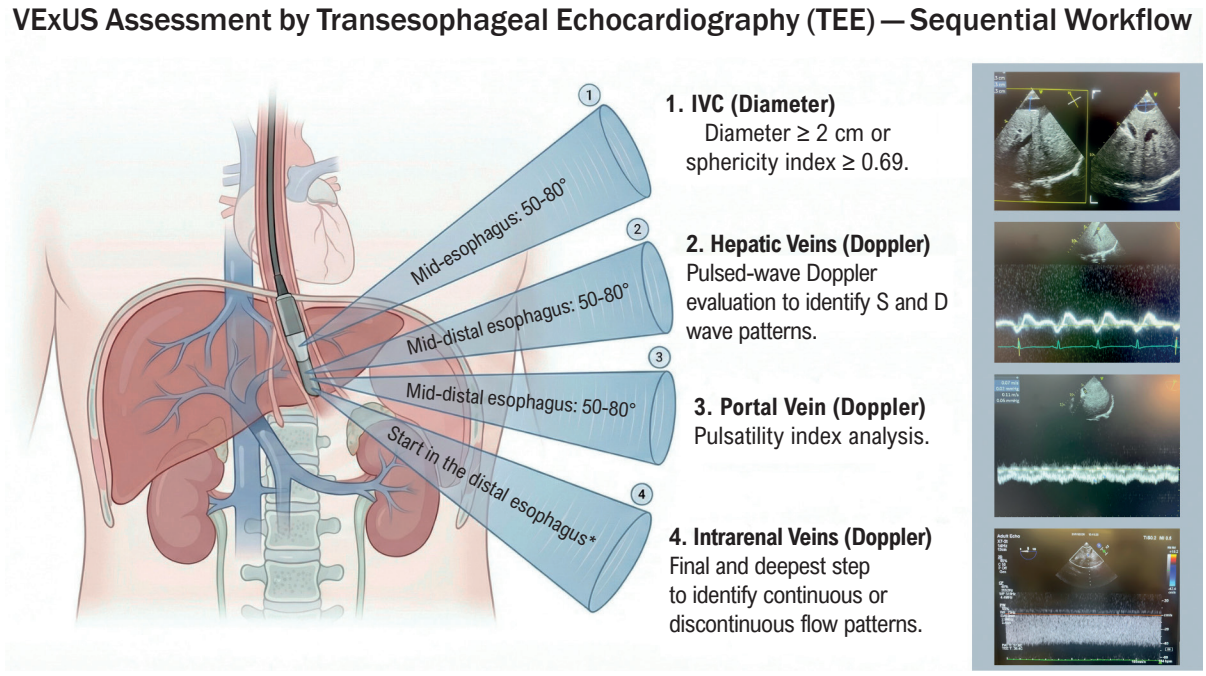

Arq Bras Cardiol: Imagem cardiovasc. 2026;39(1):e20260012

are stratified as VExUS 1 to 3 according to Doppler patterns of the splanchnic veins. More than a descriptive score, VExUS has been consolidated as a functional tool for assessing fluid tolerance (degree of fluid overload) and for guiding personalized hemodynamic decision-making, supporting the adaptation and systematic application of its criteria through transesophageal echocardiography in the perioperative setting.

In recent years, an expanding body of evidence has reinforced the prognostic impact of VExUS across different clinical scenarios, with initial application in cardiac surgery and rapid expansion to acute heart failure and intensive care settings, including incorporation into contemporary hemodynamic assessment protocols for septic shock. In acute heart failure, VExUS has proven to be a feasible, reproducible, and prognostically relevant tool from the time of admission. Saddi *et al*. demonstrated that patients hospitalized for acute heart failure who showed improvement in the VExUS score after reassessment at 72 hours had a 58% reduction in in-hospital mortality compared with those who did not respond to diuretic therapy.[7] Similarly, Lozano-Jiménez *et al*. reported that at hospital discharge, approximately 24% of patients deemed clinically compensated still had residual systemic venous congestion (VExUS ≥ 1) and experienced a higher rate of adverse events within six months, including mortality, heart failure readmissions, and emergency visits for decompensation, at a magnitude comparable to patients with clinically evident congestion at discharge.[8]

The use of Transesophageal Echocardiography (TEE) for systematic assessment of the VExUS score was protocolized beginning in 2024 by the group led by Waldron *et al*. at the Mayo Clinic, expanding the applicability of the method in the perioperative environment.[9] With TEE, image acquisition of the inferior vena cava, hepatic veins, and portal vein is, in most cases, feasible and reproducible, whereas assessment of the intrarenal veins may be technically limited. In this context, a 2025 study validated the modified VExUS, in which exclusion of intrarenal Doppler did not compromise diagnostic accuracy.[10] Compared with right heart catheterization, the modified VExUS performed similarly to the traditional score in identifying elevated right atrial pressure (RAP > 12 mmHg), with comparable areas under the curve (AUC 0.85 vs. 0.87) and near-perfect agreement between methods ($\kappa = 0.85$), outperforming isolated assessment of inferior vena cava diameter. These findings support the use of abbreviated protocols based on venous territories accessible by TEE to reliably estimate systemic venous congestion in the perioperative setting, enabling personalized hemodynamic evaluation within a multimodal monitoring framework.

Technique for Obtaining VExUS Using TEE

Image 1: Assessment of the IVC (Figure 1)

The Inferior Vena Cava (IVC) and the inferior cavoatrial junction can be imaged from either the mid-esophageal or transgastric window, provided that appropriate adjustments in probe rotation, depth, and flexion are made. In practice, the IVC is most often visualized from the mid-esophageal window, using the bicaval view as the starting reference. From there, clockwise rotation of the probe and gradual advancement allow identification of the cavoatrial junction and hepatic veins. At this stage, adjusting the multiplane angle of the bicaval view, typically from 110–120° to approximately 50–80°, provides a more suitable long-axis view of the IVC.

Measurement of the IVC in two orthogonal planes is essential, as its cross-section is typically elliptical and varies throughout the respiratory cycle. Therefore, one-dimensional long-axis measurements often fail to accurately reflect its true morphology or the relationship among vascular geometry, venous compliance, and Central Venous Pressure (CVP). In this context, Seo *et al*. demonstrated that the sphericity index—defined as the ratio between the minor and major diameters of the IVC in cross-section—best characterized the degree of systemic congestion and showed superior performance for detecting CVP > 10 mmHg, with a reference value of 0.69 and an AUC of 0.98.[11] This index appears particularly useful in patients with low body surface area, in whom IVC diameters smaller than 2.0 cm may still reflect elevated venous pressures.

Based on these findings, it is recommended to obtain IVC images approximately 2 cm from the cavoatrial junction to allow reliable diameter assessment and, when feasible, calculation of the sphericity index.

Technical pitfalls: Patients under positive intrathoracic pressure (mechanical ventilation) often have a dilated IVC, which requires cautious interpretation.

Image 2: Assessment of the Hepatic Veins (Figure 2)

In most cases, the IVC image itself already reveals the confluence of the hepatic veins, sometimes requiring only slight advancement of the probe to optimize visualization, typically in the mid-to-distal esophagus or stomach. On TEE, the hepatic vein lies inferior to the IVC, has thin walls, and drains directly into it, with flow directed toward the transducer. Under physiological conditions, systolic and diastolic flows appear in red on color Doppler and above the baseline on pulsed-wave Doppler.

The transgastric window provides an effective alternative for hepatic vein assessment, producing an image similar to the subcostal view in transthoracic echocardiography. In this approach, the hepatic veins appear in the near field, while the IVC is visualized in the far field. Under normal conditions, color Doppler shows systolic and diastolic hepatic flows in blue, indicating flow away from the probe. A key advantage of this approach is the ease of access to the portal vein: by adjusting the imaging plane between 20–60°, its branches can be visualized in long axis, allowing full application of the VExUS protocol in a manner similar to the transhepatic technique.

In the absence of significant systemic congestion, hepatic vein flow demonstrates an S wave larger than the D wave (Type 1 pattern). As venous congestion increases, the S wave progressively decreases, leading to S/D reversal (S < D) while maintaining antegrade flow (Type 2 pattern), until in advanced stages the S wave becomes reversed, defining the Type 3 pattern.

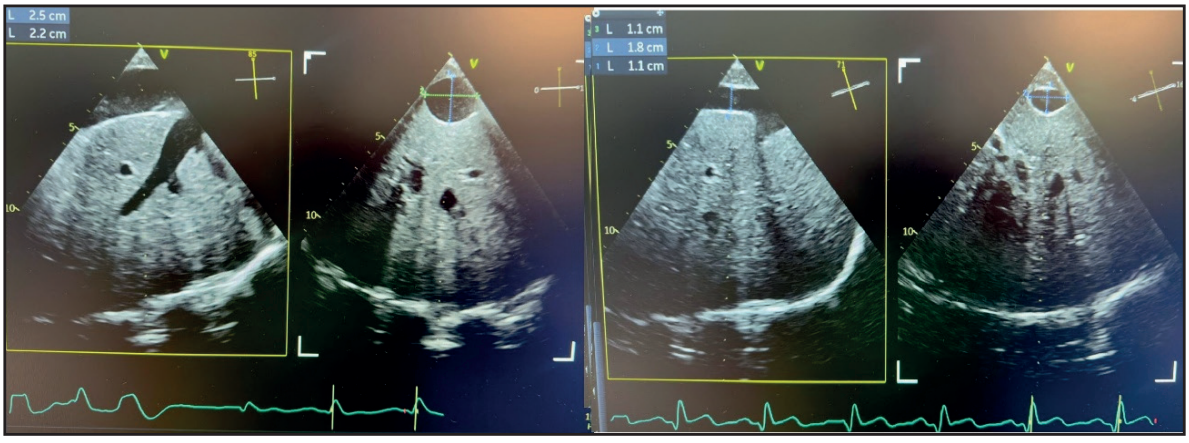

Figure 1 – *Left: IVC obtained from the mid-esophageal window with angulation approximately 50–80°, allowing optimal long-axis (LAX) visualization, and 140–170° for the short-axis (SAX) view. The IVC appears plethoric (2.5 cm) and circular on SAX, consistent with systemic congestion (sphericity index 0.88). Right: Progressive improvement in congestion, with IVC diameter: 1.8 cm and an oval shape on SAX (sphericity index: 0,61).*

Technical pitfalls: because of low flow velocities, the color Doppler scale should be set between 20–30 cm/s, and the pulsed-wave Doppler sample volume positioned 1–2 cm from the IVC junction. Another common error is failure to use ECG tracing to correctly distinguish S and D waves, which may lead to misinterpretation.

In patients with severe tricuspid regurgitation, portal vein Doppler is the most reliable ultrasound marker for monitoring decongestion, whereas hepatic and renal venous flow assessment may be significantly limited, as shown in a recent study.[12]

Image 3: Assessment of the Portal Vein (Figure 3)

The portal vein can be evaluated from the mid-distal esophagus or the transgastric window using the same approach employed for hepatic vessel visualization, sometimes requiring small rotational movements or minor advancement/withdrawal of the probe.

The portal vein is characterized by thick walls and flow directed away from the transducer (blue on color Doppler and below the baseline on pulsed Doppler). In the absence of systemic congestion, the pulsatility index [(Vmax − Vmin)/Vmax × 100] is < 30% (Type 1). As congestion develops, this variability increases (30–50%; Type 2) and becomes markedly accentuated in severe congestion (> 50%; Type 3). This occurs because progressive congestion leads to dilation of hepatic sinusoids, which act as a buffer to systemic pulsatility; as this buffering capacity is exceeded, pulsatility becomes more pronounced. The portal vein pulsatility index is among the most reliable parameters for monitoring volume removal,

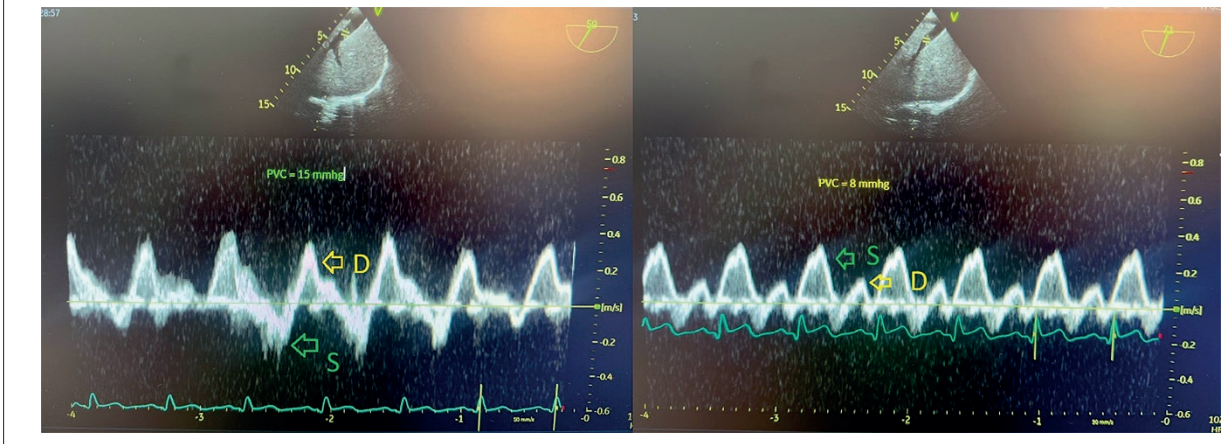

Figure 2 – *Left: Slight advancement of the probe from the IVC view reveals the left hepatic vein. Significant systemic congestion is evident by S-wave reversal (retrograde) while the D wave remains antegrade (Type 3 flow). The retrograde S wave is easily identified immediately after the QRS complex on the ECG. Right: Clinical improvement in the same patient, with antegrade S wave and S > D pattern (Type 1 flow). S wave: green arrow. D wave: yellow arrow.*

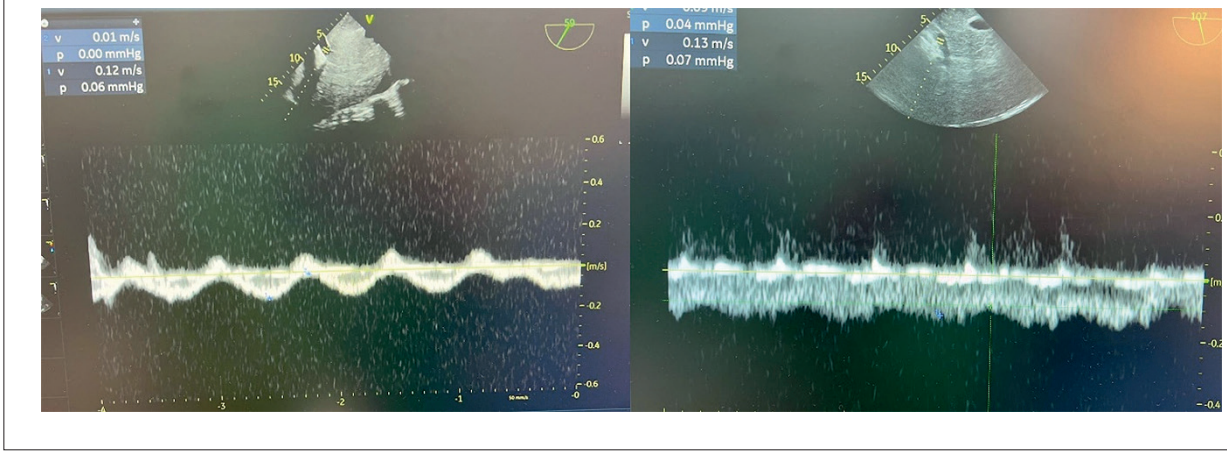

Figure 3 – *Left: Portal vein with flow variability > 50%, indicating severe congestion (Type 3 flow). Right: Restoration of normal phasicity of the portal vein, indicating resolution of congestion (Type 1 flow).*

particularly in certain congestion phenotypes such as severe tricuspid regurgitation.

Technical pitfalls: as with hepatic veins, low velocities require color Doppler settings between 20–30 cm/s. Cirrhotic patients may have altered portal flow patterns that complicate interpretation.

Image 4: Assessment of the Renal Interlobar Vein (Figure 4)

Among visceral vessels, the renal interlobar vein is the most technically challenging to assess, both by transthoracic and transesophageal echocardiography. Because these vessels are small and highly mobile with respiration, evaluation is not always feasible. Current evidence suggests that renal interlobar vein assessment is not mandatory for estimating the VExUS score; analysis of the IVC, portal vein, and hepatic veins is generally sufficient for quantifying systemic congestion, making renal assessment nonessential during surgical procedures. However, early studies indicated that impaired intrarenal flow correlated more strongly with progression to renal failure than abnormalities in other vessels. Further research is needed to clarify the diagnostic and prognostic value of renal assessment for systemic congestion during surgery.

To locate the left kidney via TEE, begin by rotating the probe to approximately 180° to identify the descending aorta in the distal esophagus. After locating it, advance the probe while applying leftward (counterclockwise) rotation until the renal parenchyma is visualized. For a longitudinal view, rotate to 90° and continue counterclockwise rotation from the aortic short-axis image while advancing until the kidney is identified. Regarding flow patterns, continuous venous flow indicates the absence of significant systemic congestion (Type 1). Type 2 is characterized by biphasic, discontinuous flow with peaks during systole and diastole. With worsening congestion, Type 3 flow appears, in which venous flow is present only during diastole. Depending on orientation, venous flow may appear above or below the baseline and is often accompanied by interlobar arterial flow in the opposite direction due to the close proximity of the vessels.

Pitfalls: Renal imaging by TEE is difficult and often yields suboptimal image quality. Because of very low velocities, the color Doppler scale should be set below 20 cm/s.

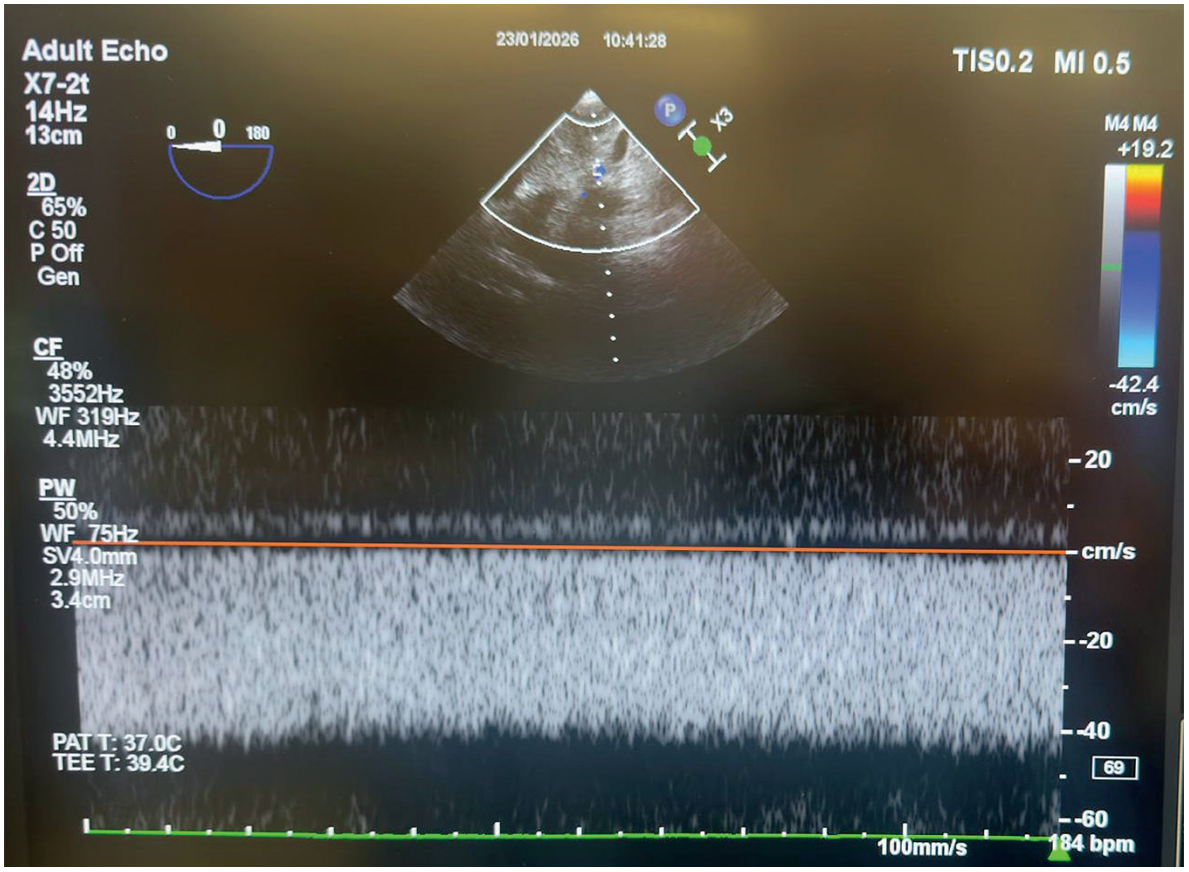

Figure 4 – *Interlobar renal venous flow showing a continuous pattern (continuous flow below baseline), characteristic of the absence of renal congestion (Type 1).*

The sequential acquisition of TEE images is summarized schematically in the central figure.

Discussion

VExUS should be viewed not as a standalone tool but as a strategic component of truly multimodal hemodynamic monitoring, aligned with contemporary physiopathological models such as the hemodynamic interfaces theory proposed by Rola *et al*.[13] This conceptual model of four interfaces offers a holistic and personalized framework for shock resuscitation, shifting the focus beyond simple normalization of Mean Arterial Pressure (MAP) and protocolized fluid administration.

- **Interface I (Ventricular-Arterial Coupling):** Focuses on the relationship between Left Ventricular (LV) contractile performance and arterial afterload.
- **Interface II (Arteriolar-Capillary Coupling):** Represents the transition from macrocirculation to microcirculation, where blood moves from arterioles into capillaries.
- **Interface III (Capillary-Venular Interface):** Centers on the venous side. Highlights that elevated central venous pressure impairs perfusion by causing stasis and edema, even when arterial flow appears adequate.
- **Interface IV (Right Ventricular–Pulmonary Artery Coupling):** Evaluates the interaction between the Right Ventricle (RV) and the pulmonary circulation. Within this framework, the goal of intraoperative hemodynamic monitoring extends beyond normalization of macro-hemodynamic variables. The primary objective becomes optimization of tissue perfusion (Interface II) and organ function. VExUS fits clearly within this model by assessing Interface III (capillary-venular), which reflects venous drainage, organ outflow, and the presence of systemic venous congestion—now recognized as a key causal mechanism of organ dysfunction.

At the same time, Interface III represents only one component of global hemodynamic assessment. Using VExUS in isolation, without considering the other interfaces, may lead to incomplete interpretation and suboptimal clinical decisions. Echocardiography, therefore, assumes a unique and central role, as it enables integrated evaluation of both the Interface I (LV–arterial coupling), Interface IV (RV–PA coupling), and Interface III (capillary/venular), through the analysis of the IVC and systemic venous flows (hepatic/portal and renal).

Especially during intraoperative management, echocardiography emerges as a comprehensive hemodynamic monitor capable of integrating flow generation, distribution, and venous drainage, overcoming fragmented approaches based on isolated parameters. Within this model, VExUS complements and refines the assessment of venous congestion and guides physiologically coherent decongestive strategies. In essence, the principal contribution of VExUS is to enhance the evaluation of Interface III by identifying scenarios in which impaired tissue perfusion results not from insufficient supply but from compromised venous drainage. When integrated into a multimodal, interface-guided approach, VExUS supports the shift from number-centered monitoring toward physiology-based monitoring focused on perfusion and clinically meaningful outcomes.

Conclusion

Performing the VExUS protocol using TEE (or its modified version, mVExUS) during surgical procedures is feasible and enables a personalized approach centered on the concept of "perfusion without congestion." It can assist in volume management and help prevent fluid overload that may lead to serious intraoperative or early postoperative complications.

Author Contributions

Conception and design of the research: Salgado AA; acquisition of data, analysis and interpretation of the data, writing of the manuscript and critical revision of the manuscript for intellectual content: Salgado AA, Bernardo MPL, Fernandes MR.

Potential Conflict of Interest

No potential conflict of interest relevant to this article was reported.

Sources of Funding

There were no external funding sources for this study.

Study Association

This study is not associated with any thesis or dissertation work.

Ethics Approval and Consent to Participate

This article does not contain any studies with human participants or animals performed by any of the authors.

Use of Artificial Intelligence

During the preparation of this work, the author(s) used ChatGPT to create the Central Figure. After using this tool/service, the author(s) reviewed and edited the content as needed and take full responsibility for the content of the published article.

Availability of Research Data

The underlying content of the research text is contained within the manuscript.

References

1. Stassen J, Falter M, Herbots L, Timmermans P, Dendale P, Verwerft J. Assessment of Venous Congestion Using Vascular Ultrasound. JACC Cardiovasc Imaging. 2023;16(3):426-31. doi: 10.1016/j.jcmg.2022.12.028.
2. Salgado AA, Bernardo MPL, Netto FM. My Approach to Evaluate Systemic Venous Congestion: VExUS Protocol. Arq Bras Cardiol: Imagem cardiovasc. 2024;37(2):e20240026. doi: 10.36660/abcimg.20240026.
3. Denault A, Vegas A, Royse C. Bedside Clinical and Ultrasound-Based Approaches to the Management of Hemodynamic Instability--Part I: Focus on the Clinical Approach: Continuing Professional Development. Can J Anaesth. 2014;61(9):843-64. doi: 10.1007/s12630-014-0203-0.
4. Denault AY, Beaubien-Souligny W, Elmi-Sarabi M, Eljaiek R, El-Hamamsy I, Lamarche Y, et al. Clinical Significance of Portal Hypertension Diagnosed with Bedside Ultrasound after Cardiac Surgery. Anesth Analg. 2017;124(4):1109-15. doi: 10.1213/ANE.0000000000001812.
5. Beaubien-Souligny W, Eljaiek R, Fortier A, Lamarche Y, Liszkowski M, Bouchard J, et al. The Association between Pulsatile Portal Flow and Acute Kidney Injury after Cardiac Surgery: A Retrospective Cohort Study. J Cardiothorac Vasc Anesth. 2018;32(4):1780-7. doi: 10.1053/j.jvca.2017.11.030.
6. Beaubien-Souligny W, Rola P, Haycock K, Bouchard J, Lamarche Y, Spiegel R, et al. Quantifying Systemic Congestion with Point-Of-Care Ultrasound: Development of the Venous Excess Ultrasound Grading System. Ultrasound J. 2020;12(1):16. doi: 10.1186/s13089-020-00163-w.
7. Saadi MP, Silvano GP, Machado GP, Almeida RF, Scolari FL, Biolo A, et al. Modified Venous Excess Ultrasound: A Dynamic Tool to Predict Mortality in Acute Decompensated Heart Failure. J Am Soc Echocardiogr. 2025;38(12):1129-41. doi: 10.1016/j.echo.2025.08.011.
8. Lozano-Jiménez S, Sebastian CG, Martín PV, Magallón BG, Centellas AM, Castro D, et al. Prevalence and Prognostic Impact of Subclinical Venous Congestion in Patients Hospitalized for Acute Heart Failure. Eur Heart J Acute Cardiovasc Care. 2026;14(12):749-53. doi: 10.1093/ehjacc/zuaf097.
9. Waldron NH, Pandompatam G, Sareyyupoglu B, Kalagara H. Transesophageal Echocardiographic Acquisition of the Venous Excess Ultrasound Exam-a Case Series and Technical Description. Can J Anaesth. 2024;71(3):422-30. doi: 10.1007/s12630-023-02688-9.
10. Martin KC, Gill EA, Douglas IJ, Longino AA. Evaluation of a Modified Venous Excess Ultrasound (VExUS) Protocol for Estimation of Venous Congestion: A Cohort Study. Ultrasound J. 2025;17(1):7. doi: 10.1186/s13089-025-00411-x.
11. Seo Y, Iida N, Yamamoto M, Machino-Ohtsuka T, Ishizu T, Aonuma K. Estimation of Central Venous Pressure Using the Ratio of Short to Long Diameter from Cross-Sectional Images of the Inferior Vena Cava. J Am Soc Echocardiogr. 2017;30(5):461-7. doi: 10.1016/j.echo.2016.12.002.
12. Alday-Ramírez SM, Leal-Villarreal MAJ, Gómez-Rodríguez C, Abu-Naeima E, Solis-Huerta F, Gamba G, et al. Portal vein Doppler Tracks Volume Status in Patients with Severe Tricuspid Regurgitation: A Proof-of-Concept Study. Eur Heart J Acute Cardiovasc Care. 2024;13(7):570-4. doi: 10.1093/ehjacc/zuae057.
13. Rola P, Kattan E, Siuba MT, Haycock K, Crager S, Spiegel R, et al. Point of View: A Holistic Four-Interface Conceptual Model for Personalizing Shock Resuscitation. J Pers Med. 2025;15(5):207. doi: 10.3390/jpm15050207.

Implantation of a Post-Dilatable Stent in Aortic Coarctation Via Carotid Access in a Newborn With Ebstein's Anomaly: Case Report

Jonathan Guimarães Lombardi,[1] Paulo Correia Calamita,[1] Orlando Carlos Barbosa,[1] Mayra Rosana Palmeira Barreto,[1,2] Giulliano Gardenghi[3,4]

Hospital Estadual de Urgências Governador Otávio Lage de Siqueira (HUGOL),[1] Goiânia, GO – Brazil
CRD Medicina Diagnóstica,[2] Goiânia, GO – Brazil
Hospital Encore,[3] Aparecida de Goiânia, GO – Brazil
Clínica de Anestesia de Goiânia,[4] Goiânia, GO – Brazil

Introduction

Ebstein's anomaly is a complex congenital heart disease that occurs in one out of every 200,000 live births. Its association with left-sided obstructive lesions is rare[1] and poses significant challenges for both clinical and surgical management. In this case report, we present a newborn patient with Ebstein's anomaly associated with supravalvular mitral stenosis and coarctation of the aorta (CoA), who underwent cardiac catheterization for the implantation of a post-dilatable stent in the aortic isthmus via the carotid approach.

Case Report

A premature newborn (35 6/7 weeks of gestational age) was admitted to the service at five days of life while receiving prostaglandin.

Echocardiography revealed Ebstein's anomaly, marked dilation of the right atrium (RA), patent foramen ovale (PFO) with bidirectional flow, right ventricular outflow tract (RVOT) with low antegrade flow, mitral valve (MV) with a supravalvular membrane and a mean gradient of 6.6 mmHg, left ventricle (LV) with moderate to severe dysfunction, tricuspid aortic valve with bicuspid opening, CoA, and a patent ductus arteriosus (Figure 1).

CT angiography demonstrated CoA, patent ductus arteriosus, and a reduced free cavity of the right ventricle (RV) (Figure 2).

The patient developed heart failure, signs of low systemic output, enterocolitis, and required antibiotic therapy and infusion of vasoactive drugs.

Keywords

Ebstein Anomaly; Aortic Coarctation; Stents; Cardiac Catheterization; Newborn Infant

Mailing Address: Giulliano Gardenghi •
Hospital Encore. Rua Gurupi, Qd.25, Lt.06/08. Postal code: 74905-350. Setor Vila Brasília, Aparecida de Goiânia, GO – Brazil
E-mail: coordenacao.cientifica@ceafi.edu.br
Manuscript received November 7, 2025, revised manuscript November 17, 2025, accepted December 3, 2025
Editor responsible for the review: Karen Saori Shiraishi Sawamura

DOI: https://doi.org/10.36660/abcimg.20250085i

Considering CoA as the most significant lesion and the high surgical risk, percutaneous treatment was chosen, which was performed at 28 days of life and 2.23 kg.

Interventional Procedure

The right carotid artery was punctured under ultrasound guidance, and a 5F slender transradial introducer was positioned. Intravenous cefazolin and heparin at a dose of 100 IU/kg were administered through the introducer. Cineangiography was performed.

With the support of a 4F JR diagnostic catheter and a 0.035" hydrophilic guidewire (150 cm), the coarctation was crossed. A 0.035" standard Teflon guidewire with J-tip (260 cm) was then positioned in the descending aorta. With guidewire support, the carotid introducer was exchanged for a 7F femoral introducer.

A PALMAZ GENESIS 1910 stent, manually crimped onto a POWERFLEX 7x20 mm balloon catheter, was implanted in the aortic isthmus. Control cineangiography demonstrated the stent to be well positioned and adequately apposed to the aortic wall, with significant improvement in antegrade aortic flow and reduction of shunting through the ductus arteriosus (Figure 3).

After removal of the arterial introducer, manual hemostatic compression was performed, followed by an occlusive compressive dressing. Heparin was reversed with protamine.

The patient had prolonged hospitalization, requiring 28 days of invasive mechanical ventilation, and was discharged after 85 days of hospital stay. Doppler ultrasound of the carotid arteries showed no abnormalities. The patient is currently stable and under outpatient follow-up, awaiting weight gain for the next surgical stage.

Discussion

CoA is a congenital malformation characterized by narrowing of the aortic isthmus, with an incidence of 1:1000 live births. The treatment of CoA has advanced considerably over the past decades, both surgically[2] and percutaneously.[3]

The implantation of a post-dilatable stent up to the diameter of the adult aorta in infant patients presents a challenge: the profile of the device is large for the traditional access route, the femoral artery, which increases the risk

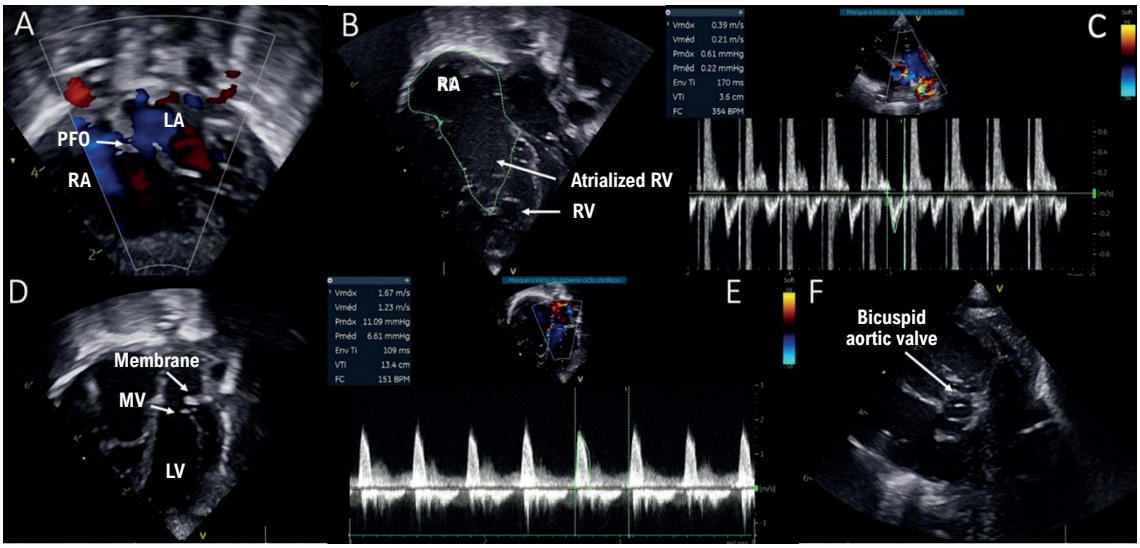

Figure 1 – *Transthoracic Doppler Echocardiogram. A) Subcostal view showing a patent foramen ovale with bidirectional flow. B) Right atrial dilation, presence of atrialized portion of the right ventricle, and a small functional right ventricle. C) Doppler in the right ventricular outflow tract plane showing low velocity–time integral (VTI). D and E) Supravalvular mitral membrane with a mean gradient of 6.6 mmHg. F) Bicuspid aortic valve. PFO: patent foramen ovale; RA: right atrium; LA: left atrium; RV: right ventricle; MV: mitral valve; LV: left ventricle.*

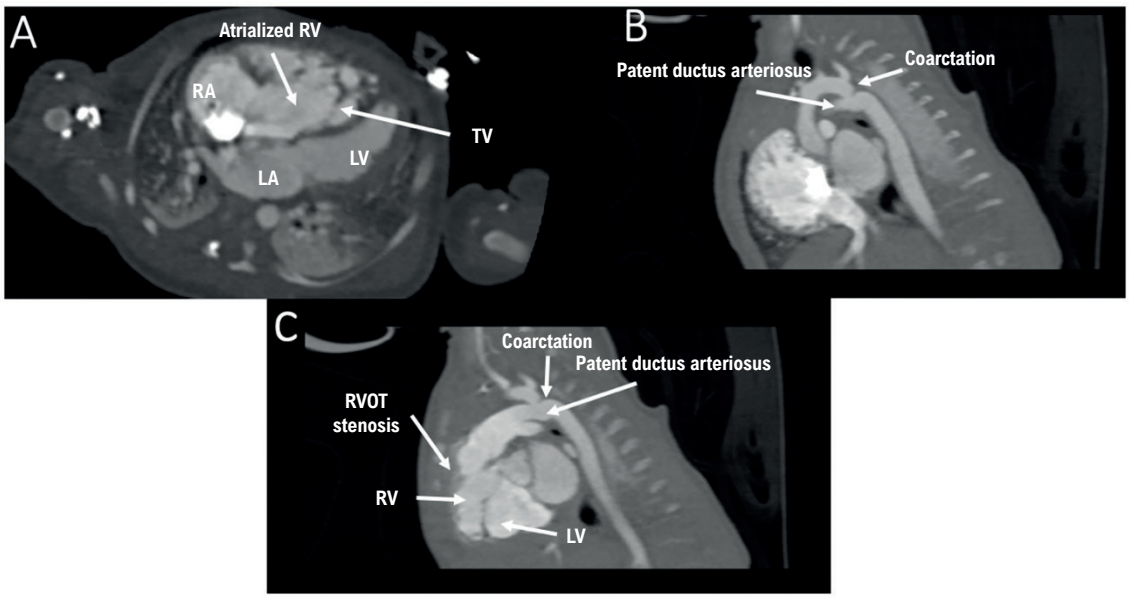

Figure 2 – *Computed tomography angiography of the aorta. A) Transverse section showing the atrialized portion of the right ventricle and tricuspid valve with apical displacement of the leaflets; B) Sagittal section demonstrating coarctation of the aorta; C) Right ventricular outflow tract with stenosis, large patent ductus arteriosus, and coarctation of the aorta; TV: tricuspid valve; RVOT: right ventricular outflow tract.*

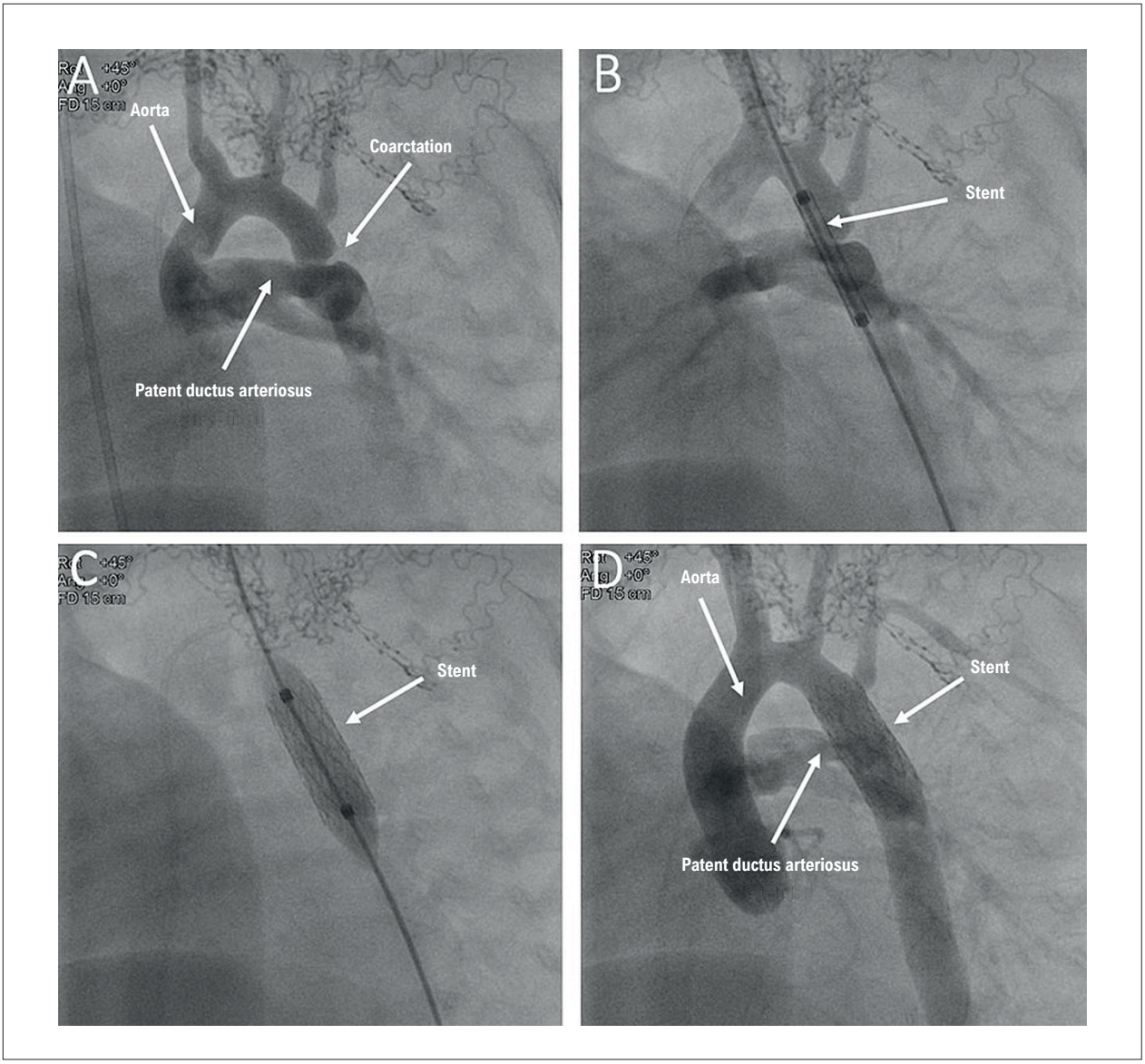

Figure 3 – *Cardiac catheterization; A) coarctation of the aorta and large patent ductus arteriosus; B) PALMAZ GENESIS 1910 stent crimped onto a POWERFLEX 7x20 mm balloon catheter being positioned in the aortic isthmus; C) stent being implanted in the aortic isthmus; D) stent implanted in the aortic isthmus with significant improvement in blood flow from the aortic arch to the descending aorta and reduction of effective flow through the ductus arteriosus via the lateral mesh of the stent.*

of severe vascular complications. In patients with CoA, the carotid arteries have significantly larger calibers than the femoral arteries. Thus, carotid access represents a viable alternative for catheterization, which can be performed either by surgical dissection or by safe puncture.[4]

The rate of aortic wall complications in patients undergoing balloon aortoplasty is higher than in those treated surgically or with stent implantation. On the other hand, hospitalization time and the incidence of acute complications are lower in patients treated with stent implantation compared to those treated surgically.[5]

The literature on the treatment of CoA in infants with stent implantation is scarce, with this approach generally reserved for patients at high surgical risk, in whom the implantation of a non–post-dilatable stent is more common.

In the case described, percutaneous treatment via carotid puncture and implantation of a post-dilatable stent in the coarctation offers the advantage of stent therapy without the drawback of failing to accommodate the patient's somatic growth, since this device can be further dilated to the diameter of the adult aorta using balloon catheters in two or three additional hemodynamic procedures over the years.[6]

The absence of vascular complications in the carotid artery, as assessed by Doppler ultrasound, together with the patient's favorable clinical course, demonstrates the efficacy and safety, at least in the short term, of this procedure.

Conclusion

In the reported case, percutaneous treatment of CoA in a newborn was chosen due to the association of cardiac defects and the patient's clinical condition. We consider that treating coarctation in infants with implantation of a post-dilatable stent up to the diameter of the adult aorta combines the benefits of stent aortoplasty – lower rates of acute complications and shorter hospital stay compared to surgical treatment – with the additional advantage of adjusting the stent size to the patient's somatic growth.

This case report demonstrates the efficacy and safety of the procedure, at least in the short term. However, further studies are needed to confirm the safety and efficacy of this technique in the medium and long term.

Author Contributions

Conception and design of the research and writing of the manuscript: Lombardi JG, Gardenghi G; acquisition of data: Lombardi JG, Calamita PC, Barbosa OC, Barreto MRP, Gardenghi G; analysis and interpretation of the data: Lombardi JG, Calamita PC, Barbosa OC; critical revision of the manuscript for intellectual content: Calamita PC, Barbosa OC, Barreto MRP, Gardenghi G.

Potential Conflict of Interest

No potential conflict of interest relevant to this article was reported.

Sources of Funding

There were no external funding sources for this study.

Study Association

This study is not associated with any thesis or dissertation work.

Ethics Approval and Consent to Participate

This study was approved by the Ethics Committee of the CEP do Hospital de Urgëncias de Goiás under the protocol number 85497418.2.0000.0033. All the procedures in this study were in accordance with the 1975 Helsinki Declaration, updated in 2013. Informed consent was obtained from all participants included in the study.

Use of Artificial Intelligence

The authors did not use any artificial intelligence tools in the development of this work.

Availability of Research Data

The data cannot be made publicly available due to legal issues related to Brazil's General Data Protection Law, as it could allow the identification of the patient in question.

References

1. Jost CHA, Connolly HM, O'Leary PW, Warnes CA, Tajik AJ, Seward JB. Left Heart Lesions in Patients with Ebstein Anomaly. Mayo Clin Proc. 2005;80(3):361-8. doi: 10.4065/80.3.361.
2. Vitullo DA, DeLeon SY, Graham LC, Eidem BW, Roughneen PT, Javorski JJ, et al. Extended End-to-End Repair and Enlargement of the Entire Arch in Complex Coarctation. Ann Thorac Surg. 1999;67(2):528-31. doi: 10.1016/s0003-4975(98)01254-5.
3. O'Laughlin MP, Slack MC, Grifka RG, Perry SB, Lock JE, Mullins CE. Implantation and Intermediate-Term Follow-Up of Stents in Congenital Heart Disease. Circulation. 1993;88(2):605-14. doi: 10.1161/01.cir.88.2.605.
4. Justino H, Petit CJ. Percutaneous Common Carotid Artery Access for Pediatric Interventional Cardiac Catheterization. Circ Cardiovasc Interv. 2016;9(4):e003003. doi: 10.1161/CIRCINTERVENTIONS.115.003003.
5. Forbes TJ, Kim DW, Du W, Turner DR, Holzer R, Amin Z, et al. Comparison of Surgical, Stent, and Balloon Angioplasty Treatment of Native Coarctation of the Aorta: An Observational Study by the CCISC (Congenital Cardiovascular Interventional Study Consortium). J Am Coll Cardiol. 2011;58(25):2664-74. doi: 10.1016/j.jacc.2011.08.053.
6. Boe BA, Armstrong AK, Janse SA, Loccoh EC, Stockmaster K, Holzer RJ, et al. Percutaneous Implantation of Adult Sized Stents for Coarctation of the Aorta in Children ≤20 kg: A 12-Year Experience. Circ Cardiovasc Interv. 2021;14(2):e009399. doi: 10.1161/CIRCINTERVENTIONS.120.009399.

Hemodynamic Impact of Hypertrophic Cardiomyopathy at Rest and During Supine Bicycle Exercise: Additional Value of Postprandial Assessment

Marília Esther Benevides Abreu,[1] *Tereza Cristina Pinheiro Diógenes,*[1] *Isadora Sucupira Machado Chagas,*[1] *Humberto Mororó Xerex,*[1] *José Sebastião De Abreu*[1]

Clinicárdio Métodos Diagnósticos,[1] *Fortaleza, CE – Brazil*

Abstract

A patient with severe, symptomatic hypertrophic cardiomyopathy (HCM) without a significant left ventricular outflow tract (LVOT) gradient at rest requires further evaluation. During exercise echocardiography (EE) performed on a supine bicycle, a latent or underestimated dynamic obstruction may be identified in real time, with postprandial assessment being particularly relevant.

Case report

A 42-year-old female patient had previous emergency department visits due to precordial discomfort radiating to the back and episodes of presyncope. During one episode, troponin elevation was observed. She subsequently underwent coronary computed tomography angiography, which demonstrated normal epicardial coronary arteries (Figure 1).

She had HCM with a septal diastolic thickness of 34 mm. Systolic anterior motion (SAM) of the mitral valve was absent at rest and under fasting conditions. The left ventricle was hyperdynamic, with an ejection fraction of 69% and global longitudinal strain of −13%. Atrial volumes were normal, and cardiac valves were competent (Figure 1).

While receiving propranolol, the patient underwent supine bicycle EE, a method that allows continuous assessment of myocardial contractility and changes in the left ventricular outflow tract (LVOT) gradient throughout the procedure (Figure 2). The first examination was performed in the morning under fasting conditions. She was then instructed to consume a meal of 1000-1500 kcal, predominantly composed of carbohydrates. On the same day, approximately 30 min after the meal, she returned for a repeat echocardiography (EE) study.

Keywords

Hypertrophic Cardiomyopathy; Exercise Test; Exercise; Postprandial.

Mailing Address: José Sebastião De Abreu •
Clinicárdio de Fortaleza e Cardioexata. Rua Doutor Jose Lourenço, 500. Postal code: 60115-280. Fortaleza, CE – Brazil
E-mail: jsabreu10@yahoo.com.br
Manuscript received June 21, 2025; revised January 28, 2026; accepted February 2, 2026
Editor responsible for the review: Andrea Vilela

DOI: https://doi.org/10.36660/abcimg.20250049i

The initial workload was 25 W, with increments of 25 W every 2 min. The test was terminated at 75 W due to exhaustion and fatigue. Heart rate ranged from 56 to 120 bpm, with no chest pain, hypotension, or arrhythmias (Table 1). No murmur was audible at rest; however, during exercise, a grade 2/4 systolic murmur emerged at the left sternal border. The highest LVOT gradients were observed during the recovery phase, with heart rate below 100 bpm.

Under fasting conditions, the resting LVOT gradient was 8 mmHg, with no SAM. During exercise in the fasting state, the gradient reached 36 mmHg. In the postprandial condition, SAM was already detectable at rest, with a baseline gradient of 16 mmHg and a gradient of 48 mmHg during exercise (Figure 3).

Discussion

HCM has an estimated prevalence of 1:200-1:500 in the general population, although only a smaller proportion of cases (10%-20%) are clinically diagnosed. Clinical presentation reflects variations in preload and afterload, which influence dynamic obstruction and symptom expression. Physiological maneuvers may intensify dynamic obstruction and cardiac murmur; however, the postprandial state may produce a meaningful increase in the LVOT gradient both at rest and during exercise, even when additional maneuvers do not demonstrate a significant effect.[1-3]

The hemodynamic impact of obstructive HCM may vary substantially within the same patient, even under pharmacological therapy. Identification of greater hemodynamic burden may indicate the need for therapeutic optimization or consideration of additional strategies such as septal myectomy, septal ablation (alcohol or radiofrequency), or pacemaker implantation.[4]

Studies evaluating HCM during exercise frequently use treadmill testing or upright bicycle protocols, with LVOT gradient measurement performed after exercise cessation. In this case, a supine bicycle was used, allowing continuous assessment of cardiac dynamics and real-time gradient measurement without interrupting the examination.

In a substantial proportion of patients with HCM, the gradient may be exacerbated in the postprandial state. Between 30-60 min after a meal, systemic vascular resistance may decrease, mainly due to mesenteric arterial vasodilation, in addition to reduced venous return and preload. Subsequent adrenergic stimulation promotes

Case Report

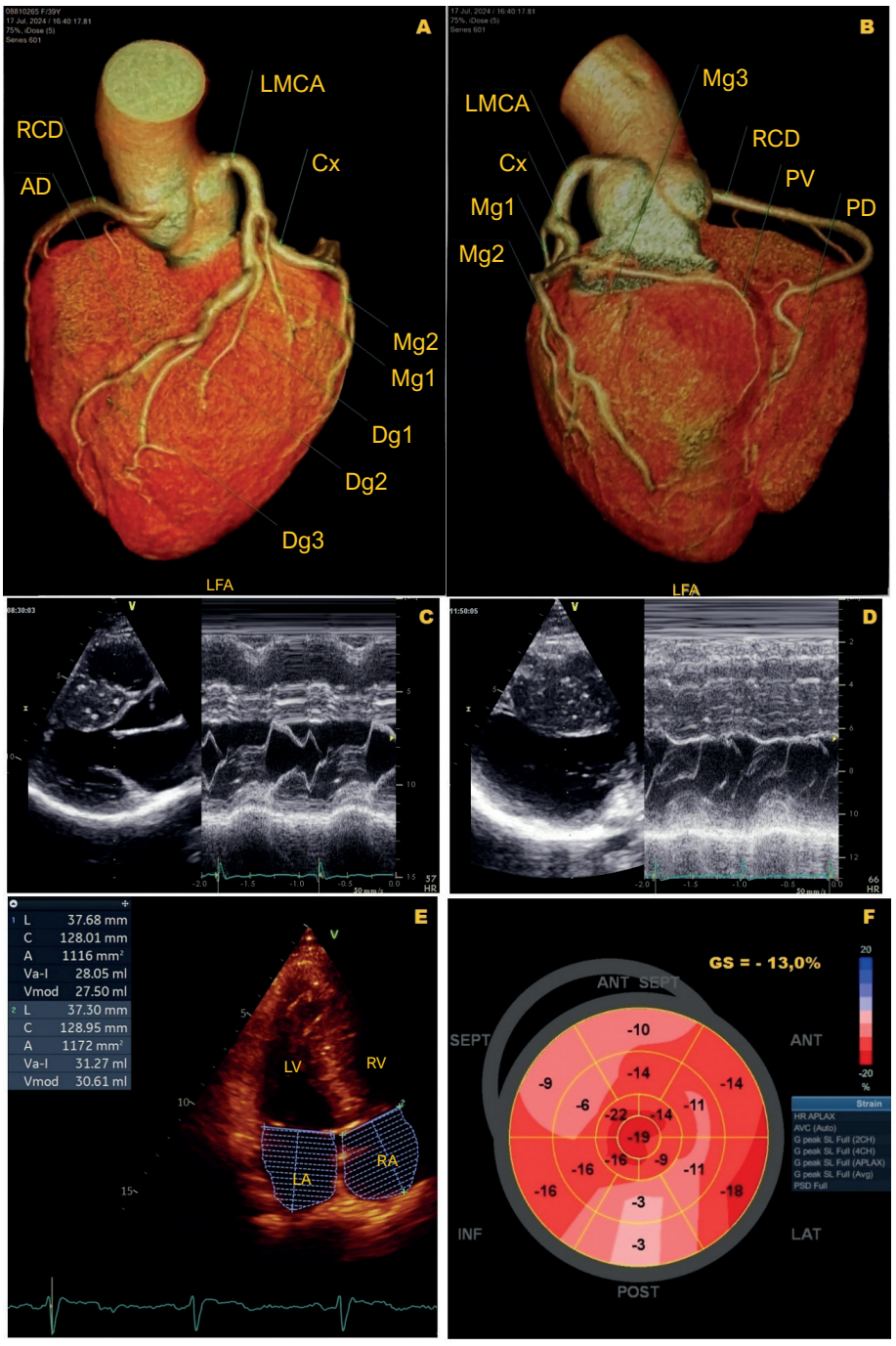

Figure 1 – *Structural and functional characterization in hypertrophic cardiomyopathy: coronary computed tomography angiography and multimodal echocardiographic assessment. A) Coronary computed tomography angiography – three-dimensional reconstruction showing the LMCA and its branches (anterior view); B) coronary computed tomography angiography – three-dimensional reconstruction showing epicardial coronary arteries and branches (complementary view); C) transthoracic echocardiography in two-dimensional and M-mode demonstrating myocardial morphology and wall thickening; D) transthoracic echocardiography in two-dimensional and M-mode with additional assessment of ventricular dynamics; E) echocardiography with atrial volumetric quantification (biplane method); F) LV GS analysis (polar map/bull's-eye). AD: left anterior descending artery; Cx: circumflex artery; Dg1: first diagonal branch; Dg2: second diagonal branch; Dg3: third diagonal branch; GS: global longitudinal strain; LA: left atrium; LMCA: left main coronary artery; LV: left ventricle; Mg1: first marginal branch (obtuse marginal); Mg2: second marginal branch (obtuse marginal); Mg3: third marginal branch (obtuse marginal); PD: posterior descending artery; PV: posterior ventricular branch; RA: right atrium; RCD: right coronary artery; RV: right ventricle.*

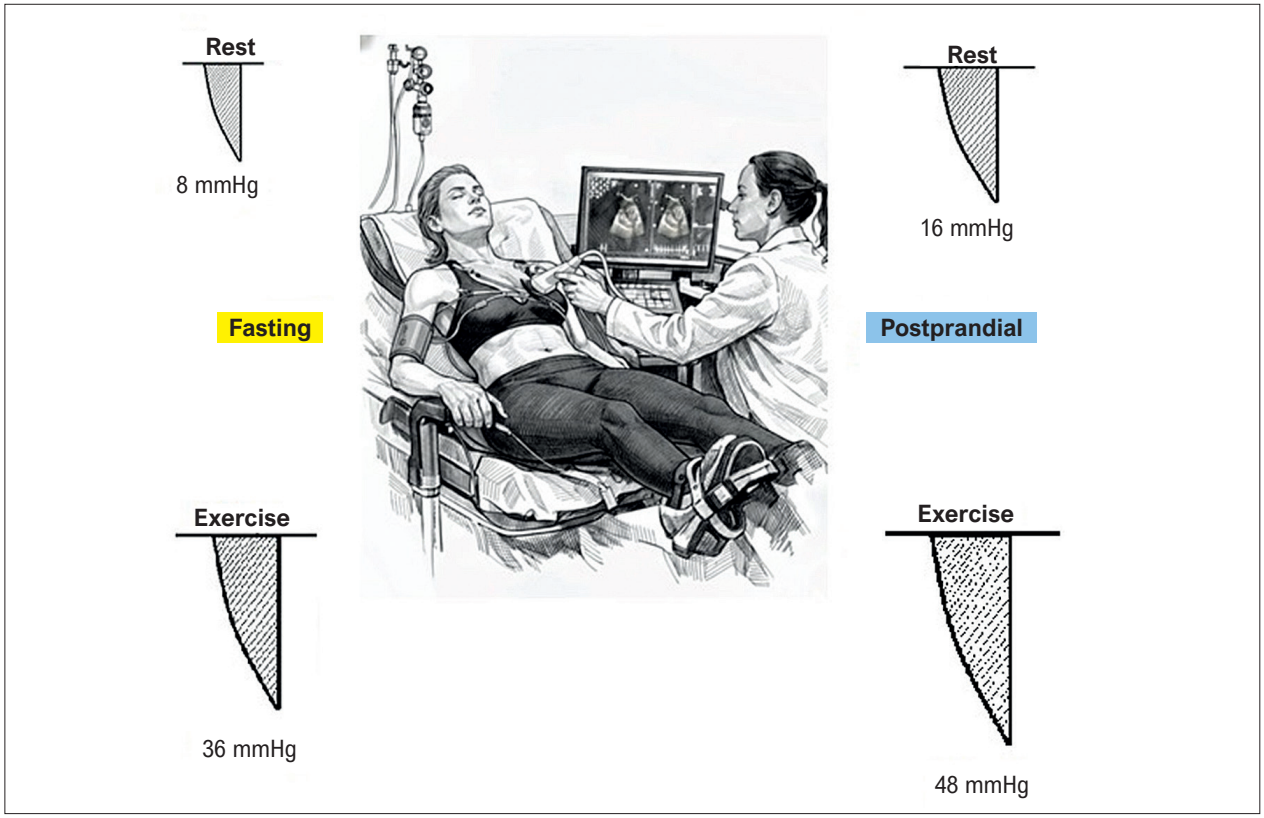

Figure 2 – *Hemodynamic Impact of Hypertrophic Cardiomyopathy at Rest and During Supine Bicycle Exercise: Additional Value of Postprandial Assessment.*

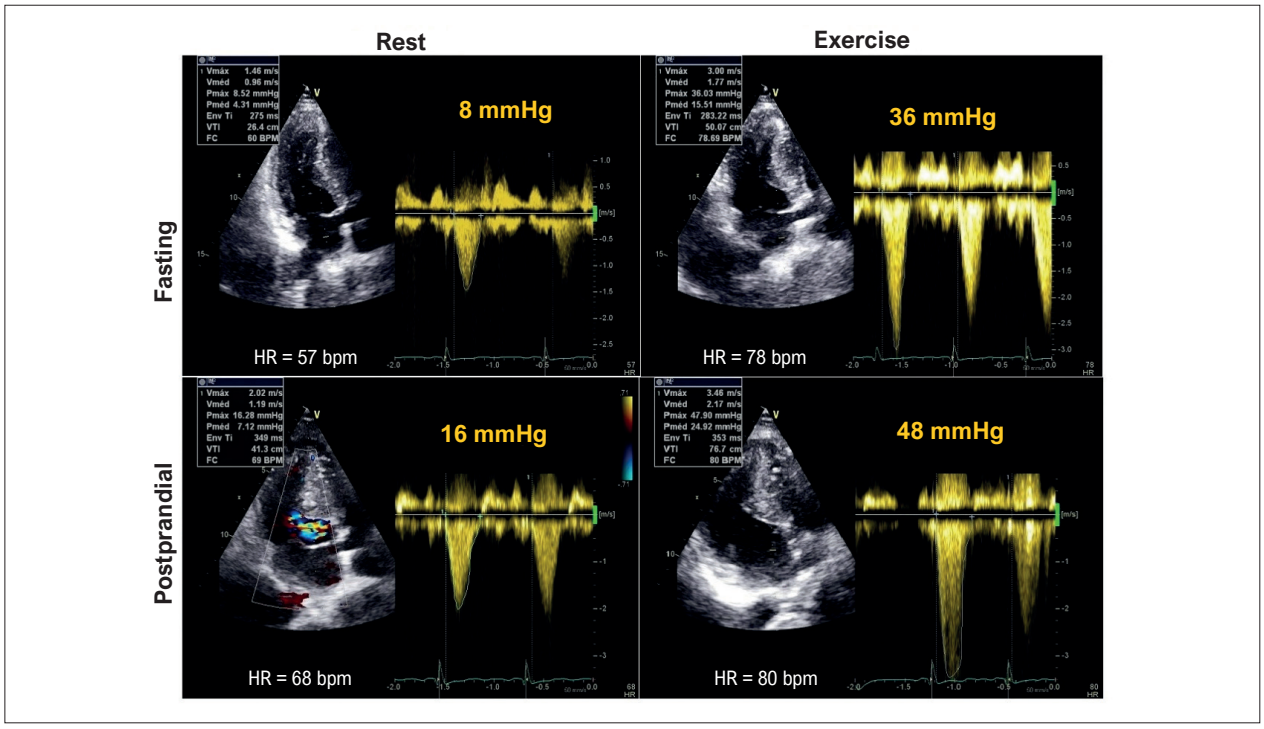

Figure 3 – *Variation in the left ventricular outflow tract gradient during fasting and postprandial states at rest and during exercise. HR: heart rate.*

Table 1 – Hemodynamic parameters

Variables	Rest	Exercise (75 W)	Recovery
Blood pressure – fasting	100 × 80 mmHg	150 × 90 mmHg	120 × 80 mmHg
Blood pressure – postprandial	100 × 70 mmHg	160 × 100 mmHg	100 × 80 mmHg
Heart rate – fasting	57 bpm	123 bpm	78 bpm
Heart rate – postprandial	68 bpm	120 bpm	80 bpm

increased inotropy and chronotropy. These hemodynamic interactions may intensify a pre-existing gradient or reveal a latent LVOT gradient.[3,5]

Studies assessing the LVOT gradient in patients with HCM during postprandial exercise generally include comparison with fasting evaluation to demonstrate potential differences. There is no standardized meal type. In general, moderate caloric intake (1000-1500 kcal) is recommended. The ideal composition remains uncertain, although carbohydrate-rich meals are frequently used.[3,5,6]

In cases of HCM with increased LVOT gradient in the postprandial state, pharmacological therapy may be initiated or adjusted. Patients should be advised to consume smaller, more frequent meals and maintain adequate hydration.[7,8]

Conclusion

In the assessment of HCM severity, postprandial evaluation is relevant both at rest and during exercise, contributing to therapeutic optimization and guidance on lifestyle modifications.

Author Contributions

Conception and design of the research: Abreu MEB, Abreu JS; Acquisition of data: Abreu MEB; Analysis and interpretation of the data: Abreu MEB, Diógenes TCP, Abreu JS; Writing of the manuscript: Machado IS, Abreu JS; Critical revision of the manuscript for intellectual content: Xerex HM, Abreu JS.

Potential Conflict of Interest

No potential conflict of interest relevant to this article was reported.

Sources of Funding

There were no external funding sources for this study.

Study Association

This study is not associated with any thesis or dissertation work.

Ethics Approval and Consent to Participate

This study was approved by the Ethics Committee of the Universidade Estadual do Ceará under the protocol number 70990923.6.0000.5534. All the procedures in this study were in accordance with the 1975 Helsinki Declaration, updated in 2013. Informed consent was obtained from all participants included in the study.

Use of Artificial Intelligence

The authors did not use any artificial intelligence tools in the development of this work.

Availability of Research Data

The underlying content of the research text is contained within the manuscript.

References

1. Ommen SR, Mital S, Burke MA, Day SM, Deswal A, Elliott P, et al. 2020 AHA/ACC Guideline for the Diagnosis and Treatment of Patients with Hypertrophic Cardiomyopathy: Executive Summary: A Report of the American College of Cardiology/American Heart Association Joint Committee on Clinical Practice Guidelines. J Am Coll Cardiol. 2020;76(25):3022-55. doi: 10.1016/j.jacc.2020.08.044.
2. Maron BJ, Desai MY, Nishimura RA, Spirito P, Rakowski H, Towbin JA, et al. Diagnosis and Evaluation of Hypertrophic Cardiomyopathy: JACC State-of-the-Art Review. J Am Coll Cardiol. 2022;79(4):372-89. doi: 10.1016/j.jacc.2021.12.002.
3. Massera D, Long C, Xia Y, James L, Adlestein E, Alvarez IC, et al. Unmasking Obstruction in Hypertrophic Cardiomyopathy with Postprandial Resting and Treadmill Stress Echocardiography. J Am Soc Echocardiogr. 2024;37(10):971-80. doi: 10.1016/j.echo.2024.06.011.
4. Valdigem BP, Correia EB, Moreira DAR, Bihan DL, Pinto IMF, Abizaid AAC, et al. Septal Ablation with Radiofrequency Catheters Guided by Echocardiography for Treatment of Patients with Obstructive Hypertrophic Cardiomyopathy: Initial Experience. Arq Bras Cardiol. 2022;118(5):861-72. doi: 10.36660/abc.20200732.
5. La Canna G, Scarfò I, Arendar I, Alati E, Caso I, Alfieri O. Phenotyping Left Ventricular Obstruction with Postprandial Re-Test Echocardiography in Hypertrophic Cardiomyopathy. Am J Cardiol. 2020;125(11):1688-93. doi: 10.1016/j.amjcard.2020.03.004.
6. Feiner E, Arabadjian M, Winson G, Kim B, Chaudhry F, Sherrid MV. Post-Prandial Upright Exercise Echocardiography in Hypertrophic Cardiomyopathy. J Am Coll Cardiol. 2013;61(24):2487-88. doi: 10.1016/j.jacc.2013.02.079.

7. Gilligan DM, Nihoyannopoulos P, Fletcher A, Sbarouni E, Dritsas A, Oakley CM. Symptoms of Hypertrophic Cardiomyopathy, with Special Emphasis on Syncope and Postprandial Exacerbation of Symptoms. Clin Cardiol. 1996;19(5):371-8. doi: 10.1002/clc.4960190509.

8. Kansal MM, Mookadam F, Tajik AJ. Drink More, and Eat Less: Advice in Obstructive Hypertrophic Cardiomyopathy. Am J Cardiol. 2010;106(9):1313-6. doi: 10.1016/j.amjcard.2010.06.061.

Aneurysm of the Suprahepatic Inferior Vena Cava: A Case Report

Gabriella Ghattas Mariano,[1] *Calina Araujo Thaines,*[1] *Gabrielle Silva Desani,*[1] *Letícia de Castro Gouvêa,*[1] *Paulo Vítor Cabral Covilo,*[1] *Rogério de Paula Garcia Caravante*[1]

Centro Universitário Católico Salesiano Auxilium,[1] *Araçatuba, SP – Brazil*

Introduction

Aneurysms of the inferior vena cava (IVC) are a rare occurrence in the cardiovascular system and can present with a variety of signs and symptoms. In many cases, patients remain asymptomatic, which makes diagnosis difficult.[1] Venous aneurysms are defined as an abnormal and persistent dilation of a vein in a specific area, with a diameter at least twice that considered normal. An IVC aneurysm is a specific type of venous aneurysm.[2] This case report is relevant because this condition is rare; by 2021, only around 70 cases had been described in literature.[3]

Aneurysms may arise due to fragility in the vessel wall and can be triggered by various factors, including hypertension, trauma, infection, and genetic conditions. Smoking, atherosclerosis, and chronic obstructive pulmonary disease are also considered risk factors for aneurysm development. Although they can occur in different regions of the body, they most frequently affect the cerebral arteries, the aorta, and the peripheral arteries.[4]

The clinical manifestations of aneurysms vary according to the size, location, and stability of the vascular dilation. They may even remain asymptomatic. However, in more severe cases, the vessel may rupture, resulting in hemorrhage, embolism, or thrombosis. These events may progress to fatal outcomes.[5] Among symptomatic patients with IVC aneurysm, the most frequently reported clinical findings include abdominal pain, lower limb edema (LLE), and dyspnea. Associated complications may include vena cava thrombosis, deep vein thrombosis (DVT), and pulmonary embolism, conditions that represent a significant risk to patients' lives.[6]

The objective of this study is to report a case of IVC aneurysm diagnosed in a private clinic in the city of Araçatuba, state of São Paulo, Brazil, classified as Type I because it is located in the suprahepatic portion of the IVC.[7] The clinical presentation, characterized by nonspecific manifestations as well as the diagnostic process and the follow-up strategy adopted, are highlighted.

Keywords

Aneurysm; Inferior Vena Cava; Cardiovascular Diseases; Case Reports.

Mailing Address: Rogério de Paula Garcia Caravante•
Centro Universitário Católico Salesiano Auxilium. Rodovia Teotonio Vilela, 3821. Postal code: 16016-500. Araçatuba, SP – Brazil
E-mail: rpgcaravante2011@gmail.com
Manuscript received August 4, 2025, revised manuscript October 29, 2025, accepted February 25, 2026
Editor responsible for the review: Tiago Magalhães

DOI: https://doi.org/10.36660/abcimg.20250055i

Case report

A 75-year-old White female patient sought care from a pulmonologist due to diffuse pain in the dorsal region and cough. Due to initial suspicions of a respiratory condition, a contrast-enhanced chest CT scan was requested. During the scan, a protruding sacular formation was identified in the upper quadrant of the abdomen.

The imaging examination demonstrated the presence of an IVC aneurysm in a suprahepatic location, classified as Type I according to the Gradman & Steinberg classification,[7] adjacent to the right atrium, without evidence of venous obstruction, measuring 4.2 cm at its greatest diameter. The cardiac silhouette was also observed to be of normal size, and the mediastinal vessels were centered, without other relevant abnormalities. These findings are illustrated in Figures 1 and 2.

According to the clinical history, the patient maintains a healthy lifestyle, with regular physical activity and a balanced diet, denying alcohol consumption and smoking. She was recently diagnosed with type 2 diabetes mellitus and is currently undergoing treatment. She reports a history of seizures during childhood and two vaginal deliveries in the second decade of life. Her surgical history includes appendectomy, gastroesophageal hiatoplasty, cholecystectomy, hysterectomy, oophorectomy, arthroplasty, and uterine curettage after an episode of ectopic pregnancy. In addition, she reports recurrent episodes of discomfort associated with palpitations throughout her life.

After the incidental finding, the patient was referred for cardiological evaluation and subsequently for consultation with a cardiovascular surgeon to undergo a more detailed investigation. At the time of the specialized evaluation, she was oligosymptomatic, presenting only persistent dorsal pain, which worsened with movement and improved with rest. On physical examination, slight abdominal prominence was observed, without pain on palpation, a finding consistent with the results of the previously performed imaging examination.

During follow-up, the patient presented significant improvement in pain after symptomatic treatment and remains under conservative clinical follow-up due to the stability of the condition. Currently, she undergoes periodic follow-up with a cardiovascular surgeon, with semiannual consultations and serial imaging examinations, with the objective of monitoring possible changes in the dimensions or characteristics of the IVC aneurysm.

Discussion

According to the classification proposed for IVC aneurysms, there are four forms of presentation (Figure 3). Type I

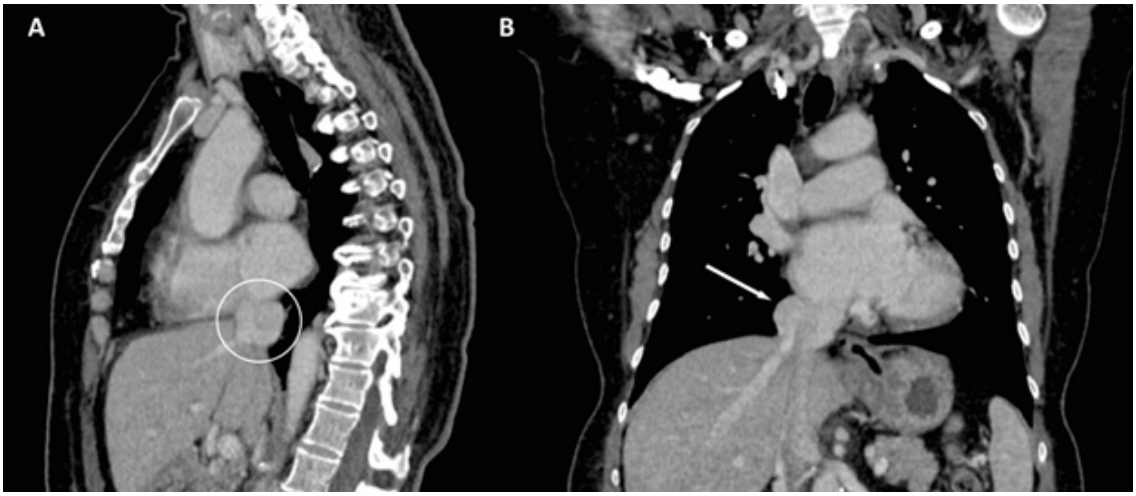

Figure 1 – *Chest CT. A) Chest CT with IV contrast administration, sagittal section, showing an IVC aneurysm (white circle); B) Chest CT with IV contrast administration, coronal section, demonstrating a suprahepatic IVC aneurysm adjacent to the right atrium (white arrow). CT: computed tomography; IVC: inferior vena cava.*

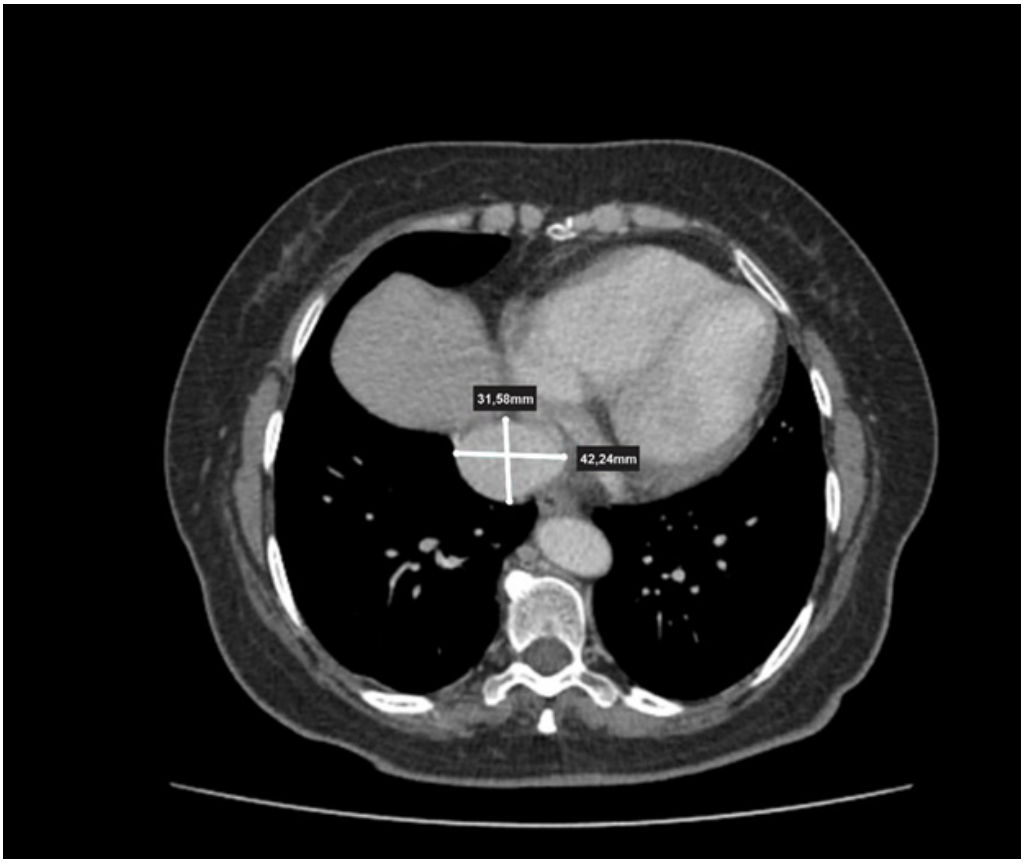

Figure 2 – *Chest computed tomography with IV contrast administration, axial section, showing an inferior vena cava aneurysm measuring 42.24 mm in the largest diameter and 31.58 mm in the smallest diameter (white lines).*

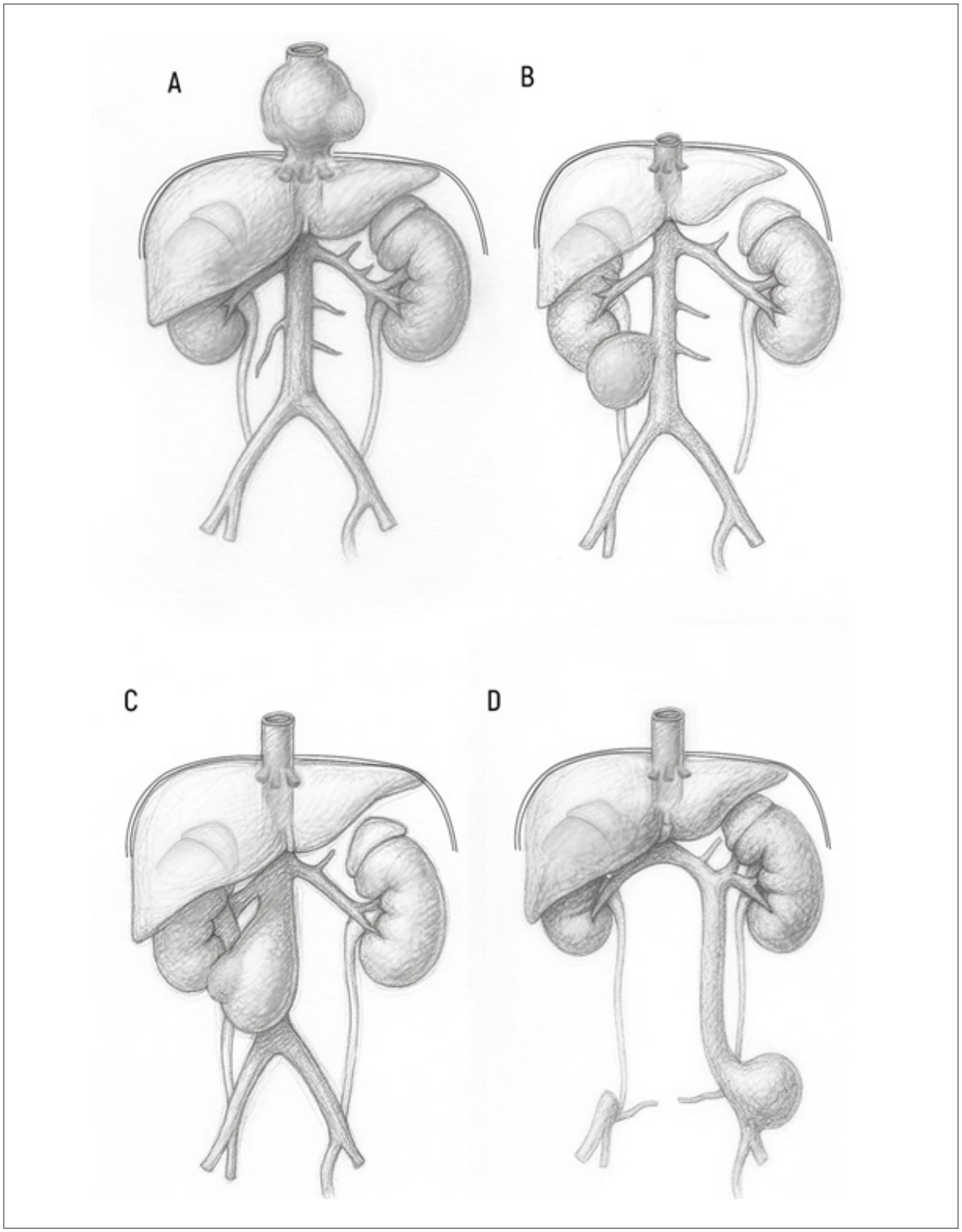

Figure 3 – *Schematic representation of the four types of IVC aneurysm. A) Type I: aneurysm located in the suprahepatic portion of the IVC, without obstruction of venous flow; B) Type II: infrarenal aneurysm associated with interruption of the suprahepatic segment of the IVC; C) Type III: aneurysmal dilation in the infrarenal region, without obstruction; D) Type IV: aneurysm involving the iliac vein, with the IVC positioned on the left side. Image adapted from Gradman & Steinberg.[7] IVC: inferior vena cava.*

corresponds to an aneurysm located in the suprahepatic portion of the IVC, without venous obstruction. Type II is associated with interruption of the IVC. Type III refers to an aneurysm located in the infrarenal portion of the IVC. Finally, Type IV corresponds to an aneurysm involving the iliac vein, associated with the presence of a left-sided IVC.[7] Based on this classification, the case presented was characterized as a Type I IVC aneurysm due to its suprahepatic location.

In the present report, the patient is female, 75 years old, and remained oligosymptomatic throughout her clinical history. Previous studies describe that most patients diagnosed with IVC aneurysm are male, with a mean age of 63.5 years among cases classified as Type I, with a large proportion of them being asymptomatic.[6] These data demonstrate that there may be variation in the epidemiological profile of individuals affected by this condition.

In this case, the diagnosis of IVC aneurysm was established after a chest CT scan. For the identification of this condition, imaging examinations constitute the main diagnostic method, particularly CT, magnetic resonance angiography, and venography, as they allow detailed evaluation of the morphology and characteristics of the venous aneurysm.[8] In the reported case, CT enabled precise visualization of the location, shape, and dimensions of the lesion.

Among the main complications associated with IVC aneurysm are rupture, DVT, pulmonary embolism, and IVC syndrome. Rupture occurs more frequently in aneurysms classified as Types II and III and may manifest with intense abdominal pain, dorsal pain, and LLE, leading to more severe clinical conditions.[9] Considering the classification of the aneurysm described in this report, Type I, as well as the patient's clinical history, no complications have been observed to date.

The literature describes abdominal pain, dyspnea, dorsalgia, LLE, and a sensation of heaviness in the lower limbs as the most common clinical manifestations in patients with IVC aneurysm. However, in aneurysms classified as Type I, asymptomatic or oligosymptomatic cases are more frequent.[6] In agreement with these findings, the patient in this report presented dorsalgia as the main clinical manifestation, which may be related to the identified aneurysm.

The treatment adopted in this case was conservative, with periodic clinical follow-up through physical examination and imaging studies, including CT performed every 6 months. This approach is consistent with the therapeutic algorithm proposed by Baker et al.,[5] which recommends conservative management with regular monitoring for IVC aneurysms classified as Type I. For Types II, III, and IV, the literature often indicates surgical intervention, such as embolization or resection, due to the higher risk of complications.[5]

Conclusion

Due to the scarcity of studies on the topic, the particularities described in this case may contribute to improving diagnosis and management in patients presenting with similar clinical features and symptoms. As a cardiovascular condition with possible systemic repercussions and often without evident clinical manifestations, IVC aneurysm may progress silently. Early identification is therefore essential for appropriate clinical management and follow-up.

Acknowledgments

We thank everyone who contributed, directly or indirectly, to the completion of this case report.

Author Contributions

Conception and design of the research, acquisition of data, analysis and interpretation of the data and writing of the manuscript: Mariano GG, Thaines CA, Desani GS, Gouvêa LCC, Covilo PV, Caravante RPG; critical revision of the manuscript for intellectual content: Caravante RPG.

Potential Conflict of Interest

No potential conflict of interest relevant to this article was reported.

Sources of Funding

There were no external funding sources for this study.

Study Association

This study is not associated with any thesis or dissertation work.

Ethics Approval and Consent to Participate

This study was approved by the Ethics Committee of the Missão Salesiana De Mato Grosso under the protocol number 7.053.378 (CAAE 79880624.0.0000.5379). All the procedures in this study were in accordance with the 1975 Helsinki Declaration, updated in 2013. Informed consent was obtained from all participants included in the study.

Use of Artificial Intelligence

The authors did not use any artificial intelligence tools in the development of this work.

Availability of Research Data

The underlying content of the research text is contained within the manuscript.

References

1. Marsafi O, Ibenyahia A, Moussaoui A, Belmekia A, Wakrim S. Aneurysm of the Inferior Vena Cava : A Case Report. Ann Cardiol Angeiol. 2022;71(4):235-9. doi: 10.1016/j.ancard.2022.05.002.
2. Hai TD, Minh LN, Dung NT, Van Dung L, Tuong CT, Van Phuoc L. Large Intra-Abdominal Venous Malformations in Associated with Inferior Vena Cava Aneurysm. Radiol Case Rep. 2023;18(5):1733-7. doi: 10.1016/j.radcr.2023.01.085.
3. Chang H, Bae J, Chung TN. A Unique Case of Inferior Vena Cava Aneurysm Complicated with Pulmonary Embolism and Cerebral Infarction. J Cardiovasc Dev Dis. 2021;8(11):147. doi: 10.3390/jcdd8110147.

4. Brito CJ, Silva RM, Loureiro E. Cirurgia Vascular: Cirurgia Endovascular e Angiologia. 4th ed. Rio de Janeiro: Thieme; 2020.

5. Montero-Baker MF, Branco BC, Leon LL Jr, Labropoulos N, Echeverria A, Mills JL Sr. Management of Inferior Vena Cava Aneurysm. J Cardiovasc Surg. 2015;56(5):769-74.

6. Wang M, Wang H, Liao B, Peng G, Chang G. Treatment Strategies for Inferior Vena Cava Aneurysms. J Vasc Surg Venous Lymphat Disord. 2021;9(6):1588-96. doi: 10.1016/j.jvsv.2021.03.017.

7. Gradman WS, Steinberg F. Aneurysm of the Inferior Vena Cava: Case Report and Review of the Literature. Ann Vasc Surg. 1993;7(4):347-53. doi: 10.1007/BF02002888.

8. Duarte ML, Abreu BFBB, Silva AQPD, Prado JLMA, Silva MQPD. Idiopathic Inferior Vena Cava Aneurysm - Tomographic Diagnosis. Rev Port Cardiol. 2017;36(10):7812. doi: 10.1016/j.repc.2016.11.014.

9. Momeni M, Momeni F. Ruptured Inferior Vena Cava Aneurysm in the Setting of Mural Vascular Malformation: A Case Report. J Clin Ultrasound. 2019;47(7):423-5. doi: 10.1002/jcu.22708.

Coexistence of Partial Anomalous Pulmonary Venous Connection and Coronary Artery Fistulas: A Rare Case Report

Mourad Haj Abdo,[1] Hussain Latsh,[2] Mathias Wagner,[2] George König,[1] Sebastian Barth[1]

Department of Cardiology, RHÖN-KLINIKUM Campus Bad Neustadt,[1] Bad Neustadt an der Saale – Germany

Department of Radiology, RHÖN-KLINIKUM Campus Bad Neustadt,[2] Bad Neustadt an der Saale – Germany

Abstract

Background

Dyspnoea is a common clinical symptom that frequently prompts hospital admission and is associated with significant morbidity. While it most often results from prevalent cardiopulmonary conditions, rare congenital cardiovascular anomalies can also manifest with dyspnoea. Partial Anomalous Pulmonary Venous Connection (PAPVC) and Coronary Artery Fistulas (CAFs) are uncommon congenital malformations of the cardiovascular system, and their simultaneous presence is exceedingly rare. Early recognition of such anomalies is critical to avoid progressive hemodynamic compromise and to guide appropriate management strategies.

Case Presentation

We present the case of a 55-year-old man who experienced an acute onset of dyspnoea lasting approximately two hours. Initial clinical assessment and routine investigations—including physical examination, echocardiography, electrocardiography, and right and left heart catheterization—raised suspicion of an underlying cardiac abnormality, prompting further evaluation. Subsequent cardiac Magnetic Resonance Imaging (MRI) and Multi-Detector Computed Tomography (MDCT) revealed the presence of a Partial Anomalous Pulmonary Venous Connection (PAPVC) accompanied by Coronary Artery Fistulas (CAFs). Given the non-complex characteristics of the shunt in this case, a shared decision was reached with the patient to proceed with conservative management.

Discussion

PAPVC and Coronary Artery Fistulas CAFs are rare entities that should be considered in the differential diagnosis. However, recommending their evaluation as initial diagnostic hypotheses may result in unnecessary investigations.

Keywords

Echocardiography; Differential Diagnosis; Coronary Vessels

Mailing Address: Mourad Haj Abdo
Rhön Klinikum AG. Salzburgerleite.1. Postal code: 97616. Bad Neustadt an der Saale – Germany
E-mail: moradhajabdo86@hotmail.de
Manuscript received May 8, 2025, revised manuscript November 30, 2025, accepted February 19, 2026
Editor responsible for the review: Tiago Magalhães

DOI: https://doi.org/10.36660/abcimg.20250030i

Introduction

A normal pulmonary venous pattern with four distinct veins is observed in approximately 60–70% of the population.[1] Developmental anomalies can result in Partial (PAPVC) or Total Aanomalous Pulmonary Venous Connection (TAPVC), with anomalous drainage patterns reported in up to 38% of individuals.[2] PAPVC may occur in isolation, in association with an Atrial Sseptal Defect (ASD), or as part of complex congenital heart disease, and often remains undiagnosed due to mild or absent symptoms.[3,4]

PAPVC involves a left-to-right shunt and is usually hemodynamically insignificant. It is often discovered incidentally, for example during imaging for a central venous catheter that appears malpositioned. Despite its subtle presentation, associated anomalies can increase the risk of morbidity and mortality.[5]

Coronary Artery Fistulas (CAFs) are rare congenital anomalies, with acquired cases being even more uncommon, and are most often detected incidentally. Small CAFs are typically asymptomatic, whereas larger fistulas can lead to cardiac chamber dilation or ischemia if left untreated.

We report a rare case of coexisting PAPVC and CAFs – an unusual combination that presents diagnostic challenges. Although each condition is individually rare, their simultaneous occurrence is exceptionally uncommon and has been seldom documented in the literature.[6,7]

Case Presentation

A 55-year-old patient presented for further evaluation of dyspnoea. He reported a mild retrosternal burning sensation radiating caudally beneath the left costal arches. The chest discomfort was non-exertional. There was no history of diabetes, connective tissue disorders, other systemic anomalies, or significant family history of disease.

On physical examination, the patient was afebrile, with no tachypnoea (respiratory rate: 13/min), oxygen saturation of 93%, and blood pressure of 150/95 mmHg. The rest of the physical examination was unremarkable. On the day of admission, the electrocardiogram demonstrated sinus rhythm with a heart rate of 92 bpm. High-sensitivity cardiac troponin levels were elevated, measuring 39 ng/L at baseline and 41 ng/L at one-hour follow-up (reference <14 ng/L), indicating myocardial injury without significant dynamic change. NT-proBNP was 89 pg/mL (normal <227 pg/mL in males aged 50-65 years).

In this case, left heart catheterization was performed prior to cardiac MRI due to clinical suspicion of a left-to-right shunt and the need to exclude coronary artery anomalies. The invasive procedure enabled precise identification of a coronary artery fistula between the Left Anterior Descending Artery (LAD) and

the pulmonary trunk, providing essential anatomical details for subsequent therapeutic planning.

Although MRI offers comprehensive structural evaluation, cardiac catheterization remains the gold standard for direct coronary visualization and hemodynamic assessment in such settings.

The patient remained largely asymptomatic, without evidence of cyanosis or angina. Following thorough medical consultation, he opted for conservative management with beta-blockers and diuretics. Given the absence of a significant left-to-right shunt, surgical intervention was not indicated.

Echocardiography and Electrocardiography

Echocardiography, which serves as both the gold standard and the primary diagnostic modality in the emergency department, demonstrated signs of right heart dilation. Both right and left ventricular systolic function were preserved, with normal ejection fractions (EF) — Right Ventricular Internal Diameter at Diastole (RVIDD) basal: 49 mm, RVIDd mid: 27 mm, FAC: 55%, TAPSE: 31 mm. Additionally, there was evidence of mild tricuspid regurgitation (Grade I), with pulmonary artery systolic pressure of 34 mmHg and a Qp:Qs ratio of 1.4. These findings are consistent with right heart volume overload, likely secondary to left-to-right shunting.

Electrocardiography revealed non-specific changes but supported the echocardiographic evidence of right heart volume overload.

To further clarify the differential diagnosis, the patient underwent comprehensive hemodynamic assessment, including both right and left heart catheterization.

Right and Left Heart Catheterization

On the same day, the patient underwent comprehensive cardiac catheterization. During right heart catheterization, direct evidence of a left-to-right shunt was observed. Oxygen saturation measurements revealed higher values in the superior vena cava compared with the inferior vena cava (SVC: 83%, IVC: 79%, RA: 81%, RV: 83%, PA: 85%).

Left heart catheterization (Figure 1) identified a fistula between the LAD artery and the pulmonary trunk. No coronary artery stenosis was detected, which allowed progression to the next step of the evaluation (Figure 1).

In light of these catheterization findings, cardiac MRI was performed to further clarify the diagnosis.

MRI (Magnetic Resonance Imaging)

To achieve better visualization of cardiac structures, cardiac MRI was performed. Left ventricular function was normal. Mild right ventricular dysfunction with right vetricular dilatation was observed, without evidence of arrhythmogenic right ventricular cardiomyopathy (Table 1). No signs of myocardial inflammation or fibrosis were detected.

A fistulous network was identified, with connections involving the proximal LAD, the conus arteriosus of the right coronary artery, and the pulmonary trunk (Figures 2 and 3).

Stress imaging or physiologic assessment was not performed to evaluate for ischemia attributable to the coronary–pulmonary

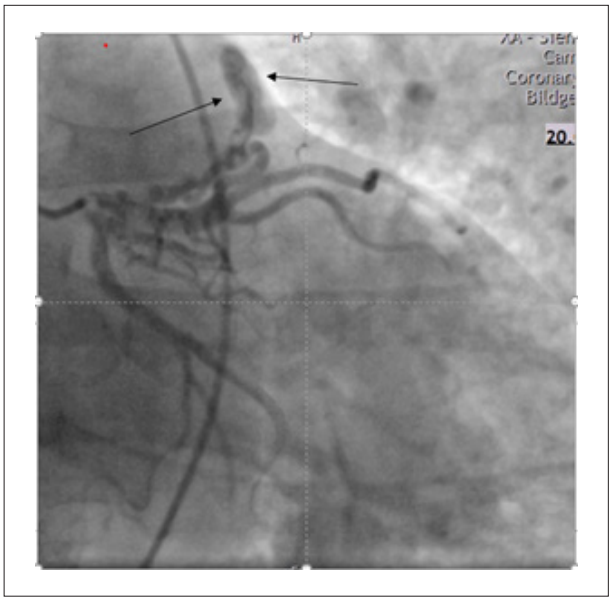

Figure 1 – *Coronary angiography showing the left anterior descending artery with a fistulous connection to the pulmonary trunk*

fistula. This decision was based on the patient's stable clinical status, the non-complex nature of the shunt, and the absence of ischemic symptoms.

MDCT (Multi-Detector Computed Tomography)

As MDCT represents the modality of choice for detailed assessment of cardiac anatomy and structural abnormalities, we elected to perform this study. MDCT revealed anomalous drainage of the upper and partially the lower left pulmonary veins into the left brachiocephalic vein. The left brachiocephalic vein was ectatic, with a maximum diameter of approximately 25 mm. The pulmonary trunk was dilated, measuring 32 mm (normal ≤29 mm in men), with associated dilatation of both pulmonary arteries. Dilatation of the right ventricle and right atrium was also noted. In addition, previously identified extensive fistulous connections between the proximal LAD and the pulmonary trunk were confirmed (Figures 4 and 5).

Discussion

PAPVC is a rare congenital defect in which one or more pulmonary veins drain into the systemic venous circulation—such as the superior vena cava or right atrium—instead of the left atrium. This results in a partial left-to-right shunt and is often detected incidentally, with a reported prevalence of 0.4–0.7%.

Both PAPVC and CAFs are rare anomalies, and their coexistence is extremely uncommon. Clinical presentation varies depending on the severity and location of the abnormal drainage.

Medium to large or symptomatic CAFs may require transcatheter closure, ideally performed in specialized centers. In cases involving large coronary aneurysms, surgical repair and anticoagulation may be necessary. Follow-up imaging is recommended to monitor for potential recanalization.

Table 1 – Left ventricle (LV) and right ventricle (RV) Volumetry: measurements of the volume of the both ventricle, including end-diastolic volume (EDV), end-systolic volume (ESV), stroke volume (SV), and ejection fraction (EF)

V- und RV-Volumetry:				
LV	**absolut**		**Norm (m)**	**(w)**
LV-EF	66	(%)	56-78	57-78
LV-EDV	156	ml	77-195	52-141
LV-ESV	53	ml	19-72	13-51
LV-SV	103	ml	51-133	33-97
LV-Mass	138	g	118-238	75-175
RV	**absolut**		**Norm (m)**	**(w)**
RV-EF	44	(%)	47-74	47-80
RV-EDV	286	ml	88-227	58-154
RV-ESV	160	ml	23-103	12-68
RV-SV	126	ml	52-138	35-98

Figure 2 – *Maximum intensity projection coronal images from a case of left-sided cardiac partial anomalous pulmonary venous connection*

Figure 3 – *Coronal maximum intensity projection images demonstrating a coronary artery fistula originating from the left anterior descending artery and draining into the pulmonary trunk; the fistulous connection is indicated by the arrow*

Conclusion

PAPVC and coronary artery fistulas are rare congenital cardiac anomalies, and their coexistence has been scarcely reported in the literature. Clinical presentation varies widely, ranging from incidental findings to symptoms influenced by the extent of abnormal venous drainage, the anatomical site of connection, and any associated cardiac defects.

Advanced imaging techniques such as MDCTA and MRA play a critical role in the precise delineation of these anomalies. Their ability to provide high-resolution, three-dimensional anatomical detail significantly aids clinicians in diagnosis, clinical assessment, and the development of appropriate management strategies.[8,9]

Author Contributions

Conception and design of the research: Abdo MH, Latsch H, Wagner M, Barth S; acquisition of data: Barth S; writing of the manuscript: Latsch H, König G; critical revision of the manuscript for intellectual content: Wagner M, Barth S.

Potential Conflict of Interest

No potential conflict of interest relevant to this article was reported.

Sources of Funding

There were no external funding sources for this study.

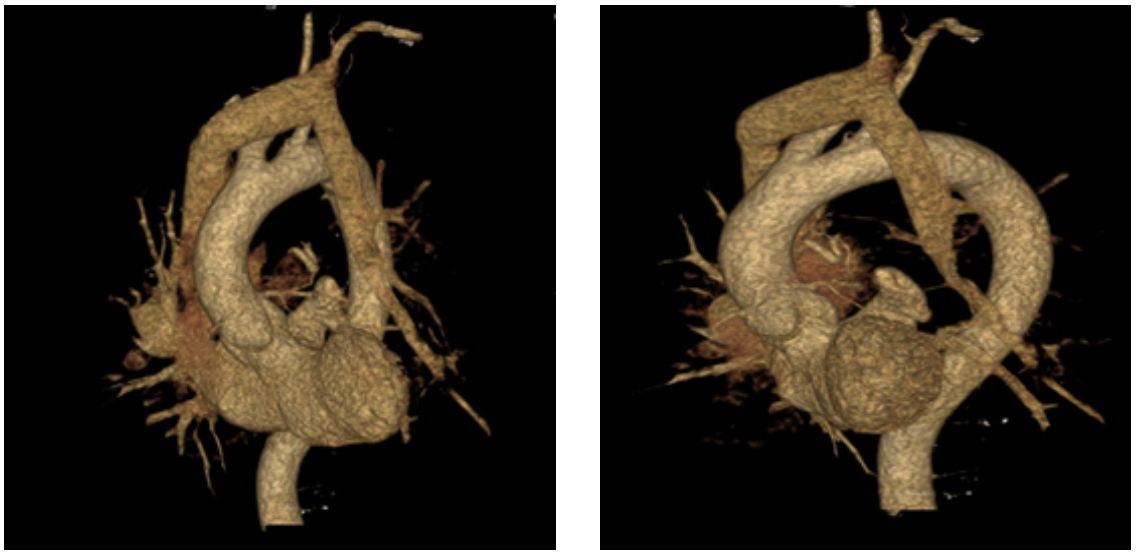

Figure 4 – *Two volume-rendered images in different orientation of our patient with partial anomalous pulmonary venous connection; the left inferior pulmonary vein is draining at the brachiocephalic vein*

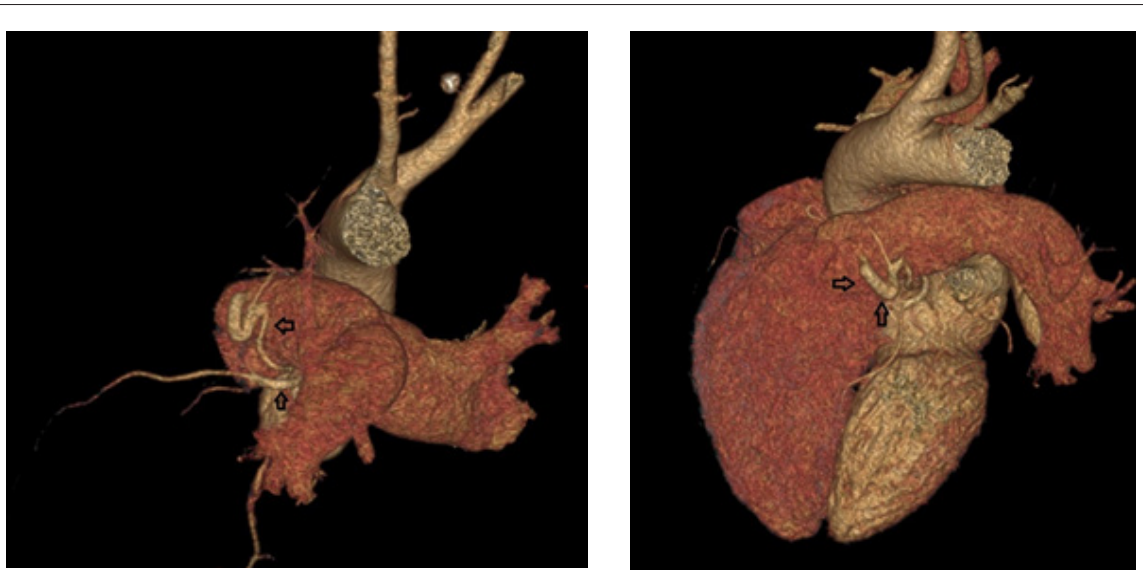

Figure 5 – *Volume-rendered computed tomography images in two different orientations depicting a coronary artery fistula originating from the left anterior descending artery and draining into the pulmonary trunk. The fistulous connection is indicated by the arrow*

Study Association

This study is not associated with any thesis or dissertation work.

Ethics Approval and Consent to Participate

The authors confirm that consent for submission and pub lication of this case report has been obtained from the patient in line with the COPE o guidance.

Use of Artificial Intelligence

The authors did not use any artificial intelligence tools in the development of this work.

Availability of Research Data

The underlying content of the research text is contained within the manuscript.

References

1. Lacomis JM, Goitein O, Deible C, Schwartzman D. CT of the Pulmonary Veins. J Thorac Imaging. 2007;22(1):63-76. doi: 10.1097/RTI.0b013e3180317aaf.
2. Kato R, Lickfett L, Meininger G, Dickfeld T, Wu R, Juang G, et al. Pulmonary Vein Anatomy in Patients Undergoing Catheter Ablation of Atrial Fibrillation: Lessons Learned by Use of Magnetic Resonance Imaging. Circulation. 2003;107(15):2004-10. doi: 10.1161/01.CIR.0000061951.81767.4E.
3. Kelle AM, Backer CL, Gossett JG, Kaushal S, Mavroudis C. Total Anomalous Pulmonary Venous Connection: Results of Surgical Repair of 100 Patients at a Single Institution. J Thorac Cardiovasc Surg. 2010;139(6):1387-1394.e3. doi: 10.1016/j.jtcvs.2010.02.024.
4. Furlanetto G, Furlanetto BH, Henriques SR, Lopes LM, Miranda ET, Porto CM, et al. Mixed Type Total Anomalous Pulmonary Venous Connection: Early Results and Surgical Techniques. World J Pediatr Congenit Heart Surg. 2015;6(1):26-32. doi: 10.1177/2150135114554660.
5. Hart A, Lee EY. Multidetector Computed Tomography of Pediatric Vascular Imaging with Advanced Postprocessing Techniques. Adv Clin Radiol 2020;2:191-211. doi: 10.1016/j.yacr.2020.06.003.
6. Yildiz A, Okcun B, Peker T, Arslan C, Olcay A, Vatan MB. Prevalence of Coronary Artery Anomalies in 12,457 Adult Patients who Underwent Coronary Angiography. Clin Cardiol. 2010;33(12):E60-4. doi: 10.1002/clc.20588.
7. Gillebert C, van Hoof R, van de Werf F, Piessens J, De Geest H. Coronary Artery Fistulas in an Adult Population. Eur Heart J. 1986;7(5):437-43. doi: 10.1093/oxfordjournals.eurheartj.a062086.
8. Dillman JR, Yarram SG, Hernandez RJ. Imaging of Pulmonary Venous Developmental Anomalies. AJR Am J Roentgenol. 2009;192(5):1272-85. doi: 10.2214/AJR.08.1526.
9. Haramati LB, Moche IE, Rivera VT, Patel PV, Heyneman L, McAdams HP, et al. Computed Tomography of Partial Anomalous Pulmonary Venous Connection in Adults. J Comput Assist Tomogr. 2003;27(5):743-9. doi: 10.1097/00004728-200309000-00011.

Left Ventricular Outflow Tract Velocity-Time Integral (LVOT VTI) as a Marker of Cardiac Performance: Mortality Data of the ELSA-Brasil Cohort

Mariana de Castro Lopes,[1] Altair Ivory Heidemann Jr.,[1] Eduardo G. Pianca,[1] Bruce B. Duncan,[2,3] Murilo Foppa,[1,2] Angela B.S. Santos[1,2]

Cardiology Division, Hospital de Clínicas de Porto Alegre,[1] Porto Alegre, RS – Brazil

Post-Graduate Program in Cardiology and Cardiovascular Sciences, Medical School, Universidade Federal do Rio Grande do Sul,[2] Porto Alegre, RS – Brazil

Post-Graduate Program in Epidemiology, Universidade Federal do Rio Grande do Sul,[3] Porto Alegre, RS – Brazil

Transthoracic Echocardiography (TTE) is a well-established tool for assessing cardiac function and hemodynamics. While Left Ventricular (LV) systolic and diastolic function are commonly used metrics, Cardiac Output (CO) remains central for evaluating hemodynamic status, especially in critical care settings. TTE-derived parameters, such as Left Ventricular Outflow Tract Velocity-Time Integral (LVOT VTI) and LVOT area, when combined with body habitus and heart rate, provide noninvasive estimates of cardiac output. However, the accuracy of CO calculations may decrease when multiple covariates are included, with LVOT diameter being a major source of error.[1] In contrast, isolated LVOT VTI may represent a simpler and more reliable surrogate of cardiac performance.

Among patients with Heart Failure with reduced Ejection Fraction (HFrEF), LVOT VTI values below 12 cm or 8 cm have been associated with worse cardiovascular outcomes, with a progressive increase in risk as VTI decreases.[2,3] Similarly, in intermediate to high-risk pulmonary embolism, LVOT VTI ≤ 15 cm has been associated with higher in-hospital mortality, cardiopulmonary arrest, shock, and need for reperfusion therapy.[4] In secondary mitral regurgitation, LVOT VTI ≤ 17 cm predicts both cardiovascular and all-cause mortality.[5] And in ambulatory adults with stable Coronary Artery Disease (CAD), LVOT VTI ≤ 18 cm was associated with heart failure hospitalization and mortality.[6] Despite these findings, there is limited data to evaluate the usefulness of LVOT VTI in free-dwelling adults.

In this study, we aimed to identify the association between LVOT VTI and mortality among participants in the ELSA-Brasil cohort, a multicenter occupational study of Brazilian adults.[7] Participants underwent standardized TTE between 2008 and 2010 based on published guidelines. All these exams were subsequently analyzed in a core lab.[7] Measurements included LVOT VTI, LV Ejection Fraction (LVEF), Stroke Volume Index (SVI), and Cardiac Index (CI). Mortality was assessed through annual follow-up and adjudicated by the investigators up to December 2022.

Keywords

Echocardiography; Risk Assessment; Mortality; Healthy Volunteers.

Mailing Address: Mariana de Castro Lopes •Hospital de Clinicas de Porto Alegre. Rua Ramiro Barcelos, 2350, Sala 2061. Postal code: 90035-903. Porto Alegre, RS – Brazil
Email: marianadecastro.lopes@gmail.com
Manuscript received February 6, 2026; revised manuscript February 9, 2026; accepted February 9, 2026.
Editor responsible for the review: Marcelo Tavares

DOI: https://doi.org/10.36660/abcimg.20260013i

Echocardiographic data were available for 2,237 participants (58.6 ± 9.1 years, 46% male). The mean of LVOT VTI was 19.6 ± 4.0 cm, and 11% had a value of LVOT VTI below the pre-specified cutoff (< 15 cm), a value similar to the other studies' cutoff and positioned between the 10th and 25th percentiles of our sample distribution. Participants with LVOT VTI < 15 cm were slightly older (57 ± 9.9 vs 58.8 ± 8.9, p = 0.009) and showed a higher proportion of males (63% vs 44%, p < 0.001) than the LVOT TVI ≥ 15 cm group. The prevalence of other parameters of cardiac performance below established abnormality thresholds[4,5] was as follows: LVEF < 50% (N = 71, 3%), SVI < 38 mL/m² (N = 1673, 74%), and CI ≤ 2 L/min/m² (N = 905, 40%). The distribution of other relevant variables is depicted in **Table 1**. Over a mean follow-up period of 11.8 ± 2.2 years, 199 (8.9%) participants died (137 males and 62 females).

Mortality was higher among participants with an LVOT-VTI < 15 cm compared with those with higher values (12.6% vs. 8.4%; log-rank test $\chi^2 = 4.68$, $p = 0.026$; **Figure 1**). The multivariable Cox proportional hazards analysis showed that this association was independent of age and sex (Model 1- HR 1.48; 95% CI 1.00–2.18; $p = 0.048$). Additionally, this association remained significant after adjustment for body surface area (Model 2), slightly attenuated after adjustment for systolic blood pressure (Model 3- HR 1.46; 95% CI 0.99–2.15; $p = 0.053$) (**Table 2**). Overall, lower LVOT-VTI was consistently associated with an increased risk of mortality across all models, even after sequential adjustment for demographic and hemodynamic covariates.

Additionally, LVOT TVI showed a weak correlation with height (r = -0.073; p < 0.001), and no significant correlation with weight (r = 0.039; p = 0.067), or with BSA (r = 0.0003, p = 0.99), reinforcing the independence of LVOT TVI with body habitus.

In summary, LVOT VTI <15 cm was associated with a higher mortality among community-dwelling adults in this middle-income country. LVOT VTI may serve as a simple screening metric for cardiac performance in cardiovascular risk stratification of general populations, independently of adjustment for demographic and hemodynamic covariates. Further research is warranted to confirm the independent role of LVOT VTI in risk classification and to define relevant thresholds in specific settings.

Author Contributions

Conception and design of the research and obtaining financing: Lopes MC, Foppa M, Santos ABS; analysis and interpretation of the data and statistical analysis: Lopes MC, Heidemann Jr. AI, Pianca EG, Foppa M, Santos ABS; writing of

Table 1 – Baseline characteristics.

	Overall N = 2,237	LVOT VTI < 15 cm N = 246	LVOT VTI ≥ 15 cm N = 1,991	p-value
Male Sex (%)	1028 (46)	157 (64)	871 (44)	< 0.001
Age (years)	58.6 ± 9	57 ± 9.9	58.8 ± 8.9	0.009
Heart rate (bpm)	67 ± 10	73.9 ± 11.6	66.7 ± 10.1	< 0.001
SBP	125.1 ± 18.8	126.1 ± 18.3	125 ± 18.8	0.38
DBP	76.1 ± 10.7	78.8 ± 11.1	75.8 ± 10.7	< 0.001
Height (cm)	163.9 ± 9.3	165.9 ± 9.7	163.7 ± 9.3	< 0.001
Weight (kg)	72 ± 13.5	72.4 ± 13.6	71.9 ± 13.6	0.57
Body surface area (m²)	1.77 ± 0.19	1.79 ± 0.2	1.77 ± -0.19	0.073
Body mass index (kg/m²)	26.5 ± 4.2	25.9 ± 3.55	26.6 ± 4.12	0.11
Hypertension (%)	1019 (45.6)	119 (48)	900 (45)	0.364
Diabetes (%)	459 (20.5)	53 (21)	406 (20)	0.675
LVEF (%)	66 ± 8.2	60.5 ± 11.7	67.1 ± 7.3	<0.001
SV index (mL/m²)	32.8 ± 8.7	25.3 ± 5.9	33.8 ± 8.5	<0.001
Cardiac output (L/min)	3.89 ± 1.1	3.3 ± 0.98	3.9 ± 1.1	<0.001
Cardiac index (L/min/m²)	2.19 ± 0.58	1.8 ± 0.5	2.2 ± 0.59	<0.001

Continuous variables are expressed as mean ± SD and categorical variables as number (percentage). SBP: Systolic Blood Pressure; DBP: Diastolic Blood Pressure; SV: Stroke Volume, LVEF: Left Ventricular Ejection Fraction.

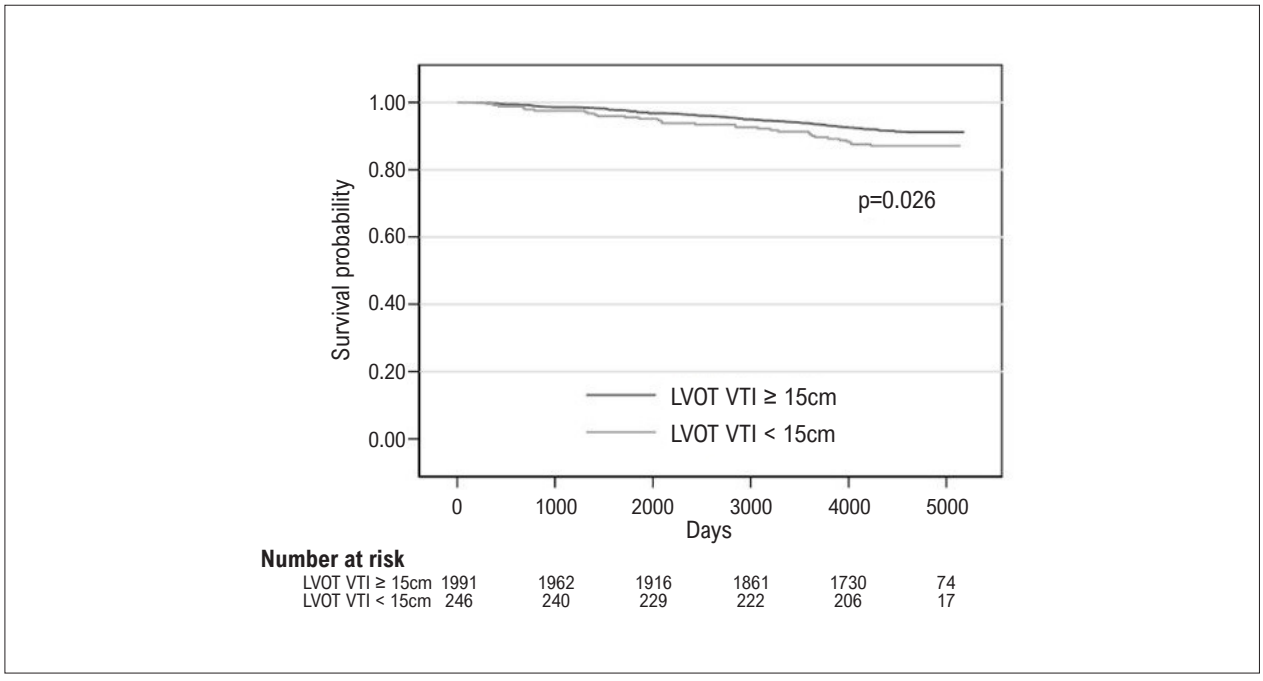

Figure 1 – *Kaplan-Meier survival according to LVOT VTI category (< 15 cm vs. ≥ 15 cm).*

the manuscript: Lopes MC, Santos ABS; critical revision of the manuscript for intellectual content: Heidemann Jr. AI, Pianca EG, Duncan BB, Foppa M, Santos ABS.

Potential Conflict of Interest

No potential conflict of interest relevant to this article was reported.

Table 2 – Multivariable Cox proportional hazards models for all-cause mortality according to LVOT-VTI (< 15 cm vs. ≥ 15 cm)

	Model 1	Model 2	Model 3
		HR (95% IC), p-value	
Age (years)	1.09 (1.07–1.12), p < 0.001	1.09 (1.07–1.12), p < 0.001	1.08 (1.06–1.11), p < 0.001
Male sex	2.58 (1.91–3.50), p < 0.001	2.70 (1.90–3.84), p < 0.001	2.47 (1.74–3.52), p < 0.001
LVOT-VTI < 15 cm	1.48 (CI 1.00–2.18), p = 0.048	1.48 (1.00–2.17), p = 0.048	1.46 (0.99–2.15), p = 0.053
BSA (m²)	—	0.81 (0.34–1.92), p = 0.637	0.83 (0.35–1.98), p = 0.682
SBP (mmHg)	—	—	1.01 (1.01–1.02), p < 0.001
p (overall model)	< 0.001	< 0.001	< 0.001

LVOT-VTI: left ventricular outflow tract velocity–time integral; BSA: body surface area; SBP: systolic blood pressure; HR: hazard ratio; CI: confidence interval.

Sources of Funding

There were no external funding sources for this study.

Study Association

This study is not associated with any thesis or dissertation work.

Ethics Approval and Consent to Participate

This study was approved by the Ethics Committee of the Hospital Clínicas de Porto Alegre under the protocol number 0017.1.069.000-06 194/06. All the procedures in this study were in accordance with the 1975 Helsinki Declaration, updated in 2013. Informed consent was obtained from all participants included in the study.

Use of Artificial Intelligence

The authors did not use any artificial intelligence tools in the development of this work.

Availability of Research Data

All datasets supporting the results of this study are available upon request from the corresponding author.

References

1. Goldman JH, Schiller NB, Lim DC, Redberg RF, Foster E. Usefulness of Stroke Distance by Echocardiography as a Surrogate Marker of Cardiac Output that is Independent of Gender and Size in a Normal Population. Am J Cardiol. 2001;87(4):499-502. doi: 10.1016/s0002-9149(00)01417-x.
2. Dini FL, Barletta V, Ballo P, Cioffi G, Pugliese NR, Rossi A, et al. Left Ventricular Outflow Indices in Chronic Systolic Heart Failure: Thresholds and Prognostic Value. Echocardiography. 2025;42(2):e70109. doi: 10.1111/echo.70109.
3. Tan C, Rubenson D, Srivastava A, Mohan R, Smith MR, Billick K, et al. Left Ventricular Outflow Tract Velocity Time Integral Outperforms Ejection Fraction and Doppler-Derived Cardiac Output for Predicting Outcomes in a Select Advanced Heart Failure Cohort. Cardiovasc Ultrasound. 2017;15(1):18. doi: 10.1186/s12947-017-0109-4.
4. Yuriditsky E, Mitchell OJ, Sibley RA, Xia Y, Sista AK, Zhong J, et al. Low Left Ventricular Outflow Tract Velocity Time Integral is Associated with Poor Outcomes in Acute Pulmonary Embolism. Vasc Med. 2020;25(2):133-40. doi: 10.1177/1358863X19880268.
5. Gentile F, Buoncristiani F, Sciarrone P, Bazan L, Panichella G, Gasparini S, et al. Left Ventricular Outflow Tract Velocity-Time Integral Improves Outcome Prediction in Patients with Secondary Mitral Regurgitation. Int J Cardiol. 2023;392:131272. doi: 10.1016/j.ijcard.2023.131272.
6. Ristow B, Na B, Ali S, Whooley MA, Schiller NB. Left Ventricular Outflow Tract and Pulmonary Artery Stroke Distances Independently Predict Heart Failure Hospitalization and Mortality: The Heart and Soul Study. J Am Soc Echocardiogr. 2011;24(5):565-72. doi: 10.1016/j.echo.2010.12.024.
7. Mill JG, Pinto K, Griep RH, Goulart A, Foppa M, Lotufo PA, et al. Medical Assessments and Measurements in ELSA-Brasil. Rev Saude Publica. 2013;47 (Suppl 2):54-62. doi: 10.1590/s0034-8910.2013047003851.